Australian Government
Geoscience Australia

Bight Basin Geological Sampling and Seepage Survey

RV *Southern Surveyor* Survey SS01/2007

Jennifer Totterdell and Cameron Mitchell (Editors)

Record
2009/24

GeoCat # 68689

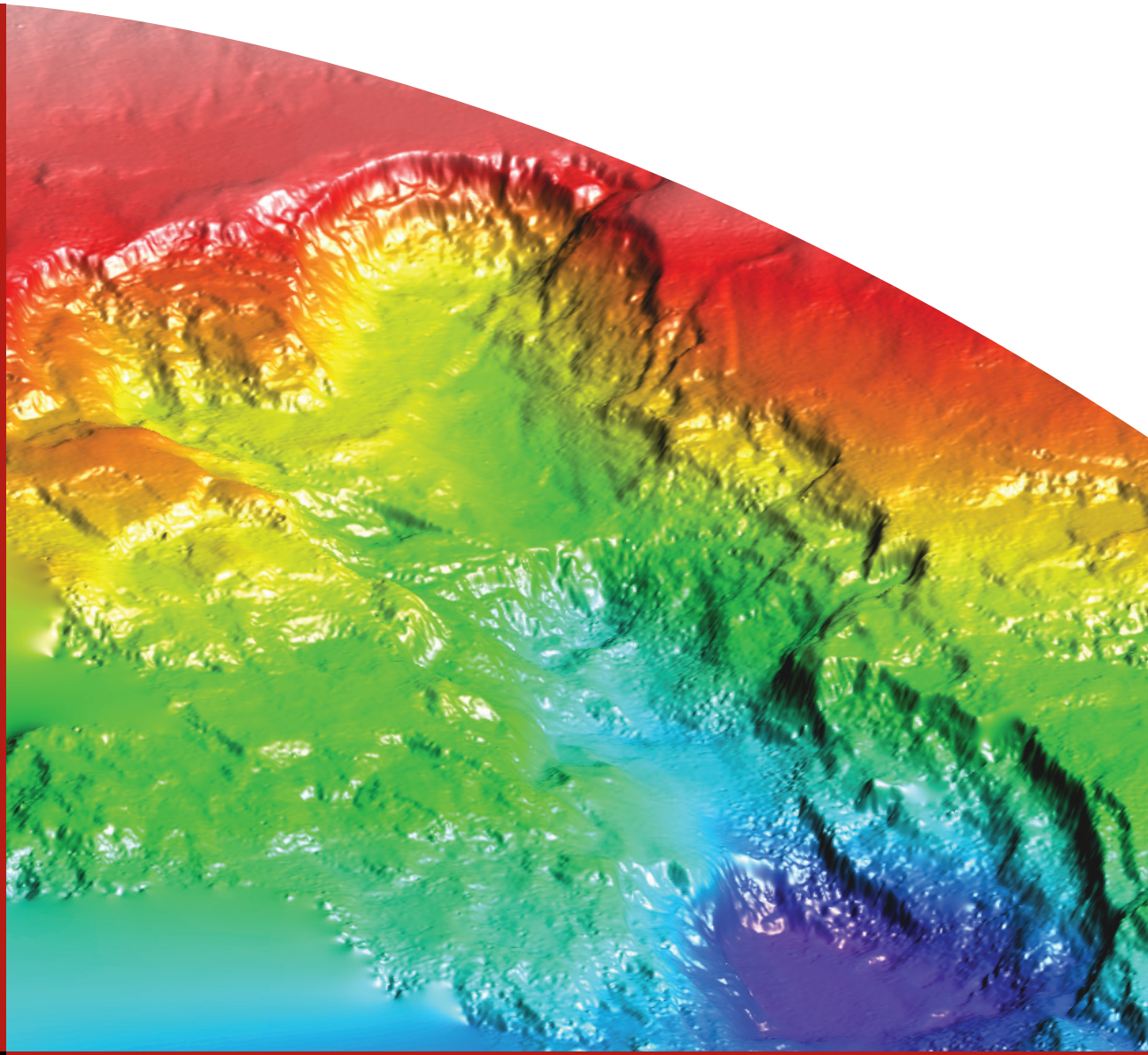

Bight Basin Geological Sampling and Seepage Survey

RV *Southern Surveyor* Survey SS01/2007

GEOSCIENCE AUSTRALIA
RECORD 2009/24

by

Jennifer Totterdell[1] and Cameron Mitchell[1] (Editors)

with contributions from Chris Boreham[1], Georgina Ryan[1], Andrew Stacey[1], Gabriel Nelson[1], Lloyd White[1], Graham Logan[1], Emma Grosjean[1] and Barry Bradshaw[1] (Geoscience Australia)
Eric Monteil (TimeMatters Biostratigraphic Services Pty Ltd)
Mike Macphail (Consultant Palynological Services)
Alan Partridge (Biostrata Pty Ltd)
John Rexilius and Scott Powell (ISC Biostrat)
James Crampton (GNS Science)
Roland di Primio and Brian Horsfield (GeoS4)

Australian Government
Geoscience Australia

1. Petroleum and Marine Division, Geoscience Australia, GPO Box 378, Canberra ACT 2601

Department of Resources, Energy & Tourism
Minister for Resources, Energy & Tourism: The Hon. Martin Ferguson, AM MP
Secretary: Mr John Pierce

Geoscience Australia
Chief Executive Officer: Dr Neil Williams PSM

ISSN 1448-2177
ISBN 978-1-921498-97-8 CD-ROM

GeoCat # 68689

Bibliographic reference: Totterdell, J. and Mitchell, C. (Editors), 2009. Bight Basin geological sampling and seepage survey: RV *Southern Surveyor* SS01/2007. Geoscience Australia Record 2009/24.

Bibliographic reference – individual chapters: Boreham, C., 2009. Organic geochemistry – source rock characterisation. In: Totterdell, J. and Mitchell, C. (Editors), Bight Basin geological sampling and seepage survey: RV *Southern Surveyor* SS01/2007. Geoscience Australia Record 2009/24, 36–60.

Contents

EXECUTIVE SUMMARY ***1***

1. INTRODUCTION ***3***

2. PETROLEUM GEOLOGY OF THE BIGHT BASIN ***5***

GEOLOGICAL SETTING 5
Regional tectonic setting 5
Structural elements 6
Tectonic evolution 8
Tectonostratigraphy 12
PETROLEUM POTENTIAL OF THE BIGHT BASIN 13
Petroleum systems model 13
Potential source rocks 13
Exploration history 14

3. BIGHT BASIN GEOLOGICAL SAMPLING AND SEEPAGE SURVEY ***16***

INTRODUCTION 16
SCIENTIFIC OBJECTIVES 16
VOYAGE OBJECTIVES 17
VOYAGE TRACK 18
PHYSICAL SAMPLING AND EQUIPMENT 18
Seabed sediment samples 18
Sampling and handling during survey 19
Post-survey laboratory analysis 21
GEOPHYSICAL EQUIPMENT 22
Bathymetry: swath (multibeam) sonar 22
Sub-bottom profiler 22
Side scan sonar 22

4. DREDGE SAMPLING RESULTS ***23***

DREDGE SAMPLE DESCRIPTIONS ***23***
Igneous rocks *23*
Modern sediments *23*
Chemical rocks *23*
Calcareous rocks *24*
Siliciclastic rocks *24*

5. BIOSTRATIGRAPHIC STUDIES ***35***

PALYNOLOGY 35
Main results 35
MICROPALAEONTOLOGY 35
MACROPALAEONTOLOGY 35

6. ORGANIC GEOCHEMISTRY – SOURCE ROCK CHARACTERISATION ***36***

SUMMARY 36
SAMPLES AND METHODS 37
RESULTS AND DISCUSSION 38
Preservation of organic matter in seafloor sediments 38
Source rock potential 39
Source facies and depositional environment 41
Pyrolysis-gas chromatogram 44
Multi-component kinetics 47
Saturated biomarker distribution 47
Metalloporphyrins 57
Photic zone anoxia 58
Carbon isotopes 58
Global Oceanic Anoxic Event 58
Implications for exploration 60

7. HYDROCARBON SEEPAGE SURVEY RESULTS *61*
INTRODUCTION 61
REGIONAL GEOMORPHOLOGY 61
REGIONAL SEDIMENTOLOGY 61
REGIONAL SHALLOW STRATIGRAPHY 62
SURVEY AREA RESULTS 65
Area 1 65
Area 2 71
Area 3 83
Area 4 91
Area 5 96
Area 6 100
Area 7 108
Area 8 111
Area 9 113
DISCUSSION AND SUMMARY 115
Geochemistry 115
Seepage indications 116
Shallow stratigraphy 117

8. SUMMARY OF SURVEY SS01/2007 RESULTS *118*
INTRODUCTION 118
DREDGE SAMPLING SURVEY 118
SEEPAGE SURVEY 119

9. ACKNOWLEDGEMENTS *120*

10. REFERENCES *121*

List of Appendices

1. SAMPLING SITES AND SURVEY LEADER'S LOG

2. DREDGE SAMPLE DESCRIPTIONS

2.1: SAMPLE CATALOGUE *
2.2: DREDGE SAMPLE DESCRIPTIONS*
2.3: CORE CATCHER SAMPLE DESCRIPTIONS*
2.4: THIN SECTION DESCRIPTIONS

3. BIOSTRATIGRAPHIC ANALYSES

3.1: PALYNOLOGICAL ANALYSES (INCLUDING 9 APPENDICES)*
3.2: MICROPALAEONTOLOGICAL ANALYSES (INCLUDING 2 APPENDICES)*
3.3: MACROPALAEONTOLOGICAL ANALYSES

4. GEOCHEMICAL ANALYSES

4.1: DESCRIPTION, AGE AND DEPOSITIONAL ENVIRONMENT FOR BIGHT BASIN SAMPLES*
4.2: ROCK EVAL PYROLYSIS, TOC AND CARBON ISOTOPES FOR BIGHT BASIN SAMPLES*
4.3: PY-GC YIELDS OF INDIVIDUAL COMPOUNDS AND COMPOUND CLASSES*
4.4: ORGANIC PETROLOGY AND MATURATION OF DREDGE SAMPLES FROM THE GREAT AUSTRALIAN BIGHT, OFFSHORE SOUTHERN AUSTRALIA
4.5: VITRINITE REFLECTANCE AND MACERAL DESCRIPTIONS FOR BIGHT BASIN SAMPLES*
4.6: YIELDS OF EXTRACTABLE ORGANIC MATTER AND ITS THREE MAIN COMPOUND CLASSES FOR BIGHT BASIN SAMPLES*
4.7: BIOMARKER RATIOS DERIVED FROM GC AND GCMS-SIR ANALYSIS OF THE SATURATED HYDROCARBONS*
4.8: DISTRIBUTION OF C_{26} DESMETHYLSTERANES DERIVED FROM GCMS-MRM ANALYSIS OF THE SATURATED HYDROCARBONS*
4.9: METALLOPORPHYRIN CONTENTS FOR BIGHT BASIN SAMPLES AND ASPHALTITES*
4.10: OIL AND GAS GENERATION CHARACTERISTICS OF A KEROGEN AND AN ASPHALTENE SAMPLE AS INFERRED FROM PHASEKINETIC ANALYSIS

5. OCEANOGRAPHIC DATA

* Excel spreadsheets for these appendices are contained in the **Data** directory on this CD-ROM

Executive Summary

The Bight Basin Sampling and Seepage Survey (SS01/2007) was undertaken in February-March 2007 as the final data acquisition activity of the Australian Government's New Petroleum Program (2003-2007). The survey was designed to address two key petroleum systems issues in the Bight Basin:

1. **Distribution of source rocks.** The survey sampled distal facies of potential source intervals of Albian-Santonian age at locations on the seaward edges of the Ceduna and Eyre Terraces to obtain new information about source facies in the basin.
2. **Presence of active petroleum systems**. The survey obtained seabed samples and geophysical data at potential natural hydrocarbon seepage sites across the Ceduna Sub-basin to assess the presence of active petroleum systems.

Nine areas of interest were identified for surveying in the eastern Bight Basin. These areas targeted outcrops of Albian-Santonian sedimentary rocks, and locations where seismic and other geophysical datasets provided evidence of possible hydrocarbon seepage. The survey took place from 24 February–17 March 2007 using the Marine National Facility vessel RV *Southern Surveyor*.

The survey successfully sampled all nine targeted areas and collected 37 dredge hauls, 69 gravity cores and 15 grab samples, as well as 8825 km^2 of multibeam swath bathymetry data, and 2400 line km of sub-bottom profiler data.

The Bight Basin Survey was very successful in addressing the most critical of its objectives – samples from the exposed up-dip northwestern edge of the Ceduna Sub-basin provide the first evidence for a world-class marine Cretaceous source rock in the Bight Basin.

Geochemical and biostratigraphic analyses of dredge samples from Area 5 identified a suite of rocks with the following characteristics:

- Good-very good organic richness: TOC 2.0–6.9% (17 samples)
- Good to excellent liquids potential: HI 274–479 mgHC/gTOC (11 samples)
- Samples with highest liquids potential have highest TOC (Dredge 17)
- Organic matter has a marine signature and was deposited under reducing (anoxic) conditions
- A close geochemical relationship exists between these samples and asphaltites from coastal bitumen strandings
- Geochemical comparisons between the potential source rocks and the asphaltites suggests the presence of richer source rocks elsewhere in the basin
- Biostratigraphic age: Latest Cenomanian–earliest Turonian
- Age and geochemistry of these organic-rich rocks suggest that they are a local expression of the global Oceanic Anoxic Event 2

The samples provide the best evidence of liquids-prone source rocks in the Bight Basin, and significantly upgrade its petroleum prospectivity.

The survey collected clastic rocks ranging in age from Cenomanian to Maastrichtian, with depositional environments ranging from delta plain to open marine. In addition, several Cenozoic carbonate rocks were collected.

The results of the seepage survey were more equivocal. No direct evidence of hydrocarbon seepage was found, despite targeting a range of promising localities across the basin. Organic geochemical analyses of gravity core samples failed to detect any thermogenic hydrocarbons.

Indirect evidence of possible shallow gas was provided by the sub-bottom profiler data collected in transit between areas 1 and 2, and in Area 3. Data collected in these areas included enhanced reflections that can be interpreted as indicating the presence of shallow gas. In addition, echo-sounder data in Area 1 captured flares of unknown origin immediately overlying a possible seepage site identified on seismic data.

There are several possible reasons for failure to directly detect any hydrocarbons during the seepage survey, including hydrocarbons not being preserved in the very shallow section (≤5 m) that was sampled by the gravity corer, poor targeting of potential seepage sites, or the lack of any hydrocarbon seepage. This question will probably not be resolved until further sampling work is carried out in the basin, using equipment capable of taking deep cores.

1. Introduction

J. Totterdell

The eastern part of the Bight Basin is potentially one of the most prospective deepwater frontier basins in offshore Australia. The Ceduna Sub-basin in particular contains a sedimentary section in excess of 15 km thick. The most prospective petroleum systems are believed to be associated with thick mid to Late Cretaceous deltaic and marine sediments, which provide reservoirs, seals and potential oil-prone source rocks at several stratigraphic levels, together with a wide range of structural and stratigraphic plays (Blevin et al., 2000; Totterdell et al., 2000; Struckmeyer et al., 2001).

The Bight Basin has seen several phases of petroleum exploration since the 1970s, but to date drilling results have been disappointing. From the 1960s to late 1990s, only nine exploration wells were drilled, six of which are located in the Duntroon Sub-basin. All wells were drilled within relatively thin and proximal successions on the margins of the basin, and only two wells encountered significant hydrocarbon indications. Oil and gas shows were reported from Greenly-1, and fluid history analysis of samples from Jerboa-1 revealed an interpreted palaeo-oil column (Ruble et al., 2001; Struckmeyer et al., 2002). The majority of wells in the region are considered to have been invalid tests (Messent 1998). During the most recent phase of exploration, Woodside Energy and its joint venture partners were awarded three large permits in the Ceduna Sub-basin in 2000; the permits were relinquished in 2007. Data acquisition included 15,636 km of 2D seismic data (Flinders 2D Marine Seismic Survey; Bruins et al., 2001) and the 1250 km^2 Trim 3D seismic survey. In April 2003, Woodside Petroleum and its partners drilled Gnarlyknots-1A in 1316 m of water aiming to test the petroleum systems within more distal Late Cretaceous depositional systems of the Ceduna Sub-basin (Tapley et al., 2005). Adverse weather conditions resulted in the abandonment of the well in Santonian age sandy coastal plain deposits, some 1500 m above the planned completion depth, with several key targets untested and no hydrocarbons encountered (Tapley et al., 2005; Walker 2007).

Hydrocarbon charge is perceived as the major exploration risk in the Ceduna Sub-basin, despite the failure of most wells to test a valid trap (Messent 1998; Somerville 2001). Potential petroleum systems occur in Middle Jurassic through to Late Cretaceous strata, with older petroleum systems located along the shallower water northern margin and younger systems located increasingly basinward in deeper water. A key uncertainty for explorers has been whether oil-prone source rocks are present in distal marine facies from the more outboard, deep water parts of the Ceduna Sub-basin. Some indications that such source rocks are present come from hydrocarbon seep studies using Synthetic Aperture Radar (SAR) and Airborne Laser Fluorosenser (ALF) data (Struckmeyer et al., 2002), and geochemical studies of asphaltite strandings along the southern margin (Edwards et al., 1998; Boreham et al., 2001). However, direct evidence for oil-prone marine source rocks in the Ceduna Sub-basin has previously been absent.

In February–March 2007, Geoscience Australia undertook a marine sampling survey in the Great Australian Bight, using the Marine National Facility vessel, RV *Southern Surveyor* (Fig. 1.1). The primary objective of the survey was to obtain samples from distal parts of the Jurassic–Cretaceous Bight Basin in order to address petroleum exploration industry concerns regarding the presence of viable source rocks in the basin. The survey successfully acquired a suite of mid-basin to distal rocks of Cenomanian–Maastrichtian age, including several samples with excellent source potential. This report documents the results of the survey, focusing on the biostratigraphic and organic geochemical analyses of the samples, and the geophysical and geochemical investigation of potential seepage indicators.

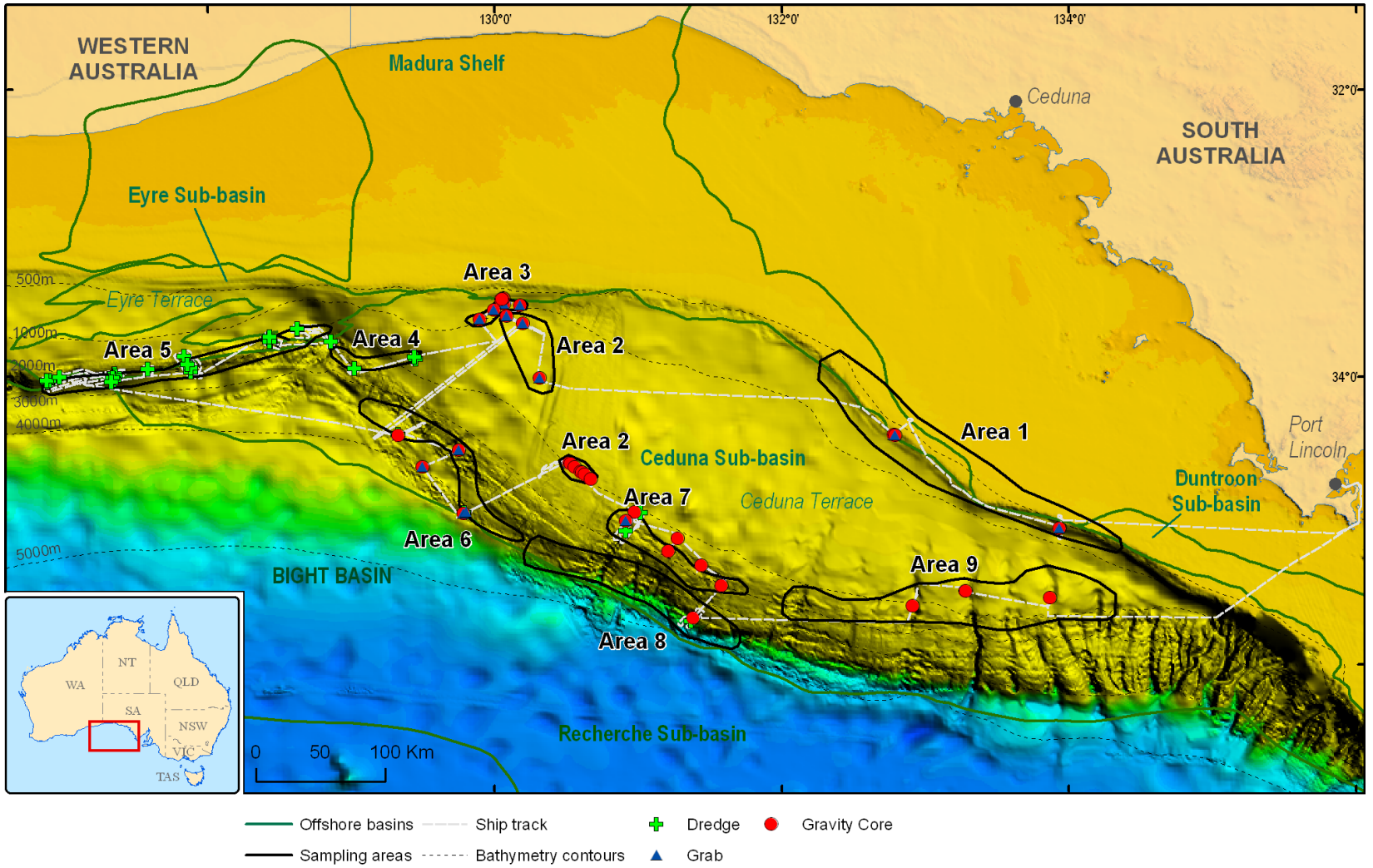

Figure 1.1. *Bight Basin Sampling and Seepage Survey SS01/2007: survey areas and location of sampling sites.*

2. Petroleum Geology of the Bight Basin

J. Totterdell and B. Bradshaw

GEOLOGICAL SETTING

Regional tectonic setting

The Jurassic–Cretaceous Bight Basin is a large, mainly offshore basin situated along the western and central parts of the continental margin of southern Australia. The basin also includes Cretaceous sedimentary rocks that extend over 300 km onshore from the coast. The Bight Basin extends from the south of Cape Leeuwin in the west, to just south of Kangaroo Island in the east, where it adjoins the Otway Basin (Fig. 2.1). The basin underlies the continental shelf and slope, including two bathymetric terraces (Eyre Terrace and Ceduna Terrace; Fig. 1.1), in water depths ranging from less than 200 to over 4000 m. The main depocentres (including the Ceduna Sub-basin) occur in the eastern part of the Bight Basin. To the east of these depocentres, a thin Bight Basin succession overlies Proterozoic basement of the Gawler Craton and deformed Early Palaeozoic rocks of the Adelaide Fold and Thrust Belt (Fig. 2.2). To the north, basement includes a variety of Proterozoic and older terranes. Basement trends had a profound influence on the structural development of the Bight Basin, controlling the location and orientation of early basin-forming structures (Stagg et al., 1990; Totterdell et al., 2000; Teasdale et al., 2003; Totterdell & Bradshaw, 2004). The Bight Basin is overlain unconformably by the dominantly cool-water carbonates of the Cenozoic Eucla Basin. To the south, the uppermost sequences of the Bight Basin onlap highly extended continental crust and rocks of the continent-ocean transition on the abyssal plain between Australia and Antarctica (Sayers et al., 2001).

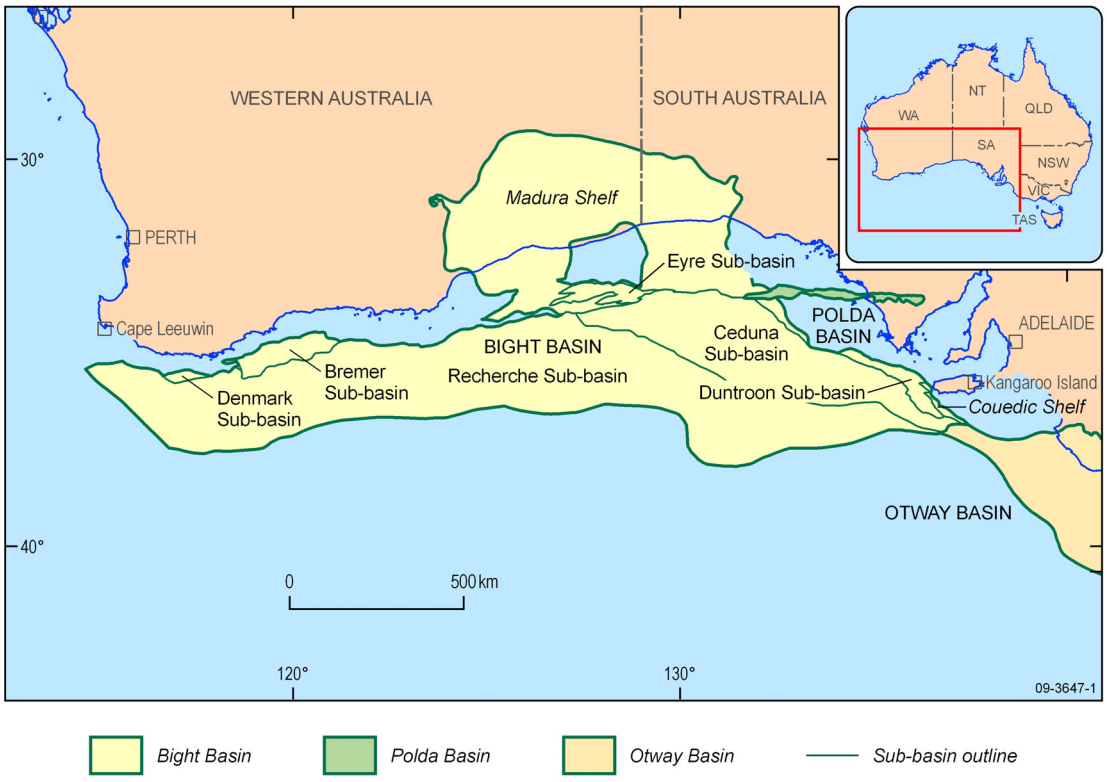

Figure 2.1. *Location of the Bight Basin, with component sub-basins (after Totterdell and Bradshaw, 2004).*

Structural elements

The Bight Basin is one of a series of Mesozoic to Cainozoic depocentres that developed along Australia's southern margin during a period of extension and passive margin evolution that commenced in the Middle–Late Jurassic (Fraser & Tilbury 1979; Bein & Taylor 1981; Willcox & Stagg 1990; Stagg et al., 1990; Hill 1995; Totterdell et al., 2000; Norvick & Smith 2001; Totterdell & Bradshaw, 2004). The basin contains five main depocentres—the Ceduna, Duntroon, Eyre, Bremer and Recherche sub-basins (Figs 2.1, 2.2). Thin sedimentary successions onlap shallow basement along the northern and eastern margins (Madura and Couedic shelves). The largest and thickest depocentre, the Ceduna Sub-basin, contains a sedimentary section approximately 15 km thick. The deepwater Recherche Sub-basin adjoins the Ceduna Sub-basin and extends west along the southern margin as far as the Leeuwin Fracture Zone. Perched half-graben systems of the Denmark, Bremer and Eyre sub-basins lie to the north of the Recherche Sub-basin. The Duntroon Sub-basin adjoins the Ceduna Sub-basin to the east, and consists of a series of oblique extensional depocentres.

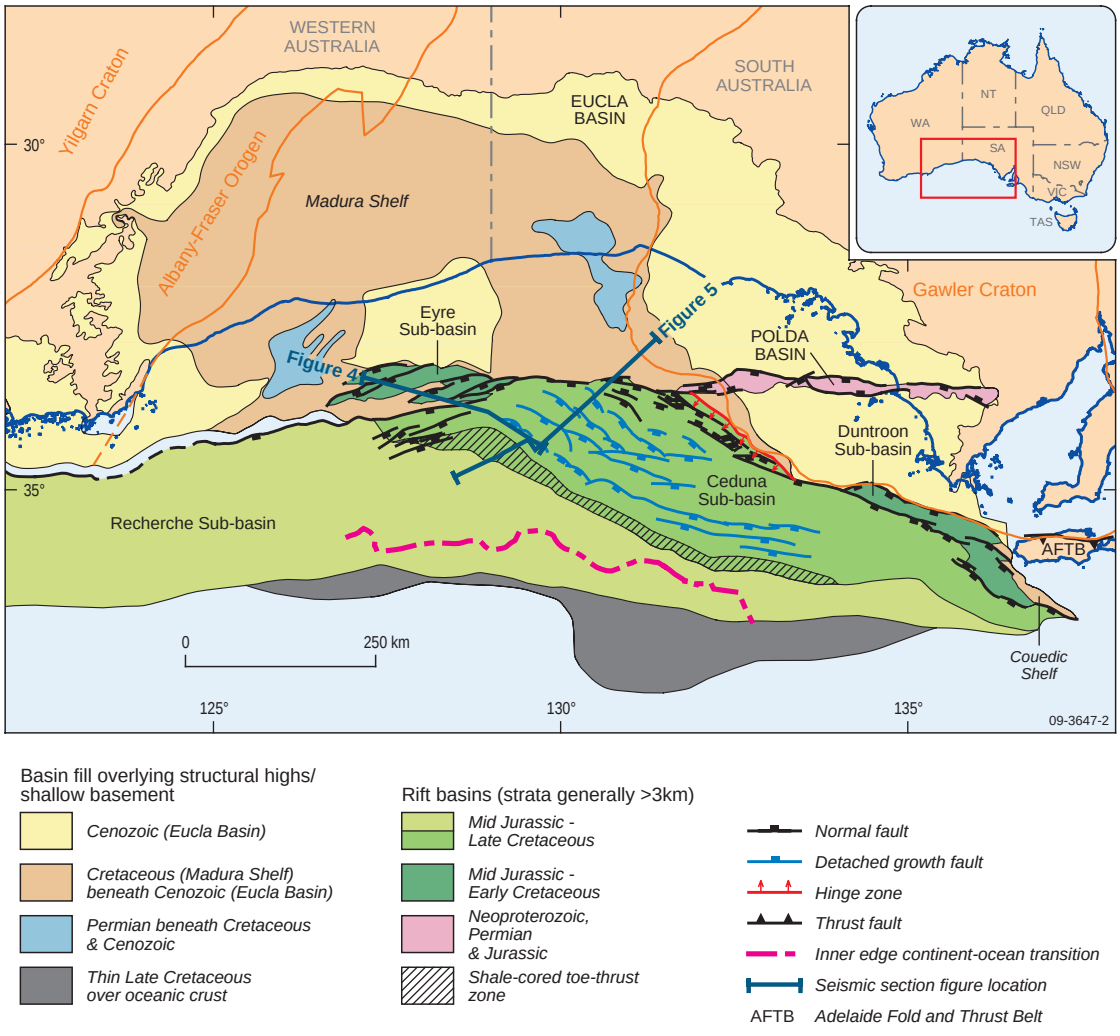

Figure 2.2. *Structural elements of the eastern Bight Basin (after Bradshaw et al., 2003).*

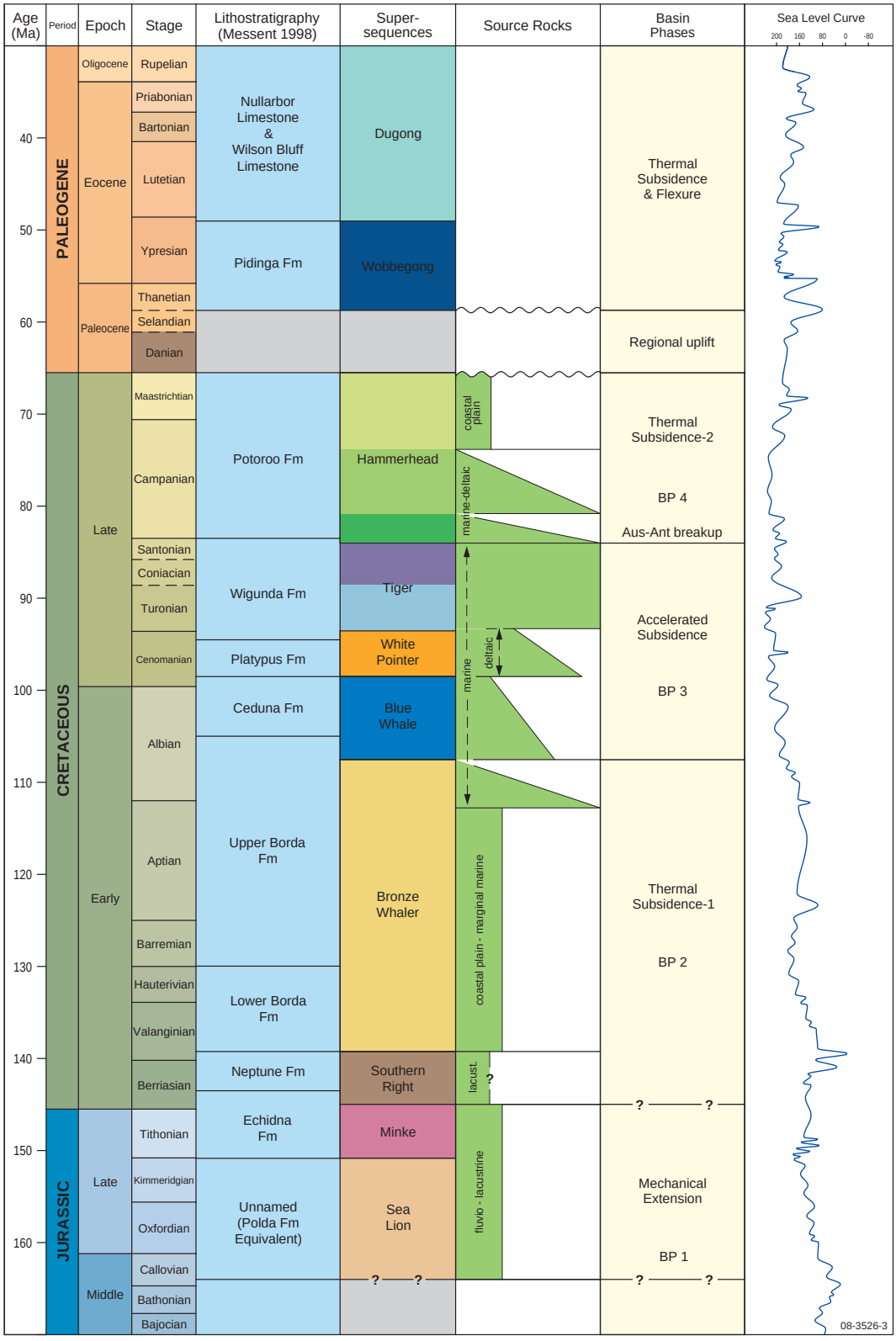

Figure 2.3. *Bight Basin stratigraphic correlation chart showing basin phases and predicted source rock intervals (modified from Blevin et al, 2000 and Totterdell et al, 2000). The sea-level curve (Haq et al, 1988) is modified to the time scale of Gradstein et al. (2004).*

Tectonic evolution

The Bight Basin formed within a tectonic framework dominated by the break-up of eastern Gondwana. The basin evolved through repeated episodes of extension and thermal subsidence leading up to, and following, the commencement of seafloor spreading between Australia and Antarctica (Totterdell & Bradshaw, 2004; Fig. 2.3).

The basin was initiated during a period of Middle–Late Jurassic to Early Cretaceous upper crustal extension. At this time a convergent margin existed on the eastern margin of the continent. Incipient rifts were developing between Australia and Antarctica, India and Antarctica, and India and western Australia, the extensional systems forming a triple junction (Norvick & Smith 2001; Fig. 2.4a). Rifting along this system eventually resulted in seafloor spreading between India and Australia/Antarctica, but the rift along the southern margin failed at that time. In the Bight Basin, a NW–SE to NNW–SSE extension direction, superimposed on east–west and northwest–southeast-oriented basement structures, resulted in oblique to strongly oblique extension and the formation of en echelon half graben in the Eyre, inner Recherche, northern and eastern Ceduna, and Duntroon sub-basins (Figs. 2.2, 2.5). The areal extent of the early extensional structures beneath the thick Ceduna Sub-basin cannot be determined due to the thickness and nature of the sedimentary section. The anomalously thick nature of the sub-basin may indicate, however, that Jurassic–Early Cretaceous rifts are present at depth.

The Early Cretaceous was characterised by post-rift thermal subsidence in the Bight Basin. In the mid-Cretaceous, open ocean lay to the west and a seaway extended along the margin to the eastern Bight area (Fig. 2.4b).

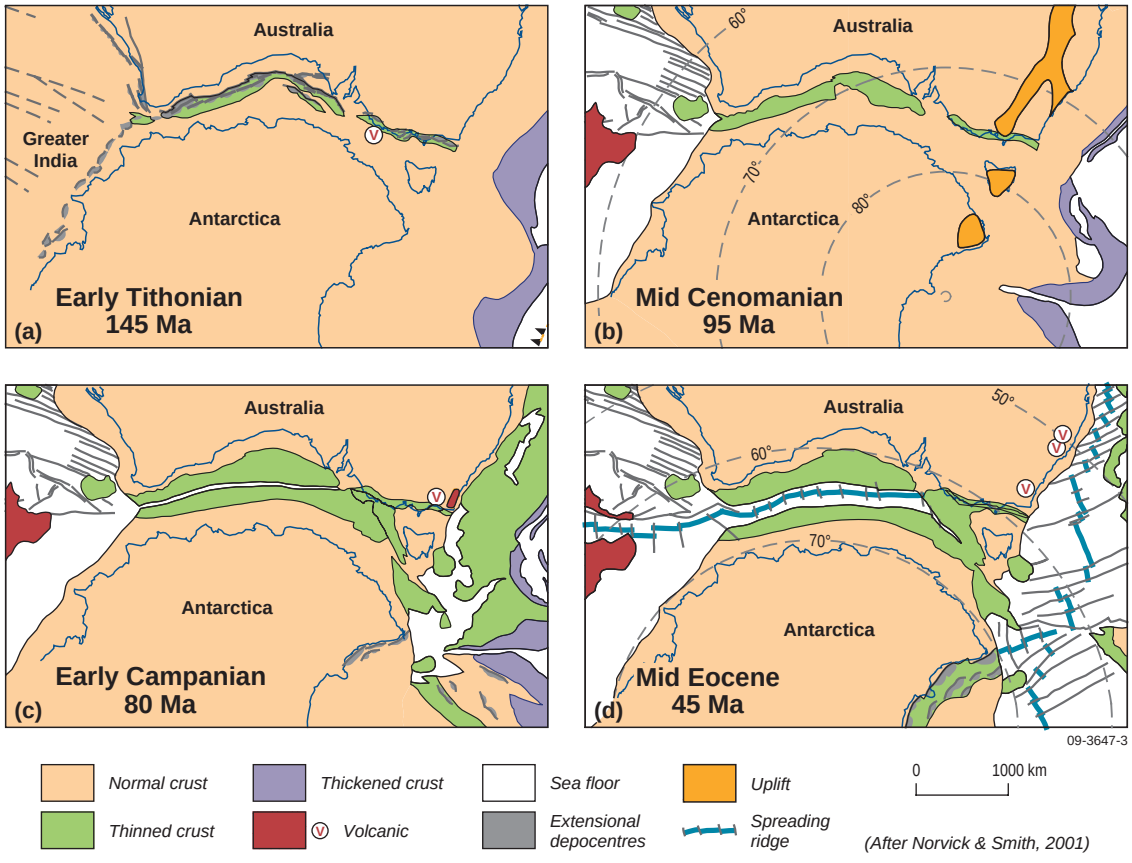

Figure 2.4. *Plate tectonic reconstructions for the southern Australia–Antarctica conjugate margin (Norvick & Smith, 2001)*

Post-rift thermal subsidence was followed by a phase of accelerated subsidence, which commenced in the mid-Albian and continued until continental break-up in the late Santonian–early Campanian. During this phase of enhanced subsidence, the dominant structural feature was a system of gravity-driven, detached extensional and contractional structures, which developed in the Cenomanian as a result of deltaic progradation (Figs. 2.6, 2.7). Several authors (Veevers et al., 1991; Raza et al., 1995; Totterdell et al., 2000; Krassay & Totterdell, 2003), have speculated that the deltas of the Ceduna Sub-basin were fed by sediments derived from the eastern Australian highlands about 1500 km to the east-northeast. Fission track studies indicate that the eastern Australian highlands were affected by a regional-scale cooling event in the mid-Late Cretaceous (100-80 Ma; late Albian-Campanian) caused by kilometre-scale uplift and denudation. At around 90-100 Ma, subduction ceased along the eastern Australian margin, resulting in dynamic rebound of the cratonic platform (Waschbusch et al., 1999). This rebound is likely to have resulted in the development of a regional drainage gradient to the west. It is possible that much of the sediment eroded from this area was transported west and southwestwards towards the Bight depocentre (Totterdell et al, 2000; Totterdell & Bradshaw, 2004).

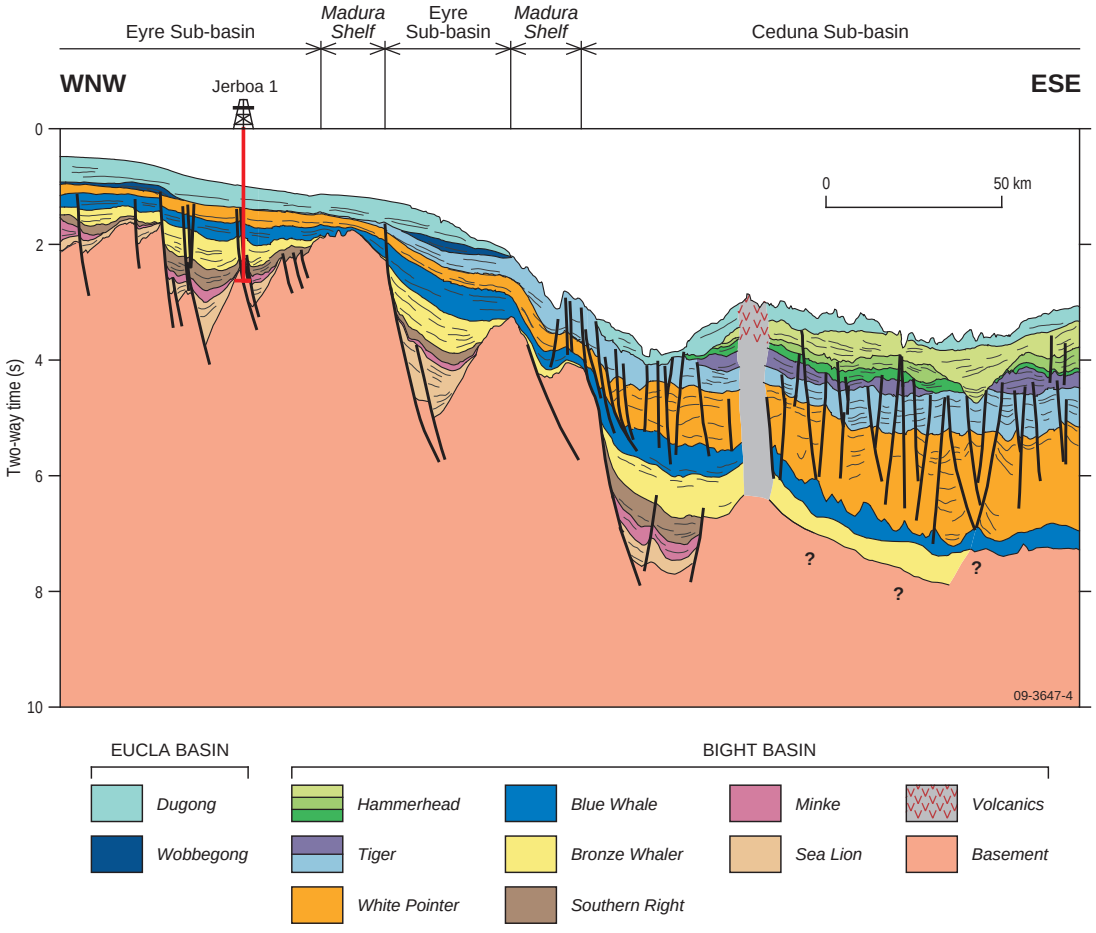

Figure 2.5. *Cross-section through the Eyre Sub-basin, Madura Shelf and Ceduna Sub-basin, showing supersequences (as per Figure 2.3). Refer to Figure 2.2 for location of cross-sections (after Totterdell and Bradshaw, 2004).*

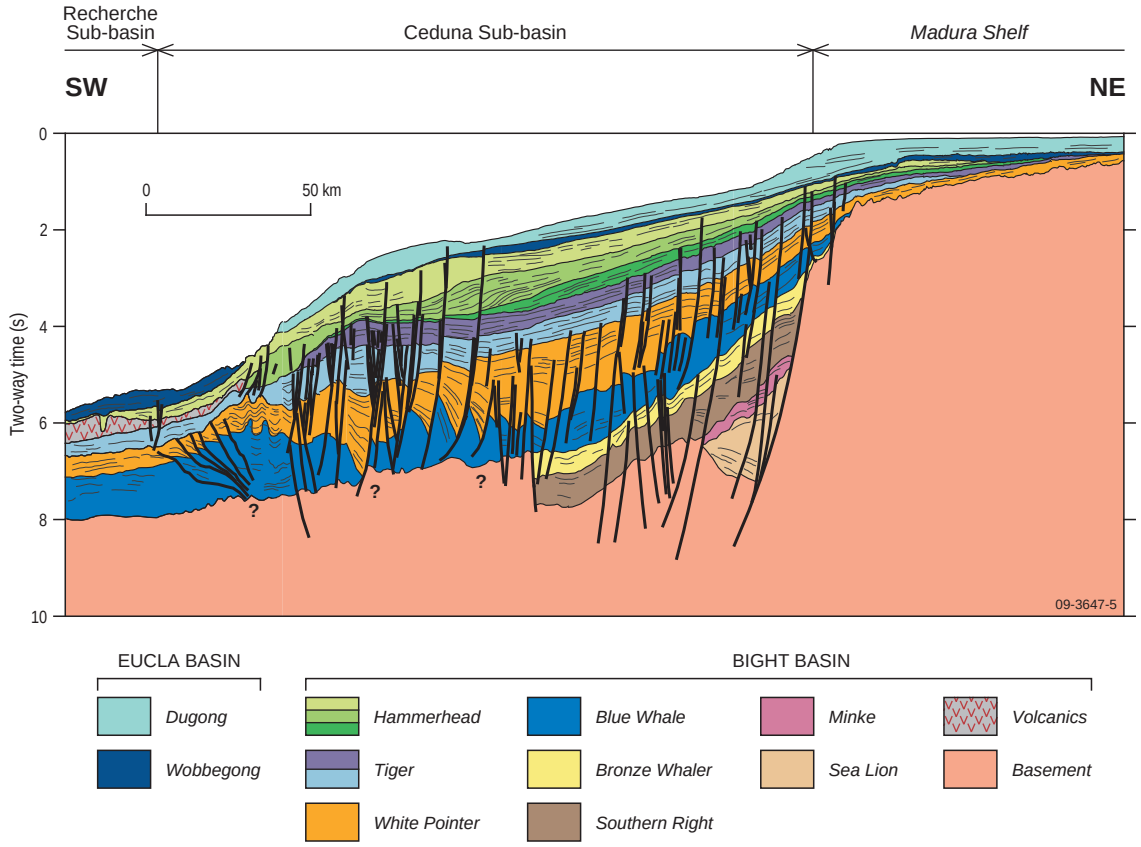

Figure 2.6. *Cross-section through the Madura Shelf, northern Ceduna Sub-basin and Recherche Sub-basin, showing supersequences (as per Figure 2.3). Refer to Figure 2.2 for location of cross-sections (after Totterdell and Bradshaw, 2004).*

Evidence for upper crustal extension during this period of accelerated subsidence preceding break-up is limited to localised Turonian–Santonian extensional faulting, including the reactivation and propagation of Cenomanian growth faults (Figs. 2.6, 2.7). The upper crustal extension that is observed is not consistent with the amount of accommodation created, so it is suggested that the accelerated subsidence rate may have been caused by depth-dependent stretching processes (i.e. where stretching of the lower crust and upper mantle is greater than that of the upper crust).

The commencement of seafloor spreading in the latest Santonian was followed by a further period of thermal subsidence and establishment of a passive margin. Ultra- to very slow spreading between Antarctica and Australia commenced around 83 Ma (Sayers et al., 2001; Fig. 2.4c) and continued for almost 20 m.y. The seaway along the southern margin would have remained narrow due to the slow rate of spreading. In the middle Eocene (Tikku & Cande 1999), there was a dramatic increase in the rate of spreading, and continental separation accelerated (Fig. 2.4d). This resulted in subsidence of the margin, which is reflected in the strongly onlapping nature of the sequence boundary at the base of the Dugong Supersequence.

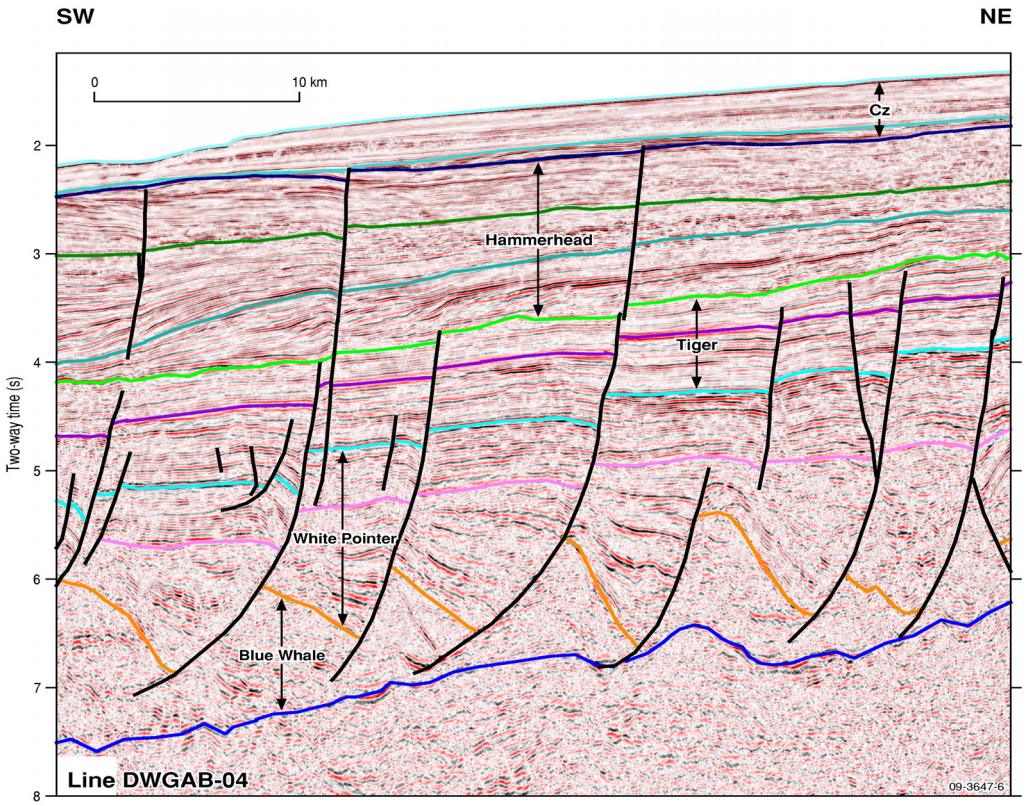

Figure 2.7. *Seismic line showing typical structural architecture, northern Ceduna Sub-basin (Totterdell & Krassay, 2003a)*

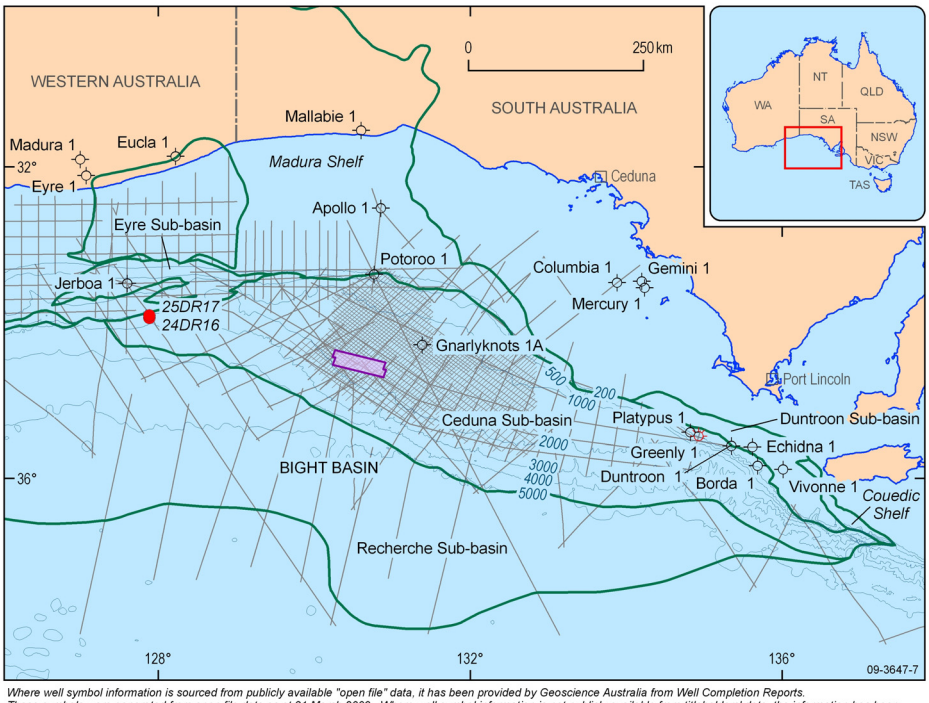

Where well symbol information is sourced from publicly available "open file" data, it has been provided by Geoscience Australia from Well Completion Reports. These symbols were generated from open file data as at 31 March 2009. Where well symbol information is not publicly available from titleholders' data, the information has been extracted from other public sources.

3D Trim seismic survey
Basin outline
2D seismic survey line
Bathymetry contour (depth in metres)
Petroleum exploration well - Dry hole
Petroleum exploration well - Gas show
Potential source rocks dredge sample location

Figure 2.8. *Location of seismic lines and wells in the eastern Bight Basin.*

Tectonostratigraphy

A tectonostratigraphic framework for the eastern part of the Bight Basin was compiled by Totterdell et al. (2000) and Totterdell and Bradshaw (2004), based on the sequence stratigraphic and structural interpretation of an extensive grid of seismic data, tied to 9 petroleum exploration wells in the offshore Bight Basin (Figs 2.3, 2.8); data from the 2003 Gnarlyknots-1A well were not available for those studies, however the drilling results are consistent with the sequence stratigraphic framework. Stratigraphic control in the Madura Shelf and northern Ceduna Sub-basin is provided by the Apollo-1 and Potoroo-1 wells, which intersect thin mid-Late Cretaceous successions at the edge of the sub-basin, and Gnarlyknots-1A, which was drilled farther basinward (Fig. 2.8). In the Eyre Sub-basin, Jerboa-1 penetrated the latest Jurassic-Early Cretaceous section. Further south, in the southern Ceduna and Duntroon sub-basins, Platypus-1, Greenly-1, Duntroon-1, Borda-1, Echidna-1 and Vivonne-1 provide information on the Early-Late Cretaceous succession.

The tectonostratigraphic development of the Bight Basin can be described in terms of four basin phases (Fig. 2.3; Totterdell et al., 2000). Basin Phase 1 (BP1) records the initiation of sedimentation during the Middle-Late Jurassic to earliest Cretaceous phase of NW–SE to NNW–SSE intracontinental extension. This resulted in the formation of a series of oblique extensional and transtensional half graben in the Bremer, Eyre and Duntroon sub-basins, and along the northern and eastern margins of the Ceduna Sub-basin (Figs. 2.2, 2.5, 2.6). The syn-rift Minke Supersequence and the drilled portion of the Sea Lion Supersequence comprise fluvial–lacustrine sandstone, siltstone, and claystone successions.

The extensional phase was followed by a period of slow thermal subsidence that lasted throughout most of the Early Cretaceous (Basin Phase 2; Fig. 2.3). This phase is represented by the Berriasian Southern Right Supersequence and the Valanginian to mid-Albian Bronze Whaler Supersequence. Deposition during this time was largely non-marine, although some marine influence is evident late in this phase. In the Eyre Sub-basin, the Southern Right Supersequence is thin and characterised by lowstand fluvial sandstones; the presence of coal is interpreted on the basis of seismic reflection character. In the Duntroon Sub-basin the Southern Right Supersequence largely comprises a thick aggradational mudstone succession. The overlying Bronze Whaler Supersequence generally consists of an aggradational succession of fluvial and lacustrine sediments. In the Eyre Sub-basin, the extent of deposition of BP2 is generally constrained by the half-graben bounding faults, but the succession does not thicken appreciably into the faults, indicating that little or no actual upper crustal extension occurred at this time. Overall, the succession has an onlapping, sag-fill geometry which indicates that accommodation was created largely by thermal subsidence and compaction, with deposition concentrated over the earlier half graben.

An abrupt increase in subsidence rate in the mid-Albian signalled the start of the third basin phase (BP3; Fig. 2.3). This period of accelerated subsidence, which continued until the commencement of seafloor spreading between Australia and Antarctica in the late Santonian, coincided with a period of rising global sea level (Fig. 2.3). This combination of factors resulted in a high rate of creation of accommodation, the first major marine flooding event in the basin and the widespread deposition of marine silts and shales of the Albian–Cenomanian Blue Whale Supersequence. The present-day distribution of the supersequence indicates that the seaway at that time extended along the southern margin from the open sea in the west towards the Otway Basin in the east. Progradation of deltaic sediments into this seaway (White Pointer Supersequence) commenced in the Cenomanian, following uplift and erosion along the eastern margin of the continent. Deposition was rapid, resulting in the development of overpressure in the underlying marine shales, and a short-lived period of shale mobilisation and growth faulting throughout the northern half of the Ceduna Sub-basin (Fig. 2.7). Interpretation of seismic facies suggests that a broad band of coaly sediments is present within the White Pointer Supersequence in the inner part of Ceduna Sub-basin. The Cenomanian deltaic sediments are overlain by the marginal marine, deltaic and

open marine sediments of the Turonian–Santonian Tiger Supersequence. In wells, the supersequence is dominated by mudstones and a few thick sandstone units. On seismic data, the supersequence has a largely flat-lying aggradational character.

Continental break-up in the late Santonian was followed by a period of thermal subsidence and the establishment of the southern Australian passive margin (BP4; Fig. 2.3). It was during this phase that the second large progradational delta developed, represented by the latest Santonian–Maastrichtian Hammerhead Supersequence (Figs. 2.6, 2.7). In contrast to the earlier deltaic system, this sand-rich delta is characterised by strongly prograding stratal geometries and shows no evidence of widespread shale tectonics. A dramatic reduction in sediment supply at the end of the Cretaceous saw the abandonment of deltaic deposition. There is widespread evidence of regional uplift at this time. The Hammerhead Supersequence, and much of the underlying Tiger Supersequence, are absent across the Eyre Sub-basin. In addition, there is an angular unconformity between the Bight and Eucla Basin successions on the Madura Shelf, where Cretaceous units are progressively eroded across the shelf (Fig. 2.6). From the late Paleocene to present, the largely cool-water carbonates of the Eucla Basin accumulated on a sediment-starved passive margin. A short phase of magmatism in the middle Eocene, coinciding with the onset of rapid spreading, affected the central Ceduna Sub-basin. This magmatic phase was characterised by both extrusive volcanism (volcanoes, flows, volcanic build-ups) and the intrusion of sills, dykes and deeper igneous bodies (Schofield & Totterdell, 2008).

PETROLEUM POTENTIAL OF THE BIGHT BASIN

Petroleum systems model

Prior to the drilling of Gnarlyknots-1A in 2003, most exploration drilling in the Bight Basin was focused around the inboard margin of the Ceduna Sub-basin or in the half-graben systems of the Eyre and Duntroon sub-basins (Fig. 2.8). Seismic and sequence stratigraphic interpretation (e.g. Totterdell et al., 2000), as well as biostratigraphic and sedimentological studies (e.g. Hill, 1991; Smith and Donaldson 1995; Morgan 1999), indicate that most wells penetrated the proximal parts of the Early–Late Cretaceous depositional systems. Therefore, organic geochemical data from these wells only provide information about the source rock potential of these proximal facies.

The sequence stratigraphic model for the basin described above was based on the interpretation of seismic data, and an understanding of the tectonic and palaeogeographic evolution of the margin within the context of a global 1st-order transgressive–regressive eustatic cycle. This tectonostratigraphic framework, describing the temporal and spatial evolution of depositional systems, formed the basis for a petroleum systems model of the likely occurrence, distribution and maturity of organic-rich rocks across the basin, away from the control provided by the wells (Blevin et al., 2000; Totterdell et al., 2000; Struckmeyer et al., 2001).

Potential source rocks

The sequence stratigraphic model predicts the occurrence of several potential source rock intervals within the Bight Basin succession (Fig. 2.3). These include: lacustrine shales of the Middle Jurassic Sea Lion Supersequence and Early Cretaceous Bronze Whaler Supersequence; coaly facies of the Early Cretaceous Southern Right Supersequence; marginal marine to coastal plain mudstone and coal of the upper Bronze Whaler Supersequence; marine shales of the Albian–Cenomanian Blue Whale and Turonian–Santonian Tiger supersequences; deltaic and shallow marine shale and coal of the Cenomanian White Pointer Supersequence; and prodelta shale of the latest Santonian–Maastrichtian Hammerhead Supersequence.

The presence of high-quality, dominantly non-marine source rocks in the basin is supported by geochemical data from the marginal wells. Several good to excellent quality source rock intervals were identified in carbonaceous shales, coals and oil shales deposited in a variety of lacustrine,

deltaic and marginal marine environments in these proximal settings (Struckmeyer et al., 2001; Boreham et al., 2001). In addition, geochemical data provided evidence of a breached hydrocarbon accumulation at Jerboa-1 in the Eyre Sub-basin, most likely sourced from lacustrine facies within the adjacent Middle–Late Jurassic half graben (Ruble et al., 2001).

The distal parts of the depositional system had not been sampled by drilling, so the presence of high quality marine source rocks in the basin could only be theorised (Blevin et al., 2000). The 1st order transgressive–regressive cycle (Fig. 2.3) reached its transgressive maximum in the mid-Cretaceous just prior to the commencement of seafloor spreading in the central Bight Basin. Therefore, an increasing marine influence from the Aptian to the eustatic sea-level peak in the late Albian–mid-Turonian, was likely to have led to a basinward improvement in source rock quality for the uppermost Bronze Whaler, Blue Whale, White Pointer and Tiger supersequences. Source rock quality may also have been enhanced by the palaeogeography of the margin. By the mid-Cretaceous, open ocean lay to the west and a narrow, possibly restricted, seaway would have existed along the southern margin, at least as far east as the western Otway Basin. Accelerated subsidence prior to the commencement of seafloor spreading led to increased marine accommodation in the Bight Basin, with an enhanced potential for the deposition and accumulation of organic-rich rocks.

Another factor potentially influencing source rock quality was that deposition during the mid–Late Cretaceous coincided with several global marine organic carbon burial events or Oceanic Anoxic Events (OAE) (Schlanger and Jenkyns 1976; Jenkyns 1980; Schlanger et al., 1987; Arthur et al., 1987). Elevated primary productivity during these periods is generally credited with causing an increased flux of planktonic material to the seafloor and creating oxygen-poor conditions in bottom waters, both factors favouring the preservation of organic matter (Kuypers et al., 2002). The most significant Oceanic Anoxic Event occurred during the late Cenomanian–early Turonian (OAE 2; Schlanger et al., 1987). Evidence for oceanic anoxic events in the Jurassic and Cretaceous is recorded in deep and shallow marine carbonates, marine organic matter, and terrestrial organic matter and further, each event has been successfully correlated between globally distributed and facies-independent sections. Pelagic intervals deposited during these events are characterised by a range of factors, notably the presence of elevated organic-carbon levels (black-shale deposits; e.g. Jenkyns and Clayton 1986), and facies changes suggestive of eustatic sea-level rise (e.g. Hallam 1981, 1992; Haq et al., 1988; Hesselbo and Jenkyns 1998).

Most information regarding these short-lived but widespread periods of enhanced deposition of marine organic-rich shales comes from locations in the Northern Hemisphere, particularly Europe, Africa and North America. OAE2 has not previously been recognised on the Australian southern margin. However, recent Ocean Drilling Project drilling on the Kerguelen Plateau sampled organic-rich sediments of Cenomanian-Turonian age that have been interpreted as representing OAE2 (Mohr et al., 2002; Meyers et al., 2007). Furthermore, analysis of the benthic foraminiferal assemblages associated with these rocks has revealed a palaeoceanographic change during the Cenomanian–Turonian that reflects the existence of open oceanic gateways and trans-hemispheric global circulation (Holbourn and Kuhnt 2002).

Exploration history

The eastern part of the Bight Basin is potentially one of the most prospective deepwater frontier basins in offshore Australia. From the 1960s to late 1990s, only 9 exploration wells were drilled (Fig. 2.8), six of which are located in the Duntroon Sub-basin. All wells were drilled within relatively thin successions on the margins of the basin and none encountered significant hydrocarbons. The majority of wells in the region are considered to have been invalid tests (Messent 1998). During the most recent phase of exploration, Woodside Energy and its joint venture partners were awarded three large permits in the Ceduna Sub-basin in 2000; the permits

were relinquished in 2007. Data acquisition included 15,636 km of 2D seismic data (Flinders 2D Marine Seismic Survey; Bruins et al., 2001) and the 1250 km^2 Trim 3D seismic survey.

Hydrocarbon charge was perceived as a major exploration risk in the Ceduna Sub-basin, despite the failure of most wells to test a valid trap (Messent 1998; Somerville 2001). Potential petroleum systems occur in Middle Jurassic through to Late Cretaceous strata. The most prospective petroleum systems are inferred to be associated with thick mid to Late Cretaceous deltaic and marine sediments, which provide reservoirs, seals and potential oil-prone source rocks at several stratigraphic levels, together with a wide range of structural and stratigraphic plays (Blevin et al., 2000; Totterdell et al., 2000, Struckmeyer et al., 2001). A key uncertainty for explorers in the Ceduna Sub-basin is how far outboard the source rocks and cross-fault seals are suitably well developed for mid-Late Cretaceous plays to contain large volumes of oil. Well data from the northeastern sub-basin margin show that Cretaceous strata contain a range of proximal fluvio-lacustrine, deltaic and marine source rocks with good to excellent potential for generating oil and gas from Type II and III organic matter (Blevin et al., 2000; Totterdell et al., 2000; Somerville 2001; Struckmeyer et al., 2001; Boreham et al., 2001). Indications that an oil-prone marine source rock is present in the Ceduna Sub-basin come from hydrocarbon seep studies using SAR and ALF data (Struckmeyer et al., 2002), and geochemical studies of asphaltite strandings along the southern margin (Edwards et al., 1998; Boreham et al., 2001).

In April 2003, Woodside Petroleum and its partners drilled Gnarlyknots-1A aiming to test the petroleum systems within more distal Late Cretaceous depositional systems of the Ceduna Sub-basin (Tapley et al., 2005). The well aimed to penetrate four stratigraphic horizons with fault-dependant closure within a low-side fault block trap. Adverse weather conditions resulted in the abandonment of the well at the top of the Tiger Supersequence, some 1500 m above the planned completion depth, leaving several key targets untested. Although Gnarlyknots-1A failed to recover hydrocarbons, several encouraging indications were observed, including: a methane-depleted wet gas to gas-condensate response in the primary objective (observed using Fluid Inclusion Stratigraphy) consistent with a highly mature palaeo-charge; strong proximity to pay indicators within local shale seals below 4600 m, which may indicate proximity to an oil column below the TD of the well; and indications that thermogenic gas has migrated into the structure from mud gas isotope analysis in the primary objective. The failure of Gnarlyknots-1A to discover a hydrocarbon accumulation was considered to be primarily due to the absence of valid cross-fault seals within the sand-prone coastal plain deposits that were penetrated (Tapley et al., 2005).

3. Bight Basin Geological Sampling and Seepage Survey

C. Mitchell & J. Totterdell

INTRODUCTION

Geoscience Australia's Bight Basin Geological Sampling and Seepage Survey (Fig. 1.1) was designed to address the question of hydrocarbon charge in the Bight Basin by targeting potential source rock facies from the pre-Campanian section for dredging, and investigating sites of potential natural hydrocarbon seepage.

The survey's main goal was to obtain geological samples that could provide direct evidence regarding the nature and distribution of potential source rock intervals in the Bight Basin. As outlined above, Geoscience Australia's previous basin analysis studies had identified a series of potential source rock intervals at different stratigraphic levels, including marine or marine-influenced sediments whose source rock character was predicted to improve farther basinward. The most prospective section was considered to be the Albian–Santonian Blue Whale, White Pointer and Tiger supersequences.

A study of all available seismic data indicated that these rocks cropped out on the seafloor at the seaward edge of the Eyre Terrace where canyon formation, slumping and faulting have exposed the mid-Cretaceous section. This area (Area 5; Fig. 1.1) was the prime dredging target for the survey. The seismic study also identified a range of sites where, if other geological conditions were met, seepage of hydrocarbons was most likely to occur. These included areas where recent reactivation of deep-seated faults was evident at the seafloor, basin margin areas where seal facies thin or deteriorate sufficiently to allow seal failure, and areas high-graded by the presence of slicks detected by SAR.

Nine areas of interest were identified for surveying and sampling, using swath bathymetry, side-scan sonar, 12 and 120 kHz echo-sounder, 3.5 kHz sub-bottom profiler, gravity cores and dredges. Detailed illustration of the sampling sites and sampling details are presented in Appendix 1.

Conducted from 22 February to 17 March 2007 using the Marine National Facility vessel RV *Southern Surveyor* (survey SS01/2007), the survey gathered geophysical data and geological samples via deep-sea dredging and gravity coring. Good sea and weather conditions enabled sampling to be completed in all nine target areas (Fig. 1.1). Thirty-seven dredge samples, 69 gravity cores and 15 grab samples were collected, as well as approximately 8825 km^2 of multibeam swath bathymetry data and 2400 km of sub-bottom profiler data. The SS01/2007 Voyage Plan and Voyage Summary documents are available on the CSIRO Marine National Facility web site at http://www.marine.csiro.au/nationalfacility/voyagedocs/2007/index.htm

Following the survey, the samples were catalogued, described and sub-sampled for a range of lithological, geochemical and biostratigraphic analyses. The results of these analyses are documented in the following sections of this report and the accompanying appendices.

SCIENTIFIC OBJECTIVES

The main survey objectives were to:

- Increase our understanding of the geological evolution and petroleum potential of the Bight Basin, primarily through:
  - acquiring geological samples from the pre-Campanian section of the basin in order to assess their petroleum source rock potential; and

- investigating, identifying, characterising and sampling sites of potential natural hydrocarbon seepage.

Prior to the survey, knowledge of the hydrocarbon source potential of the basin was based on samples from wells drilled in proximal areas of the basin and geological models of the basin fill derived from seismic interpretation. This survey aimed to sample the distal facies of potential source intervals of Albian-Santonian age at locations on the seaward edges of the Ceduna and Eyre Terraces. The survey also aimed to investigate potential natural hydrocarbon seepage at sites across the Ceduna Sub-basin, which could provide evidence for the presence of active petroleum systems.

VOYAGE OBJECTIVES

Sites of geological significance, particularly areas where potential source rock intervals were interpreted to outcrop at the seabed and locations of possible hydrocarbon seepage, were identified from existing seismic, seabed sampling, swath and interpolated bathymetry and SAR data. These sites were divided into nine areas of interest for surveying and sampling (Fig. 1.1; Appendix 1).

Area 1. Continental shelf-break, northeastern margin of the Ceduna Sub-basin: Investigate and sample potential seepage sites above the pinch-out edge of Cretaceous sealing units and basin-margin fault system;

Area 2. Northern and central Ceduna Sub-basin: Investigate and sample potential seepage and palaeo-seepage sites associated with SAR slicks, and above possible shallow gas concentrations;

Area 3. Northern margin of the Ceduna Sub-basin: Investigate and sample potential seepage sites above reactivated basin-margin faults;

Area 4. Cenozoic volcanic build-ups in the northern Ceduna Sub-basin: sample for age-dating;

Area 5. Seaward edge of the Eyre Terrace: dredge sampling of Albian-Santonian age rocks of the western Ceduna Sub-basin exposed by faulting and erosion in canyons;

Area 6. Lower continental slope above the northern Ceduna-Recherche sub-basin transition: Sampling of exposed interpreted Turonian-Santonian age rocks, and mounded seabed features overlying Albian-Cenomanian mud diapirs and toe-thrusts;

Area 7. Seaward edge of the central Ceduna Terrace: Investigate and sample potential seepage sites associated with Late Cretaceous growth faults extending to the seafloor;

Area 8. Lower continental slope above the central Ceduna-Recherche sub-basin transition: Sampling of exposed interpreted Santonian-Maastrichtian age rocks, and potential seepage sites above Late Cretaceous shale ridges;

Area 9. Southern Ceduna Sub-basin: Investigate and sample potential seepage targets where Late Cretaceous faults are exposed by canyons.

Priorities: The highest priority sampling sites were those in Area 5 on the margin of the Eyre Terrace (Figure 1.1), where faulting, slumping and erosion in canyons provide the best access to rocks of Albian-Santonian age that may contain potential source rocks. Other high priority sampling sites were Areas 2, 6 and 3, which were considered to be the most likely sites in the basin for hydrocarbon seepage. The lesser priority areas were 1, 7, 8, and 9, in that order.

The key survey equipment and tools to be utilised were multibeam swath bathymetry, side-scan sonar, 12 & 120 kHz echo-sounder, 3.5 kHz sub-bottom profiler, gravity cores, and dredges. The operational strategy for the survey was to identify and prioritise potential targets using the depth-appropriate geophysical tools and the underwater video camera, followed by sampling. The success of the survey was dependent on fully operational dredging, gravity coring, multibeam swath and sub-bottom profiler systems.

VOYAGE TRACK

Figure 1.1 shows the SS01/2007 voyage track starting at Port Lincoln, and intersecting the nine geologically significant sampling areas in a counter-clockwise direction. The linear deviation from Area 3, to the southwest, occurred when winch maintenance had to be carried out in deep water. Upon completion of the repairs the survey returned to Area 3 and continued on the planned course, with no further significant deviations. Throughout the survey the weather remained fine with moderate to calm seas except for a few rougher days later in the survey which did not hinder progress. Details of the day-to-day operations of the survey are presented in Appendix 1 (Sampling sites and survey leader's log).

PHYSICAL SAMPLING AND EQUIPMENT

Sampling equipment and methods used on this survey were similar to those documented by Jones et al. (2007), from which the following section is modified.

Seabed sediment samples

Smith-McIntyre Grab

Unconsolidated seabed surface sediments were collected using a Smith-McIntyre sediment grab deployed from the starboard side A-frame winch. The grab is mounted on a sturdy, weighted, steel frame, with springs to force the two-jaw bucket into the sediment substrate when released. Tripping pads, positioned below the square-based frame on which the bucket is suspended, make first contact with the seabed and are pushed upward to release two latches holding the spring-loaded bucket jaws. Retrieving the deployment wire exerts tension on cables connected to the end of each bucket-jaw arm causing the jaws to pivot tightly shut. The grab was deployed at mid-ships on the starboard side to minimise excessive movement from pitch during sampling procedure.

Rock dredge

The rock dredge, consisting of a 0.5 x 1 m rectangular metal collar to which a 1 x 1 m chain bag was attached, was used to sample lithified and cemented sediments on the seabed. A closed and a 10 mm sieved pipe dredge were attached to the bottom of the dredge to collect smaller samples. The dredge was operated using the port trawling winch, and was lowered to the seabed at the start of the dredge, the vessel laying out cable as it transited beyond the finish of the dredge. At this point the vessel held position and then winched the dredge along the seabed for approximately 500–1000 m before retrieval.

Sediment core samples

Sediment cores were collected using Geoscience Australia's gravity corer, which has a 1 tonne core head and a 6 m barrel attached. A core cutter and catcher at the bottom of the barrel ensured collection of sample while a 6 m PVC core barrel liner housed the sample during the sampling and retrieval process. Penetration generally varied between 2 to 6 m with best results in more unconsolidated and finer sediments.

Video camera

Only a single camera station was recorded during the survey. Video footage of the seabed was collected to provide a visual recording of the substrate, morphology, potential seepage indicators,

and benthic biota. The digital video camera was housed within Geoscience Australia's Deep Underwater Camera System DUC 2, in a watertight housing attached to a steel frame.

Underwater lighting was provided by 4 quartz halogen lamps, two lamps of 100 watts and 2 of either 150 watts or 250 watts. The lamps were mounted on the four corners of the camera housing frame, above and below the camera pressure housing. The footage was recorded on a Sony Digital Camcorder, Model DSR-PDX10P, using Mini DV digital video cassettes, and was also fed to VHS tape and a monitor on-board the vessel. This "live" video feed enabled the winch control operator to raise and lower the camera in order to image a representative area of the seabed and specific features while the vessel drifted beam-on to the swell. The video data was transcribed from the DV mini cassettes using Ulead Media Studio Pro 7 software version or Roxio Easy Media Creator 7 Basic DVD Edition.

Sampling and handling during survey

Bulk sediment samples

Sediment samples were collected from the Smith-McIntyre Grab for geochemical analysis. Surface water were syphoned off prior to sampling. Between 0.5–1 kg of sediment was placed in clear plastic snap-lock bags and given a Munsell colour and grain-size description. Samples were double bagged and labelled, and an aluminium label tag also inserted in the outer bag.

Geochemical samples were snap-frozen at -20°C, and sedimentological samples were stored at 4°C.

Geochemical cores

A total of 67 gravity cores were taken for geochemical analysis. These cores were initially cut into 1 m sections on deck, which were then immediately sub-sampled in the vessel's laboratory as per the scheme shown in Figure 3.1. Each core was sampled differently depending on the total length retrieved. For the upper parts of the core, only the lower 10 cm of each 1 m section, as well as the uppermost 10 cm of the core, were sampled for biomarker analysis (but not for headspace gas analysis).

Since samples were collected starting from the base of each core, and the total recovered length varied, the sub-seabed depth of samples varies from core to core (Fig. 3.1). The uppermost un-sampled portion of each core remaining after headspace gas and biomarker analysis was retained as a sedimentary sample.

During sampling, care was taken to remove mud that had been in contact with the PVC liner, to avoid organic contamination, and only the interior portion of the core was collected for geochemical analyses. Samples collected for high molecular weight biomarker analysis were double bagged within plastic zip lock bags, labelled, and snap frozen at -20°C.

Two methods for headspace gas collection/sampling were utilised during the survey. The lower 20 cm of each 1 m core section was extruded from the PVC liner by pushing a metal cutting device (core divider) up through a 20 cm section of core liner. The core divider has two intersecting metal plates that divided the extruded core into quarters (Fig. 3.2). After extrusion, the exterior of the core was trimmed with a metal spatula to remove mud that had been in contact with the core liner. Each quarter was then removed from the cutter and placed in either a 500 ml tin (duplicate samples; tins provided by TDI-Brooks) or a plastic disrupter canister (duplicate samples; disrupters provided by EGI).

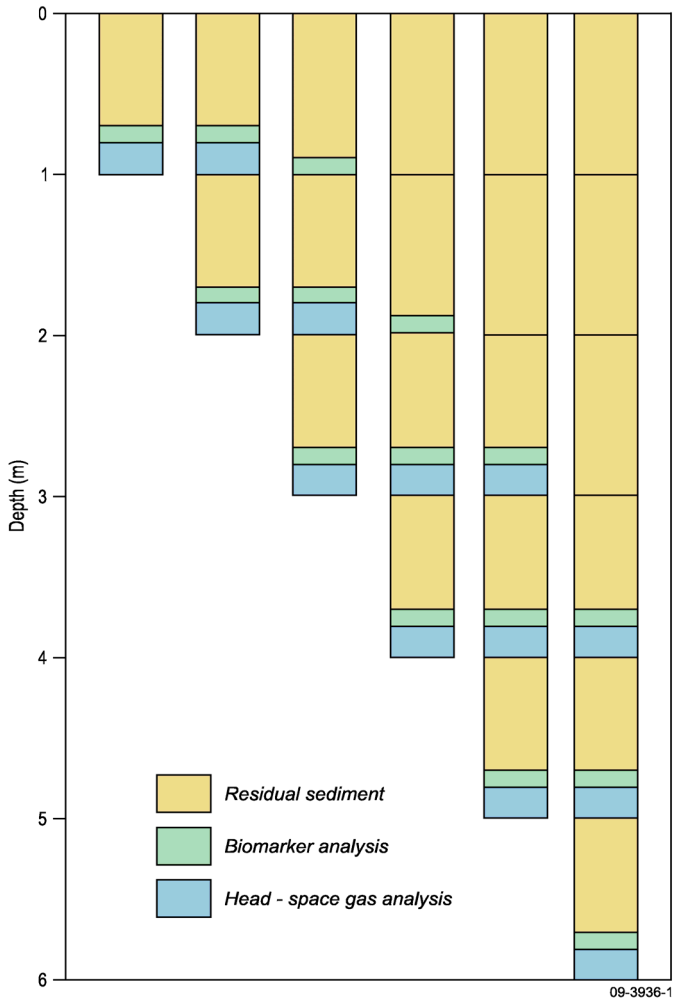

Figure 3.1. *Geochemical core sampling system for varying lengths of core.*

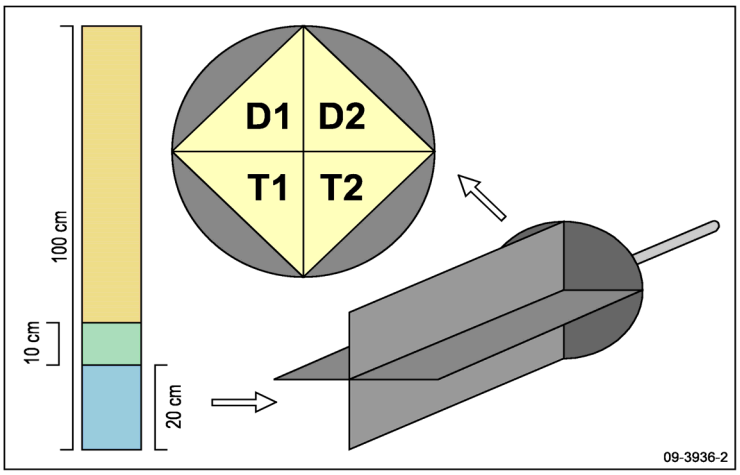

Figure 3.2. *Illustration of samples taken from 1 m gravity core sections. The lower 20 cm of the core section was quartered and placed into tins and disrupters for headspace gas analysis. The adjacent 10 cm was sampled for biomarker analysis. T – Tins; D - Disrupters.*

Sampling Using Tins and Disrupters

The 500 ml metal paint tins used for the headspace gas analysis were provided by TDI-Brooks and are the same as used during their own surface geochemical sampling surveys. The plastic disrupters were supplied by EGI to compare with the more traditional tin containers for headspace gas analysis. One quarter of a 20 cm section of core filled a tin to around one-third full. This was the volume of mud required for headspace gas analysis. Once the mud was placed inside a tin, three tablespoons of salt were added to the disrupters but not the tins. A further one-third of the volume (150 mL, using a graduated measuring cylinder) was then filled with filtered sea water which had been poisoned with sodium azide and degassed by bubbling with chemical-grade nitrogen. The headspace of the tin was then flushed with nitrogen and the lid of the tin was sealed. Once sealed, the tin was shaken and placed upside down in the -20°C blast freezer.

Dredge samples

The contents of each dredge were sorted into buckets on deck and representative rock samples described and stored at 4°C. In some cases samples were cut and trimmed using a small, on-board, rock saw before storage.

Post-survey laboratory analyses

Seepage study geochemical analyses

Samples collected for headspace gas analysis were transported frozen and analysed by TDI-Brooks, College Station, Texas, USA. Concentration data (ppm) was reported for C_1-C_5 hydrocarbons and CO_2 for one set of replicate tins. The second set of tins was retained at Geoscience Australia at -20°C to provide back-up in case of shipping problems or sample loss.

Headspace gas analysis

The can is thawed approximately 24 hours prior to analysis, heated to 40°C for approximately 4 hours, and shaken vigorously using a conventional paint shaker. Ten (10) ml of water is syringed into the can headspace using silicone sealant septa. Ten (10) ml of headspace gas is collected using a syringe and injected in the gas chromatogram for compositional analysis. The mud to headspace ratio for volume calculations is estimated using the weight and assumed density. The parts per million values are calculated using partition coefficients which represents a fraction of the total gas in sample container after equilibration. Bernard (1978) calculated approximately 85% to 95% of the gas is removed during each removal and re-equilibration as part of his doctoral thesis. The TDI-Brooks headspace gas composition data is reported as ppm by volume (mole %).

High-molecular weight hydrocarbon analysis

Samples collected and frozen for high molecular weight biomarker analysis (20 cm core sections and grab samples) were analysed in the organic geochemistry laboratory at Geoscience Australia, using protocols outlined in the *University of Utah* study *Surface Geochemistry Calibration Study* (Abrams et al., 2004).

The sampling and analytical techniques used to assess the dredge samples for their source rock potential are documented in Chapter 6.

GEOPHYSICAL EQUIPMENT

Survey SS01/2007 utilised geophysical sampling equipment and methods also similar to those documented by Jones et al. (2007) to delineate bathymetry, identify seafloor and near-surface features, and identify water column features. These are swath (multibeam) sonar, sub-bottom profiler, side-scan sonar and echo-sounders. The acquisition and processing parameters are outlined below.

Bathymetry: Swath (multibeam) sonar

Swath bathymetric data were collected using a Kongsberg Simrad EM 300 multibeam echo-sounder mounted in a gondola beneath the vessel hull. Good performance from the multibeam system and fair-to-good sea-state allowed for optimal angular coverage and data quality for the majority of the survey. The nominal sonar frequency is 30 kHz with 135 beams, each with a 1° beam width, giving a total angular coverage of 135°. The system has roll and pitch stabilization, with optional yaw compensation; utilised in cross winds or currents.

In water depths less than 100 m, a swath width of 200–500 m was achieved. In water depths great than 1000 m, the swath width was about 2000–3000 m, and in water depths greater that 4000 m swath widths reduced to about 2000 m due to limited return from the outermost beams. The processed swath grid provides a 10 m spatial resolution and approximate 1 m vertical resolution of bathymetry, and a measure of seafloor reflection intensity (i.e. backscatter).

Sub-bottom profiler

Shallow seismic reflections data were collected using a Topas PS 18 Parametric Sub-bottom Profiler fitted to the gondola below the hull. The Topas PS 18 system is a narrow beam, high resolution sub-bottom profiler capable of recording substrate reflections of greater than 150 m in optimal conditions. Sea-state, water depth, substrate character and the transmitted signature all influence the return signature. The survey observed good substrate penetrations up to ~80 m. These were achieved in water depths of ~2000 m where thick sediment occurred on the outer shelf.

Fault scarps were readily observed in the sub-bottom profiler data and targets were routinely picked on-screen during acquisition. Additionally, sub-bottom profiler date were saved in the RAW Topas format; processed data were output in SEG-Y format. File sizes were limited to ~100 Mb.

Side scan sonar

Side scan sonar data were collected in Area 1 in order to detect evidence of natural hydrocarbon seepage. The equipment and methods utilised are the same as those documented by Jones et al. (2007).

4. Dredge Sampling Results

A. Stacey & C. Mitchell

DREDGE SAMPLE DESCRIPTIONS

A total of 37 dredge hauls were undertaken during the Bight Basin survey (Table 1). Most dredges contained a range of rock types, although mudrocks were the dominant lithotype. In addition, lithified material was also obtained from the base of several gravity cores. The following section describes the dredged rocks. Detailed descriptions of the dredge and core catcher samples, thin section descriptions and the dredge sample catalogue are presented in Appendix 2. The gravity cores are described in the Hydrocarbon Seepage Survey Results section.

Igneous rocks

Anorthosite

Igneous rocks comprised a very small component of the rocks returned by dredge sampling during the Bight Survey. The samples collected were cobble sized and elongate with rounded to sub-rounded exteriors. Several thin sections were made of these rocks to aid their identification. The samples were phaneritic and granular, dominated by up to 40 mm euhedral plagioclase crystals and minor K-feldspar with interstitial quartz and rare amphibole and apatite. Secondary minerals include magnetite, epidote (after feldspar) and chlorite. The plagioclase feldspars commonly exhibit undulatory extinction and deuteric alteration along fractures.

Modern sediments

Pelagic ooze

Pelagic ooze was commonly recovered by dredging and in gravity cores and therefore it is thought to be widespread across the survey area. Ooze samples were highly calcareous, with abundant foraminifera tests. The samples were generally beige to pale brown in colour, mostly clay with silt to fine sand-sized grains scattered throughout. Sponge spicules were present in some samples. The samples were unlithified, sloppy to moderately dewatered and often plastic. Dredge 60DR37 recovered clay rich, tan-coloured ooze with only scattered foraminifera tests. The lack of foraminifera may be because this sample was taken from the base of the continental slope (4580 m) and probably close to the Carbonate Compensation Depth (CCD) for this region.

Chemical rocks

Phosphates

Phosphatic rocks were routinely recovered in dredges from the edge of the Eyre Terrace (Dredges 17DR07–34DR27). The phosphate nodules were up to 10 cm wide and 30 cm long (a 0.5 m fragment was retrieved by 25DR17) and varied in shape from well rounded spheres and lozenges to a variety of irregular forms (Figs 4.1 & 4.2). The rocks were well-lithified with common radiating and concentric fractures often filled by calcite, and most have prominent iron oxide weathering rinds with varying degrees of manganese encrustation (Figs 4.1 & 4.2).

Fresh surfaces were grey/brown, grey/green and grey in colour and occasionally mottled indicating bioturbation of the protolith prior to being phosphatised (Figs 4.1 & 4.2). In many samples remnant textures, clasts and sorting can be identified, indicating their protoliths ranged from mudrocks to fine- and coarse-grained sandstone. Sand-sized glauconite pellets were common and similarly-sized quartz grains were identified in some samples. Many samples contained very

fine, very dark green to black carbonaceous or glauconitic grains, which were either disseminated or confined to zone or occurred as stringers. One sample (21DR13D) has a 3 cm core of such material (Fig. 4.3). Some samples contain very well preserved casts and moulds of several Late Cretaceous species of the bivalve *Inoceramus* (Fig. 4.4; Appendix 3.3).

Pyrite

A single pyrite nodule was recovered in dredge 31DR24 at the western edge of the Ceduna Sub-basin. The tabular, rounded nodule has dimensions of 40 x 40 x15 mm and comprises medium to coarse sand-sized, euhedral pyrite crystals and crystal clusters set in a very dark grey/brown mudstone matrix (Fig. 4.5).

Calcareous rocks

Calcareous rocks were very rare and only recovered from three sites (32DR25, 52DR35 & 53DR36) only in areas 5 and 7 of the survey.

Limestone

Argillaceous limestone was sampled by dredges 52DR35 (Fig. 4.6), 16DR06 and 21DR13. The rocks were well lithified, massive and very fine-grained. Fresh surfaces were very dark grey in colour. Sample 52DR35 contains numerous, small (<1 mm), black to brown flattened grains (?carbonaceous) with a local preferred orientation and ?rare pyrite. The sample margins were generally weathered to a soft clayey rind many mm thick and were often encrusted in botryoidal dark brown (?iron stained) calcite, well burrowed and manganese-encrusted. Some samples have weak lamination with parallel, often syntaxial, calcite veins. Samples from dredges 16DR06 and 21DR13 were thin-sectioned and further descriptions can be found in Appendix 2.4.

Oolitic wackestone and packstone

Brecciated phosphate-rich oolitic wackestone and packstone were identified in dredges 15DR03 and 18DR08. The rocks were generally pale green/yellow in colour and contain often angular phosphatised ooid clasts in carbonate cement. These samples were thin-sectioned and further descriptions can be found in Appendix 2.4.

Chalk

Samples of chalk were identified at all three sites where calcareous rocks were recovered. The samples were weathered, ranging in colour from pure white and grey/white to cream (Fig 4.7). They were very fine-grained, generally soft and powdery, one sample has a weak horizontal lamination. Most samples contain burrows and were manganese encrusted.

Siliciclastic rocks

Mudrocks

Mudstone

A large variety of mudstones were dredged from throughout the survey area. The rocks range in colour from light grey through brown, olive, and green to blue/black for the carbonaceous samples. They contain clasts of quartz, fine mica and very rare glauconite pellets. Sponge spicules, foram tests and shell material were common in the more calcareous samples, while the

carbonaceous samples were rich in plant fragments. The samples were partially lithified to friable, weakly laminated and poorly to moderately sorted, with a few well sorted examples (Fig. 4.8). Graded bedding was observed in sample 27DR19 B3. Sandy mudstones were common and comprise fine- to medium-grained sand clasts in a mud matrix (Figs. 4.9 & 4.10). They were partially lithified and poorly sorted with weak laminations or weak, irregular beds. Burrows were common in all of the samples; fossil bivalves and ichnofossils were rare. Some samples have weathered to clay at their margins, and manganese and iron oxide staining were common on the weathered surfaces.

Siltstone

Siltstones were rare and were only obtained from the northwestern margin of the Ceduna Sub-basin (Area 5). The samples were generally micaceous and varied in colour from blue/black to green/grey and brown (Fig. 4.11). The rocks were lithified, becoming friable towards their weathered margins, and commonly well-laminated. Samples were burrowed to varying degrees; several have none, while one sample has abundant burrows disrupting bedding. Bivalve fossils were relatively common and abundant in some samples (Fig. 4.12). Iron oxide staining was common on weathered surfaces (Fig. 4.11).

Clays and claystones

Clays and claystones were the most common and widespread lithology recovered by dredging during the Bight Survey.

Clay:
The clays sampled were generally grey/brown to olive brown in colour (occasionally mottled), very fine-grained and massive to weakly laminated (Fig. 4.13). The clays were soft, plastic and often sticky; some samples were dewatered (drier), but still very malleable. Many samples appear to have been contorted and mixed with modern pelagic sediments during dredging. Several samples contain rare silt sized grains of quartz and mica, whilst others were distinctly silty with rare sand-sized quartz and mica. Sample B from dredge 20DR12 contains angular carbonaceous fragments ranging from 0.5 – 16 mm in size, and remnant fossil plant fragments. Sample 52DR35 E contains zones of angular, fine-grained ferruginous material. A number of samples display internally burrowing.

Claystone:
A diverse range of claystones were retrieved from across the survey area. The rocks were dark, ranging in colour from olive, grey/green, grey/brown and blue/grey to black. The samples were well-sorted with rare silt and sand-sized grains (Fig. 4.14). Two samples (21DR13 B & 22DR14 D) from the NW edge of the Ceduna Sub-basin were less well-sorted, containing stringers and lenses of fine-grained sand. The rocks generally comprise quartz and disseminated fine mica. Plant and carbonaceous fragments and zones of amorphous organic material were common, but not observed in all of the samples. The rocks were partially lithified to friable, weakly laminated to massive and rarely bioturbated. Many samples were weathered to dark brown clay at their margins. Iron oxide staining and manganese encrusting the exterior surfaces was common. Weathered surfaces were commonly burrowed and fossils rare.

Silty claystone was recovered by dredges 21DR13 and 60DR37. The rocks from dredge 21 were organic-rich and high in silt to sand-sized clasts of mica and rare quartz. Sample A2 contains several lenses of very fine-grained sand. Sandy claystone was recovered by dredge 21DR13 and contains lenses and stringers of alternating light and dark, fine sand.

Interbedded sedimentary rocks

Interbedded rocks were obtained from one area, on the north-western margin of the Ceduna Sub-basin. The rocks recovered by dredge 22DR14 comprise ferruginous sandstone, irregularly to chaotically interbedded with dark brown claystone (Fig. 4.15). The sandstone consists of well sorted and rounded, iron oxide-coated grains of quartz, ?feldspar and mica. The rocks were partially lithified and often friable, weathering to clay. The weathered surface was iron oxide-stained with minor manganese encrustation.

Rocks with thin interbeds of fine sandstone and mudstone were recovered by dredge 26DR18. The rocks were well lithified; containing quartz, mica, organic material, iron oxide coated bivalve fragments and sand-filled burrows.

Sandstone

An assortment of sandstones were recovered mainly along the north-western margin of the Ceduna Sub-basin. The rocks vary in colour from yellow, orange and brown to green and grey (Fig. 4.16). The grainsize generally fines towards the east varying from fine to medium-grained sand, with a coarse pebbly sandstone retrieved by dredge 36DR29. In general, the samples were partially lithified and friable and while many samples were massive, weak laminations and layering were common. Most of the samples exhibit some degree of weathering, with alteration to clay, internal iron oxide staining, iron oxide coated grains and loss of coherence all commonly observed. The rocks very commonly comprise quartz, fine mica (often disseminated) and clay. Glauconite is common and its occurrence becomes more frequent towards the west. Feldspar is less common, lithic clasts (mudstone intraclasts and igneous material) and carbonaceous material were rare and calcareous material is very rare. The matrix material is commonly clay or silty clay and both matrix and clast supported fabrics were observed. Several samples contain bands/layers of muddy or carbonaceous material. Fossils were rare; however, several samples contain burrows, while mottling resulting from bioturbation is not uncommon. Manganese deposits and iron oxide staining on external surfaces were rarely observed.

Conglomerate

Conglomeratic rocks were recovered from the west of the survey (Area 5). The rocks were matrix-supported with small pebble to cobble-sized, generally rounded to well rounded clasts of quartz, feldspar, rare ?chert and many clasts of altered igneous/metamorphic rock (Fig. 4.17). Bimodal sorting is common. The matrix is more varied, including granular ferruginous shelly material, poorly sorted granular to coarse sandstones and well sorted coarse sandstone. All the samples were weathered, iron-stained and manganese-encrusted and often friable. (Fig.4.18).

Table 4.1. *Dredge haul summary.*

Survey Area	Dredge	Water Depth (m)	Dredge Location		Main Rock Types	Recovery Weight Kg	Date Acquired
			Dredge Start	Dredge Finish			
4	13DR01	1436 - 1360	-33.846136 129.445826	-33.842276 129.440381	Light grey, siliceous mudstone, fine sandstone, calcareous ooze.	150	28-Feb-07
4	14DR02	1315 - 1314	-33.839585 129.445630	-33.832804 129.445599	Calcareous mudstone.	150	01-Mar-07
4	15DR03	2270 - 1902	-33.917623 129.027809	-33.923003 129.022515	Brecciated phosphatic-rich oolitic wackestone/packstone, calcareous ooze.	25	01-Mar-07
4	15DR04	n/a	n/a	n/a	No recovery. Site Abandoned	0	01-Mar-07
4	15DR05	n/a	n/a	n/a	No recovery. Site Abandoned	0	01-Mar-07
5	16DR06	2184 - 1925	-33.645589 128.631247	-33.644779 128.616569	Argillaceous Limestone, claystone, calcareous ooze.	100	01-Mar-07
4	17DR07	2173 - 1950	-33.640999 128.634401	-33.630583 128.622102	Phosphate nodule, mudstone, claystone, mudstone, calcareous ooze.	40	01-Mar-07
4	18DR08	2336 - 2089	-33.729919 128.867760	-33.729263 128.859945	Brecciated phosphatic-rich oolitic wackestone/packstone, calcareous ooze.	7	03-Mar-07
5	19DR09	2144 – 1855	-33.708392 128.434280	-33.713046 128.420458	Clay.	5	03-Mar-07
5	19DR10	2150 - 1848	-33.708825 128.434626	-33.716160 128.413877	Phosphate nodule, claystone, calcareous ooze.	60	03-Mar-07
5	20DR11	2144 - 1989	-33.728600 128.443144	-33.733845 128.434555	Claystone, calcareous ooze.	2	03-Mar-07
5	21DR12	2152 - 1989	-33.729430 128.441565	-33.736271 128.431688	Phosphate nodule, clay, calcareous ooze.	50	03-Mar-07
5	21DR13	2198 - 2066	-33.702977 128.438810	-33.686808 128.443084	Sandy claystone, silty claystone, mudstone, fine sandstone, phosphate nodule, argillaceous limestone, calcareous ooze.	60	04-Mar-07
5	22DR14	2011 - 1612	-33.833457 127.842223	-33.811243 127.839496	Phosphate nodule, arkosic sandstone, claystone, interbedded sandstone and claystone, fine sandstone, calcareous ooze.	180	04-Mar-07
5	23DR15	2059 - 1629	-33.836825 127.842223	-33.817418 127.823457	Phosphate nodule, sandy mudstone, coarse sandy mudstone, fine sandy mudstone, calcareous mudstone to fine sandy mudstone.	180	04-Mar-07
5	24DR16	3066 - 2622	-33.945075 127.894853	-33.937723 127.880340	Siltstone, phosphate.	200	05-Mar-07
5	25DR17	2611 - 2172	-33.911500 127.890000	-33.892860 127.901927	Mudstone, very fine sandstone, phosphate nodule.	200	06-Mar-07
5	26DR18	2607 - 2121	-33.891143 127.867831	-33.873618 127.845152	Interbedded mudstone and very fine sandstone, fossiliferous fine to very fine sandstone, phosphate nodule, calcareous ooze.	200	06-Mar-07
5	27DR19	1926 - 1836	-33.923288 127.589299	-33.906942 127.588616	Fine sandstone, very fine sandstone, siltstone, mudstone, calcareous ooze.	80	06-Mar-07

5	28DR20	2243 - 1951	-33.954500 127.357667	-33.948678 127.367357	Siliciclastic siltstone, silty clay, sandstone.	120	06-Mar-07
5	29DR21	2231 - 2085	-33.956320 127.360381	-33.952575 127.377480	Siliciclastic siltstone, silty clay, micaceous sandstone, ferruginous sandstone.	40	07-Mar-07
5	30DR22	2538 - 2258	-33.970415 127.362191	-33.962552 127.377168	Claystone, fossiliferous ferruginous fine sandstone, calcareous ooze.	50	07-Mar-07
5	31DR23	2672 - 2512	-33.987973 127.348050	-33.981102 127.355217	Claystone.	10	07-Mar-07
5	31DR24	2670 - 2597	-33.987224 127.349095	-33.976798 127.360586	Muddy sandstone, sandstone, claystone, phosphate nodule, pyrite nodule.	60	07-Mar-07
5	32DR25	2735 - 2495	-33.995103 127.355253	-33.983471 127.353381	Claystone, calcareous glauconitic sandstone, glauconitic sandy mudstone, chalk, phosphate nodule, glauconitic sandstone, sandstone.	120	26-Feb-07
5	33DR26	2567 - 2369	-33.980667 127.344500	-33.976067 127.350123	Claystone.	30	08-Mar-07
5	34DR27	2831 - 2620	-34.014639 127.336957	-34.005554 127.331208	Claystone, sandy mudstone, phosphate nodule.	30	08-Mar-07
5	35DR28	2179 - 1920	-34.016145 126.898876	-34.004840 126.900990	Pebble to cobble conglomerate, anorthosite, calcareous ooze.	40	08-Mar-07
5	36DR29	2089 - 1806	-34.013048 126.893382	-33.997993 126.891700	Pebble to cobble Para-conglomerate, pebble Para-conglomerate, pebbly sandstone, anorthosite, clay.	120	08-Mar-07
5	37DR30	1991 - 1756	-34.003321 126.906129	-33.994192 126.893916	Sandy-pebbly Para-conglomerate, anorthosite cobbles.	60	08-Mar-07
5	38DR31	1838 - 1643	-34.000167 126.887833	-33.984751 126.892678	Clay	20	08-Mar-07
5	39DR32	1998 - 1717	-33.978775 126.977428	-33.967385 126.975688	Claystone, clay.	15	09-Mar-07
6	40DR33	3640 - 3510	-34.378000 129.332000	-34.369875 129.347704	Claystone, glauconitic sandstone, calcareous ooze.	60	09-Mar-07
6	43DR34	3990 - 3900	-34.917108 129.794640	-34.929003 129.777351	Clay	10	12-Mar-07
7	52DR35	3068 - 2360	-35.047388 130.911308	-35.037512 130.942662	Argillaceous limestone, ferruginous sandy mudstone, claystone, chalk, calcareous ooze.	20	12-Mar-07
7	53DR36	2175 - 1926	-34.918602 131.017306	-34.917644 131.024848	Chalk, calcareous ooze.	60	13-Mar-07
8	60DR37	4580 - 4430	-35.677353 131.368062	-35.669996 131.374871	Silty claystone, clay, carbonate ooze.	20	14-Mar-07

Figure 4.1

Figure 4.2

Figure 4.3

Figure 4.4

Figures 4.1–4.4. *Phosphatic rocks recovered during the Bight Survey: 4.1) Phosphate nodules demonstrating typical morphology, weathering rind and calcite veining; 4.2) Mottling - probably due to bioturbation prior to being phosphatised; 4.3) Examples of the distribution of dark grains: a) disseminated, b) zoned (stringers circled) and c) with a circular core; 4.4) Phosphatised Inoceramus fossils.*

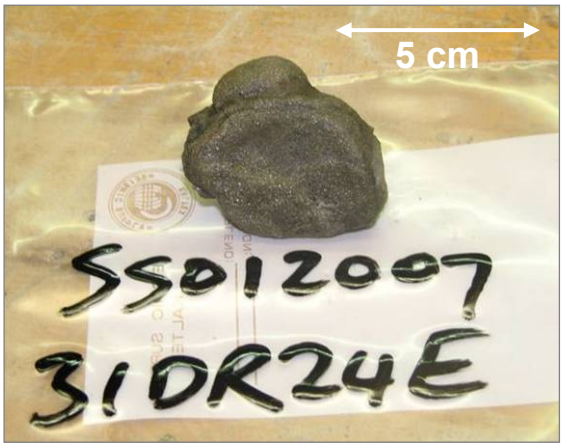

Figure 4.5. *Pyrite nodule*

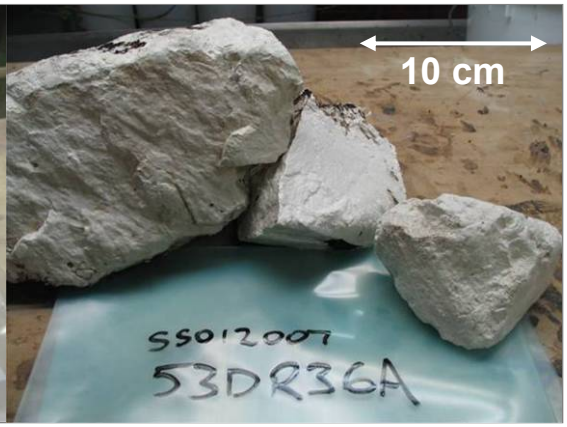

Figure 4.6 *Figure 4.7*

Figures 4.6–4.7. *Calcareous rocks: 4.6) Argillaceous limestone; 4.7) chalk*

Figure 4.8 *Figure 4.9*

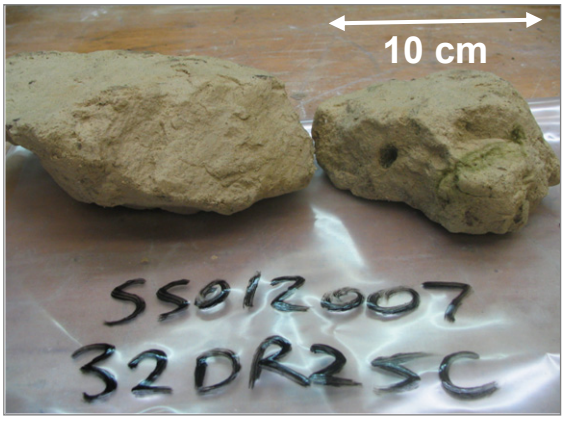

Figure 4.10

Figures 4.– 4.10. *Mudstones: 4.8) clean mudstone; 4.9) sandy mudstone; 4.10) glauconitic sandy mudstone.*

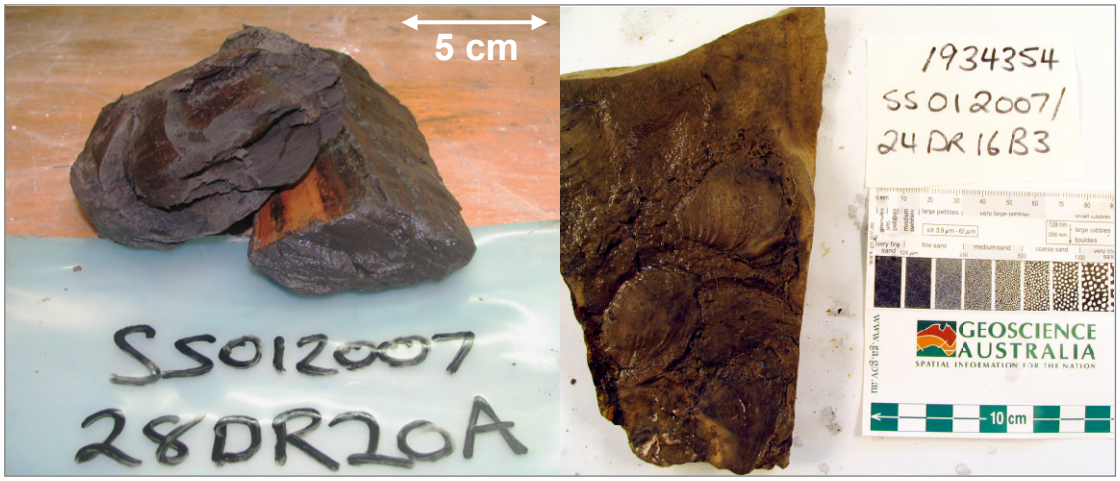

Figure 4.11 *Figure 4.12*

Figure 4.11–4.12. *Examples of 4.11) siltstone; 4.12) fossiliferous siltstone*

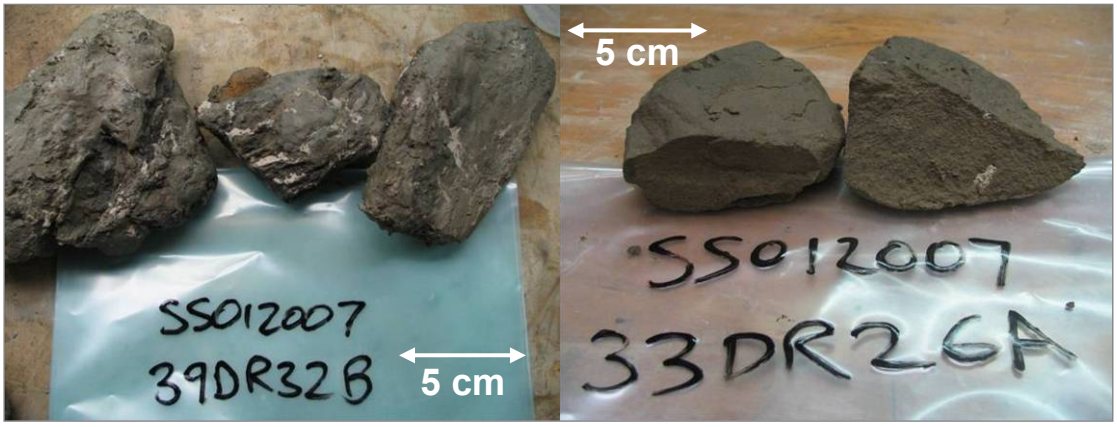

Figure 4.13 *Figure 4.14*

Figures 4.13–4.14. *Examples of 4.13) soft malleable clay with minor pelagic ooze, and 4.14) more lithified claystone.*

Figure 4.15. I*nterbedded sandstone and claystone.*

Figure 4.16. *Examples of sandstone recovered during the Bight survey: a) fine, micaceous sandstone, b) fine sandstone, c) fossiliferous, ferruginous fine sandstone and d) glauconitic sandstone (greensand).*

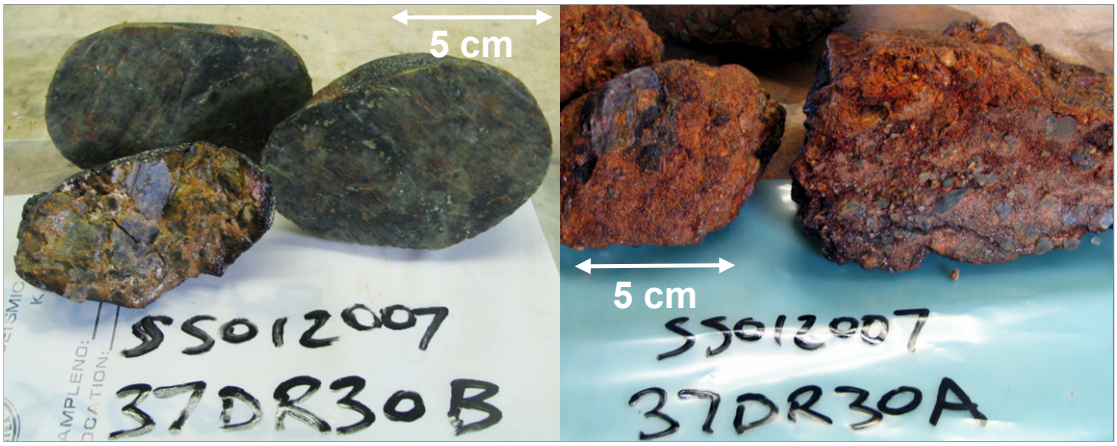

Figure 4.17 *Figure 4.18*

Figures 4.17–4.18. *Examples of coarse-grained rocks: 4.17) Well rounded cobble sized clasts; 4.18) weathered, pebbly conglomerate.*

5. Biostratigraphic Studies

E. Monteil, M. Macphail, A. Partridge, J. Rexilius, S. Powell & J. Crampton

PALYNOLOGY

The results of the palynostratigraphic and palaeoenvironmental analyses of 281 dredge and core samples from the Bight Basin Sampling and Seepage Survey (SS01/2007) are presented in Appendix 3.1. The palynostratigraphic study was undertaken by Eric Monteil (microplankton), Mike MacPhail (spore/pollen) and Alan Partridge (microplankton and spore/pollen) through a contract with TimeMatters Biostratigraphic Services.

The aims of this study were to provide an initial age/zone determination, and to assess age and palaeoenvironment based on a quantitative analysis of up to 250 palynomorphs per sample. The report in Appendix 3.1 documents the age and palaeoenvironment assessments, microplankton and spore/pollen biozone identification, and reworking.

Main results

- Samples from dredge sites on the Ceduna Terrace (Areas 2-4 and 6-9) yielded palynological assemblages of early middle Campanian to late Middle Eocene age, deposited in open marine, prodelta, delta front and terrestrial environments.
- Samples from dredge sites on the outer edge of the Eyre Terrace (Area 5) were mostly Turonian to Cenomanian age, and were deposited in environments ranging from deltaic to open marine.
- Cenomanian-Turonian boundary assemblages were identified in a suite of samples from Area 5. The identification of similar dinoflagellate cyst assemblages to those found in Cenomanian-Turonian "Black Shale" sequences of northern Europe and the abundance of organic matter in these samples suggests a possible correlation with the Cenomanian-Turonian boundary Oceanic Anoxic Event (OAE2).

MICROPALAEONTOLOGY

Micropalaeontological analysis of 14 samples was undertaken by ISC Biostrat. The results of these analyses are presented in Appendix 3.2. The age of the samples range from late Campanian to Early Miocene, based on the identification of planktonic foraminiferal, benthonic foraminiferal and calcareous nannofossil assemblages.

MACROPALAEONTOLOGY

Large bivalve fossils collected in dredges from Area 5 were studied by James Crampton (GNS Science), who identified the bivalves as Inoceramids of probable Coniacian age (Appendix 3.3; Fig. 4.4).

6. Organic Geochemistry – Source Rock Characterisation

C. Boreham

SUMMARY

The Geoscience Australia survey in the Bight Basin (SS01/2007) collected hundreds of dredge samples of early Cenomanian to late Maastrichtian age. Given the location of these samples, near the updip northern edge of the Ceduna Sub-basin, they are all immature for hydrocarbon generation with vitrinite reflectance ≤ 0.5% Rvmax, Tmax < 440^{o}C and PI < 0.1.

Excellent hydrocarbon generative potential is seen for marine, outer shelf, black shales and mudstones with TOC up to 6.9% and HI values up to 479 mg hydrocarbons/g TOC. These sediments are exclusively of late Cenomanian-early Turonian (C/T) in age. The high hydrocarbon potential of the C/T dredge samples is further supported by a dominance of the hydrogen-rich exinite maceral group (liptinite, lamalginite and telalginite macerals), where samples with the highest HI (>200 mg hydrocarbons/g TOC) contain >70% of the exinite maceral group. Pyrolysis-gas chromatography of the C/T kerogens reveal moderate levels of sulphur compounds and the relative abundances of aliphatic and aromatic hydrocarbons predict the generation of a paraffinic-naphthenic-aromatic low wax oil in nature.

The C/T organofacies is characterised by a diagnostic molecular signature. There is only minor dilution by allochthonous refractory terrestrial land plant inputs that variably lowers the overall hydrocarbon potential of the C/T marine rocks. For the most prolific potential source rocks, an anoxic marine depositional environment is consistent with the saturated hydrocarbons showing a *n*-C_{17} maxima, Pr/Ph < 1, high abundance of 28,30-bisnorhopane, the presence of the marine-specific C_{30} 24-propylcholestane and C_{30} 4,23,24-trimethylcholesterane (dinosterane). The Cretaceous age derived from palaeontological analysis is supported by the distribution of C_{26} desmethylsteranes. The biomarker assemblage of the C/T bitumens are very similar to those of the marine asphaltites (stranded coastal bitumens) that occur along the southern Australian coastline. However, subtle differences do occur. For example, the asphaltites are dominated by vanadyl porphyrins and contain isorenieratane (C_{40} arylisoprenoid), indicating photic zone anoxia. In comparison, the Bight C/T marine potential source rocks are dominated by nickel porphyrins and isorenieratane is absent or in trace amounts, suggesting that the oxic-anoxic boundary is at, or just below, the sediment-water interface. Therefore, source areas where even higher organic preservation has occurred under more anoxic conditions in euxinic seas may provide additional oil-prone ‘sweet-spots’. More mature and generative equivalent successions may lay down-dip towards the centre of the Bight Basin and have possibly contributed to the generation of the asphaltites. Acceptance of such an oil-source relationship infers the existence of an active petroleum system in the Bight Basin.

The C/T black shales in the Bight Basin draw the obvious comparison with world-wide black shales that characterise the oceanic anoxic event (OAE) at the C/T boundary, i.e. OAE2. Organic matter from the Bight Basin outer shelf, black shale shows a small enrichment in ^{13}C but not as much as that found in ‘classical’ OAE2 black shales. Nevertheless, the occurrence of extremely hydrogen-rich and organic-rich C/T sediments at ODP Site 1138 on the Kerguelen Plateau in the southern Indian Ocean would suggest that mid-Cretaceous anoxic conditions extended to extremely high southern latitudes and that OAE2 affected the entire global ocean.

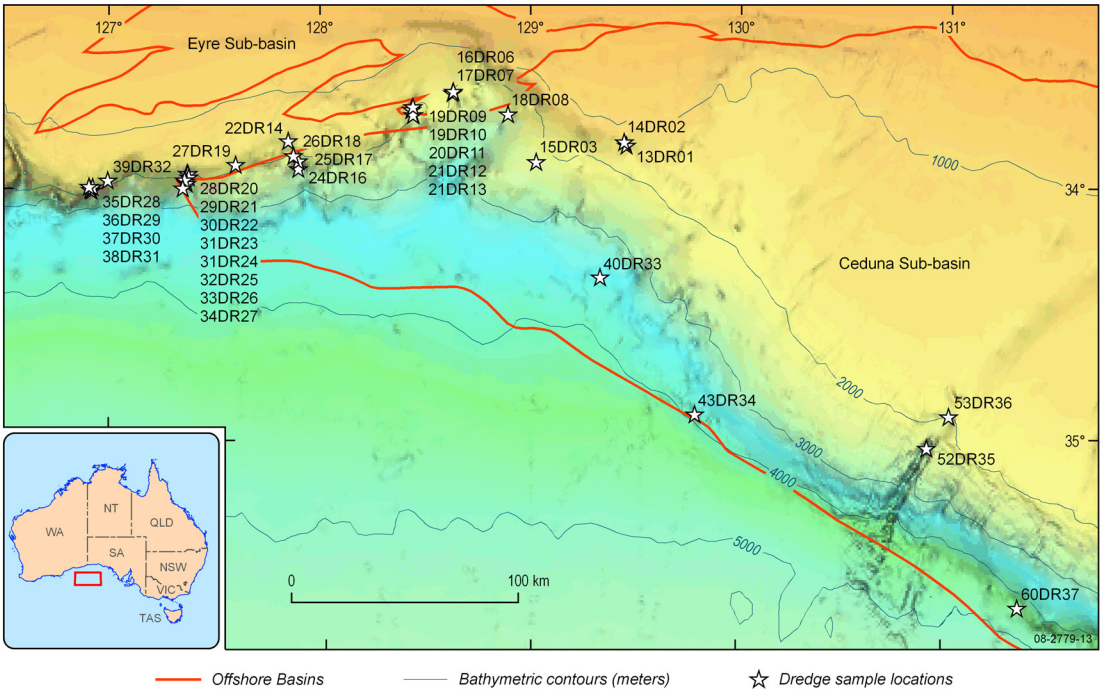

Figure 6.1. *Survey dredge locations in the western Ceduna Sub-basin / Eyre Sub-basin transition.*

SAMPLES AND METHODS

Dredge samples were selected for source rock assessment based primarily on their dark coloration and fine-grained nature, resulting in a total of 264 samples from 39 dredge and gravity core sites (Fig. 6.1 and Appendix 4.1). A sub-sample (50 g) was taken from the unexposed centre of the bulk specimen, washed with distilled water and air dried at 40°C. After lightly crushing to pass through a 3 mm sieve, representative splits were taken for organic petrographic, organic geochemistry and palaeontolgical analyses. For the latter analysis, acid-resistant plant, marine and algal microfossils were extracted using standard oxidation and filtration techniques designed to eliminate fines with maximum diameters of less than 5 µm. Age determinations are found in Monteil et al. (2008; Appendix 3.1) and summarised in Appendix 4.1.

Rock-Eval pyrolysis and TOC contents of powdered whole rock and kerogen isolate were determined using a Rock Eval 6 instrument and the results are listed in Appendix 4.2. Following solvent extraction (see below) of the powdered sediment, removal of mineral matter for kerogen isolation was done using the HF/BF_3 method of Robl and Davis (1993). The kerogen was thoroughly dried at 105°C in an inert atmosphere under a stream of nitrogen (30 ml/min) for 3 hours. Rock Eval and TOC of the kerogen are given in Appendix 4.2. The carbon isotopes of the kerogen were analysed at the Research School of Biological Sciences, Australian National University and the results given in Appendix 4.2.

Pyrolysis gas chromatography was performed using the Quantum MSSV-2 Thermal Analysis System©. Thermally extracted (300°C for 10 minutes) kerogens were heated in a flow of helium, and products released over the temperature range 300-600°C (40°C/minute) were focussed using a cryogenic trap, and then analysed using a 50 m x 0.32 mm BP-1 capillary column equipped with a flame ionisation detector. The GC oven temperature was programmed from 40°C to 320°C at 8°C/minute. Boiling ranges (C_1, C_2–C_5, C_6–C_{14}, C_{15+}) and individual compounds (*n*-alkenes, *n*-alkanes, alkylaromatic hydrocarbons, phenols and alkylthiophenes) were quantified by external standardisation using *n*-butane (Appendix 4.3). Response factors for all compounds were assumed the same, except for methane whose response factor was 1.1.

Based on the bulk geochemical results, 34 samples were high-graded for further detailed molecular and organic petrographic analyses. Vitrinite reflectance and maceral descriptions were carried out by Keiraville Konsultants (Appendix 4.4) and are summarised in Appendix 4.5. All samples were extracted with dichloromethane:methanol (9:1) at 100^{o}C using the accelerated solvent extraction (ASE) technique and extract yields measured after removal of the solvent (Appendix 4.6). The isolated extractable organic matter was separated into saturated hydrocarbons, aromatic hydrocarbons and polars (NSO compounds) by open column chromatography on solid silica gel support using *n*-hexane, dichloromethane:*n*-hexane (1:1) and dichloromethane:methanol (1:1), respectively (Appendix 4.6). The saturated hydrocarbons were further purified by passing through a column of elemental Cu in order to remove elemental S. Gas chromatography (GC) of the saturated hydrocarbons (Appendix 4.6) followed the procedures outlined in Boreham and Ambrose (2007). Gas chromatography-mass spectrometry (GCMS in full scan and single ion recording (SIR) mode) of the saturated hydrocarbons (Appendix 4.7) were done using the procedures outlined in Boreham and Ambrose (2007). GCMS-metastable reaction monitoring (MRM) using a Micromass Autospec were used to further characterise the C_{26}–C_{30} desmethylsteranes and C_{30} methylsteranes (Appendix 4.8). The aromatic hydrocarbons were analysed by GCMS-SIR using the same GC conditions as for the saturated hydrocarbons (Edwards et al., 2004). The C_{40} arylisoprenoid distribution was determined by monitoring selected ions at 133 and 134 Daltons (Boreham and Ambrose, 2007). The identification of isorenieratane was confirmed by co-injection with the aromatic hydrocarbons isolated from the Barney Creek Formation, McArthur Basin (sample 2887) as characterised by Brocks et al. (2005).

Metalloporphyrin contents (Appendix 4.9) were determined by UV-Vis spectrometry using the method of Boreham and Fookes (1989) for Ni porphyrins and Boreham (1992) for vanadyl porphyrins.

RESULTS AND DISCUSSION

Preservation of organic matter in seafloor sediments

Prolonged exposure of rock in outcrop can adversely affect petroleum potential assessment. Oxidative weathering typically leads to loss of organic carbon and reduction in bulk petroleum potential (Copard et al., 2002). However, there is generally little change at the molecular level and detailed geochemical assessments (e.g. pyrolysis-GCMS) of original unaltered petroleum potential will remain valid (Petsch et al., 2000) even though bulk parameters are less optimistic. Furthermore, vitrinite reflectance is little affected by weathering, however, Tmax and OI can show increases proportional to the degree of weathering (Copard et al., 2002).

The effect of sub-marine exposure was qualitatively assessed during organic petrographic analysis by observing the degree of alteration of various mineral (e.g.. pyrite) and organic phases. A weathering index (WI) from 1 to 5 was devised (Appendix 4.4) to assess the effects of weathering and corrosion with 1 representing no alteration and 5 being severely altered (Appendix 4.5). Encouragingly, for the high-graded samples analysed, 23 remained fresh and unaltered with pyrite being preserved and the organic matter showing no corroded margins. The 3 samples with the highest alteration (WI = 3) showed moderately strong weathering indicated by abundant iron oxides and moderate evidence of organic matter corrosion. Interestingly, the samples with the best hydrocarbon potential encompass the full range of observed WI (1 to 3; Appendix 4.5), suggesting that bulk geochemistry parameters have been little influenced by sub-marine exposure. This is further supported by the lack of a simple relationship between Tmax and OI (Appendix 4.2). Therefore, the organic petrology and geochemistry results suggest that the exposed Bight Basin samples have been only mildly affected by oxidative weathering and this has had little impact on source rock assessment. A similar result was found for dredge samples collected from the Bremer Sub-basin (Boreham et al., 2005).

Source rock potential

Source richness

Since all the samples are considered immature with mean maximum vitrinite reflectance (Rvmax) ≤ 0.5% (Appendix 4.5), the present-day geochemical parameters can be considered as initial values and do not need to be adjusted for losses due to petroleum generation. TOC contents range from 0.04 to 6.91%. Seventeen of the samples show good to excellent organic richness (TOC > 2%; Fig. 6.2a and Appendix 4.2) across four dredge sites; 25DR16, 25DR17, 32DR25, 52DR35 (Fig. 6.1), and one gravity core, 62GC63. The ability of this organic matter to be converted to petroleum (gas and oil) was further assessed using the Rock Eval pyrolysis technique. Pyrolysate yields (S2) range from extremely low 0.04 to extremely high 29.68 mg hydrocarbons/g rock with eleven samples having good to excellent generative potential (S2 > 5 mg hydrocarbons/g rock in Fig. 6.2a). The samples came from two dredge sites – 25DR16 and 25DR17 (Fig. 6.1). TOC-normalised pyrolysis yields, or Hydrogen Indices (HI), range from 24 to 479 mg hydrocarbons/g TOC, with the highest value representing potential conversion of up to 40% of the TOC into both gas and oil. The eight samples with TOC > 2% and HI > 300 mg hydrocarbons/g TOC (Type II/III to Type II kerogen) from dredge sites 24DR16 and 25DR17 (Appendix 4.2; Fig. 6.1) are considered excellent potential source rocks for the generation and expulsion of black oil. Only at dredge site 32DR25 was there any further evidence of limited liquids potential (wet gas) with two samples having TOC > 1% and HI > 150 mg hydrocarbons (Type III kerogen), with the bulk of the samples showing only limited gas or no hydrocarbon potential (Fig. 6.2).

S2 pyrolysate yields can be influenced by the mineral matrix, especially for samples with TOC< 4–5%, giving rise to lowered HI for the whole rock (Boreham and Powell, 1987),. A more realistic measure of the hydrocarbon potential is gained after removal of the mineral matter with strong acids and Rock Eval of the organic concentrates (kerogen). For the most prospective potential source rocks, $HI_{kerogen}$ up to 530 mg hydrocarbons/g TOC are observed (Appendix 4.2). For the more organically leaner whole rock samples, pyrolysis yields on the kerogen (Appendix 4.2) generally resulted in a considerable 2-fold increase in $HI_{kerogen}$ over the HI_{whole} (Fig. 6.3). However, even with such enhancements in $HI_{kerogen}$ there is little change in the overall interpretation of the hydrocarbon potential given the low values of the initial $HI_{whole\ rock.}$

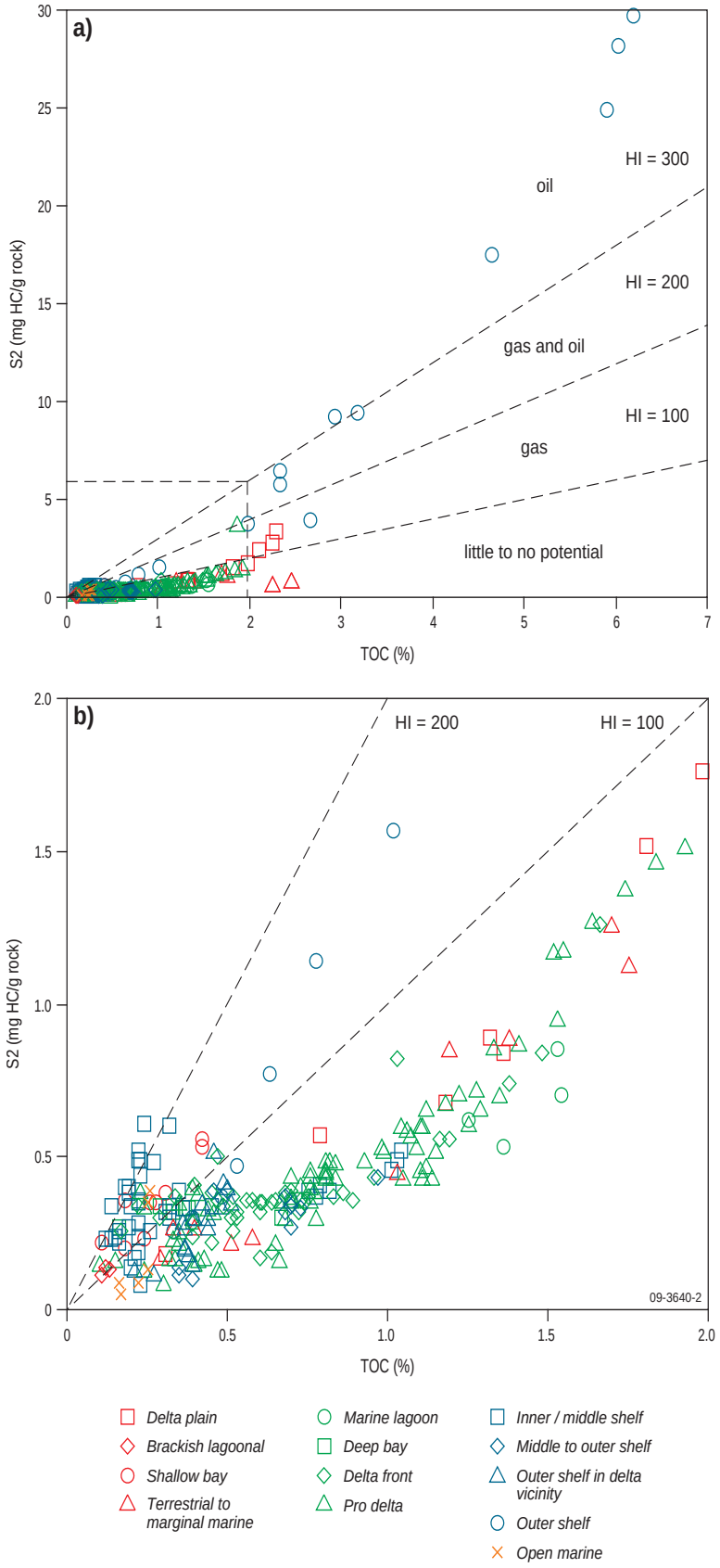

Figure 6.2. *Plot of total organic carbon (TOC %) versus Rock-Eval pyrolysis S2 (data from Appendix 4.2) for a) total data set, and b) for samples with TOC < 2 %. Note: HI = 100*S2/TOC with the various source richness and quality fields modified after Peters (1986) and Espitalié and Bordenave (1993).*

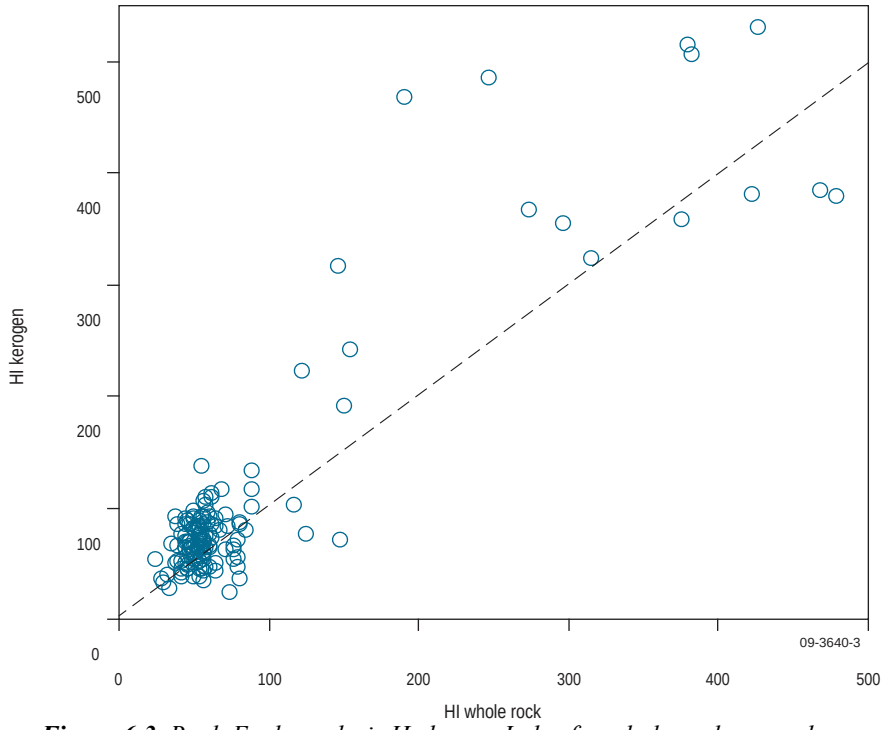

Figure 6.3. *Rock-Eval pyrolysis Hydrogen Index for whole rock versus kerogen.*

The dominance of the liptinite maceral group in those Bight dredge samples with the highest hydrocarbon potential is a further indication of hydrogen-rich organic matter. Thus, samples with the highest HI (> 200 mg hydrocarbons/g TOC) have the greatest proportion of the liptinite maceral group representing over 70% of the dispersed organic matter (Fig. 6.4). With these samples, lamalginite is the most abundant maceral (Appendix 4.5).

Maturity

The majority of the samples have Tmax < 440^{o}C (Fig. 6.5) and PI < 0.1 confirming their immaturity (Appendix 4.2). The high-graded samples analysed for molecular geochemistry are all immature with Rvmax < 0.5%, Tmax < 434^{o}C and PI < 0.06 (Appendices 4.2 and 4.5). Additionally, there is a smaller group of samples that appear to be overmature with Tmax > 600^{o}C (Fig. 6.5 and Appendix 4.2). Characteristic of this group are low TOC values (generally < 0.5 %) and a dominant high temperature contribution to the S2 profile, attributed to ionisation of salts, which monotonically increases at the higher pyrolysis temperature and never reaches a 'peak'. Thus, the highest detector response is at the final pyrolysis temperature resulting in the maximum instrument value for Tmax (Boreham et al., 2005).

Source facies and depositional environment

The Bight Basin samples analysed for organic geochemistry range in age from early Cenomanian to late Maastrichtian and cover depositional environments from delta plain to open marine (Appendix 4.1 and Monteil et al., 2008; Appendix 3.1). The best potential source rocks were deposited in an outer shelf environment (Fig. 6.2a). TOC-poor outer shelf samples also show elevated hydrocarbon potential (Fig. 6.2b). Although the remaining, vast majority, of the Bight samples encompass a wide variation in depositional environments, from delta plain to open marine, there is a limited range in generative potential, with all showing a similar relationship between TOC and S2 (Fig. 6.2b). Nevertheless, the TOC-poor outer shelf samples still show elevated hydrocarbon potential (Fig. 6.2b).

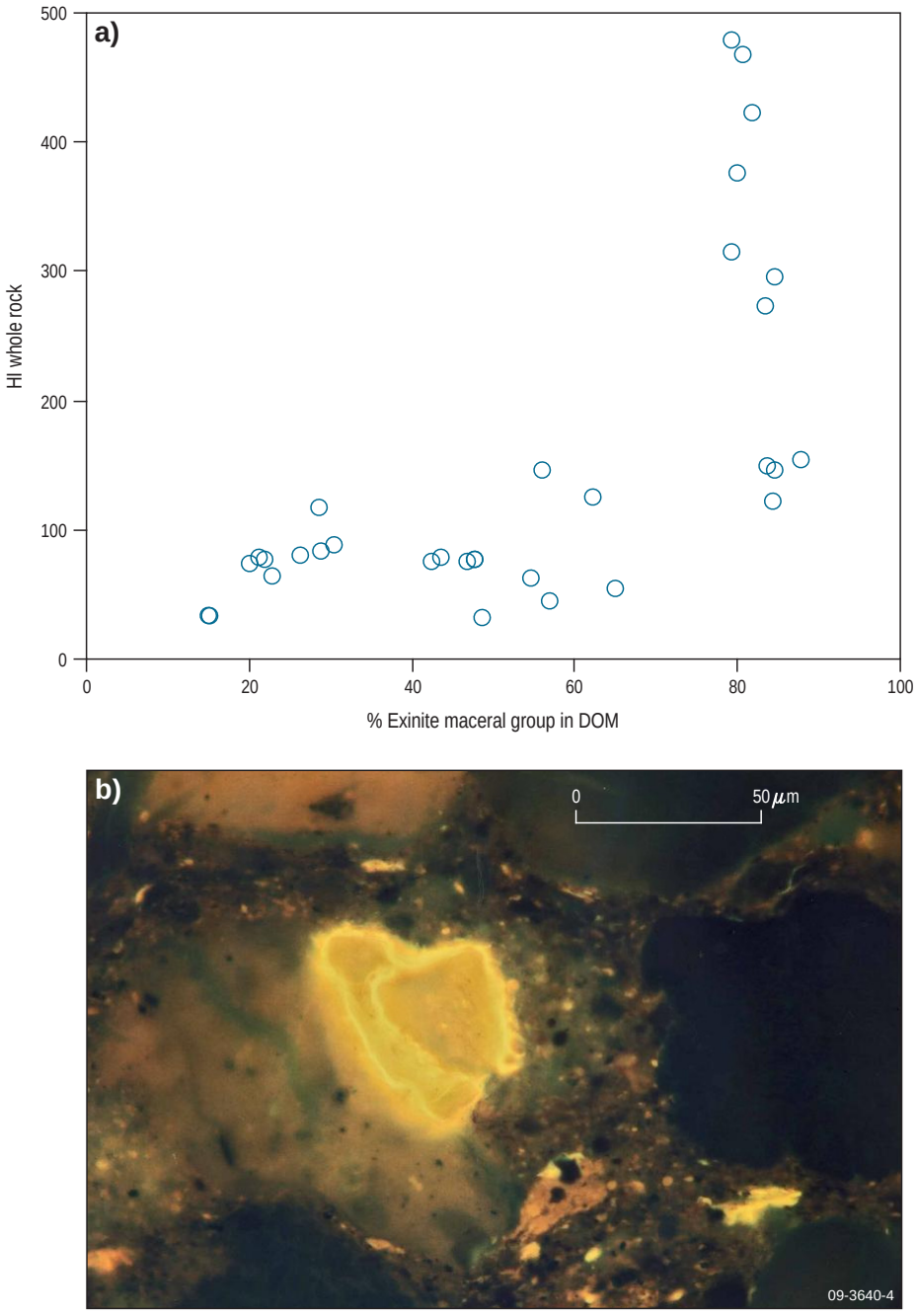

Figure 6.4. *a) Plot of HI versus relative proportion of liptinite maceral group compared to the sum of exinite, vitrinite and inertinite maceral groups, and b) SS012007/25DR17 B1.1(#1935256); Dinoflagellate tests and lamalginite in claystone; Fluorescence-mode; Field width 0.22 mm; vitrinite reflectance (Rvmax) 0.34%.*

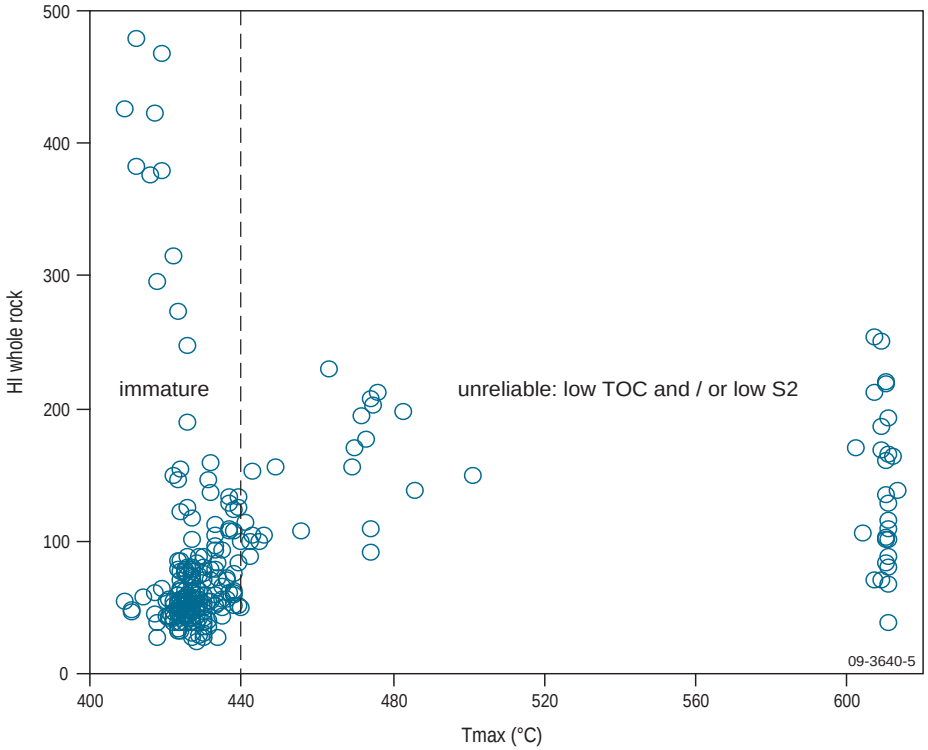

Figure 6.5. *Source quality—maturity plot of Hydrogen Index versus Tmax.*

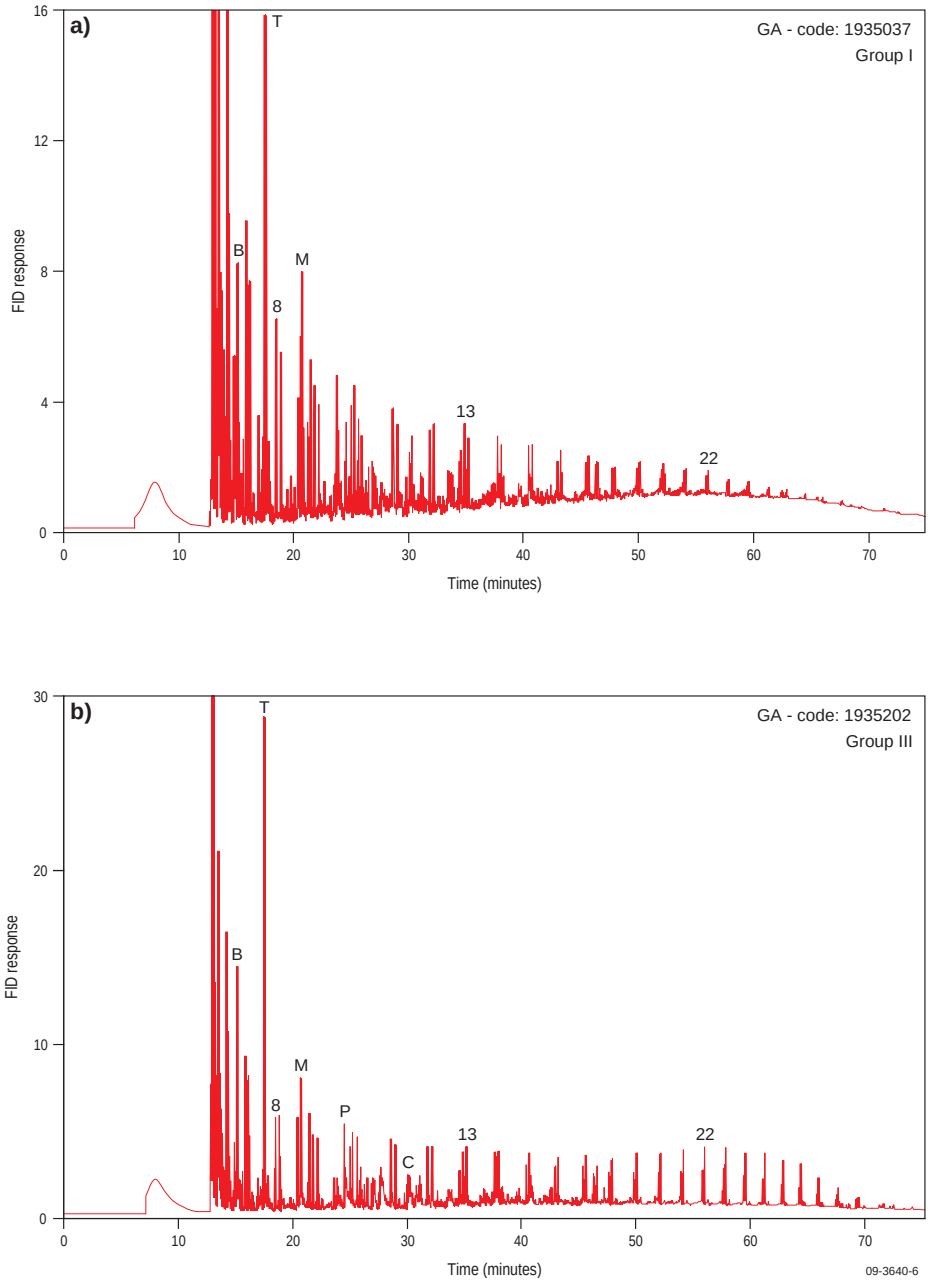

Figure 6.6. *Pyrolysis-gas chromatograms of a) 25DR17 B5 (#1935037; Cenomanian-Turonian boundary, outer shelf), and b) 52DR35 E1 (#1935202; early Maastrichtian, delta plain). B= benzene; T = toluene; M= = meta+para xylenes; P = phenol; C =1,2,3,4-tetramethylbenzene; 8, 13, 22 = carbon number of alkene/alkane pairs.*

Pyrolysis-gas chromatogram

Pyrolysis-gas chromatography addresses the molecular composition of the kerogen and can be used to predicted organofacies and depositional environments. Appendix 4.3 lists the yields of different compound classes, C_1–C_5 gaseous hydrocarbons, C_6–C_{14} and C_{15+} hydrocarbons, alkylaromatics, alkylphenols and alkylthiophenes. Pyrolysis gas chromatograms are shown in Figure 6.6. Based on the chain length distribution of *n*-alkyl moieties, and the relative abundances of hydrocarbons versus alkylthiophenes versus alkylaromatics, the samples fall into three groups (Fig. 6.7). The Group I samples represent the Cenomanian-Turonian boundary, outer shelf organic-rich mudstones with the best hydrocarbon potential (2.34% < TOC < 6.02% and 274 < HI < 468 mg hydrocarbons/g TOC; Type II/III to Type II kerogen), Group II represents Cenomanian and Cenomanian-Turonian boundary, outer shelf samples with lower hydrocarbon potential

(0.63% < TOC < 2.66% and 122 < HI < 154 mg hydrocarbons/g TOC; Type III kerogen) while Group III includes prodelta and delta plain samples of Cenomanian and early Maastrichtian age with Type III/IV kerogen.

The gas chromatograms of all samples belonging to Group I (Fig. 6.6a) show the strong presence of gaseous hydrocarbons and normal hydrocarbon doublets (*n*-alk-1-enes and *n*-alkanes) whose homologues extend to *n*-C_{28}. Gas chromatograms are characterized by a relative decrease in abundance of alkene/*n*-alkane doublets with increasing carbon number from C_6 to C_{28} with little to no odd-to-even carbon number predominance, which is typical of many marine kerogens (e.g. van de Meent et al., 1980; Muscio et al.,1994; Clegg et al., 1997). Additionally, benzene and the alkylbenzenes (toluene, o-m-p-xylenes) represent the second-most abundant compound group in these samples. Meanwhile, phenol and methylphenols (cresols), typical of land plant lignocellulosic pyrolysis products were essentially absent. 1,2,3,4-tetramethylbenzene (TeMB) is one of the prominent peaks in the pyrolysis-gas chromatograms of many samples in Group I, eluting between the *n*-C_{11} and *n*-C_{12} doublets. This compound is often assumed to be a pyrolysis product released from ß-cleavage of bound diaromatic carotenoids (e.g. C_{40} isoprenoids isorenieratene and/ or chlorobactene) from anaerobic photosynthetic green sulphur bacteria (e.g. *Chlorobiaceae*), which populate zones of photic zone anoxia (Summons & Powell, 1987; Hartgers et al., 1994; Muscio et al.,1994; Clegg et al., 1997; Wanglu et al., 2007) though it may simply be of algal kerogen (Hoefs et al., 1995). The absence of the C_{40} isoprenoids in the aromatic hydrocarbons from the extractable organic matter suggests the latter origin. The alkylthiophenes are present in high concentration, namely in the range from 830 to 2700 (µg/g sample).

The gas chromatograms of samples in Group II are closely similar to those of Group I. However, Group II produces more toluene, but generally less 2,5-dimethylthiophene than that from Group I (Fig. 6.7a). This is likely to reflect the greater input of reworked, more refractory organic matter.

The pyrolysis-gas chromatograms of samples in Group III, shown in Figure 6.6b, are distinctly different from the other two groups. They show a strong presence of gaseous hydrocarbons and aromatic hydrocarbons, such as benzene, toluene and m-p-o-xylenes. Normal hydrocarbon doublets are less abundant and extend to long chain length (*n*-C_{30}) with a high relative abundance of waxy (> C_{22}) *n*-hydrocarbons. Phenol and cresols, which are typical of land plant lignocellulosic pyrolysis products, are also found in Group III samples. As shown in Figure 6.7a, this sample group produces more toluene but less S-compounds (70-410 µg/g sample) than do the other two groups. The distribution of pyrolysis products documented for Group III is therefore typical of organic matter having a variable type II/III to type III composition (Figs. 6.4 and 6.5). It commonly occurs in lower delta plain and inner shelf environments (Horsfield, 1997). This interpretation is consistent with environments deduced from the palaeontological assessment.

The type of petroleum products that may be generated from the investigated samples are illustrated in the triangular plot of Horsfield (1989, 1997) in Figure 6.7b. Groups I and II distribute within the “paraffinic-naphthenic-aromatic low wax” oil generating field, which are usually associated with marine depositional settings. On the other hand, Group III samples are expected to produce a paraffinic-naphthenic-aromatic high wax product, more consistent with the dominance of land plant input to the depositional environment.

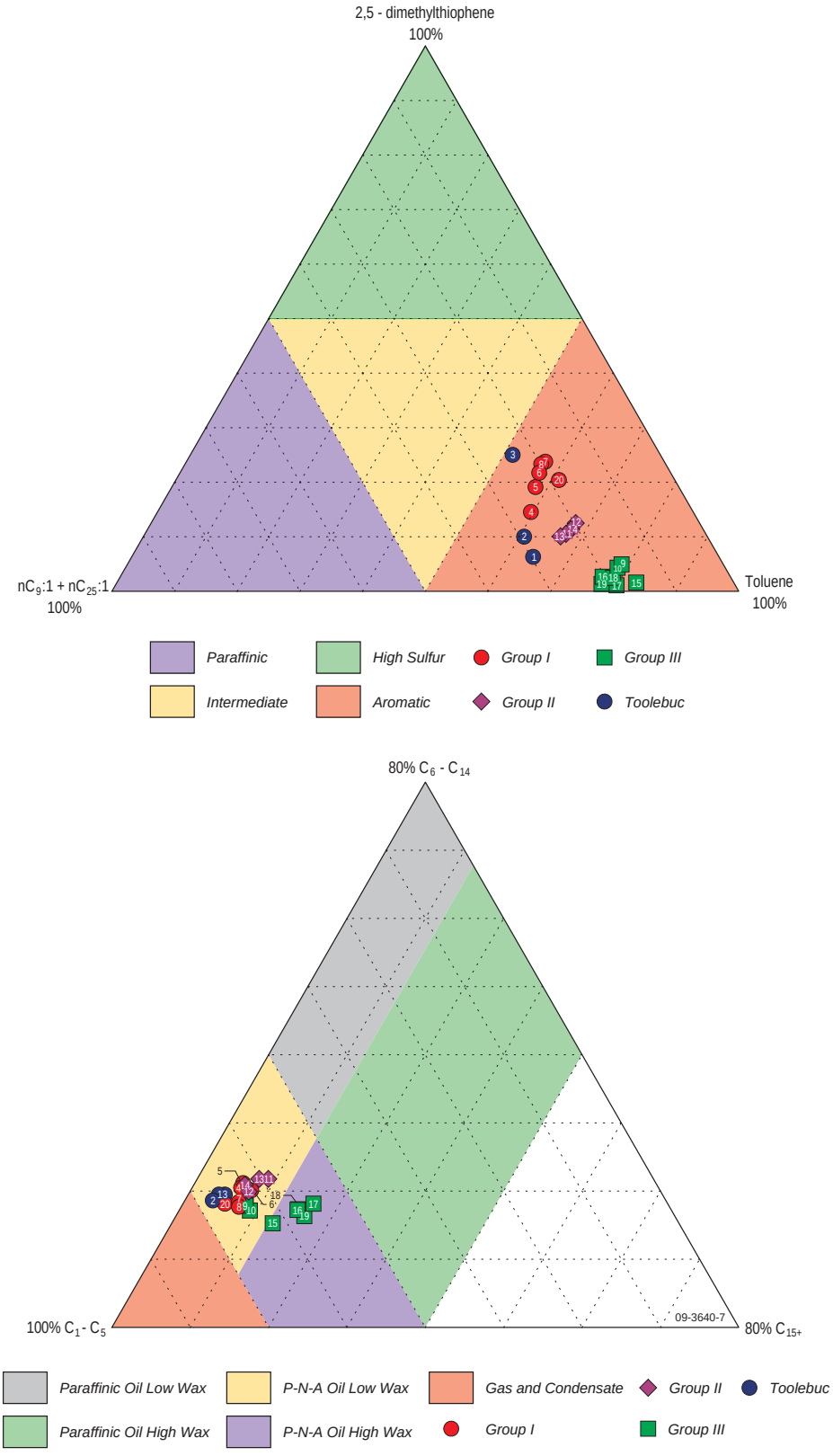

Figure 6.7. *Triangular plot of a) relative abundances of C_9–C_{25} n-hydrocarbons versus 2,5-dimethylthiophene versus toluene, and b) relative abundances of C_1–C_5 versus C_6–C_{14} n-hydrocarbons versus C_{15+} n-hydrocarbons.*

Multi-component kinetics

Multi-component kinetics for a kerogen from the late Cenomanian-early Turonian black shale (25DR17 B4) and an asphaltene isolated from the marine asphaltite (GA# 20010763) from Kangaroo Island (Edwards et al, 1998) were analysed to determine their oil and gas generating characteristics. Both samples were analysed using the PhaseKinetic approach (di Primio and Horsfield, 2006) in order to develop phase predictive compositional kinetic models of hydrocarbon generation (Appendix 4.10). The 15-component phase kinetics derived on the potential source rock was used to define the kinetic characteristics of the marine source rock units in subsequent petroleum systems modelling (Totterdell et al., 2008).

The source rock kinetic parameters for bulk petroleum generation indicate that 10% conversion occurs around 107°C and 127°C for the kerogen and asphaltene samples respectively at a 3°C/My heating rate. The kerogen sample is relatively heterogeneous, in that it displays a comparatively wide activation energy distribution, and generates petroleum with a broad GOR span covering a range from 73.1 to 196.2 Sm3/Sm3 over a temperature range of roughly 60°C at a geologic heating rate of 3°C/Ma. The asphaltene sample shows a narrower activation energy distribution with over 50% of the potential concentrated in two main activation energies (54 and 55 kcal/mol). This indicates a more homogeneous organic matter type. The asphaltene sample generates petroleum with a limited GOR span ranging from 107.4 to 189.5 Sm^3/Sm^3 over a temperature range of 45°C at a geologic heating rate of 3°C//Ma. Both samples belong to the paraffinic-naphthenic-aromatic low wax petroleum type organofacies (also see Pyrolysis-gas chromatography section above). The hydrocarbon phases generated by the samples are characterised by constantly increasing GORs with increasing thermal stress. The fluids generated fall within the black oil class, are highly undersaturated at low levels of conversion and reach saturation pressures of over 160 bars at the highest transformation ratios monitored.

There is a strong genetic affinity between the potential source rock and the asphaltite. The residual activation energy distribution of the asphaltite falls within the higher temperature envelope of the activation energy distribution of the source rock, consistent with an oil-source relationship.

Saturated biomarker distribution

Molecular geochemical analysis of the extractable organic matter, combined with micro-palaeontology and palynology analyses (Appendix 4.2) of the organic facies, can define source inputs and depositional environments. Thirty-three dredge samples were chosen, ranging in age from early Cenomanian to latest Maastrichtian (Appendix 4.6), encompassing the measured range in petroleum potential and interpreted depositional environments (terrestrial to marine, derived from palaeontological assessments. The low extract yields (Appendix 4.6) are further evidence of the immaturity of the samples.

For 25DR17 B4, of late Cenomanian-early Turonian age and prolific source rock potential (TOC = 6.2 % and HI = 479 mg HC/g TOC), the GC trace of the saturated hydrocarbons (Fig. 6.8a) is dominated by a homologous series of *n*-alkanes from *n*-C_{15} to *n*-C_{23} with a maximum at *n*-C_{17} and a slight odd-over-even carbon number predominance (OEP(*n*-C_{17}) = 1.24), dominance of phytane over pristane (Pr/Ph = 0.47), and a high content of tetracyclic (sterane) and pentacyclic (hopane) hydrocarbons. Such an assemblage of molecular biomarkers is consistent with a major source input of marine algal organic matter and preservation in an anoxic depositional environment (Peters et al., 2005). This is confirmed by the presence of the marine-specific C_{30} 24-*n*-propylcholestane and C_{30} 4,23,24-trimethylcholesterane (dinosterane) while the distribution of C_{26} desmethylsteranes supports the Cretaceous age (Peters et al., 2005). Although the source organic matter and age are similar for 24DR16 A1 (Fig. 6.8b), the reduction in bulk oil generative potential is reflected at the molecular level by a higher Pr/Ph ratio of 1.26, which results from a slightly more oxygenated (dysoxic) depositional environment. The younger organic-rich sample

52DR35 C1 of late Campanian-early Maastrichtian age, which has a low hydrocarbon generative potential, has a GC trace (Fig. 6.8c) dominated by waxy *n*-alkanes (> *n*-C_{22}), maximising at *n*-C_{29}, together with the strong odd-over-even carbon number predominance (OEP(*n*-C_{27}) = 3.23), indicating a pronounced higher land plant source input (Tissot and Welte, 1984).

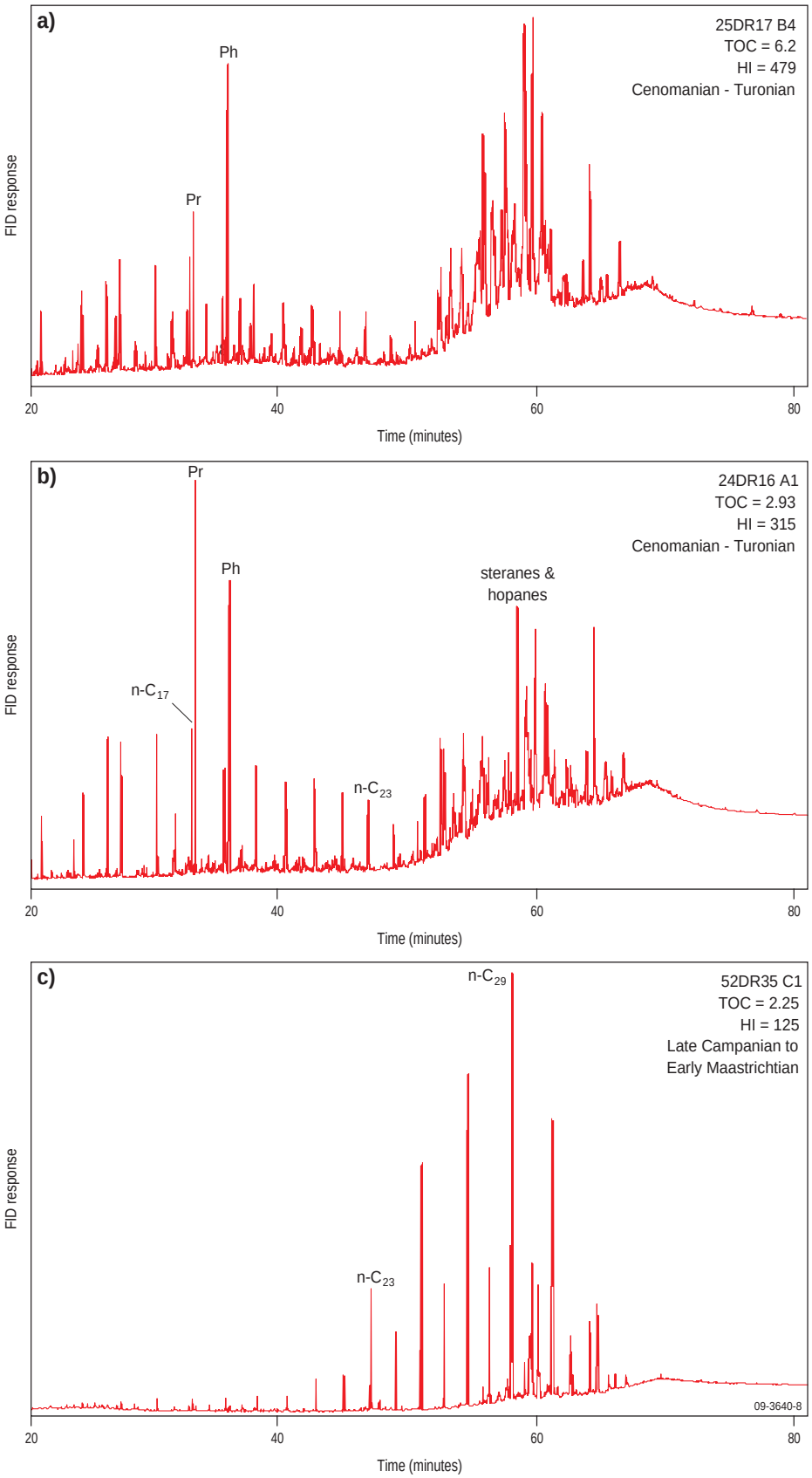

Figure 6.8. *Gas chromatography of saturated hydrocarbons on Bight Basin dredge samples for a) 25DR17 B4 (Cenomanian-Turonian boundary, outer shelf), b) 24DR16 A1 (Cenomanian-Turonian boundary, outer shelf), and c) 52DR35 C1 (late Campanian to early Maastrichtian, delta plain).*

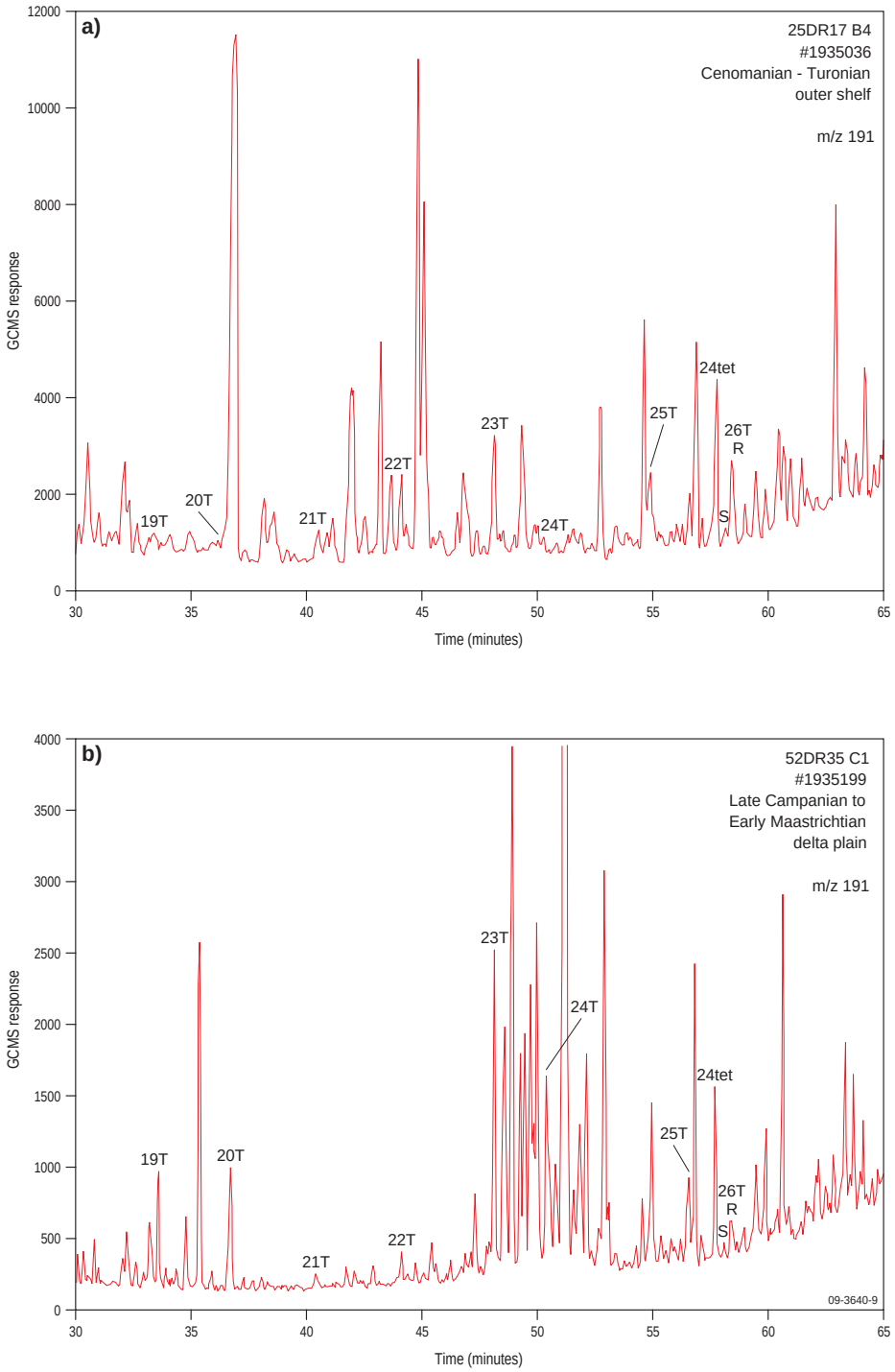

Figure 6.9. *Gas chromatography-mass spectrometry selected ion recording (GCMS-SIR) at m/z 191 for the saturated hydrocarbons of a) 24DR17 B4 (Cenomanian-Turonian boundary, outer shelf), and b) 52DR35 C1 (late Campanian to early Maastrichtian, delta plain). Note: time window shows the tri- and tetracyclic hydrocarbons.*

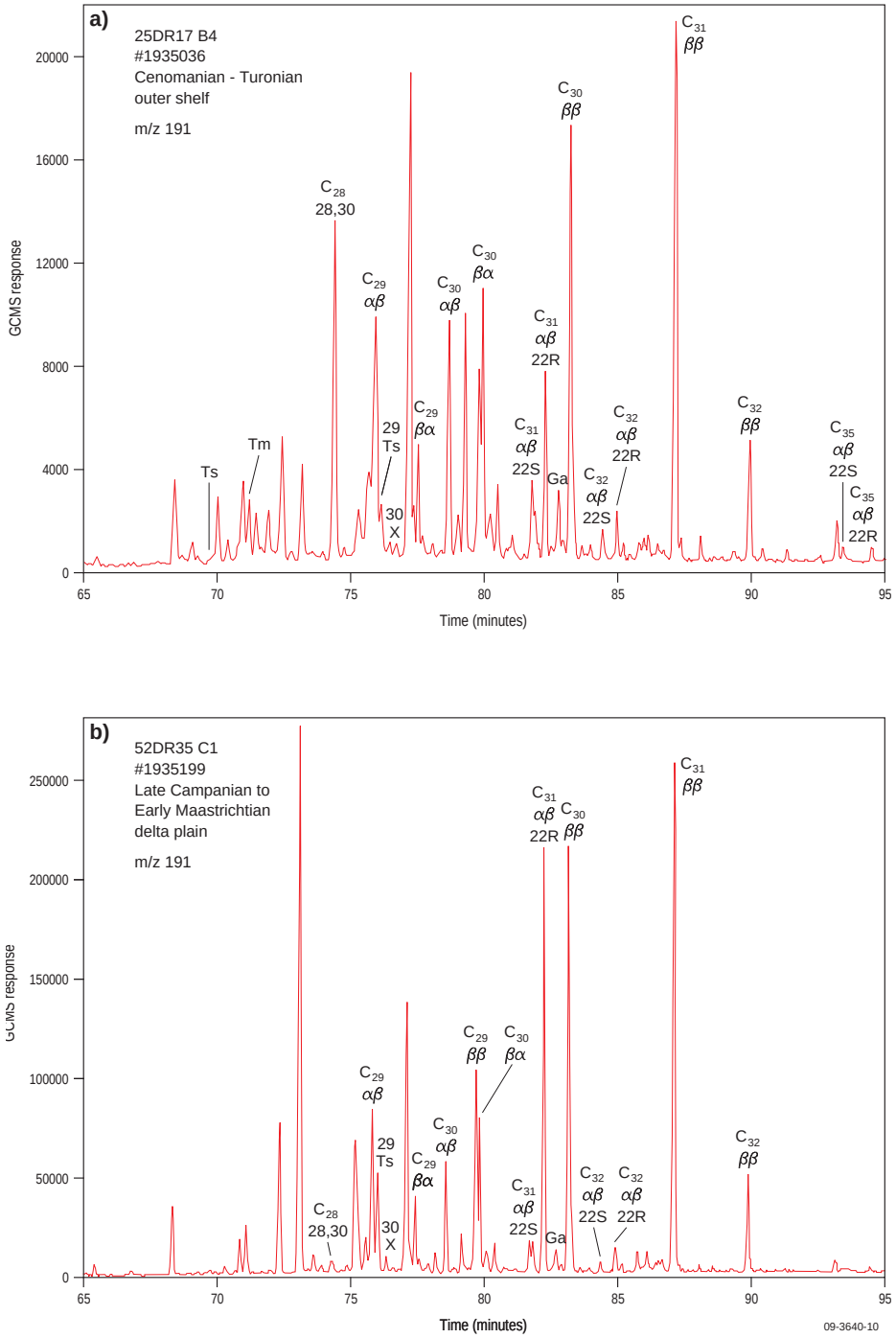

Figure 6.10. *Gas chromatography-mass spectrometry selected ion recording (GCMS-SIR) at m/z 191 for the saturated hydrocarbons of a) 24DR17 B4 (Cenomanian-Turonian boundary, outer shelf), and b) 52DR35 C1 (late Campanian to early Maastrichtian, delta plain). Note: time window shows the pentacyclic hydrocarbons.*

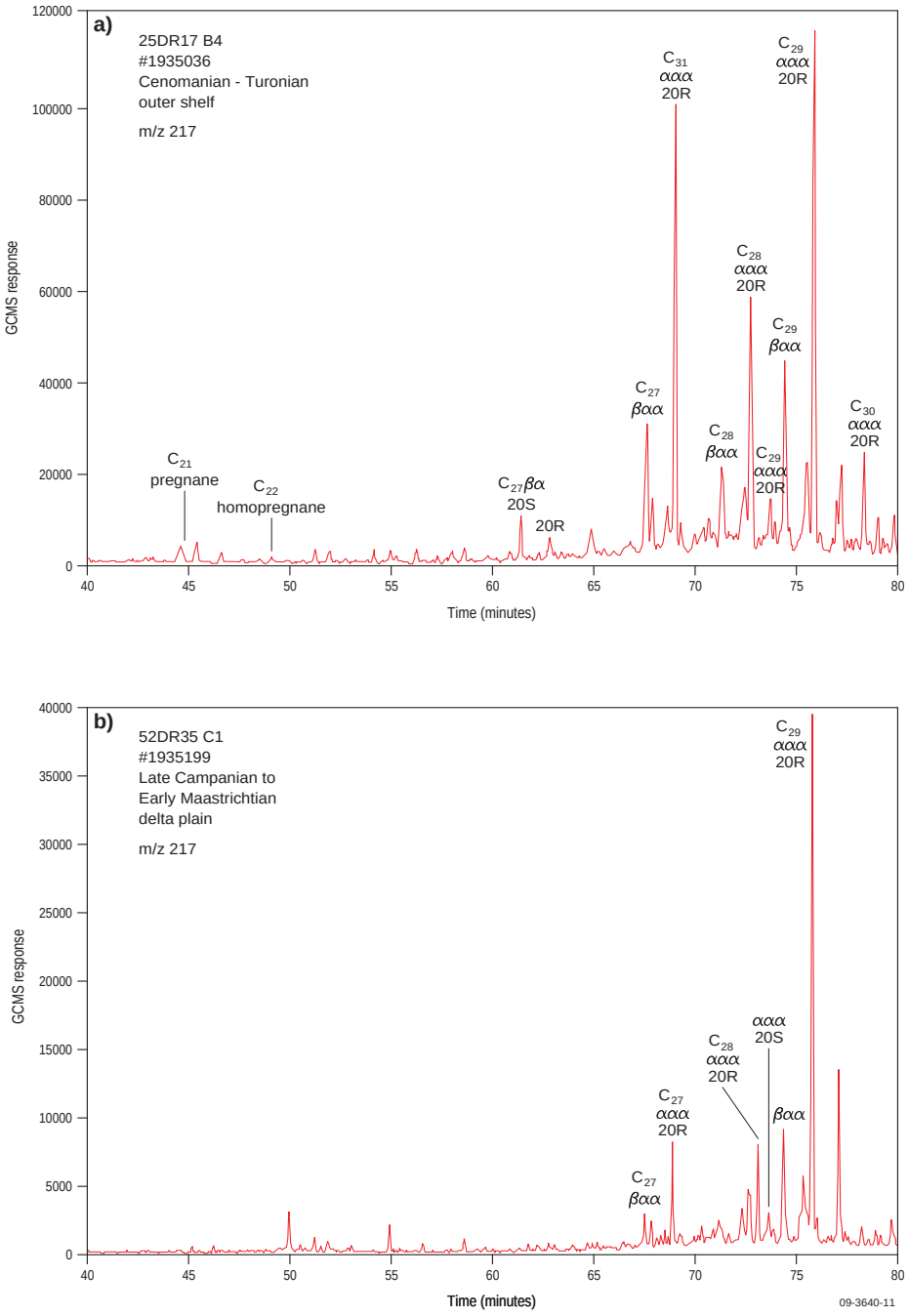

Figure 6.11. *Gas chromatography-mass spectrometry selected ion recording (GCMS-SIR) at m/z 217 for the saturated hydrocarbons of a) 24DR17 B4 (Cenomanian-Turonian boundary, outer shelf), and b) 52DR35 C1 (late Campanian to early Maastrichtian, delta plain).*

Representative GCMS-SIR traces for the saturated hydrocarbons isolated from the end-member outer shelf and delta plain samples are shown in Figure 6.9 for the C_{19}–C_{26} tricyclic and tetracyclic hydrocarbons, Figure 6.10 for the C_{27}–C_{35} pentacyclic triterpanes and Figure 6.11 for the C_{27}–C_{30} desmethylsteranes. Surprisingly, there is not a strong relationship between Pr/Ph and the proportion of C_{27} steranes (Fig. 6.12a), where a preference for the latter is another notably marine marker (Peters et al., 2005). Interestingly, the organic-rich sediments are characterised by low C_{27} steranes and a dominance for C_{29} steranes (Fig. 6.12b), especially in the majority of the outer shelf sample set. The organofacies from the delta plain depositional environment is characterised by elevated *n*-C_{27}/*n*-C_{17} ratios (i.e. high wax content) together with a preference for C_{29} steranes. The sterane content is not a sensitive marker to distinguish between the other depositional environments with C_{27} steranes still subordinate to C_{29} steranes (Fig. 6.12 and Fig. 6.13a). There

are three distinct organofacies with the outer shelf depositional environment that are readily distinguished by the biomarker ratios in Figure 6.13. The outer shelf-I are samples from 25DR17, outer shelf-II from 24DR16 and outer shelf-III from 32DR25 and 26. With a decrease in organic richness from outer shelf-I to outer shelf-III there is an increase in Pr/Ph and the proportion of C_{27} steranes (Appendix 4.2 and Fig. 6.12a). This most likely reflects the decline in organic matter preservation caused by an increase in oxidation and accompanying change in the algal community. The outer shelf depositional environment is also characterised by low C19/C23 tricyclics (Fig. 6.13c) and high relative abundances of 28,30-bisnorhopane (generally 28H/30H > 1; Fig. 6.13d), the latter indicative of anoxia (Farrimond et al., 1990), with the outer shelf-I organofacies showing the highest C28H/30H ratios (up to 13.5).

In order to obtain a broader overview of the biomarkers used to characterise the different organofacies from the Bight Basin samples, a multivariate statistical approach was employed using a wide range of biomarker ratios based on tricyclic and tetracyclic hydrocarbons, triterpane, hopane and sterane contents in the saturated hydrocarbon fractions (Appendices 4.7 and 4.8). Hierarchical cluster analysis (Einsight^{TM}) of the samples is shown in Figure 6.14, while principal component analysis is depicted by the plots of Factors 1 (defines the maximum variance) and Factors 2 (defines the maximum variances in the residues of Factor 1) for the samples and set of biomarker ratios in Figures 6.15a and 6.15b, respectively. The outer shelf-I organofacies is geochemically distinct from the other organofacies. The latter separate into three main sub-groups; eg.the outershelf-II and -III (each still retain their individuality), the prodelta/delta front/marine lagoon, and the delta plain to very near shore terrestrial–marginal marine organofacies. The distinction is mainly based on the increasing input of land plant material and associated bacterial reworking and increased oxygenation from the outer shelf-I to the delta plain end-member organofacies. The biomarker ratios that best differentiate the outershelf-I organofacies from the other organofacies are predominance of C_{29} steranes (%29), elevated C_{35} homohopane (35S/34S), high relative abundance of C_{30} *n*-propylcholestane (30/27-30S), high steranes relative to hopanes (Ster/Terp), high relative abundance of 2- and 3-methylhopanes (2+3MeH/H) and high C22/C21 ratio for the tricyclic hydrocarbons (Fig. 6.15).

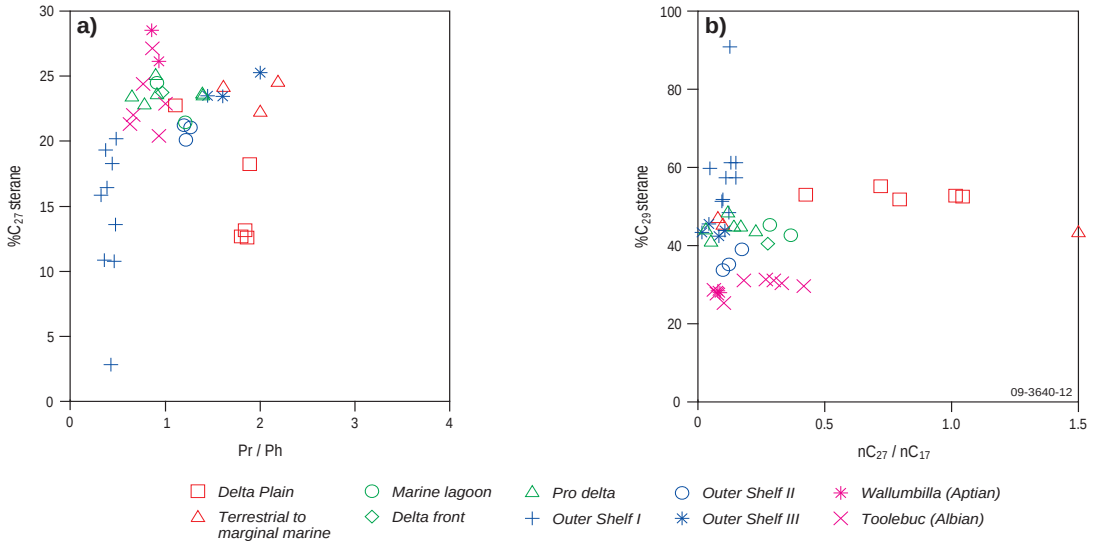

Figure 6.12. *Combined GC and GCMS-SIR biomarker ratio plot of a) Pr/Ph versus % C_{27} steranes and b) n-C_{27}/n-C_{17} versus % C_{29} steranes.*

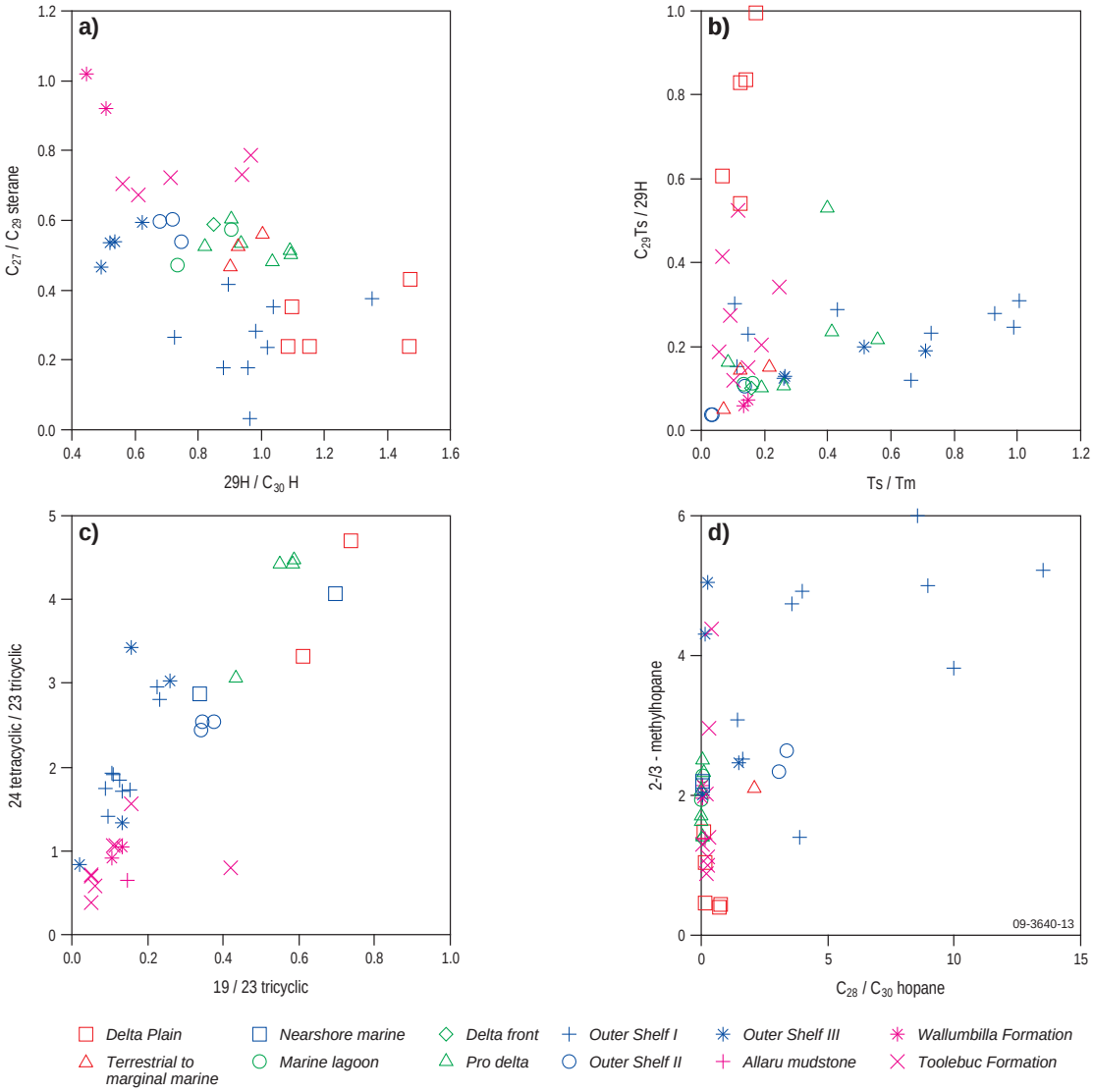

Figure 6.13. *Biomarker ratio plots based on GCMS-SIR of saturated hydrocarbons showing a) 29/30 hopane versus C_{27}/C_{29} sterane, b) Ts/Tm versus 29Ts/29H, c) 19/23 tricyclic versus 24 tetracyclic/23 tricyclic, and d) 28/30H versus 2-/3-methylhopane.*

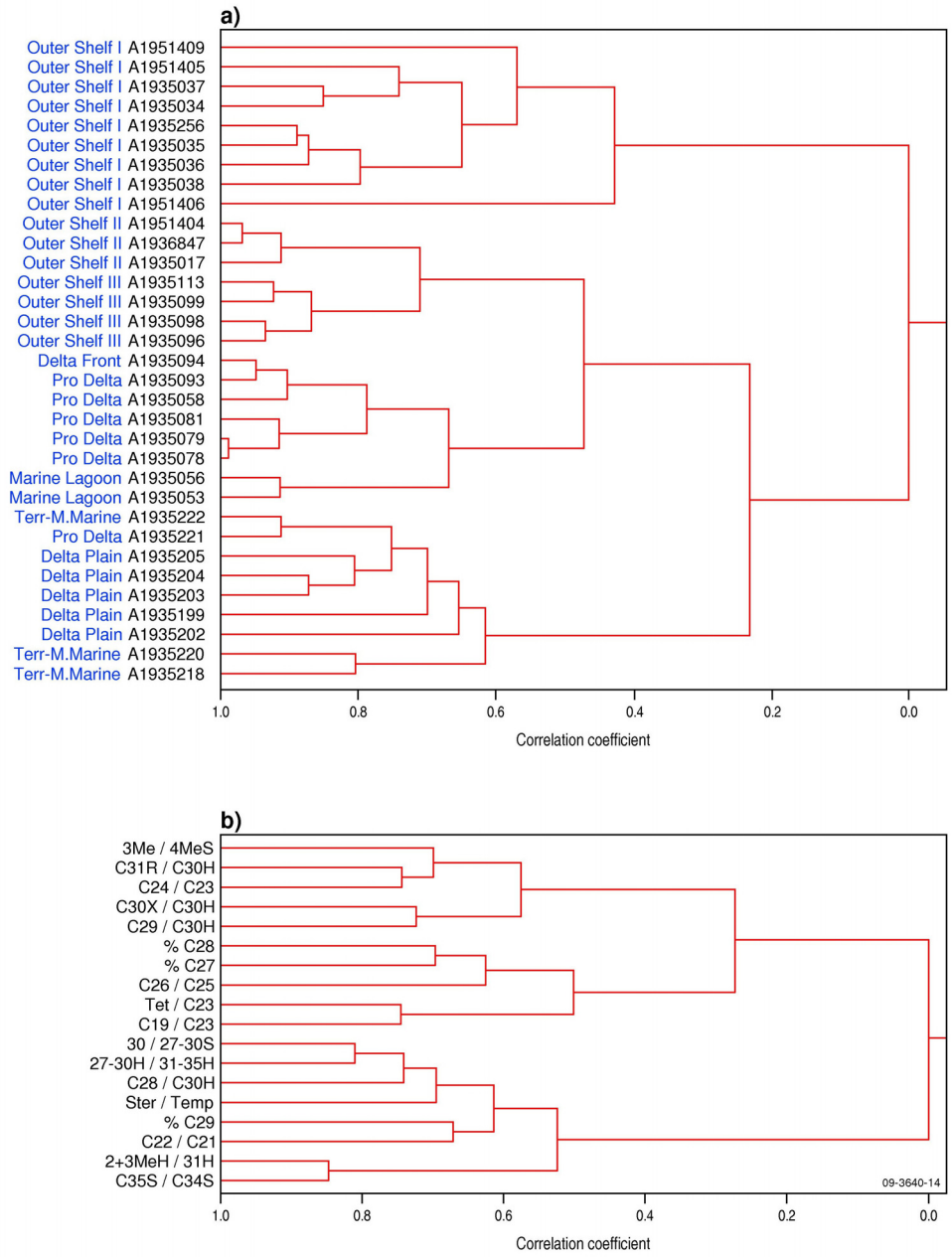

Figure 6.14. *Dendrograms from hierarchical cluster analysis of Bight Basin samples. Note: biomarker ratios are defined in Appendix 4.6.*

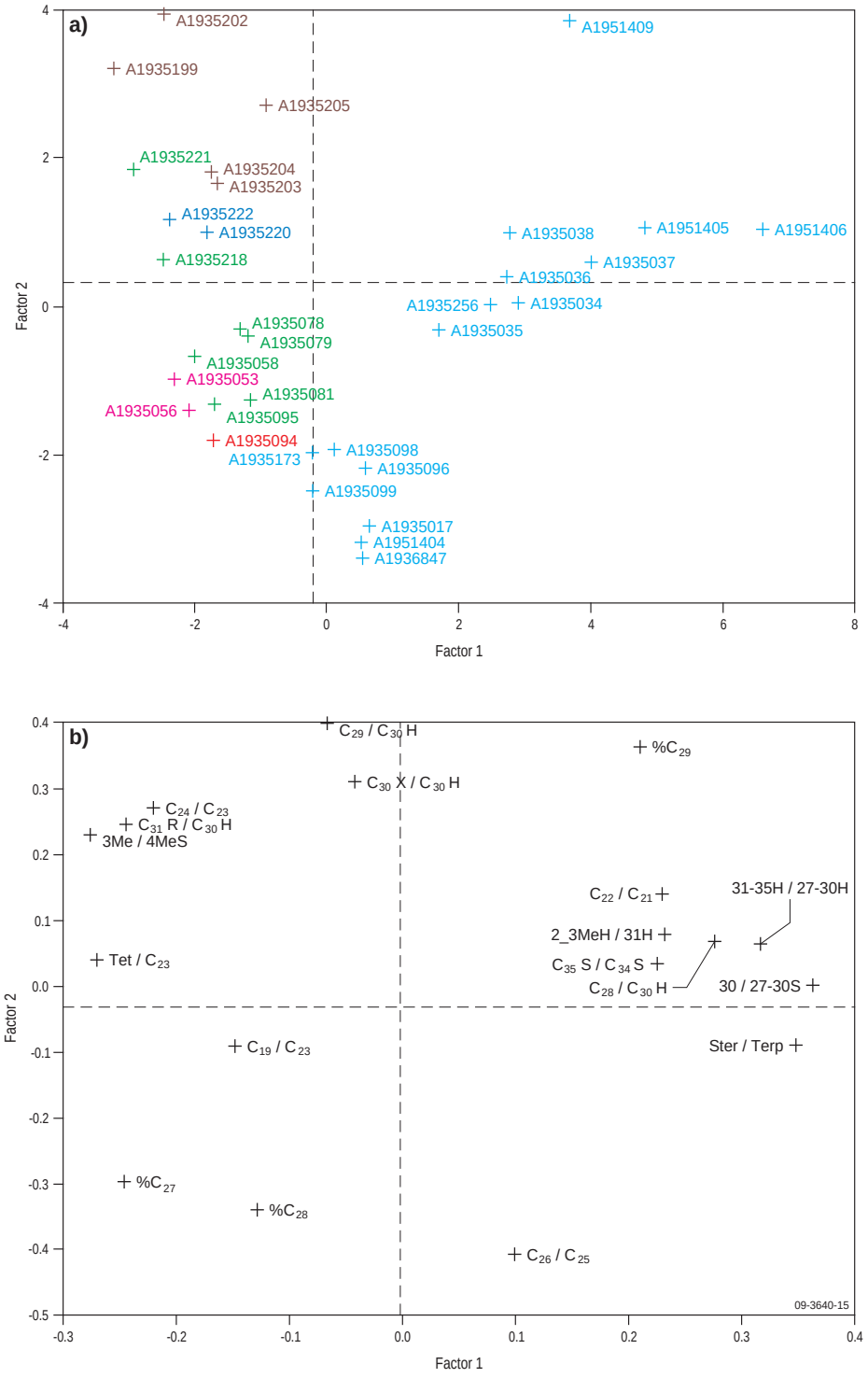

Figure 6.15. *Cross plot of the Factors 1 and Factors 2 from Principal Component Analysis for a) the Bight Basin samples and b) the biomarker ratios.*

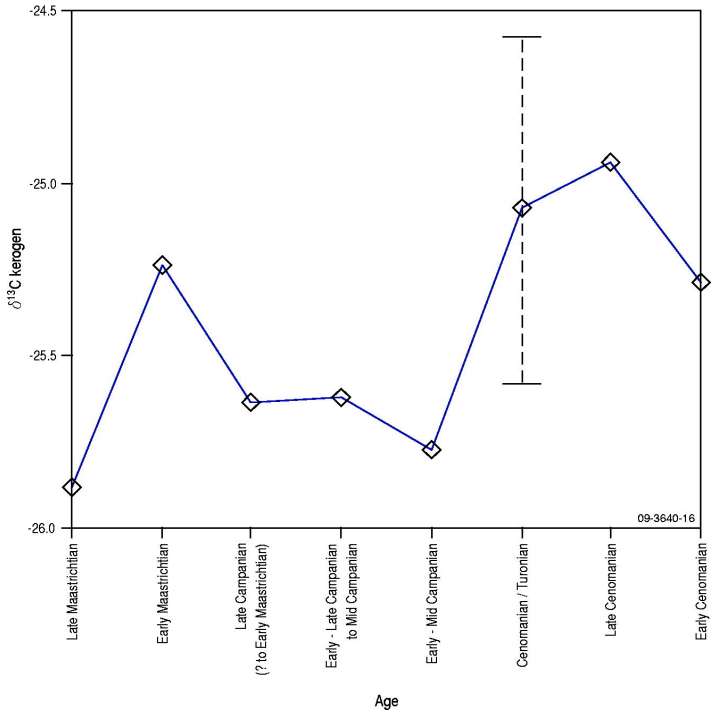

Figure 6.16. *Age distribution of average $\delta^{13}C$ kerogen.*

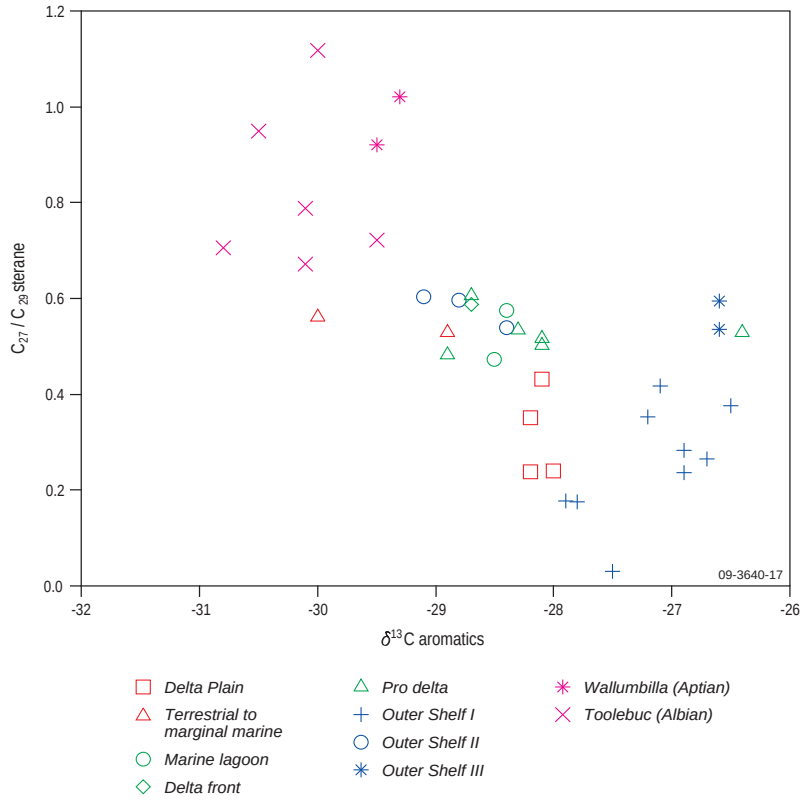

Figure 6.17. *Plot of $\delta^{13}C$ of aromatic hydrocarbons versus C_{27}/C_{29} steranes.*

Metalloporphyrins

The proportion of nickel (Ni) to vanadyl (VO) porphyrins is strongly controlled by the Eh/pH conditions within the water column and shallow sediment. Highly reducing and slightly acidic conditions, together with the presence of excess H_2S, favours the preservation of VO porphyrins

over Ni porphyrins (Lewan, 1984). The high Ni/VO porphyrin ratio (6.1 to 18.3; Appendix 4.9) for the late Cenomanian-early Turonian black shales is consistent with other geochemical parameters, which suggest anoxic conditions only existed below the sediment/water interface. In contrast, VO porphyrins are more abundant than Ni porphyrins in asphaltites (Boreham et al., 2001), which are stranded coastal bitumens that occur along the southern Australian coastline (Edwards et al., 1998), indicating a more reducing depositional environment for their effective source rocks.

Photic zone anoxia

The expansion of the oxic-anoxic boundary within the water column into the photic zone (i.e. photic zone anoxia) can be addressed by the occurrence of C_{40} arylisoprenoids and their degradation products (Summons and Powell, 1987; Koopmans et al., 1996; Brocks et al., 2005). The occurrence of C_{40} isorenieratane, a C_{40} arylisoprenoid biomarker for photosynthetic green sulphur bacteria (Brocks et al., 2005 and references therein), in the Bight Basin samples and some related mid-Cretaceous samples that record oceanic anoxic events (OAE1c and OAE2) is listed in Table 6.1. The Bight Basin samples are characterised by the absence to trace amounts of isorenieratane, while isorenieratane is found in the asphaltites (coastal bitumens), the Albian Toolebuc Formation of the Eromanga Basin (OAE 1c) and 'classical' OAE2 black shales (Kolonic et al., 2005). Such differences are consistent with the metalloporphyrin distributions (Table 6.1).

Carbon isotopes

The carbon isotopic composition of organic matter offers a powerful tool for the characterisation and differentiation of source inputs, as well as providing secular constraints on changes in organic inputs (Tissot and Welte, 1984; Hayes et al., 1999; Peters et al., 2005). Figure 6.16 shows the average carbon isotopic composition of kerogen for eight time intervals between the early Cenomanian and late Maastrichtian. The rather narrow range in $\delta^{13}C_{kerogen}$ of 1.06‰ indicates that the bulk carbon isotopic composition allows minimal differentiate between the various organofacies/depositional environments given that the standard deviation $(\sigma) = \pm 0.3‰$. Nevertheless, kerogens of early Cenomanian–early Turonian age are slightly enriched in ^{13}C compared to younger kerogens. Such a small increase in ^{13}C for the outer shelf C/T black shales is in contrast to the large positive carbon isotopic excursion of up to 6–7‰ for organic carbon found in OAE2 black shales (Tsikos et al., 2004; Erbacher et al., 2005; van Bentum et al., 2007). Additional resolution using carbon isotopes is obtained with the carbon isotopic composition of the aromatic hydrocarbons. Figure 6.17 plots the $\delta^{13}C_{arom}$ against the C27/C29 sterane ratio. The late Cenomanian–early Turonian outer shelf-I and -III organofacies are consistently enriched in ^{13}C compared to the other organofacies/depositional environments.

Global Oceanic Anoxic Event

The mid-Cretaceous was a time when sea levels were the highest of the Phanerozoic, atmospheric CO_2 levels were up to an order of magnitude greater than present day levels and the Earth's (proto)oceans experienced restricted circulation and became stagnated compared to modern oceans due to the arrangement of the land masses (Thurow et al., 1992; Lüning et al., 2004). Hence, the mid-Cretaceous oceans were predisposed to the deposition and preservation of organic matter. The apex of stagnation was reached during the late Cenomanian to early Turonian. During that time there was globally significant deposition of marine, hydrogen-rich Type II organic matter (OM) in black shales. Total organic carbon (TOC) contents of these black shales approached 10%, and therefore represent excellent potential source rocks for oil (Kuypers et al., 2002; van Bentum, 2007). Even some previously euxinic basins fleetingly experienced anoxia extending into the photic zone (Kolonic et al., 2005; Hautevelle et al., 2007).

Superimposed on this black shale deposition was the oceanic anoxic event (OAE) at the Cenomanian/Turonian (C/T) boundary (i.e. OAE2). The cause of this OAE is likely to be the rapid emplacement of new seafloor, via oceanic plateaus and magmatic flows, which resulted in fertilization of oceans (with nutrient-rich hydrothermal fluids) and the atmosphere (with more CO_2), and even higher sea levels. Importantly, these processes occurred over a relatively short timeframe (Kerr, 1998; Turgeon and Creaser, 2008). The Earth's feedback mechanisms became rapidly overloaded and lagged in their response by tens of thousands of years but eventually, after about 500,000 years (the OAE2 interval), had started to approach pre-OAE2 conditions (Lüning et al., 2004). The Earths' oceans still appeared to be very heterogeneous during OAE2 with productivity or preservation models, or a combination of both, being used to explain black shale distribution across high northern latitude epicontinental seas, the northern and southern (proto)Atlantic, the western and southern Tethyan and the equatorial Pacific oceans (e.g. Kuypers et al., 2002 and references therein).

Evidence for OAEs relies on the use of proxies such as biomarkers reflecting environmental niches (e.g. isorenieratane as a marker for photic zone anoxia), redox-sensitive and nutrient-related metal enrichments, organic matter accumulation rates and faunal distributions (e.g. types of foraminifera and dinoflagellates). During the late Cenomanian-early Turonian, organic matter-rich layers were deposited across shallow nearshore to deep pelagic environments in rock types ranging from shales to carbonates, however the outer shelf and upper slope became the main loci for organic matter deposition. The most notable expression of the OAE2 is the prolific preservation of hydrogen-rich, marine organic matter with TOC commonly >10% and up to 50%. Furthermore, with the vast amount of organic carbon being deposited and stored, stable carbon isotopic excursions with enrichments in ^{13}C in organic and inorganic carbon exclusively define the OAE2 within the context of black shale deposition during the late Cenomanian-early Turonian. One feedback mechanism that ensued was a lowering in pCO_2 resulting in a drop in ocean temperatures. Ongoing tectonic movement that opened up oceanic circulation patterns, which are most reminiscent of today, has not again led to such an intense geological storage of marine organic matter.

The Bight Basin contains marine, organic-rich potential oil prone source rocks (TOC to 6.9% and HI to 479 mgHC/gTOC) of late Cenomanian-early Turonian age. Table 6.1 summarises the critical geochemical parameters that define OAE2 and shows how these compare with the Bight Basin C/T sediments and the asphaltites. Also included is the Albian marine Toolebuc Formation, which was previously thought to be an organofacies analogue for the source of the asphaltites (Boreham et al., 2001). For the Bight Basin outer shelf black shales, the notable differences with 'classical' OAE2 black shales are their lack of notable isorenieratane and no predominance of vanadyl porphyrins. Furthermore, no current Bight Basin sediments show prolific (TOC > 10%) organic matter enrichments. However, the most notable difference is the lack of large enrichment in ^{13}C that characterise the OAE2 black shales. Nevertheless, there is sufficient evidence to suggest that the Bight Basin C/T outer shelf-I sediments analysed are part of this intense OAE2 that extended to high southern latitudes.

The asphaltites from strandings along the southern Australian coastline (Edwards et al., 1998) show all the attributes in common with OAE2 organic matter (Table 6.1). Furthermore, the asphaltites are thought to be generated from Cretaceous effective source rocks in the Bight Basin (Boreham et al., 2001). Therefore, it is conjectured that source areas where higher organic matter preservation has occurred under more anoxic conditions in euxinic seas may provide oil-prone 'sweet-spots' of OAE2 black shales. Furthermore, the up-dip position of these dredge site samples suggests that more prospective, mature and generative equivalent successions may lay down-dip towards the Bight Basin's centre and have possibly contributed to the generation of the asphaltites (Totterdell et al., 2008).

Table 6.1. *Comparison of characteristic geochemical parameters between Bight Basin black shales, asphaltites and well-characterised mid-Cretaceous OAE 'black shales'*

Geochemistry	OAE2	Bight Basin	Asphaltite	Toolebuc (OAE1C)
TOC > 10%	Y	N		Y
HI > 400-500 (900)	Y	Y		Y
Marine OM	Y	Y	Y	Y
Anoxic depositional environment	Y	Y	Y	Y
Euxinic (H_2S)	Y	Y	Y	Y
Photic zone anoxia (C_{40} isorenieratane)	Y	N	Y	Y
Outer shelf/upper slope	Y	Y		Y
VO > Ni porphyrins	Y	N (Ni > VO)	Y	Y
+ve $\delta^{13}C$ excursion (up to 6‰)	Y	N?		N

Implications for exploration

For the first time, a world class, marine, oil-prone potential source rock has been proven in the Bight Basin. For these black shales, which are of late Cenomanian-early Turonian age, the most organic-rich and hydrogen-rich sediments were deposited in an outer shelf depositional environment under reducing conditions. The C/T black shales in the Bight Basin draw obvious comparison with world-wide black shales that characterise the oceanic anoxic event (OAE) at the Cenomanian/Turonian boundary, i.e. OAE2. The occurrence of extremely hydrogen-rich and organic-rich C/T sediments at ODP Site 1138 on the Kerguelen Plateau in the southern Indian Ocean (Meyers et al., 2007) would suggest that mid-Cretaceous euxinic seas extended to extremely high southern latitudes and that OAE2 most likely affected the entire global ocean.

Although source richness is not a risk factor in the Bight Basin, the low maturity of the dredged Bight Basin black shales precludes the generation of petroleum at these sites. The location of the sample sites is at the up-dip exposure of the sedimentary succession, however, a sequence boundary at the base of the Turonian has been interpreted across the basin, and reaches depths of up to 9 km (i.e. gas mature) in the thickest part of the Ceduna Sub-basin. Source areas where higher organic preservation has occurred under more anoxic conditions in euxinic seas may provide oil-prone 'sweet-spots'. Burial and maturation history modelling suggests that these intervals have made a significant contribution to black oil prospects in the Bight Basin (Totterdell et al., 2008). Furthermore, the close geochemical similarity between the Bight C/T black shales and the marine asphaltites (coastal bitumens) would suggest a genetic relationship between the two and an active petroleum system in the Bight Basin.

7. Hydrocarbon Seepage Survey Results

G. Ryan, G. Logan & E. Grosjean

INTRODUCTION

The analysis of the Bight Basin survey data with respect to potential hydrocarbon seepage is discussed in this section. Data sets analysed in order to detect potential seepage include: sidescan sonar, echosounder profiles and swath multibeam bathymetry for geomorphology; sediment samples (grabs, gravity cores and dredges) for surface sedimentology; sub-bottom profiler data and gravity cores for the shallow stratigraphy; and underway Acoustic Doppler Current Profiler (ADCP) recordings for oceanography. The geomorphological and sedimentological analyses are used to identify seafloor features that can be indicative of seepage including carbonate hard-grounds and pockmarks. Analysis of the shallow stratigraphy can identify indicators of shallow gas or fluid within sub-bottom profiler data or anomalous concentrations of hydrocarbons from geochemical analysis of the gravity cores. The underway ADCP data, which was not recorded down to the seabed during this survey, was of limited use for the assessment of seafloor processes and current affects on seepage plumes. Therefore, this data is included as an appendix (Appendix 5).

The geomorphology, sedimentology, and shallow stratigraphy is described for each area of interest. Geochemical analysis of selected gravity cores is included for high priority areas 2c, 3 and 6.

REGIONAL GEOMORPHOLOGY

The Great Australian Bight (GAB) comprises a broad continental shelf, a wide continental slope including two marine terraces (Eyre and Ceduna terraces), and a narrow continental rise (Rollet et al., 2001). The shelf reaches a maximum width of 260 km in the centre of the GAB and the shelf-break is identified at around the 200 m isobath (Richardson et al., 2005; Rollet et al., 2001). The lower shelf slopes down onto the wide submarine terraces before the seafloor plunges to abyssal depths (Hine et al., 2004). The location of the survey areas of interest is shown in Fig. 1.1, and their geomorphic setting is summarised in Table 7.1.

A comprehensive review of the geomorphology, sedimentology and oceanography of the survey area is provided in Hughes et al. (2009).

REGIONAL SEDIMENTOLOGY

Most of the GAB continental shelf is dominated by a thin veneer of modern skeletal carbonate grains (Holocene) and older carbonate material (Late Pleistocene) covering Cenozoic limestone (Richardson et al., 2005; Hughes et al., 2009). Carbonate sedimentation dominantly occurs on the outer shelf, resulting in oceanward progradation of the platform over time (James et al., 2001). Below about 300 m water depth the surface sediment is dominantly spiculitic carbonate and on the terraces there is a thin veneer of pelagic calcareous ooze and mixed terrigenous-carbonate sand, silt and mud rich in skeletal carbonate fragments (Davies et al., 1989; James et al., 2001; Richardson et al., 2005). The middle to lower slope sediments consist of foraminiferal-nannofossil oozes (Feary et al., 1993; Richardson et al., 2005). The surface sediment was sampled during this survey by grabs, gravity cores and dredges.

Table 7.1. Geomorphic setting of the survey areas.

Survey Area	Geomorphic setting	Water Depth
1	Shelf-break	130 – 700 m
2	Marine terrace (Ceduna Terrace)	1000 – 1750 m
3	Lower shelf slope to marine terrace (Ceduna Terrace)	550 – 1100 m
4	Marine terrace (Ceduna Terrace) to continental rise	1100 – 2600 m
5	Continental rise	2000 – 3000 m
6	Continental rise to abyssal	3000 – 4000 m
7	Marine terrace (Ceduna Terrace)	1800 – 2800 m
8	Continental rise to abyssal	3700 – 4700 m
9	Marine terrace (Ceduna Terrace)	1400 – 2300 m

REGIONAL SHALLOW STRATIGRAPHY

The Ocean Drilling Program (ODP) Leg 182 drilled 27 holes at nine sites over the slope and continental rise in the western Great Australian Bight, on the Eyre Terrace (Fig. 7.1; Feary et al., 2004; Li et al., 2004). This drilling has provided a good understanding of the shallow stratigraphy and its age constraints. Therefore, the ODP data were used in this study to help constrain and interpret the sub-bottom profiler data from this survey.

The Cenozoic succession intersected by Leg 182 drilling comprises Paleocene to mid-Eocene sequences of terrigenous clastics, and mid-Eocene to Quaternary primarily carbonate marine sediments (Li et al., 2004). Carbonate deposition during the Middle Eocene to early Middle Miocene occurred in a cool-water ramp environment. A barrier reef system developed during the early middle Miocene, and is located under the present day mid shelf. Late Middle Miocene gentle uplift, tilting and global sea level fall (mega-hiatus 1 (MH1) of Li et al., 2004) terminated the reef growth (Feary & James, 1998). The Late Miocene to Early Pliocene is represented by cool water lowstand wedge and ramp deposition followed by marine erosion (mega-hiatus 2; Feary & James, 1998; Li et al., 2004). The Pliocene to Quaternary section comprises a thick succession of cool-water carbonates. The Pliocene and Quaternary packages are separated by the Neogene mega-hiatus 3 (Li et al., 2004). In the absence of any other stratigraphic control, tentative correlation of the mega-hiatuses identified by Li et al. (2004) to breaks identified in the stratigraphic succession imaged in the sub-bottom profiler data in the GAB, has been used to provide a possible control on the age of that succession.

In the ODP holes drilled on the Eyre Terrace (Fig. 7.2), Lower Miocene sediments are characterised by brown-dark grey wackestone and light grey-cream packstone, both with abundant quartz silt in a carbonate (low Mg calcite) matrix. The middle Miocene succession comprises buff coloured, low-Mg calcite mudstone to mud-rich wackestone. The upper Miocene section contains massive, white to light grey wackestone to mudstone with burrowings. The Pliocene unit is characterised by slumps and gravity flow deposits at the middle and lower slope. These sediments include bioclastic packstones at the upper slope sites (Li et al., 2004).

The early Miocene corresponds to a time of cyclical carbonate deposition and active quartz silt transport from the continent (Li et al., 2004). The sedimentation rate during the Early and Middle Miocene was 10–15 m/Myr, and during the late Miocene, 14–28 m/Myr (Li et al., 2004). The Pliocene had similar sedimentation rates to the late Miocene. The upper slope had rapid sedimentation during the Pleistocene (180–200 m/Myr) reflecting an increased productivity during sea level lowstands that triggered prolific bryozoan growth (Li et al., 2004).

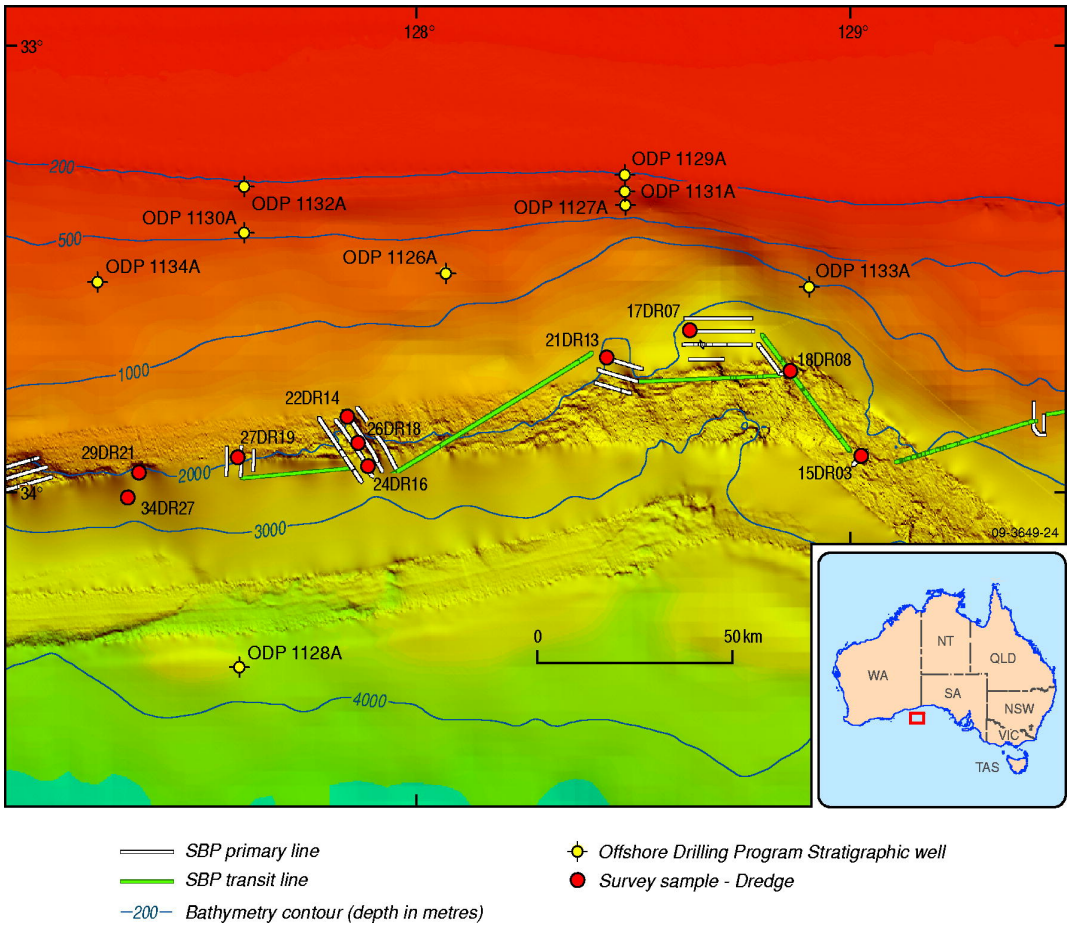

Figure 7.1. *Location of ODP Sites on regional bathymetry (250 m GA bathy grid red=100 m blue=4000m). Location of Area 5 sub-bottom profiler lines and samples illustrated.*

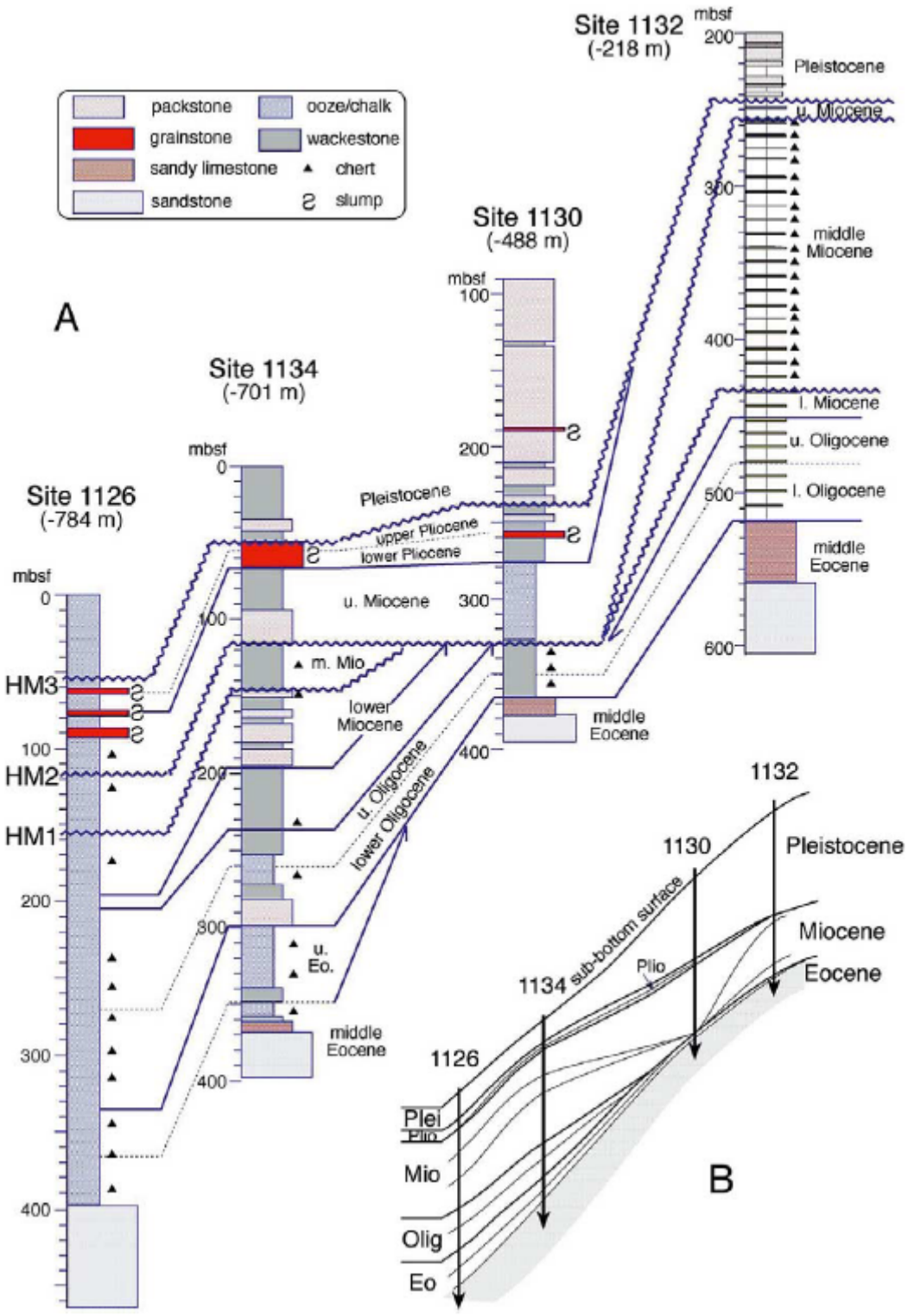

Figure 7.2. *Stratigraphic correlation diagram for ODP Leg 182 sites on the Eyre Terrace (from Li et. al., 2004)*

SURVEY AREA RESULTS

Area 1

Introduction

Area 1 is located on the continental shelf-break above the northern margin of the Ceduna Sub-basin (Fig. 1.1). This area was targeted for a study of potential seepage due to the presence of basin margin faults in close proximity to the pinchout edge of Cretaceous units (Fig. 7.3). Third rank Synthetic Aperture Radar (SAR) slicks occur along the sub-basin margin within Area 1 (Fig. 7.4), and three second rank slicks about 25 km north of the southeastern end of Area 1.

The third rank SAR slicks are located over areas of shallow basement overlain by Late Cretaceous and Tertiary sediments. These SAR features may be an indication of liquid hydrocarbons that have migrated from the Ceduna Sub-basin down-dip, and accumulated in stratigraphic or structural traps near the basin margin (Struckmeyer et al., 2002). The thinning or increasing grain size of the regional seal and faults intersecting the seafloor at the shelf break could lead to leaking of the hydrocarbon accumulations (Struckmeyer et al., 2002).

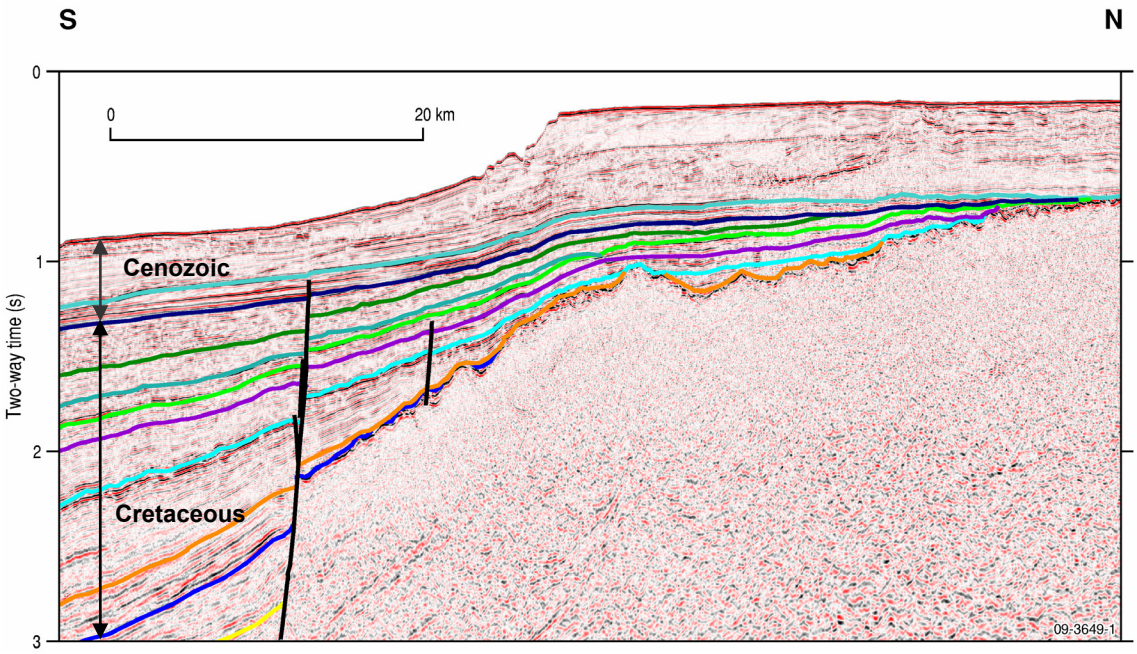

Figure 7.3. *Regional seismic line over Area 1 displays mid-Late Cretaceous strata pinching-out over shallow basement.*

Seabed Morphology and Sedimentology

In Area 1, the continental shelf break has a 1 to 6° slope between 150 and 700 m water depth, decreasing onto the wide submarine Ceduna Terrace (James & von der Borch, 1991; Hine et al., 2004). There is very little surface drainage into the GAB, resulting in a very low supply of terrigenous material to the ocean. Therefore, the shelf sediments are mostly carbonate (James & von der Borch, 1991). The shelf contains a very thin layer of Holocene carbonate sediment that is underlain by Cenozoic (Eocene-Middle Miocene) limestone (James et al., 2001).

The multibeam swath data acquired during this survey indicates that the shelf edge has an uneven surface, probably a karst-weathered limestone surface. Where imaged in Area 1, the shelf break forms an abrupt and highly irregular 30-50 m high cliff-like feature between 180 to 210 m water depths, with boulders or rubble present at its base. In the southern part of Area 1 there are numerous southwest trending channelised canyon features around 1 km wide that are almost regularly spaced (4-8 km) (Fig. 7.4).

Sidescan sonar data were collected over the southern shelf transect in Area 1. The features observed in this data on the shelf include dark reflections on the seafloor that might be related to limestone outcrop or patches of bryozoans (Fig. 7.5). The data collected over the shelf break also indicates a very dark seafloor reflection that is likely to be related to outcropping limestone. No obvious seafloor features that could be related to seepage were detected in the sidescan sonar data collected over this area

Several interesting water column features, however, were observed in both the echosounder and sidescan sonar data in the northwestern end of Area 1. These features could be either biological (e.g. plankton or fish) or related to seepage flares (Fig. 7.6) Other possible evidence for seepage in this area is provided by two 3rd rank SAR slicks and the presence of vertical disruption zones in the underlying regional seismic data (Fig. 7.7).

Details of the seabed samples collected in Area 1 are provided in Table 7.2. The seabed at the base of the slope comprised grey-green calcareous mud with abundant corals and shell grit in some areas. No underwater video footage was acquired in Area 1.

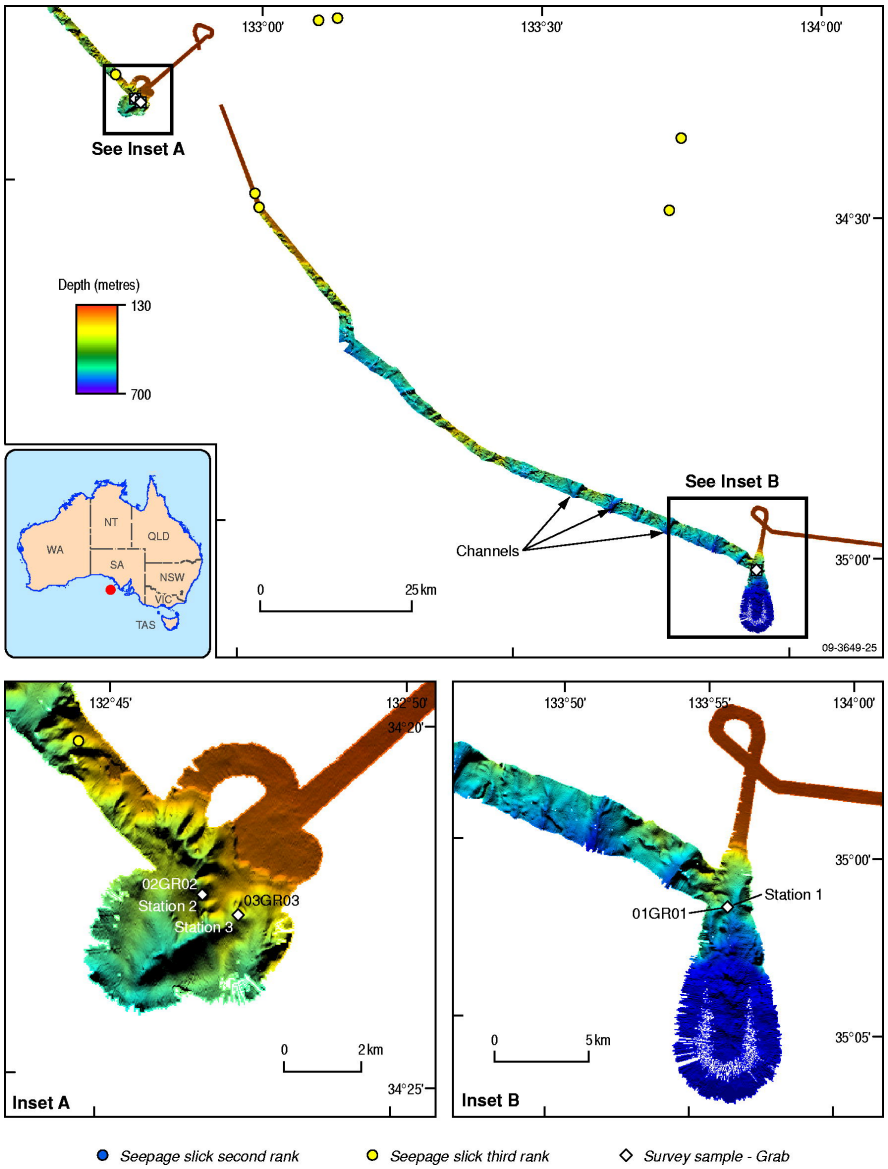

Figure 7.4. *Multibeam swath data acquired over Area 1 with sample locations. SAR slicks from Struckmeyer et al. (2000).*

***Table 7.2**: Area 1 samples*

Sample Type	Station number	Sample number	Brief description
Grab	Station 01	01GR01	Grey-green calcareous mud. Contains some forams and minor very delicate bivalve fragments. Fine grained and generally homogeneous with minor grey patches.
Grab	Station 02	02GR02	Poor recovery due to coarse coral. Shell grit, shell fragments and coral fragments.
Grab	Station 03	03GR03	Mud with fine–medium grained shell and coral fragments.
Gravity Core	Station 01	01GC01	4 m. Base of core is greyish-green, unstructured, sticky calcareous mud. Upper core is slightly different colour but has similar lithology.
Gravity Core	Station 02	01GC02	1.2 m. Pale green, unstructured, sticky calcareous mud, no bedding or coarser fragments.
Gravity Core	Station 03	02GC03	5.1 m. Pale greenish grey, poorly sorted, clay to sand size fragments. Coarser clasts mainly bioclasts, horizons with abundant bryozoan fragments to 4 cm. H_2S smell.
Gravity Core	Station 04	02GC04	5 m. Pale greenish grey, poorly sorted, clay to sand size fragments. Coarser clasts mainly bioclasts, horizons with abundant bryozoan fragments to 4 cm. Slight H_2S smell.
Gravity Core	Station 05	03GC05	5.3 m. Pale greenish-grey mud, poorly sorted mixture of clay and sand size bioclasts. Sparse horizons with abundant bryozoan fragments. H_2S smell.
Gravity Core	Station 06	03GC06	5.1 m. Pale greenish-grey mud, poorly sorted mixture of clay and sand size bioclasts. Sparse horizons with abundant bryozoan fragments. H_2S smell.

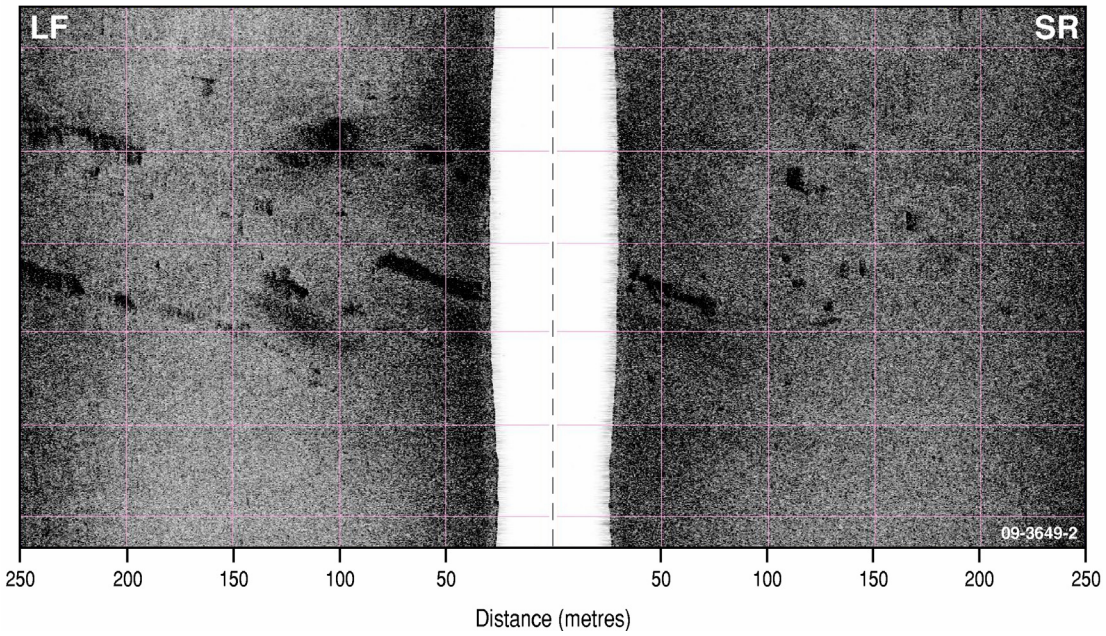

Figure 7.5. *Sidescan sonar image of dark reflections imaged on the shelf.*

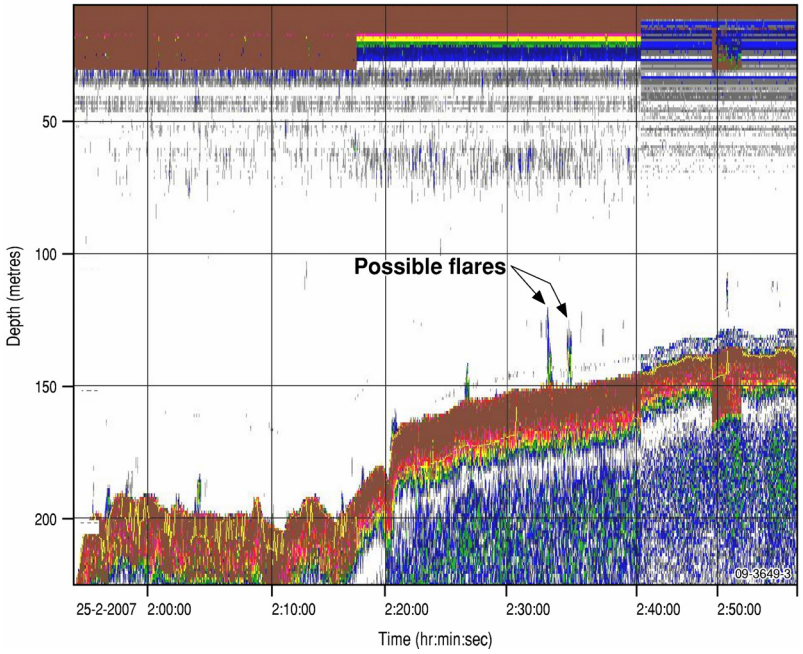

Figure 7.6. *Echosounder data from Area 1 displaying water column flares.*

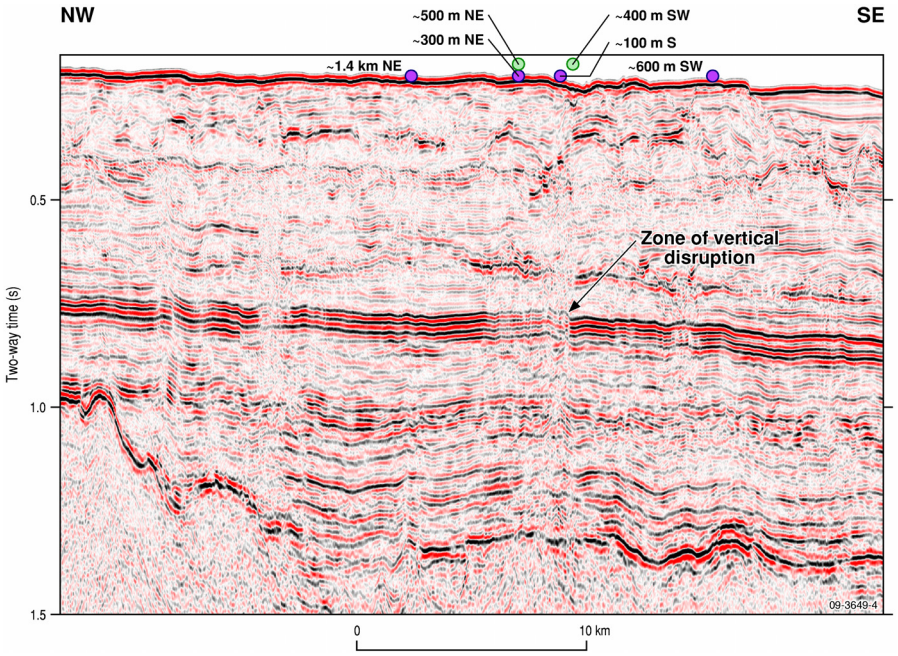

Figure 7.7. *Seismic line s216-206m underlying the echo-sounder flares (purple circles - text indicates distance and direction the feature is offset from the seismic line) and SAR slick locations (green circles). Both third rank SAR slicks and some of the echo-sounder flares are located above an area of vertical disruption in the seismic data.*

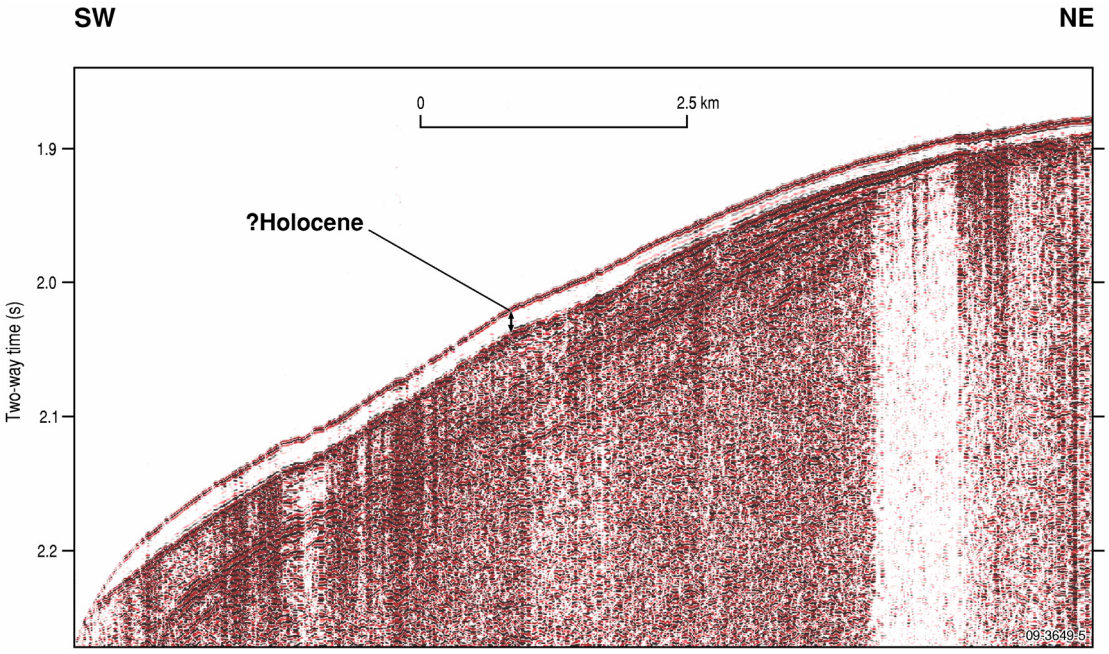

Figure 7.8. *Sub-bottom profile showing stratigraphy of the shelf slope in Area 1.*

Stratigraphy

The regional seismic data from Area 1 indicate the presence of a zone of normal faulting and slumping along the shelf edge (James et al., 2001). The shallow stratigraphy of Area 1 interpreted from sub-bottom profiler data includes probable Cenozoic limestone overlain by a thin veneer od sediment, isolated pockets of sediment cover of possible late Pleistocene to Holocene age (Fig. 7.8), and an older hard unit (limestone) overlain by a stratified unit (possibly early Pleistocene in

age), which is overlain in turn by a thin probable late Pleistocene to Holocene sediment cover (0.01s) (Fig. 7.9). The unit interpreted as a Cenozoic limestone is represented by a strong reflection that results in a loss of seismic penetration in the sub-bottom profiler data below. This unit is present in the area where the 3rd rank SAR slicks occur, and the subsequent poor seismic quality precludes identification of any fluids possibly seeping through these units.

Two gravity cores were taken on the southern shelf break transect in Area 1, one with 4 m penetration and one with 1.2 m penetration. Both these cores were taken in the same location on the shelf slope and both recovered greyish-green, unstructured sticky calcareous mud (Table 7.2). Four gravity cores were taken on the shelf break on the northern transect in Area 1. All these cores penetrated about 5 m into greenish grey mud that was poorly sorted with clay to sand sized fragments and bryozoan fragments. These four cores were noted to have an H_2S odour and may have penetrated the well stratified unit interpreted in the sub-bottom profiler data.

The transit from Area 1 to Area 2b contained some possible shallow gas indicators within the sub-bottom profiler data. These indicators are located over an area of intense basin margin faulting, where the Oligocene and younger sediments are not present and where there is a topographic depression at the base of slope (Fig. 7.10). Attribute analysis of the sub-bottom profiler data indicates enhanced amplitudes with low frequency and reversed polarity. However, as there were no raw sub-bottom profiler data available over this line the interpretation of the attribute analysis is tentative.

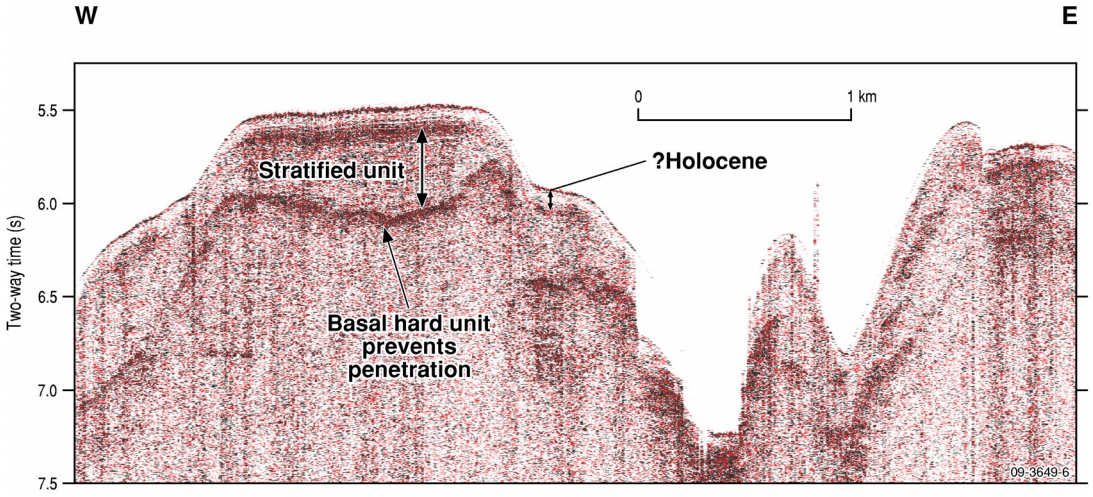

Figure 7.9. *Sub-bottom profile illustrating the stratigraphy on shelf slope in Area 1. The stratified unit above hard layer (?limestone) is draped with acoustically transparent, thin ?Holocene sediment.*

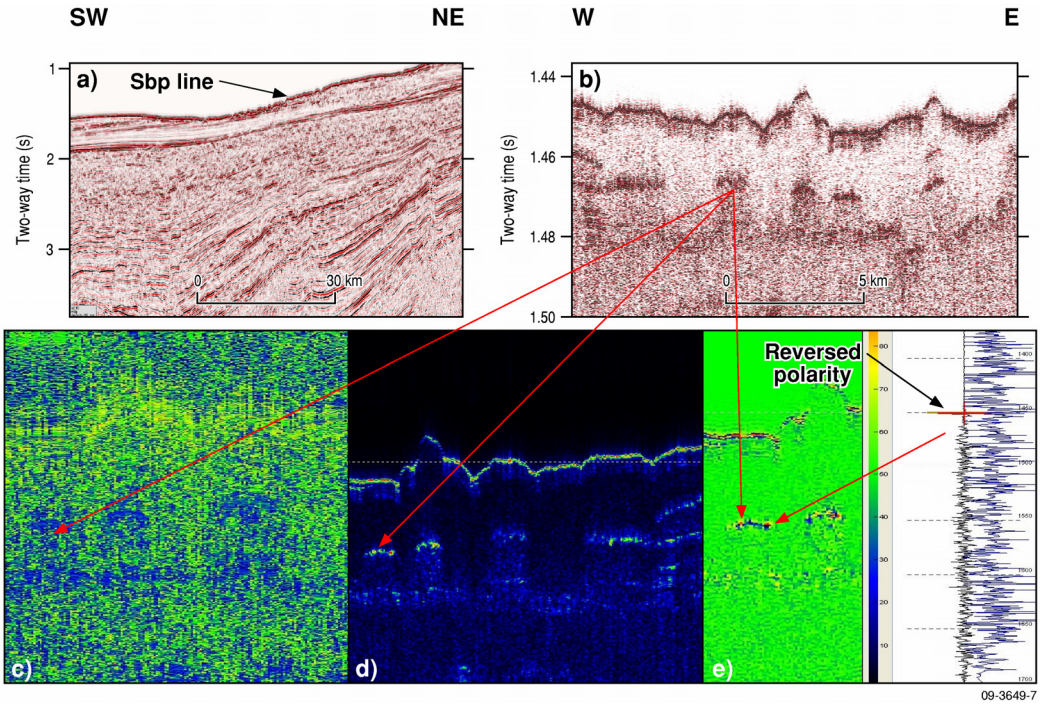

Figure 7.10. *Possible indications for shallow gas/fluid. (a) Seismic line DWGAB-10r illustrates sub-bottom profiler (sbp) line location where the Oligocene and younger units are interpreted to be missing. (b) sbp image of shallow enhanced reflections within upper acoustically transparent layer. (c) Instantaneous frequency displays enhanced reflections as low frequency (blue). (d) Instantaneous amplitude displays the reflections as high amplitude (light colours). (e) Apparent polarity indicates the enhanced reflections are reversed in polarity (dark colours)y, also indicated in wiggle trace.*

Area 2

Introduction

Area 2 is located on the Ceduna Terrace above the central Ceduna Sub-basin (Fig. 1.1). This area was targeted for potential seepage sites associated with SAR slicks above possible shallow gas concentrations, as indicated in regional seismic data (Fig. 7.11).

Area 2 is subdivided into three sub-areas (Fig. 7.12). Area 2a is located about 15 km south of the northern Ceduna Sub-basin boundary. This area is associated with two third rank SAR slicks and one second rank SAR slick. The regional seismic data in Area 2a show a canyon that cuts down to a horizon interpreted as a major Oligocene unconformity. This horizon shows variable seismic reflection characteristics, with very bright positive amplitudes in places, particularly where the horizon shallows and outcrops (Fig. 7.13). Given the presence of SAR slicks in this area, which may indicate present-day seepage, sampling sites in Area 2a were chosen to test the possibility that these bright amplitudes may be Hydrocarbon-Related Diagenetic Zones (HRDZ; O'Brien & Woods, 1995) related to palaeo-seepage. Area 2b is located about 30 km south of Area 2a and is associated with two second rank SAR slicks. This area transects a canyon where the Oligocene sediments are shallow or exposed at the seabed (Fig. 7.14). Regional seismic data indicate a series of enhanced reflections with reversed polarity, within the Hammerhead Supersequence, that are interpreted as coaly beds. Area 2c is located about 65 km southwest of Area 2b. This area overlies reversed polarity, enhanced reflections within the sediments above the base Oligocene horizon (Fig. 7.15).

***Table 7.3**: Area 2a samples*

Sample Type	Station number	Sample number	Brief description
Grab	Station 05	05GR05	Pale green/grey calcareous mud; contains minor forams.
Grab	Station 06	06GR06	Grey calcareous ooze, very fine-grained; contains minor fine-grained dark material.
Gravity Core	Station 05	05GC09	4.5 m. Pale greenish grey, sticky clay, and sandy clay as mottles and thin bands. Sandy areas comprise slightly greener zones with fine- to medium-sized sand grains of quartz, rare brown grains and shell fragments.
Gravity Core	Station 05	05GC10	4.75 m. Pale greenish-grey, very sticky calcareous ooze, minor gritty components (?forams). Slight H_2S smell. Shelly material (pteropods?) abundant near top of core, and bioturbation.
Gravity Core	Station 06	06GC11	5.1 m Pale greenish-grey, very sticky, slightly calcareous ooze. Minor gritty components (?forams), pteropods common. Bioturbated.
Gravity Core	Station 06	06GC12	5.17 m. Pale greenish-grey, very sticky, slightly calcareous ooze. Minor gritty components (?forams), pteropods common. Bioturbated.

***Table 7.4**: Area 2b samples*

Sample Type	Station number	Sample number	Brief description
Grab	Station 04	04GR04	Fine sticky ooze (2.5Y 7/1)
Gravity Core	Station 04	04GC07	4 m. Pale, slightly bluish-grey, sticky, calcareous ooze. Slightly gritty in part (?forams). Bioturbation near surface.
Gravity Core	Station 04	04GC08	4 m. Pale, slightly bluish-grey, sticky, calcareous ooze. Scattered small pebbles of white, chalky limestone.

***Table 7.5**: Area 2c samples*

Sample Type	Station number	Sample number	Brief description
Grab	Station 45	45GR17	Pale brown/beige calcareous ooze.
Gravity Core	Station 45	45GC35	2.1 m. Calcareous foraminiferal ooze. Light greenish grey, at top to white at base. Common forams and spicules.
Gravity Core	Station 45	45GC36	1.5 m. Light greenish grey, calcareous foraminiferal ooze. Abundant forams and minor spicules.
Gravity Core	Station 46	46GC37	2.4 m. Calcareous foraminiferal ooze; forams more abundant towards surface. Colour changes from pale yellow at surface to light grey and white at base.
Gravity Core	Station 46	46GC38	2.6 m. Calcareous foraminiferal ooze. Colour changes from pale yellow at surface to light grey and white at base.
Gravity Core	Station 47	47GC39	3.1 m. Calcareous foraminiferal ooze. Light grey at top, white at base
Gravity Core	Station 47	47GC40	4.5 m. Calcareous foraminiferal ooze. Light grey to white at base with dark grey streaks throughout.
Gravity Core	Station 48	48GC41	3.4 m. Light grey calcareous foraminiferal ooze with dark grey streaks
Gravity Core	Station 48	48GC42	2.5 m. Light grey at top to white at base calcareous foraminiferal ooze with dark grey streaks.
Gravity Core	Station 49	49GC43	1.8 m. Light grey to pale yellow at base calcareous foraminiferal ooze
Gravity Core	Station 49	49GC44	3.6 m. Grey calcareous foraminiferal ooze with local zones of light greenish grey and grey to black.
Gravity Core	Station 50	50GC45	3.2 m. Pale grey, sticky, stiff foraminiferal mud, slightly calcareous. Top 50 cm is beige, loose, calcareous ooze.
Gravity Core	Station 50	50GC46	3.4 m. Pale grey stiff, sticky foraminiferal mud. Gritty texture from forams and has minor darker mottles.
Gravity Core	Station 51	51GC47	2.2 m. Pale greenish grey calcareous foraminiferal gritty mud.
Gravity Core	Station 51	51GC48	2.3 m. Pale grey calcareous foraminiferal mud. Very smooth to slightly gritty.

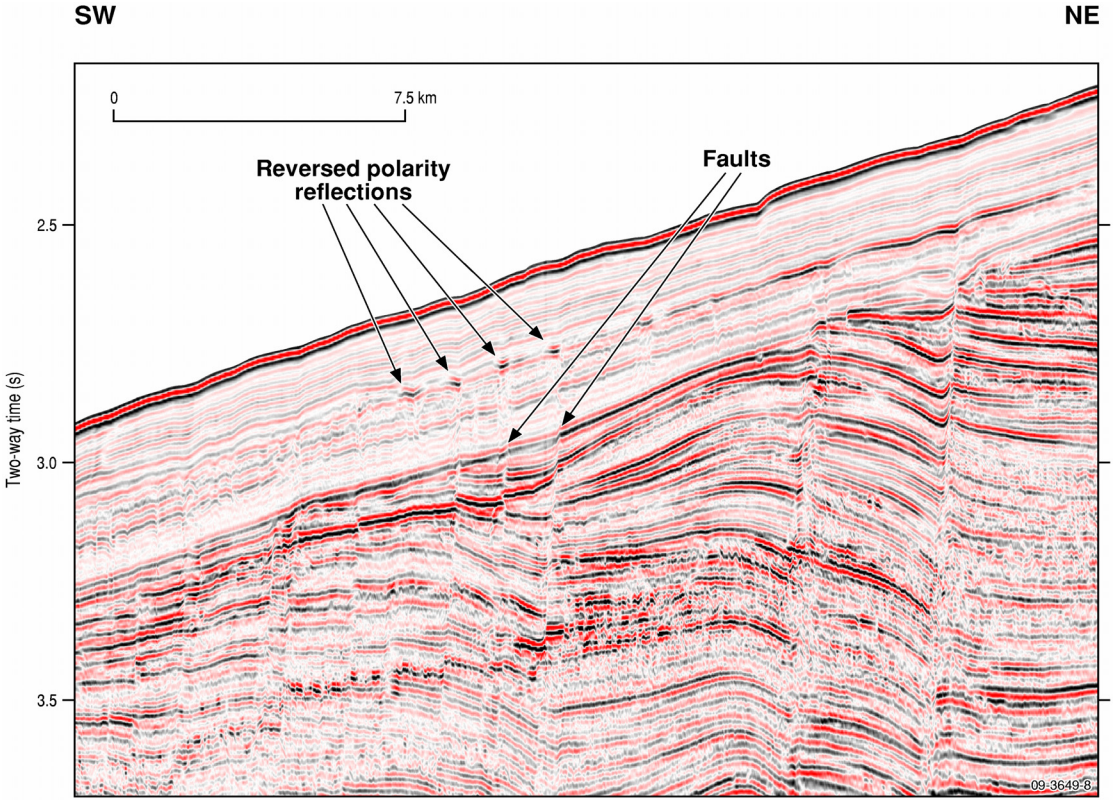

Figure 7.11. *Reversed polarity reflections above faults may be an indication of migrating hydrocarbons and minor shallow gas accumulations (Flinders survey line 17).*

Seabed Morphology and Sedimentology

Area 2 is located on the wide submarine Ceduna terrace which dips seaward at less than 1° (James & von der Borch, 1991).

Area 2a

The multibeam swath data collected over Area 2a show that the seabed slopes from northwest and southeast into the centre of the area where a shallow canyon extends to the south (Fig. 7.16). The area is the shallowest in the northwest at 1000 m water depth and has a series of shallow canyons (100 to 400 m width; ~ 2 km long) that initiate from the break in slope and trend south-southeast. Samples of the seabed in Area 2a include 2 grabs and 4 gravity cores (Table 7.3). The samples taken in the western end of Area 2a (Station 06) are located above a topographic rise between two channels and consist of pale greenish-grey sticky calcareous ooze. The samples taken in the centre of Area 2a (Station 05) within the canyon (~1200 m) are pale green-grey calcareous mud. These sediments are likely to be younger than those found at Station 06.

Area 2b

The multibeam swath data acquired over Area 2b indicate a NE-SW trending shallow canyon (~8 km wide) that runs through the centre of the area and is about 100 m deep (between 1350-1450 m) (Fig. 7.17). The canyon is floored by at least 3 narrowly incised, very straight rills of the same orientation as the canyon. Samples of the seabed were taken at one station (Station 04) located near the centre of the canyon. The sediment collected from one grab and two gravity cores was pale, slightly bluish-grey, sticky calcareous ooze (Table 7.4).

Area 2c

The multibeam swath data acquired over Area 2c indicates the presence of a gentle slope (about 1°) down to the southwest with a highly irregular, very subtle escarpment at around 1670 m (Fig. 7.18). A series of very shallow, NE-SW oriented channels extend from the escarpment. Samples of the seabed in Area 2c include 1 grab and 14 gravity cores (Table 7.5). The grab (Station 45) collected pale brown/beige calcareous ooze and the gravity cores (Stations 46–51) recovered light grey to beige and pale yellow calcareous foraminiferal ooze at the seabed.

No underwater video footage or side-scan data were acquired in Area 2 and there were no obvious indications on the seafloor that could be related to potential seepage.

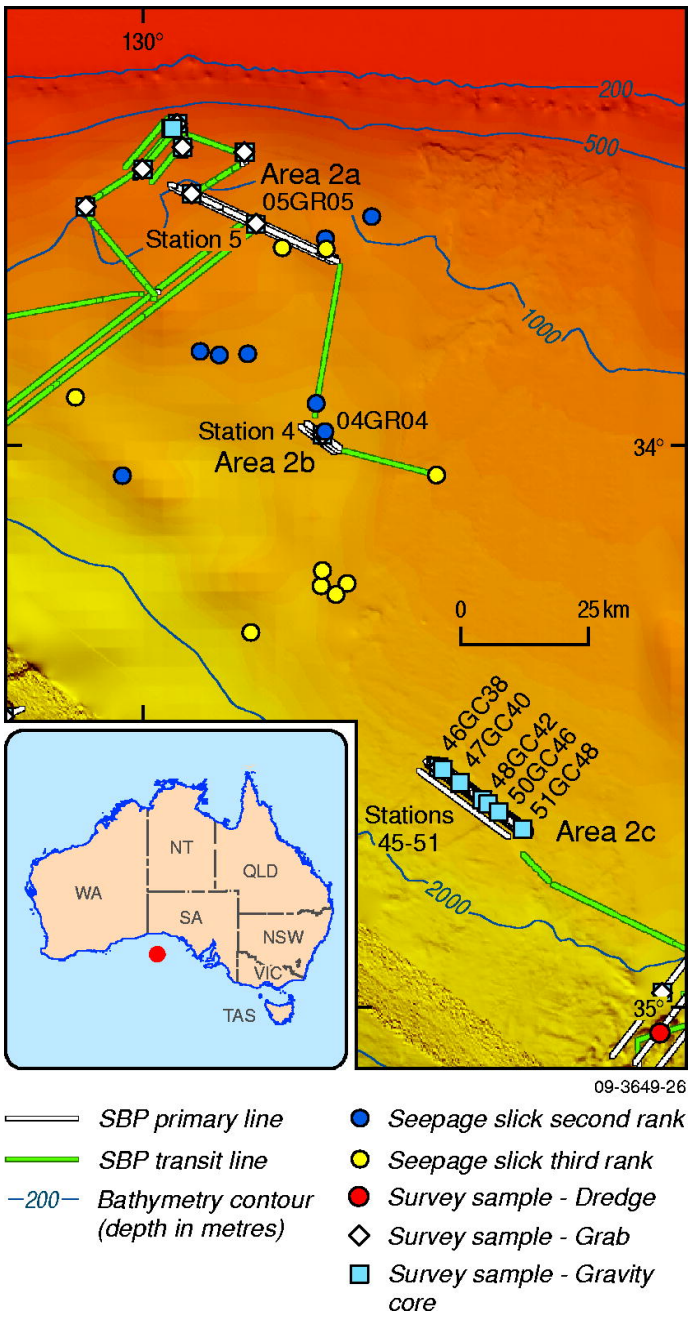

Figure 7.12. *Area 2 subdivision with sample and SAR slick locations (Struckmeyer et al., 2000).*

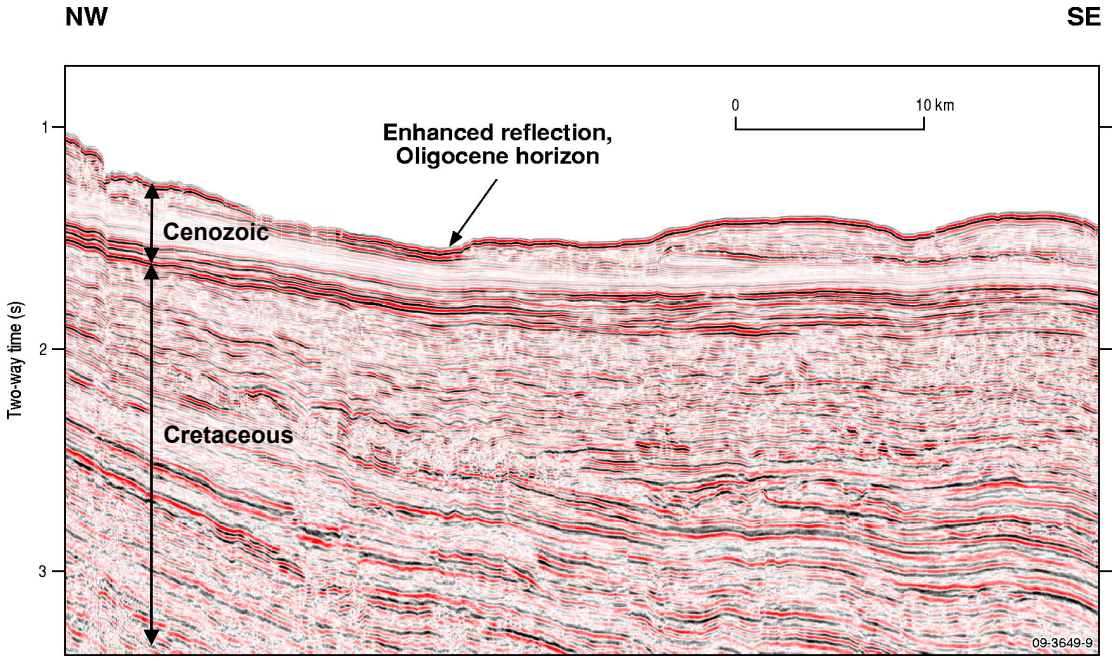

Figure 7.13. *Regional seismic line in Area 2a. Note the enhanced reflector, interpreted to be the Oligocene unconformity, exposed near the seabed.*

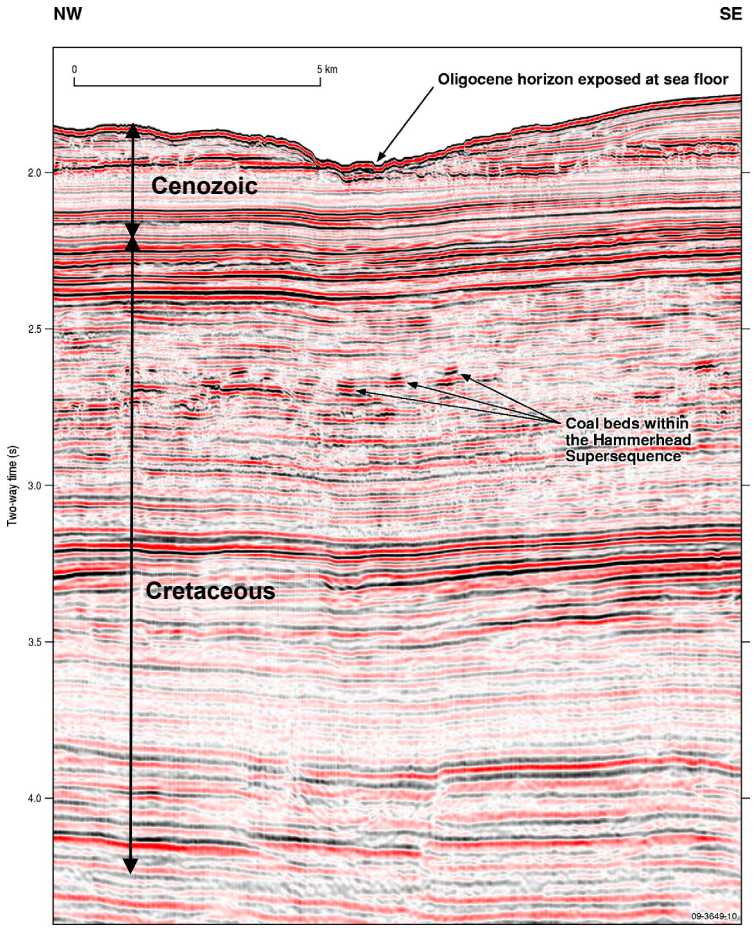

Figure 7.14. *Regional seismic line in Area 2b displaying the near-surface Oligocene horizon (bright reflection at 2.0 s (TWT) on left of image) and interpreted coal beds within the underlying Hammerhead Supersequence.*

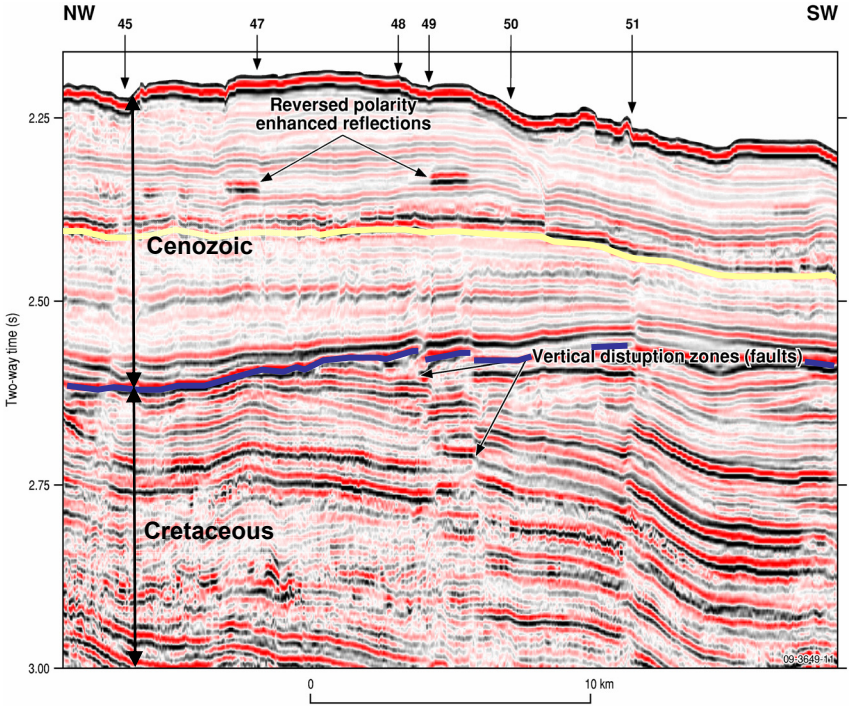

Figure 7.15. *Regional seismic line in Area 2c. Station numbers of sample locations are labelled, and the Oligocene horizon (yellow) and base Cenozoic horizon (dark blue) are shown. Note disrupted reflection character in upper Cenozoic section at around 2.25 s (TWT), top left of image.*

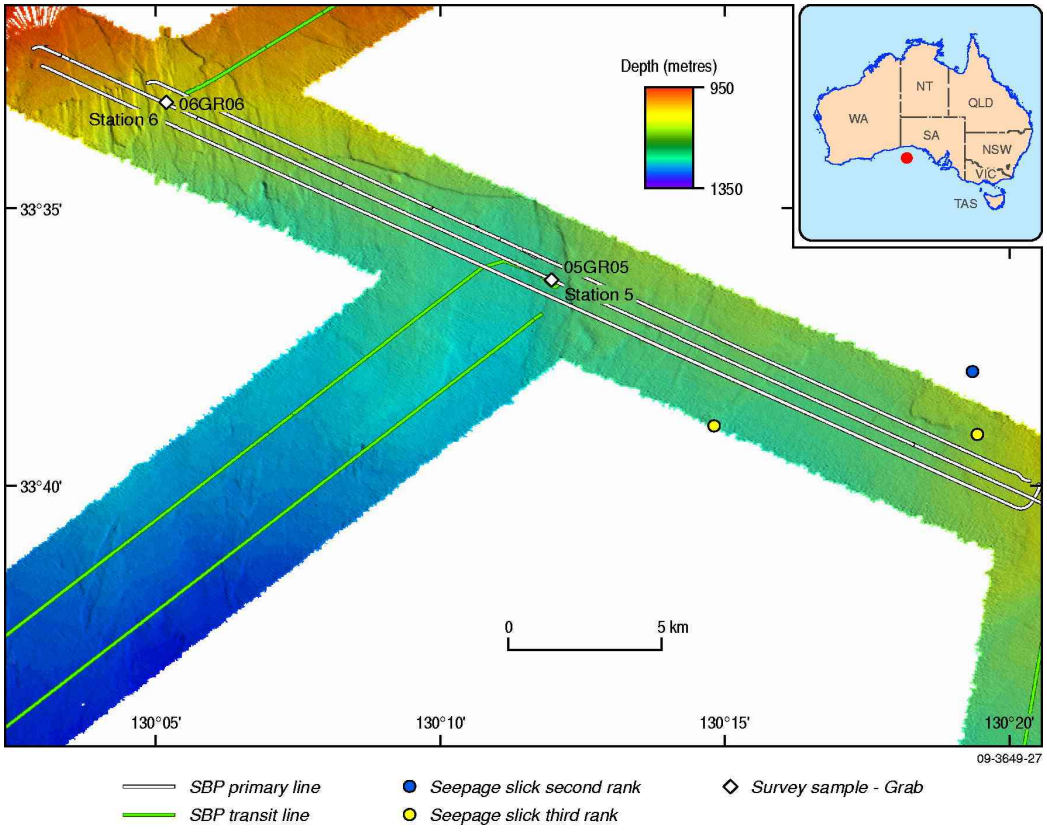

Figure 7.16. *Multibeam swath bathymetry over Area 2a showing location of SAR slicks (Struckmeyer et al., 2000).*

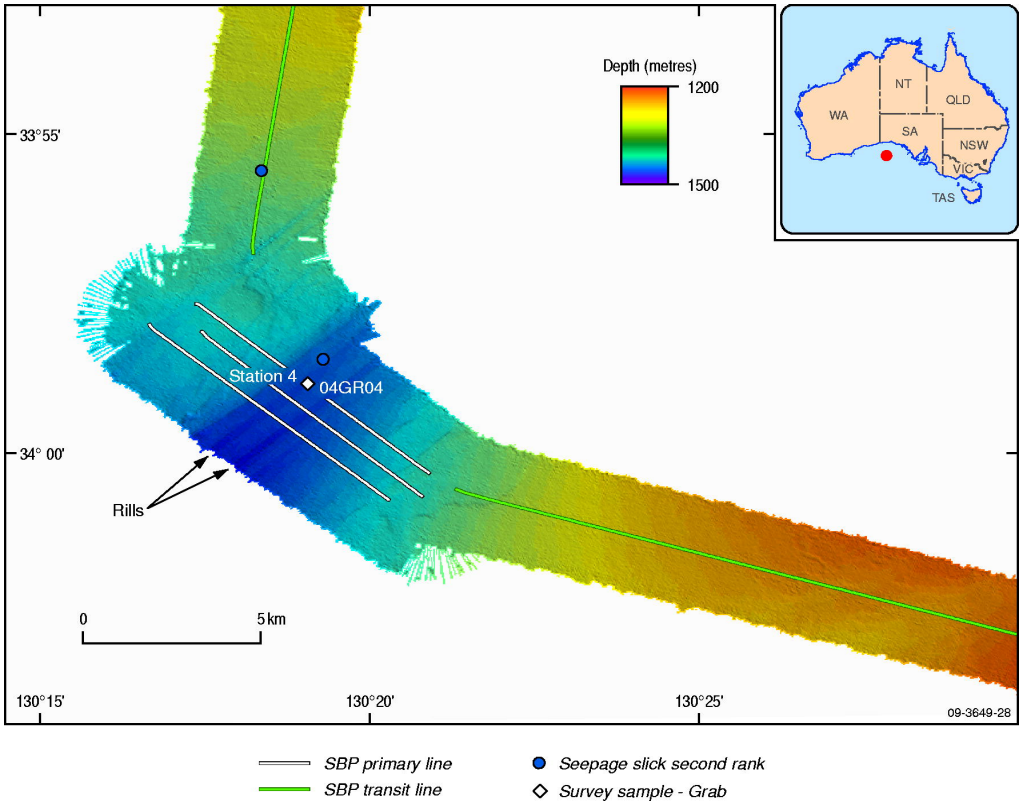

Figure 7.17. *Multibeam swath bathymetry over Area 2b showing location of SAR slicks (Struckmeyer et al., 2000).*

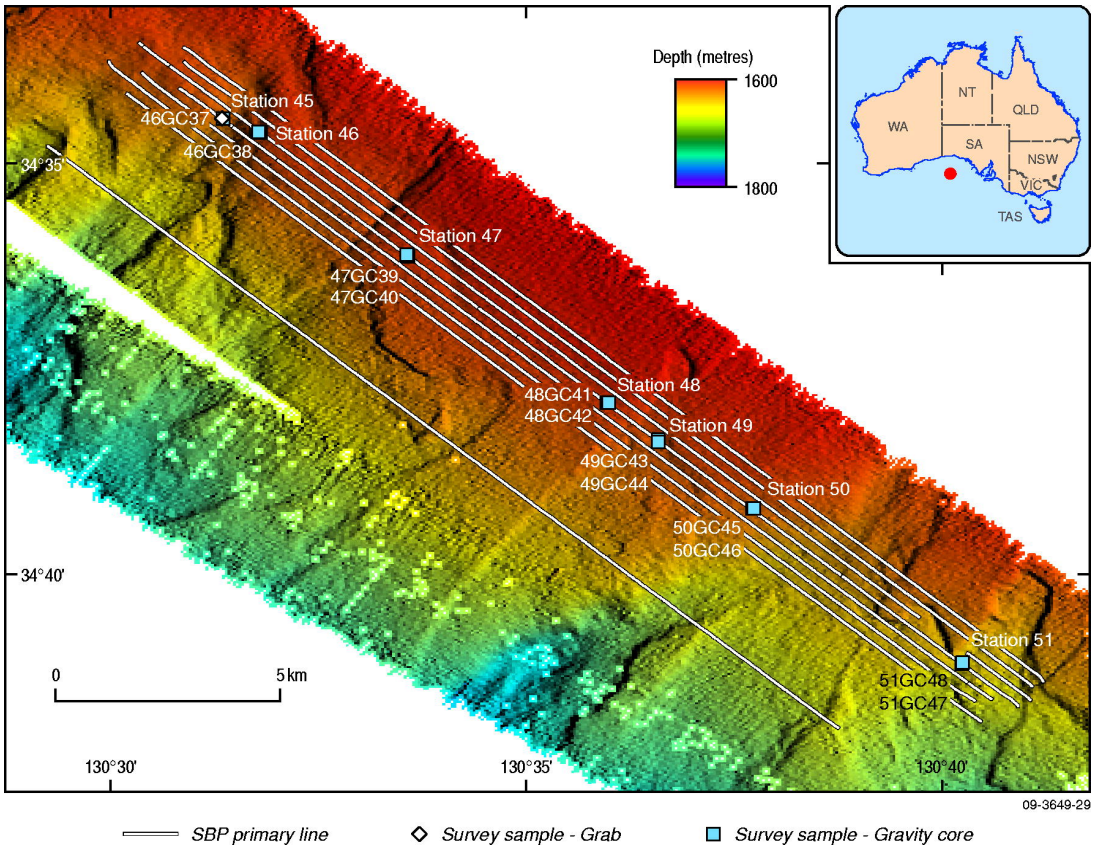

Figure 7.18. *Multibeam swath bathymetry over Area 2c.*

Stratigraphy

Area 2a

The sub-bottom profiler data in Area 2a images 4 main units (Fig. 7.19). The oldest unit is hard and causes a loss of penetration below its surface. Comparison with the regional seismic data suggests that the top of this unit may correspond to the Oligocene horizon. Alternatively, it may be of late Miocene age. In the eastern part of Area 2a this unit is overlain by an acoustically transparent unit of possible Pliocene age. Overlying this is a well stratified unit imaged on the topographic highs of the eastern and western parts of the area. This unit may consist of early Pleistocene deposits. The overlying unit is an acoustically transparent package that is most likely to consist of late Pleistocene to Holocene sediments. This youngest unit is thickest in the canyon and continues as a thin cover over the topographic high in the west.

The gravity cores taken within Area 2a all penetrated about 5 m into the sediments. At both sample locations (Stations 05 & 06), the gravity cores may have just penetrated into the well stratified, interpreted early Pleistocene sediments. One of the gravity cores recovered at the edge of the canyon in the centre of Area 2a was noted to have a slight H_2S odour.

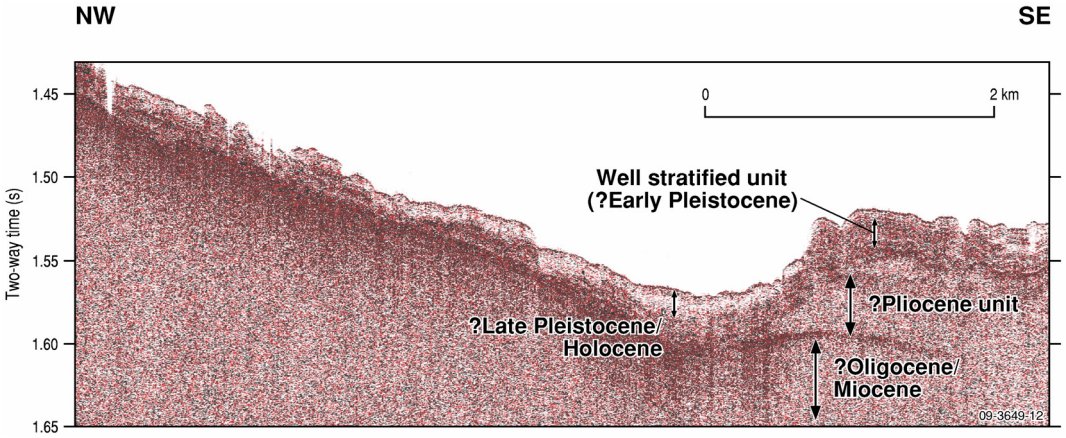

Figure 7.19. *Interpreted stratigraphy from sub-bottom profiler data in Area 2a.*

Area 2b

This area was targeted because of the presence of a canyon cutting down to the Oligocene horizon, as in Area 2a, and the presence of two second rank SAR slicks nearby. As in Area 2a, the Oligocene horizon has enhanced positive amplitudes in places, which could be an indicator of well-cemented zones (possibly HRDZs) (Fig. 7.14). Deeper in the section, within the Hammerhead Supersequence, there are many small enhanced reflections with reversed polarity, however these are likely to be related to coaly beds (Krassay & Totterdell, 2003; King & Mee, 2004).

The sub-bottom profiler data in this area do not image the stratigraphy very clearly due to rapid changes in slope. However, 2 units are discernible. These units can be tied to those observed in Area 2a. The lower unit probably corresponds to the interpreted early Pleistocene well-stratified sediments. The interpreted Oligocene/Miocene horizon and Pliocene unit are not imaged in this locality but are present in the sub-bottom profiler lines that transit in and out of Area 2b. The interpreted late Pleistocene/Holocene acoustically transparent unit occurs as a very thin drape over the margins of the canyon and may also exist in the base of the canyon, although this is not imaged well in the data.

Two gravity cores were taken at the base of the canyon (Station 04) and both penetrated to about 4 m depth. The sediment retrieved is pale, slightly bluish-grey, sticky calcareous ooze, most likely derived from the youngest late Pleistocene/Holocene unit. One of the cores recovered small pebbles of white chalky limestone which could be derived from an older unit, possibly the Oligocene/Miocene.

Area 2c

The Flinders Deep Water seismic line (fdw-0111) that runs the length of Area 2c images a zone of vertical disruption (faulting) below the eastern part of this area. These deeper faults terminate at the interpreted Oligocene horizon (Fig. 7.15). The interpreted Pliocene unit in the western part of Area 2c contains sediments that appear disrupted (Fig. 7.15). Possible causes of such disruption are channelling and mass sediment transport, or the movement of fluids. In the central and eastern parts of Area 2c there are distinct, flat, enhanced reflections with reversed polarity within the Oligocene to Recent sequence (Dugong Supersequence) (Fig. 7.15). In this region the faults may provide migration pathways for hydrocarbons from deeper in the basin which could possibly form minor accumulations within this section.

The sub-bottom profiler data in Area 2c display good penetration (up to 0.05s / ~ 40 m) (Fig. 7.20). It is assumed that the basal sediments imaged here correspond to the interpreted Pliocene unit. The sediments in the western part of Area 2c on Figure 7.20 appear disrupted and correspond to the interpreted Pliocene disrupted sediments observed in the regional seismic data (Fig. 7.15). There are no indications of fluid/hydrocarbons within the sub-bottom profiler data in this area, so it is unlikely that the disruption is the result of fluid migration. The central topographic high in Area 2c contains a well-stratified sediment package that probably correlates to the interpreted Early Pleistocene unit identified in Areas 2a and 2b. The overlying acoustic transparent unit probably corresponds to late Pleistocene/Holocene deposits.

Gravity cores taken in Area 2c are all very similar with calcareous foraminiferal ooze that generally changes from light grey at the top of the core to white near the base. Foraminifera are generally more abundant towards the top of the cores. Most of the cores penetrated the stratified unit with sediment recovery ranging from 2 to 4.5 m (Fig. 7.20). However, samples from Station 45 likely terminated in older sediments (possibly Pliocene) and only penetrated 1.5 m of recent late Pleistocene/Holocene sediments.

There are no indications of fluid or shallow gas within the sub-bottom profiler data within Area 2. However, Area 2c had very clear indications in the regional seismic data of possible shallow gas (reversed enhanced reflections) within the Oligocene to Recent sequence. It is possible that this gas has not leaked to the shallow sediments and therefore, were not sampled during this survey or imaged by the sub-bottom profiler.

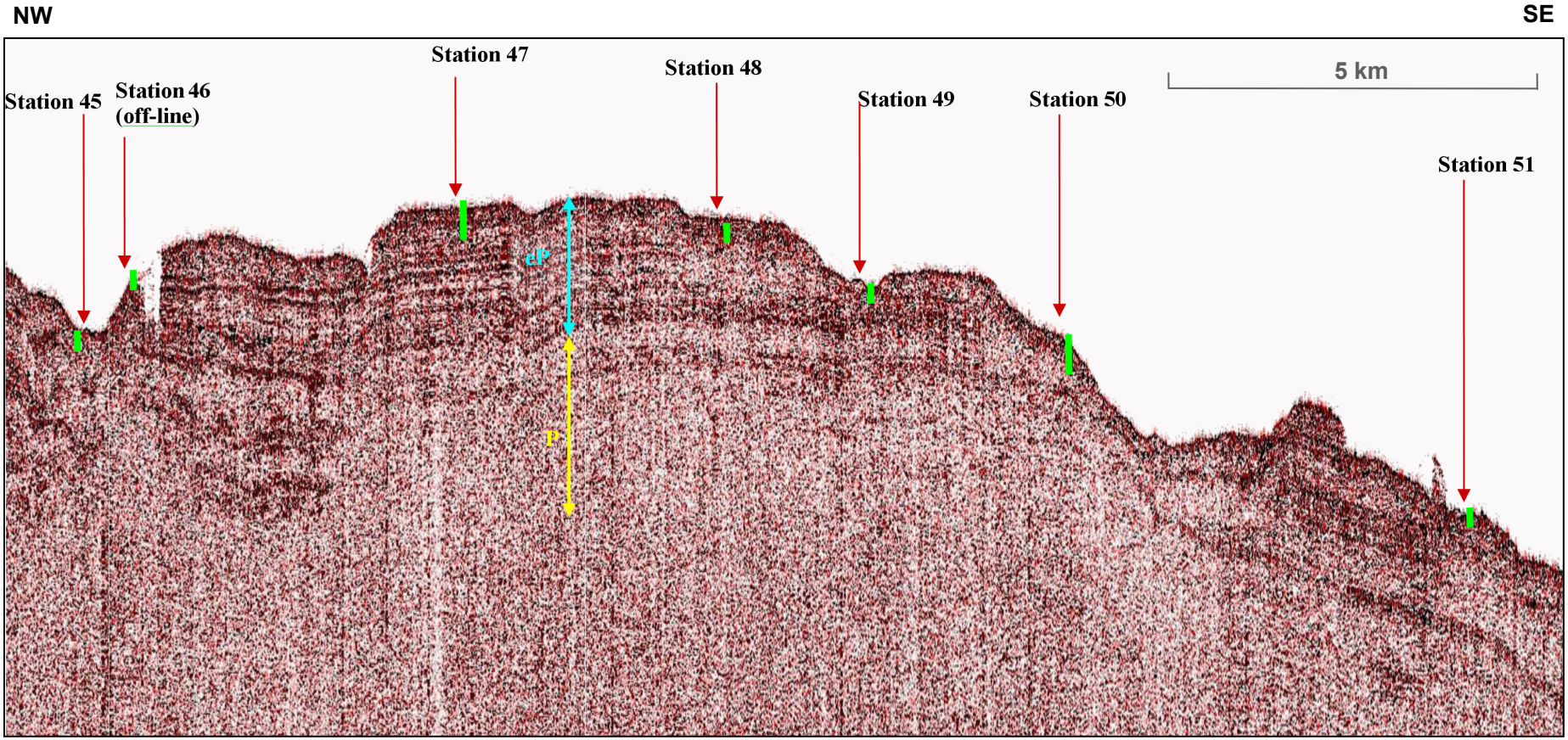

Figure 7.20. *Interpreted stratigraphy from sub-bottom profiler data in Area 2c. Location of gravity core samples displayed with green lines indicating the estimated core penetration. eP = interpreted early Pleistocene unit; P = interpreted Pliocene unit*

.

Geochemistry (Area 2c)

Core samples in Area 2c were screened for thermogenic gas (C_1 to C_5) and liquid hydrocarbons (C_{12} plus) to search for evidence of natural hydrocarbon seepage. All gravity core samples had extremely low concentrations of headspace gases consistent with background levels. High-molecular weight thermogenic hydrocarbons were also not detected in any of the samples. Therefore, geochemical screening revealed no evidence for natural hydrocarbon seepage in Area 2c.

Core sample depth in Area 2c extended from 0.5 to 3.5 m below seafloor (bsf). Biomarker distributions from these core samples are dominated by high molecular weight linear alkanes and alkan-1-ols at all core depths (Fig. 7.21). Linear alkanes in the C_{27}-C_{33} range show an odd over even carbon number predominance with a maximum at C_{31}, whereas C_{24}-C_{32} linear alkan-1-ols display an even to odd carbon number predominance with a maximum at C_{28}. These distributions are typical of terrestrial higher plant waxes (Eglinton & Hamilton, 1967) and are therefore indicative of a strong terrigenous input to the samples. Only minor marine inputs could be evidenced through the occurrence in low relative amounts of long-chain C_{37} and C_{38} alkenones deriving from haptophyte algae (Marlowe et al., 1984; Brassell et al., 1986) and of microalgal biomarkers C_{30} 1,15-diol and associated C_{30} 15-keto,1-ol (Volkman et al., 1998). All core samples taken from Area 2c consistently presented the same biomarker patterns down core suggesting strong terrigenous inputs across the region and from the interpreted early Pleistocene unit.

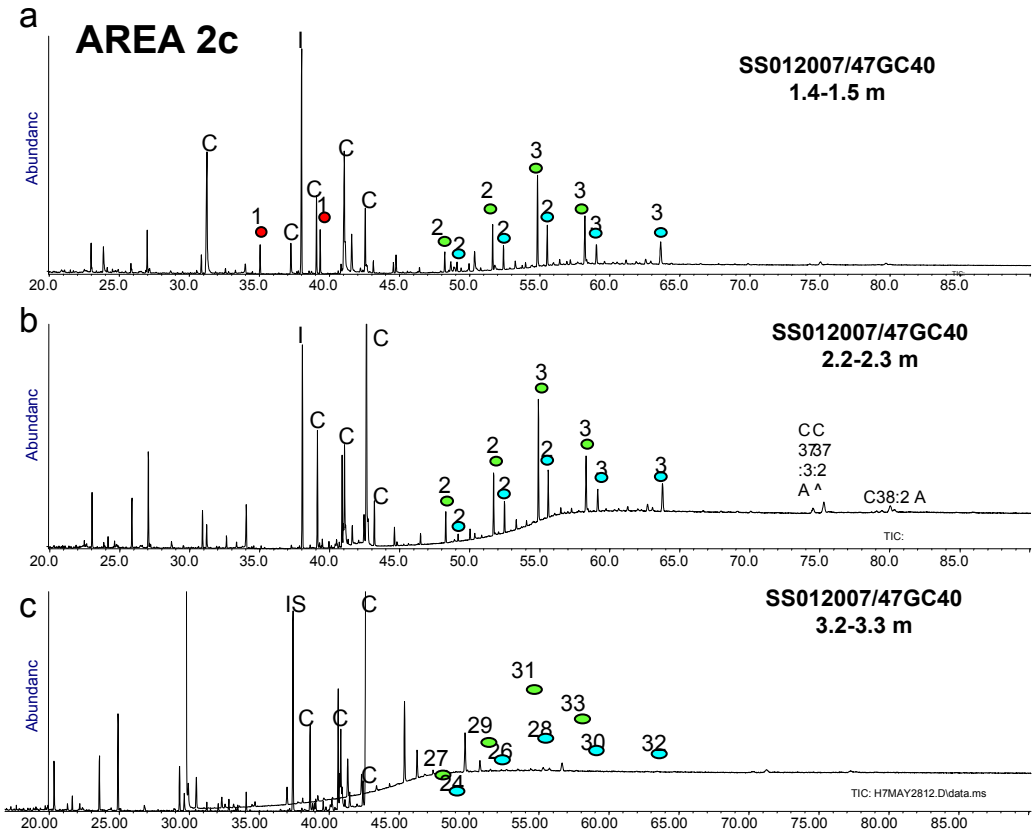

Figure 7.21. *Total ion chromatograms of silylated organic extracts from Area 2 SS012007/47GC40 core samples: (a) 1.4-1.5 m, (b) 2.2-2.3 m and (c) 3.2-3.3 m. IS: Internal Standard; A: Alkenone; C: Contaminant. Red circles: Fatty acids; Green circles: linear alkanes; blue circles: linear alkanols.*

Area 3

Introduction

Area 3 is located on the northern Ceduna Terrace, and straddles the northern margin of the Ceduna Sub-basin (Fig. 1.1). This area was targeted for potential seepage sites above reactivated basin margin faults that have formed seafloor scarps (Fig. 7.22). These faults may provide vertical migration pathways for hydrocarbons; enhanced reflections that may indicate the presence of hydrocarbons are observed in the Hammerhead Supersequence adjacent to the faults.

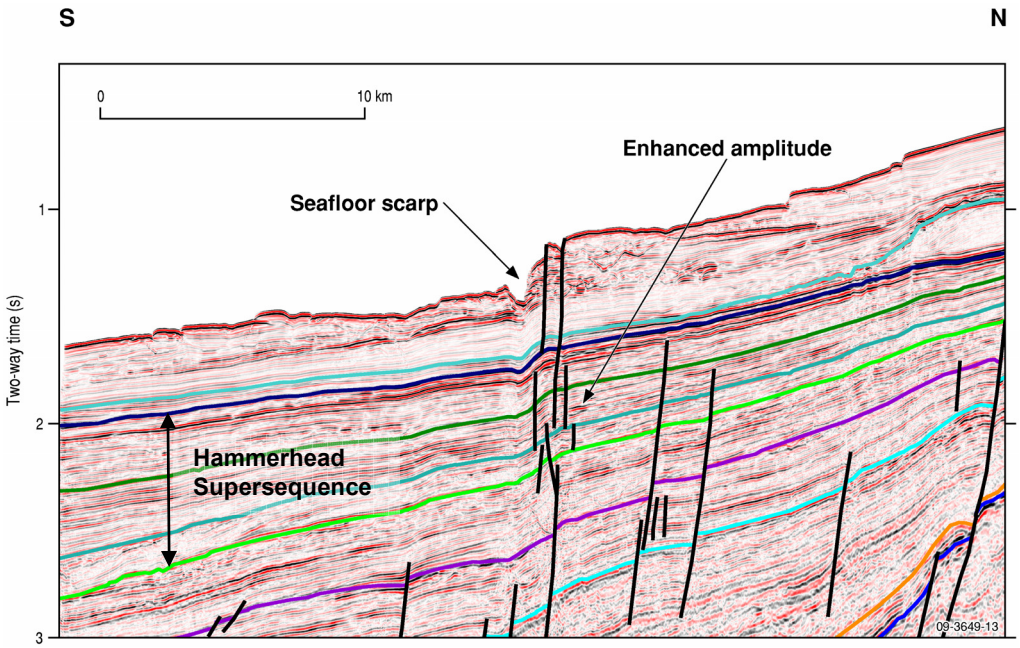

Figure 7.22. *Regional Seismic line s216-108 illustrating recent reactivation of basin-forming faults causing seafloor scarps, with some enhanced reflections near the reactivated fault within underlying Hammerhead Supersequence*

Seabed Morphology and Sedimentology

The multibeam swath data collected over Area 3 cover the outer part of the shelf and the transitional slope between shelf and terrace, where underlying basin margin faults have been reactivated to form seafloor scarps (Fig. 7.23). The scarps are separated by relatively smooth, gently sloping substrates. An area of seabed with circular depressions was identified on a plateau in the northern part of Area 3 in about 700 m water depth (Fig. 7.24). These depressions are about 150 m in diameter, about 5 m deep and are located on a ~5° SE slope. These may be pockmark features related to fluid escape that is currently active, or represent palaeo-fluid escape features. If they are palaeo-features they must have been active during the late Pleistocene due to their formation within interpreted Recent sediments. In comparison, the average size of a pockmark in the North Sea is generally 50 to 100 m in diameter with depths ranging from 1 to 3 m (Judd & Hovland, 2007).

Samples of the seabed in Area 3 include 5 grabs and 12 gravity cores (Table 7.6). The shallowest samples taken (Station 09) on the shelf slope in 680 m water depth consist of grey sticky ooze and pale yellow-grey slightly calcareous ooze. Cores taken over the ‘pockmarked’ seafloor (Station 11) recovered pale green-grey calcareous mud. The remaining samples (Stations 07, 08, 10 and 12) were taken off the edge of various escarpments and consist of fine-grained, grey to pale greenish-grey calcareous mud, and pale yellow-grey calcareous ooze (Station 10).

Table 7.6: *Area 3 samples*

Sample Type	Station number	Sample number	Brief description
Grab	Station 07	07GR07	Fine-grained, grey, calcareous ooze. Some minor darker patches and fine-grained dark material (organic?).
Grab	Station 07	08GR08	Very fine-grained, calcareous ooze (2.5Y 7/2).
Grab	Station 07	09GR09	Grey, sticky ooze.
Grab	Station 07	10GR10	Small quantity of pale yellowish-grey ooze.
Grab	Station 07	12GR11	Very fine-grained, grey, calcareous ooze containing minor forams and very fine dark grains (?organic).
Gravity Core	Station 07	07GC13	5.1 m. Fine-grained, grey mud containing some minor forams and dark fine organic-rich material. Strong H_2S smell. Only slight fizz with HCl indicating a calcareous clay mix.
Gravity Core	Station 07	07GC14	4.9 m. Fine-grained, grey mud. Plastic texture; contains forams; strong H_2S smell. Fine-grained, dark material is dispersed throughout the sample.
Gravity Core	Station 08	08GC15	5 m. Grey-green, clay-rich, calcareous mud. Fine-grained, homogeneous. Strong H_2S odour. Minor forams and shell fragments.
Gravity Core	Station 08	08GC16	4.7 m. Grey-green, clay-rich, calcareous mud. Fine-grained, homogeneous. Strong H_2S odour. Minor forams and shell fragments.
Gravity Core	Station 09	09GC17	4.9 m. Pale yellowish-grey, slightly calcareous ooze. Scattered shelly material (pteropods and minor bryozoans, slightly gritty forams?), bioturbation and H_2S odour.
Gravity Core	Station 09	09GC18	4.8 m. Pale yellowish-grey, slightly calcareous ooze. Sparse shelly material (mainly pteropods), bioturbation and H_2S odour.
Gravity Core	Station 10	10GC19	4.8 m. Pale yellowish-grey ooze, slightly calcareous, sparse shelly material (mostly pteropods), H_2S odour and bioturbation.
Gravity Core	Station 10	10GC20	3.6 m. Pale yellowish-grey ooze, slightly calcareous, layers of shelly material, weak H_2S odour and bioturbation.
Gravity Core	Station 11	11GC21	4.3 m. Grey-green, calcareous, clay mud. Homogeneous fine-grained, slightly silty in part. Moderate H_2S odour. Minor fizz with dilute HCl.
Gravity Core	Station 11	11GC22	3.5 m. Pale green-grey, calcareous mud, fine-grained. Large articulated and dis-articulated bivalves from 2.5-2.3 m. Bivalve shells up to 4 cm in diameter, pale grey in colour. Also contains zones with numerous shell fragments.
Gravity Core	Station 12	12GC23	4.9 m. Greyish-green, sticky, plastic, calcareous mudstone with minor shell and braided coral fragments (up to 10 cm long). Moderate H_2S smell. 2.9 - 3.9 m coarser grained comprising bioclasts (forams, shell fragments, coral fragments).
Gravity Core	Station 12	12GC24	2.9 m. Grey-green, calcareous mud. Fine-grained, slightly bioturbated, contains minor forams. Occasional zones with grey staining. Sandier towards base (fine to medium-grained, grey bioclastic calcareous sand).

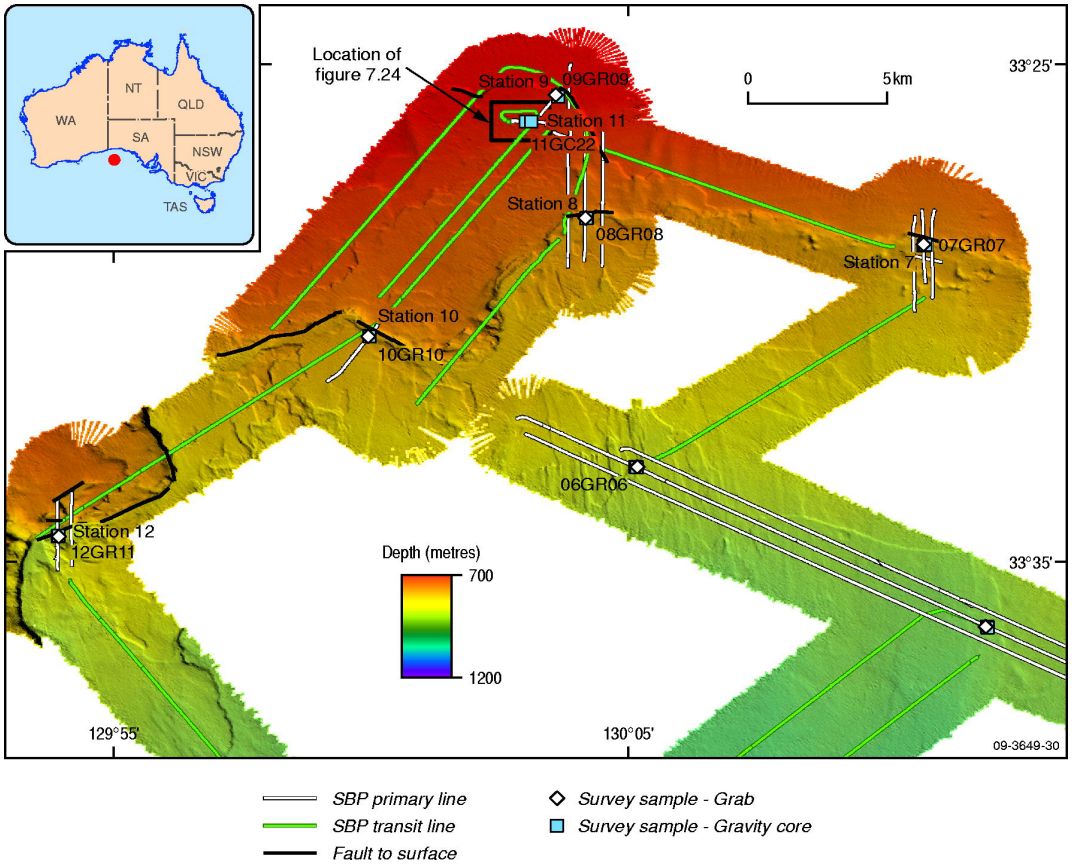

Figure 7.23. *Multibeam swath bathymetry over Area 3 with location of sub-bottom profiler lines and location of faults that penetrate the seafloor to form scarps. The fault scarps are interpreted from regional seismic and sub-bottom profiler data and in places have been inferred from multibeam swath data.*

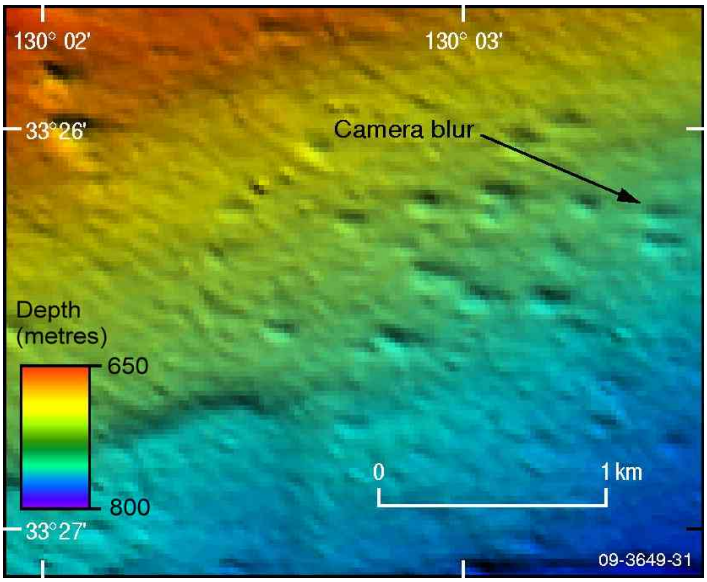

Figure 7.24. *Multibeam swath bathymetry over Area 3 pockmarks. The location of this are is displayed in Fig. 7.23. The camera transect displayed blurred images when transecting the edge of the labelled pockmark.*

One video transect was taken over the area of pockmarked seafloor. The transect recorded a mounded, heavily burrowed seabed (Fig. 7.25) with occasional fish, shrimp, and sessile organisms. One depression appeared to have a greater amount of burrowing on the seafloor. The water column contained plankton and appeared to become more turbid (focus blurs and camera shudders) near the last pockmark (refer to Fig. 7.24 for location). This camera blurring may be due to fluid escape from the pockmark or currents near the seafloor. Therefore, there were no unequivocal direct indicators of seepage could be interpreted from the video footage.

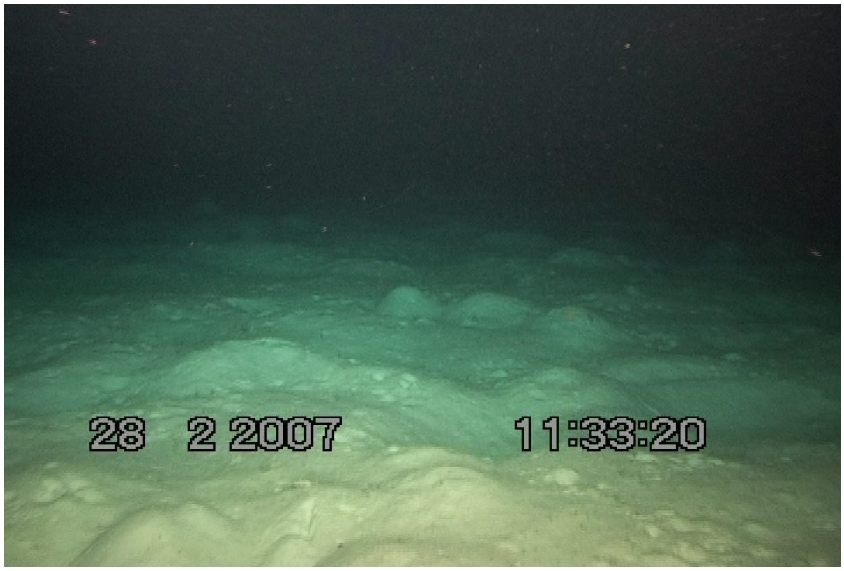

Figure 7.25. *Image taken from video footage taken over the area of pockmarked seafloor in Area 3. Note the mounded and heavily burrowed seafloor.*

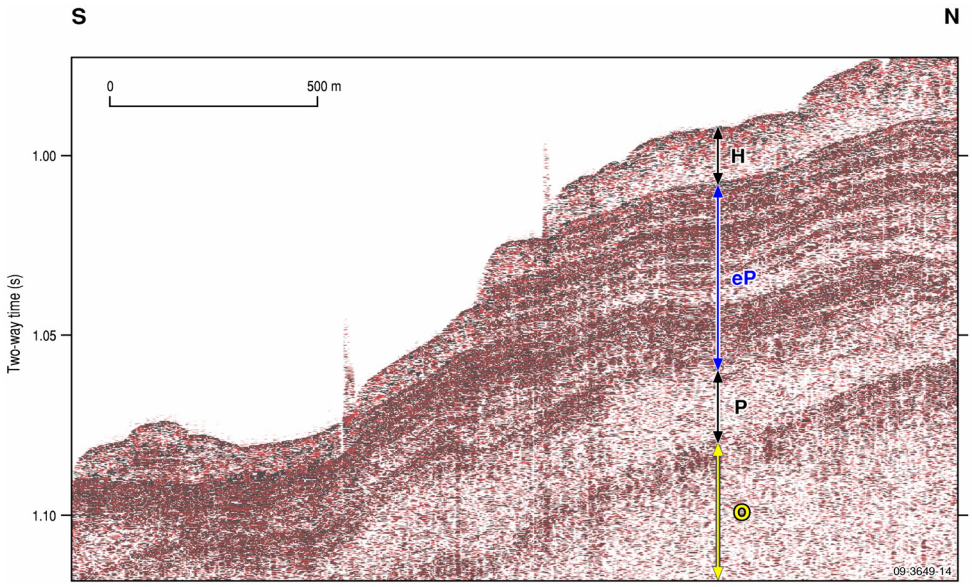

Figure 7.26. *Interpreted stratigraphy from sub-bottom profile in Area 3. O = Oligocene or Miocene unit; P = Pliocene unit; eP = early Pleistocene unit; H = late Pleistocene/Holocene unit.*

Stratigraphy

Area 3 targeted seafloor scarps that formed as a result of the reactivation of basin margin faults. It is possible that these faults may be migration pathways for hydrocarbons.

The sub-bottom profiler data in Area 3 have good penetration (up to 0.110 s TWT / ~83 m) and four units have been interpreted (Fig. 7.26). The basal unit underlies an extremely reflective surface that causes a loss of seismic penetration below. This unit is interpreted as a hard limestone of probable Oligocene or Miocene age. Overlying this is an acoustically transparent unit that probably corresponds to sediments deposited during the Pliocene. Unconformably overlying the Pliocene unit is a well-allystratified package of sediments that are probably early Pleistocene in age. The youngest unit is a thin acoustic transparent unit that is likely to be late Pleistocene/Holocene in age. The Oligocene/Miocene to Pleistocene section is exposed in some steep fault scarps.

In Area 4, 12 gravity cores were collected (Table 7.6). An H_2S odour was detected in a number of samples. This was generally only encountered when the interpreted early Pleistocene well-stratified sediments were sampled, either directly or as reworked late Pleistocene/Holocene deposits. Wells drilled by ODP Leg 182 encountered high levels of H_2S in brines from a thick progradational Pleistocene succession. Feary et al. (2004) proposed that the high concentration of H_2S was the result of the oxidation of organic matter within the sediments by sulphate-reducing bacteria.

The gravity cores taken at Station 11 in the pockmark field recovered sediments containing some large bivalves and shell fragments. The sub-bottom profiler data indicate that these cores penetrated the late Pleistocene sediments on the edges of the pockmarks. Minor diffractions or enhanced reflections have been identified beneath the imaged pockmarks in the sub-bottom profiler data (Fig. 7.27). These features could be an indication of the presence of shallow gas or may simply be related to the sub-bottom profiler line imaging the edges of the pockmarks. The diffractions/enhanced reflections were not penetrated by the gravity cores.

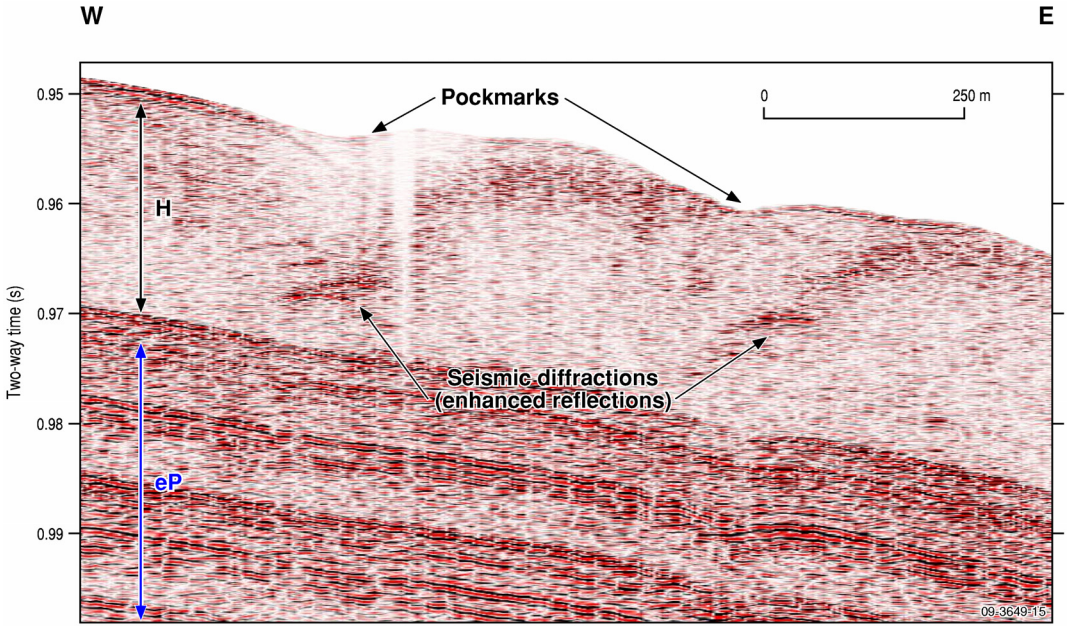

Figure 7.27. *Sub-bottom profile over the pockmark field in Area 3. Minor diffractions / enhanced reflections observed below the imaged pockmarks. H = late Pleistocene/Holocene unit; eP = early Pleistocene unit.*

Geochemistry

Headspace gas and high-molecular weight hydrocarbon analyses revealed no evidence for natural hydrocarbon seepage in Area 3.

Biomarker distributions of surface samples from Area 3 were very similar to those of Area 2 grabs (Fig. 7.28), reflecting mixed marine and terrigenous contributions. In contrast to cores from Area 2c, core samples from Area 3 clearly show increasing marine contributions down core. A down-core shift towards elevated marine inputs is evidenced by an increase in concentrations of haptophytes-derived biomarkers, i.e. long-chain unsaturated C_{37}-C_{39} alkenones as well as of microalgal lipids C_{30} 1,15-diol and ketol (Fig. 7.29). Terrestrial contributions are indicated by the presence of C_{24}-C_{32} linear alcohols and fatty acids and by C_{27}-C_{33} linear alkanes. The respective contributions of marine versus terrestrial material to the sediments can be assessed with the following ratio:

$$\text{Marine/Terrestrial ratio} = \frac{\Sigma\,(C_{37:2}\ \text{Alkenone} + C_{30}\ \text{1,15-diol} + C_{30}\ \text{15-keto,1-ol})}{\Sigma\,(C_{27}\text{-}C_{33})\ \text{odd}\ n\text{-alkanes}}$$

This ratio increases from ca. 0.9 in grab samples to ca. 2.5 (on average) below 3 mbsf in Area 3 (Fig. 7.30b). In contrast, samples from Area 2c had Marine/Terrestrial ratios lower than 0.2 (Fig. 7.30a). Samples from Area 3 are mainly recently deposited marine carbonates (as suggested by the thick late Pleistocene cover mainly comprising calcareous ooze/mud) mixed with some reworked sediments transported from the shelf or eroded from fault scarps. This is consistent with the biomarker distributions showing a well preserved marine signal.

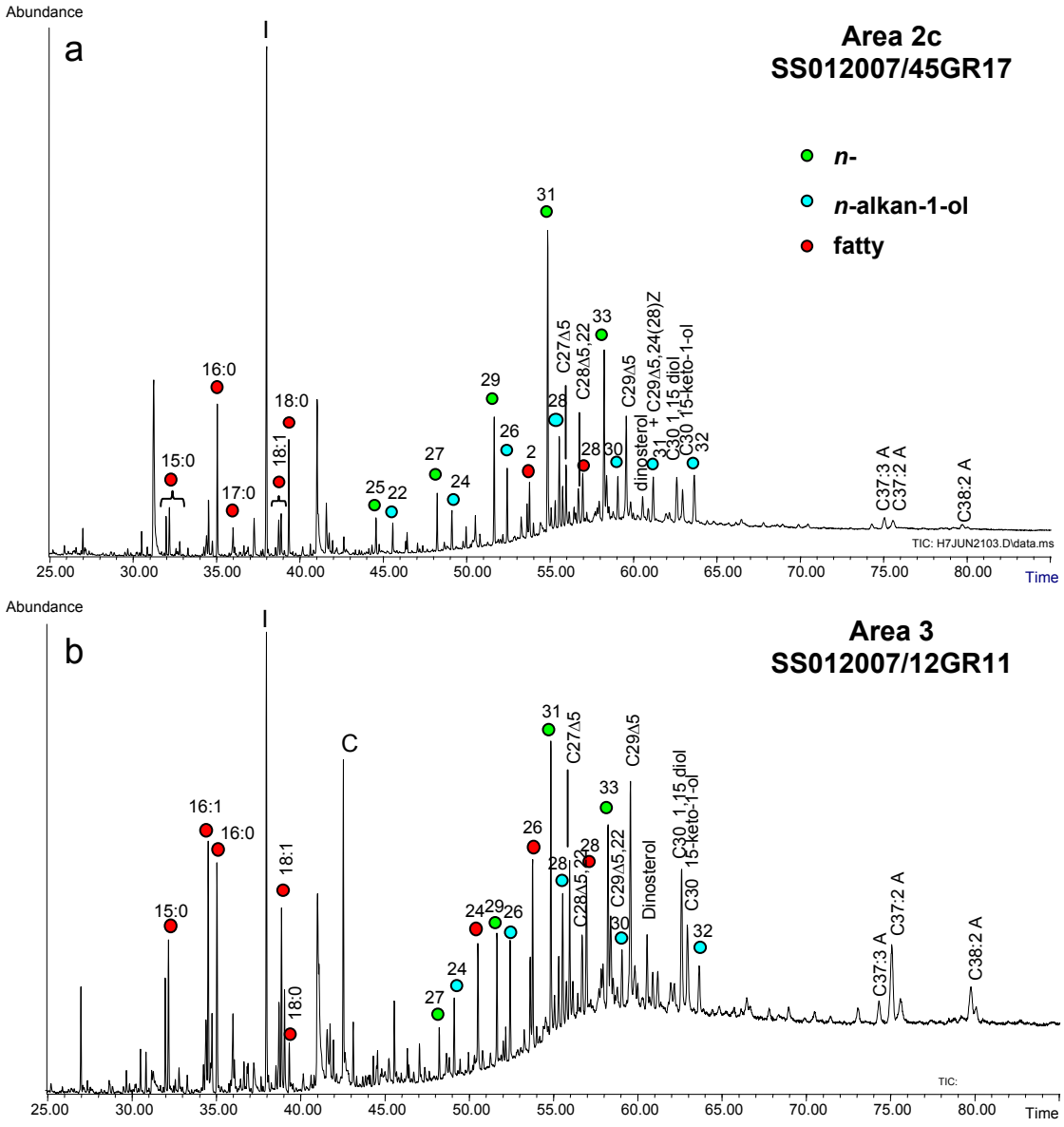

***Figure 7.28**. Total ion chromatograms of silylated organic extracts from grab samples: (a) SS012007/45GR17B (Area 2c) and (b) SS012007/12GR11B (Area 3). IS: Internal Standard; A: Alkenone; C: Contaminant; $C_{27}\Delta^5$: cholesterol; $C_{28}\Delta^{5,22}$: 24-methylcholesta-5,22E-dien-3β-ol; $C_{29}\Delta^{5,22}$: 24-ethylcholesta-5,22-dien-3β-ol; $C_{29}\Delta^5$: 24-ethylcholest-5-en-3β-ol; $C_{29}\Delta^{5,\ 24(28)Z}$: 24-ethylcholesta-5,24(28)Z-dien-3β-ol.*

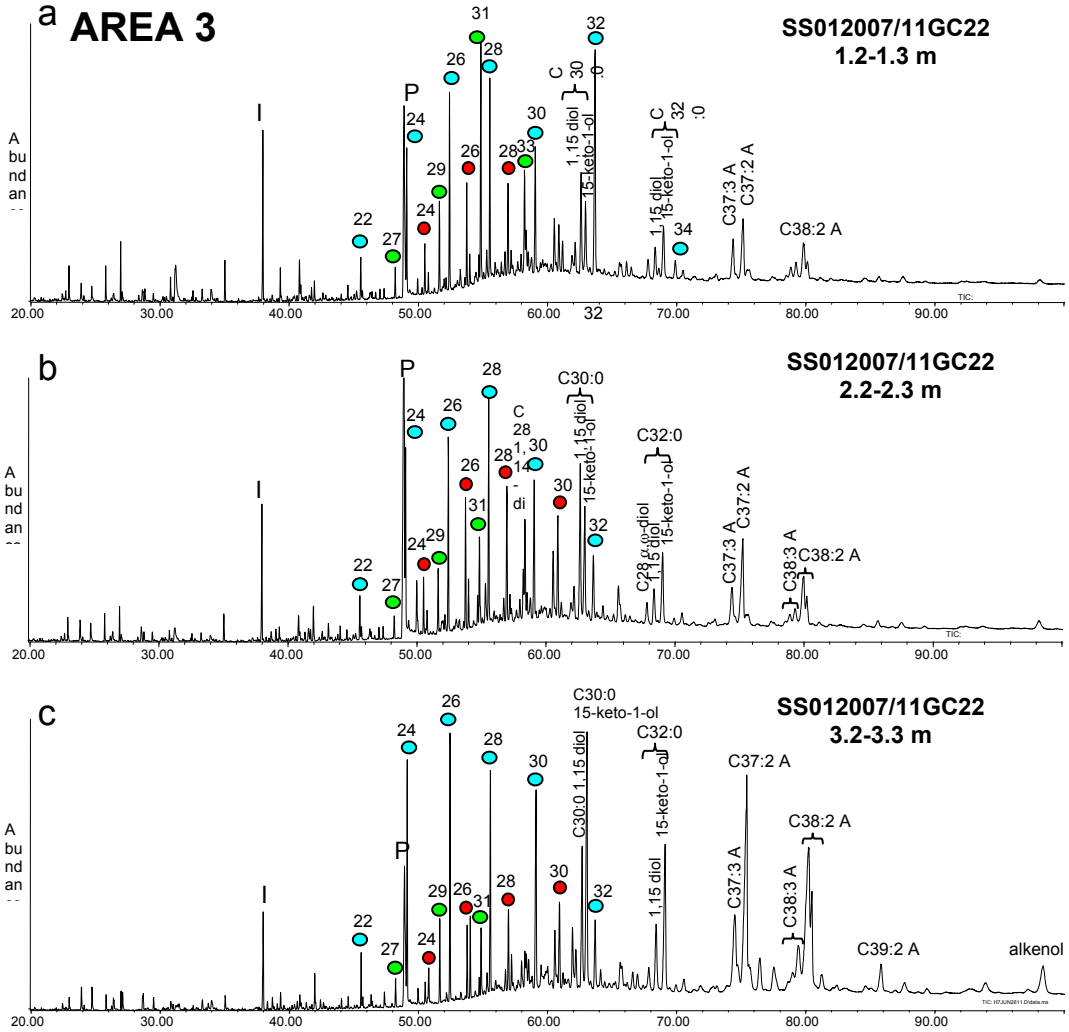

Figure 7.29. *Total ion chromatograms of silylated organic extracts from Area 3 SS012007/11GC22 core samples: (a) 1.2-1.3 m, (b) 2.2-2.3 m and (c) 3.2-3.3 m. IS: Internal Standard; A: Alkenone; P: Phthalate.*

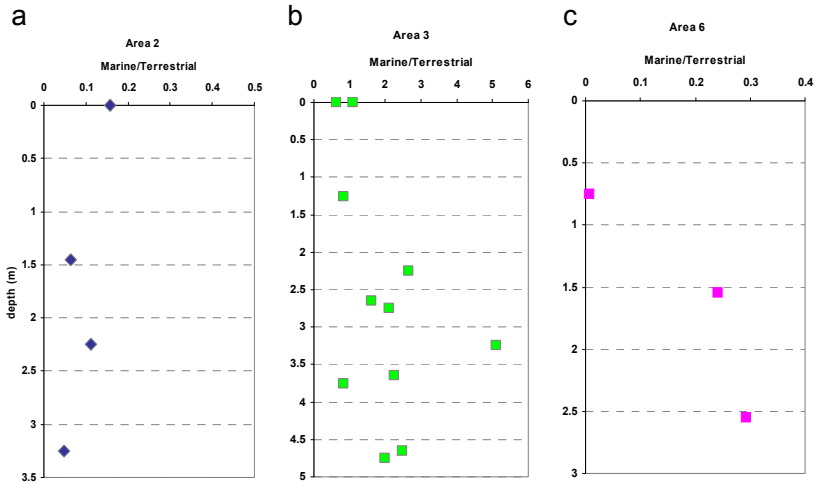

Figure 7.30*. Depth profiles of Marine to Terrestrial ratio for cores of (a) Area 2, (b) Area 3 and (c) Area 6.*

Area 4

Introduction

Area 4 is located in the northwestern corner of the Ceduna Terrace (Fig. 1.1). This area was not a potential seepage target but was surveyed in order to image and sample interpreted Cenozoic volcanic build-ups (Fig. 7.31). The area is sub-divided into 3 data acquisition sub-areas: Area 4a, Area 4b and Area 4c (Fig. 7.32).

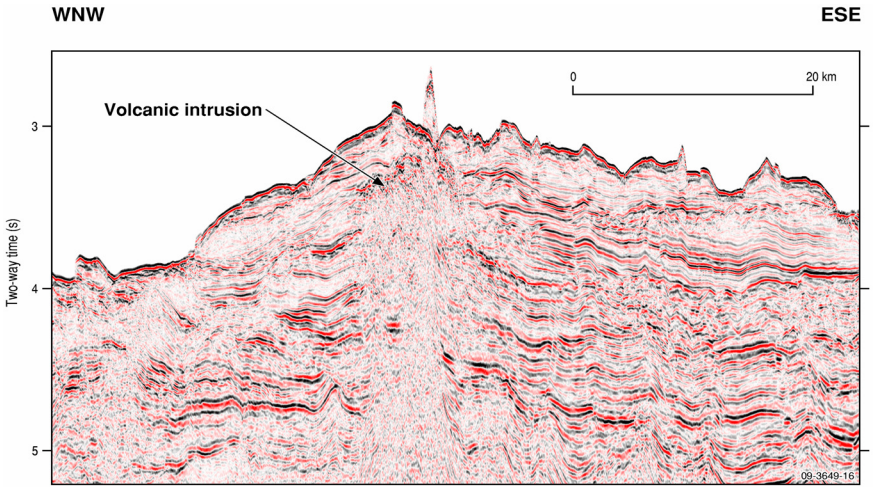

Figure 7.31. *Regional seismic line showing volcanic intrusion and volcano on seabed.*

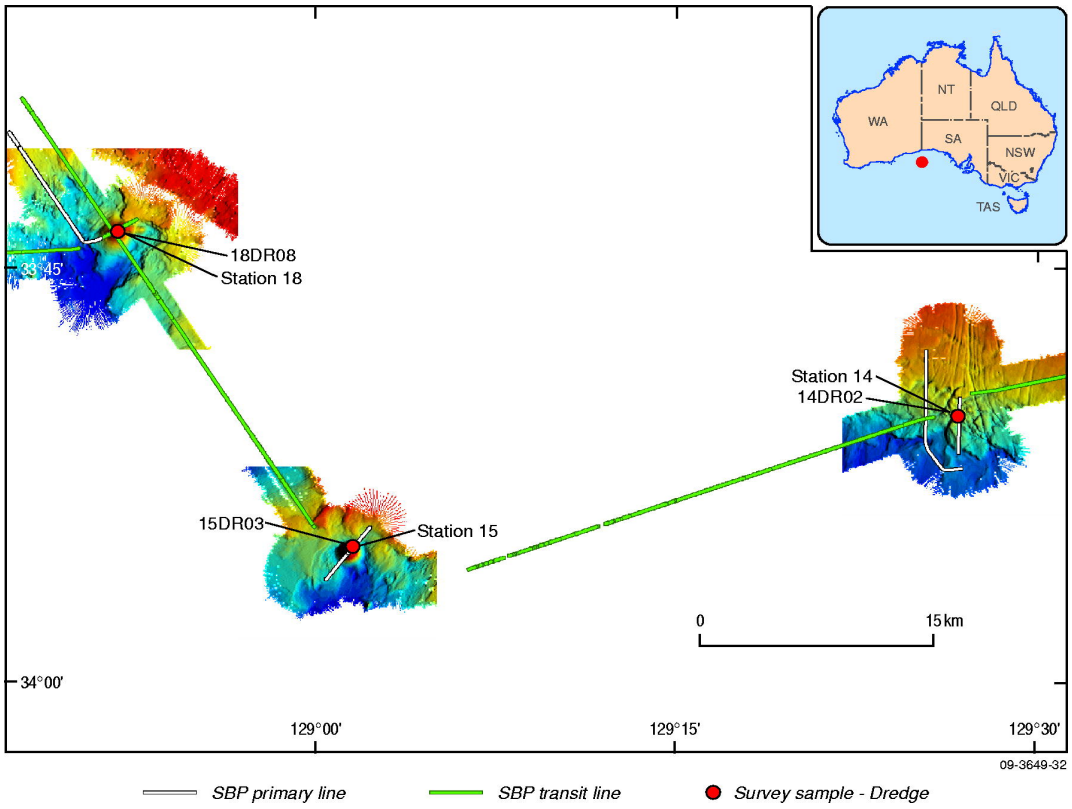

Figure 7.32. *Area 4 subdivision with sample locations and multibeam swath bathymetry.*

Seabed Morphology and Sedimentology

Area 4a

The multibeam swath data collected over Area 4a image a deeply incised seabed sloping to the south (Fig. 7.33). The northern part of Area 4a is incised by at least 7 significant, slightly curved N-S rill systems, up to 20 m deep. In the south the topography becomes more irregular and comprises a series of minor slide features that are incised by the rills. The rills appear to diverge to the south. Samples of the seabed in Area 4a include light grey mudstone and pale yellow, fine-grained sandstone fragments recovered from the pipe dredges at Stations 13 and 14 (Fig. 7.33).

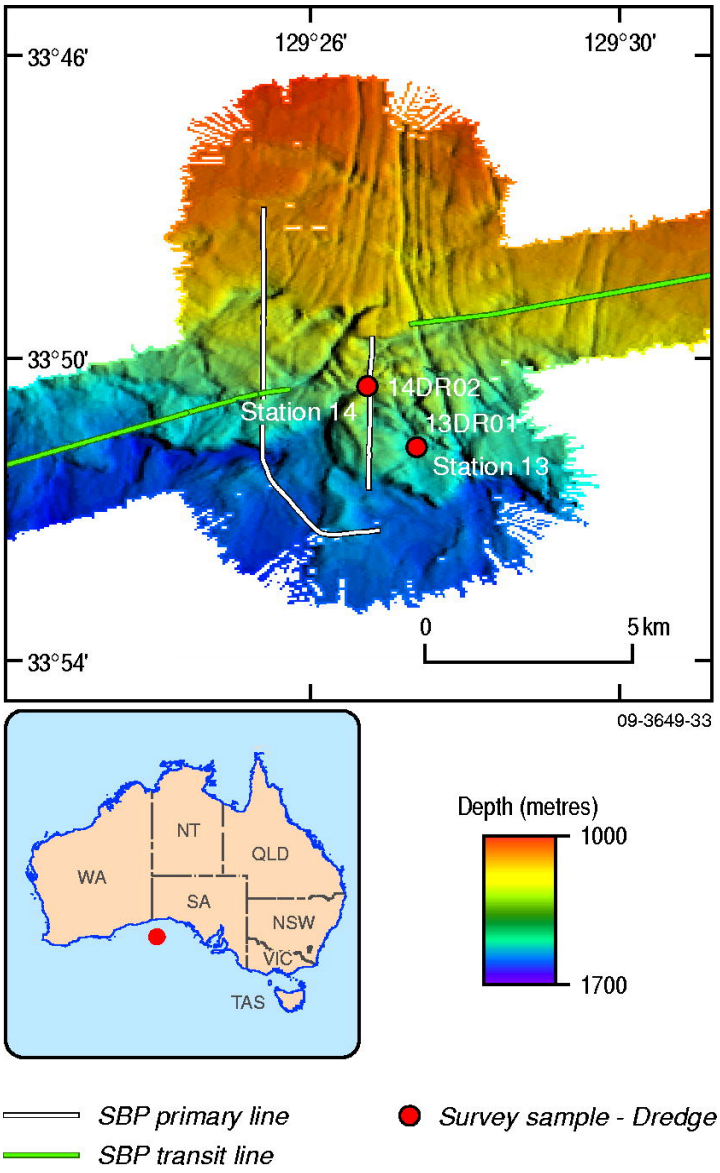

Figure 7.33. *Multibeam swath bathymetry over Area 4a.*

Area 4b

The multibeam swath data collected over Area 4b image an overall southwest-dipping seafloor. In the centre of the area is a steep volcanic cone rising from 2300 m water depth to 1900 m with no obvious crater at the apex. The cone is 1600 m wide at the base and sits on a canyon floor, with little evidence of surrounding lava flows beyond the base of the cone (Fig. 7.34). Nearby seismic data imaging similar volcanic build-ups show that basal volcanic flows are buried beneath younger Cenozoic sediments (e.g. Fig. 7.31). Samples of the seabed in Area 4b were taken from the pipe dredges and chain bag at Station 15. The sediments collected from this area include very fine-grained, white to grey calcareous ooze and fragments of highly weathered volcaniclastic sediments with a fine- to coarse-grained groundmass and sparse infilled vesicles.

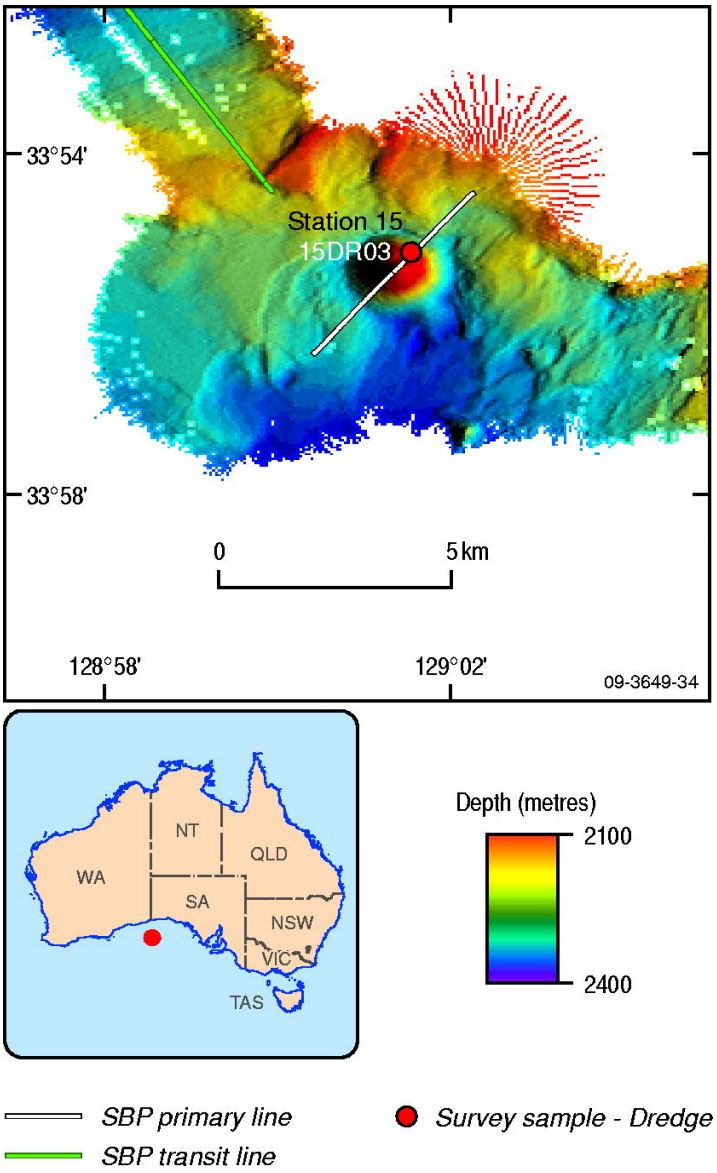

Figure 7.34. *Multibeam swath bathymetry over Area 4b.*

Area 4c

Multibeam swath data collected over Area 4c show a distinct volcanic cone within a highly rugose canyon floor (Fig. 7.35). The cone is about 2000 m wide at the base in 2500 m water depth and has an indistinct crater at the apex (at 2053 m). Samples of the seabed taken in Area 4c were from one dredge taken at Station 18 (Fig. 7.35). Sediment collected from the seabed includes calcareous ooze and fragments of weathered basalt.

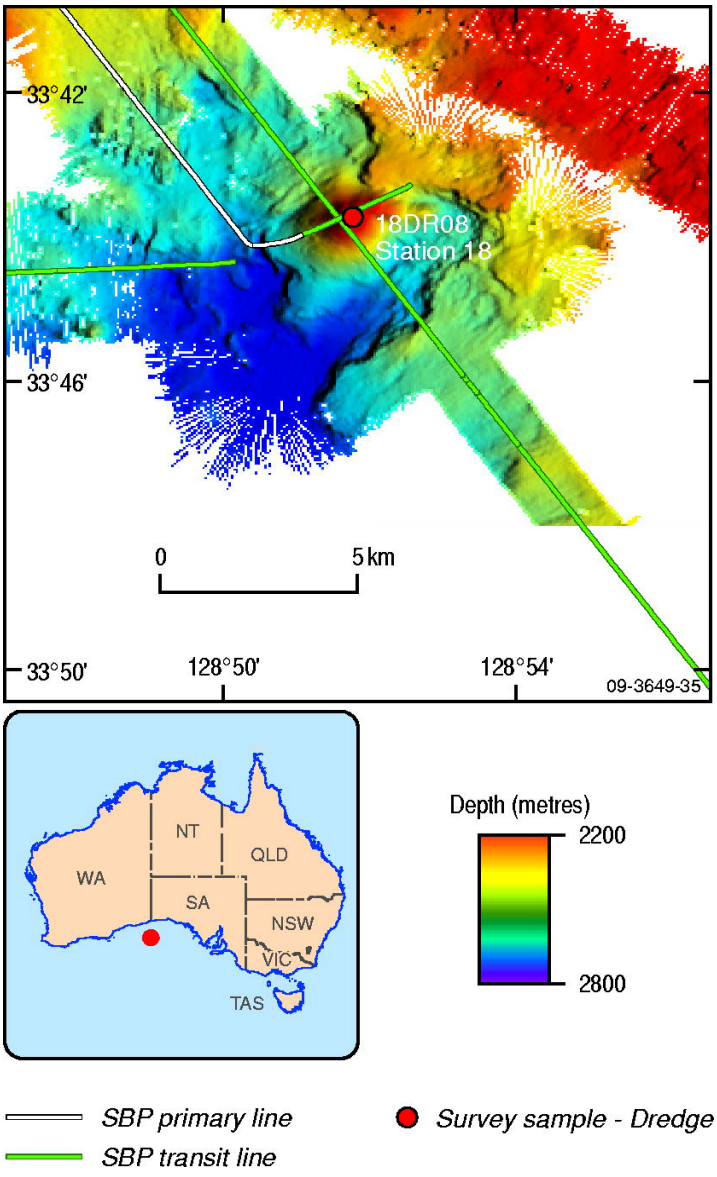

Figure 7.35. *Multibeam swath bathymetry over Area 4c.*

Stratigraphy

The sub-bottom profiler data collected over Area 4 has very limited penetration. The basal unit observed on the transit from Area 3 to Area 4a appears layered, has limited seismic penetration below and is often exposed near the seabed (Fig. 7.36). This unit possibly correlates to the interpreted early Pleistocene unit identified in Area 3. In places a thin, probably late Pleistocene/Holocene, cover overlies the interpreted early Pleistocene unit. The remainder of Area 4 appears to have a hard surface at the seafloor as there is no penetration in the sub-bottom profiler data. The limited penetration in this area may be related to the water depth and high boat speed during sub-bottom profiler data acquisition.

There is no evidence of hydrocarbon seepage within the sub-bottom profiler data in Area 4.

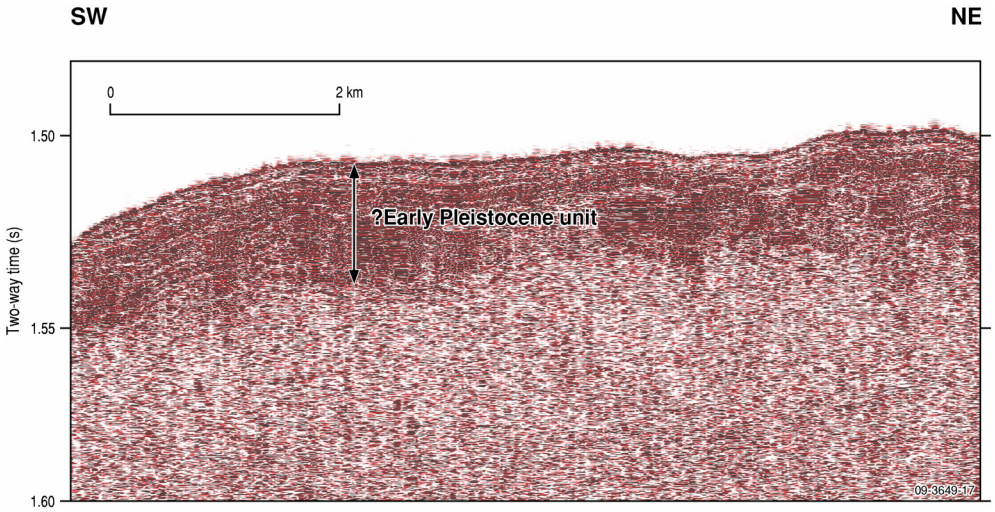

Figure 7.36. *Sub-bottom profile of transit line from Area 3 to Area 4a.*

Area 5

Introduction

Area 5, located on the seaward edge of the Eyre Terrace (Fig. 1.1), was not targeted for its seepage potential. This main purpose of sampling in Area 5 was to collect rocks from the exposed Albian-Santonian succession for assessment of source rock potential (Fig. 7.37). Area 5 has been divided into 3 sub-areas for the purpose of the following discussion (Fig. 7.38).

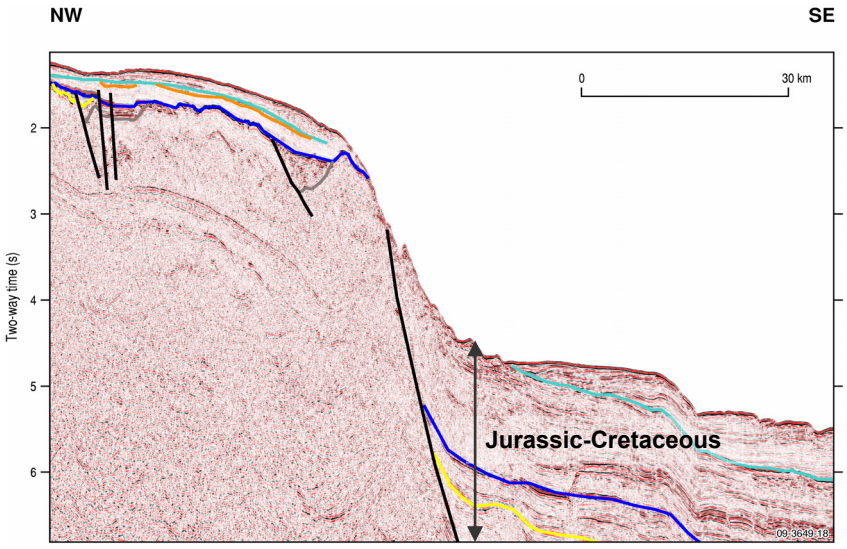

Figure 7.37. *Regional seismic line across the edge of the Eyre Terrace in Area 5. Older rocks exposed from faulting and slumping on the lower slope.*

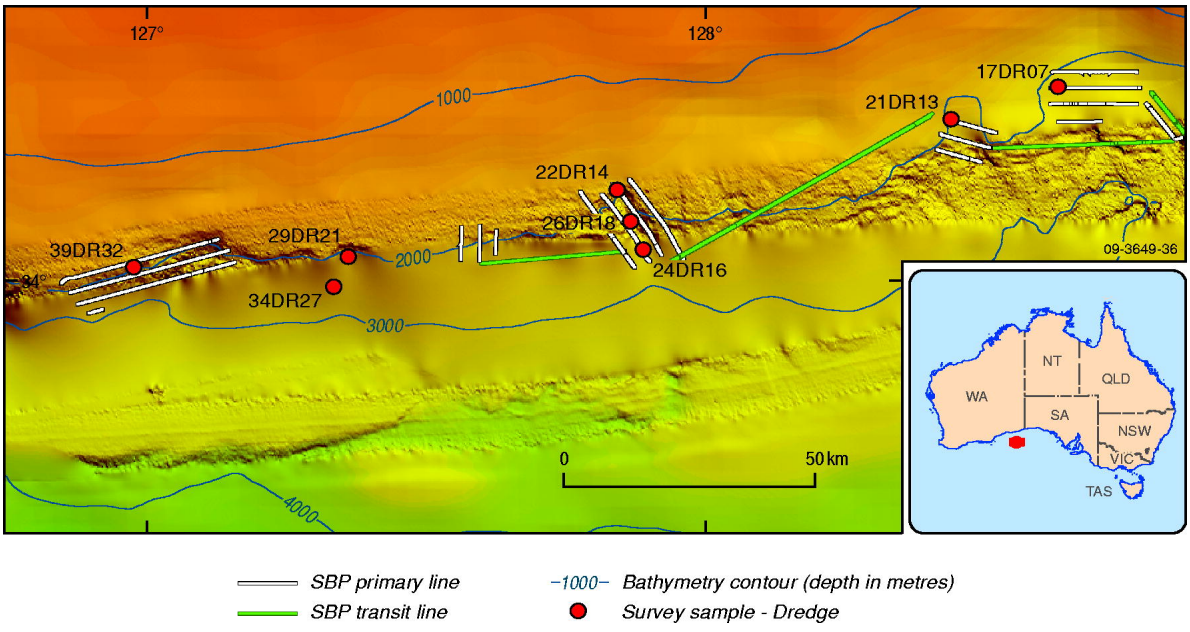

Figure 7.38. *Area 5 subdivision with sample locations.*

Seabed Morphology and Sedimentology

Area 5a

The multibeam swath data collected over Area 5a images the heads of three 100 m deep canyons and two significant and irregular escarpments (Fig. 7.39). The escarpments drop from a plateau at 1700 m water depth down to an irregular canyon floor which reaches a water depth of 2600 m. The upper plateau is characterised by at least two straight, NW-SE trending, sharply incised rills (north of Station 17; Fig. 7.39). The escarpments have an irregular, cuspate appearance with blocks or large-scale slide features at their bases. Samples of the seabed in Area 5a were taken from dredges from stations 17 and 21. Sediments collected include dark grey mudstone with yellow patches (Station 17), and olive coloured mudstone of possible non-marine to restricted marine origin (Station 21). Station 21 samples also included fragments of silt to clay grain sized limestone, and phosphate nodules were collected from both stations.

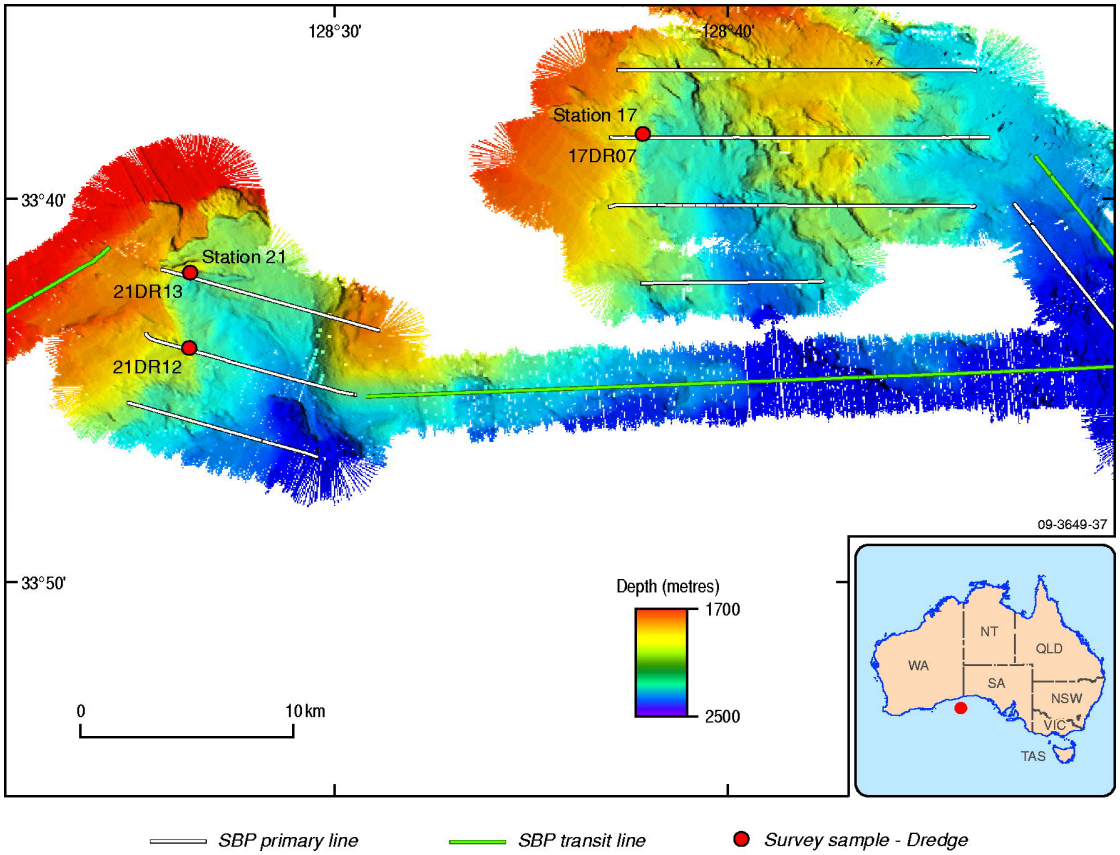

Figure 7.39. *Multibeam swath bathymetry over Area 5a with sample locations.*

Area 5b

Multibeam swath data collected over Area 5b image the head of a significant canyon system (Fig. 7.4). The canyon trends NNW-SSE and begins abruptly at around 1650 m water depth. The head of the canyon is a distinctive cuspate shape with a radius of 2000 m. This drops sharply to a step feature at 1850 m, then falls away gradually to greater than 3000 m water depth. The walls of the canyon are highly irregular and show evidence of slumping.

Samples of the seabed in Area 5b are from 4 dredges at stations 22, 24, 25, and 26. The sediments recovered from Station 22 include arkosic sandstone, very dark grey claystone and dark greenish brown lithified sandy mudstone. Sediment samples collected from Station 24 include greenish-grey to very dark grey lithified siltstone. Very fine grained, well-lithified mudstone and very fine-grained sandstone were collected from Station 25, and interbedded mudstone with very fine-grained sandstone, including fossiliferous sandstone, from Station 26. All stations in Area 5b recovered phosphate nodules.

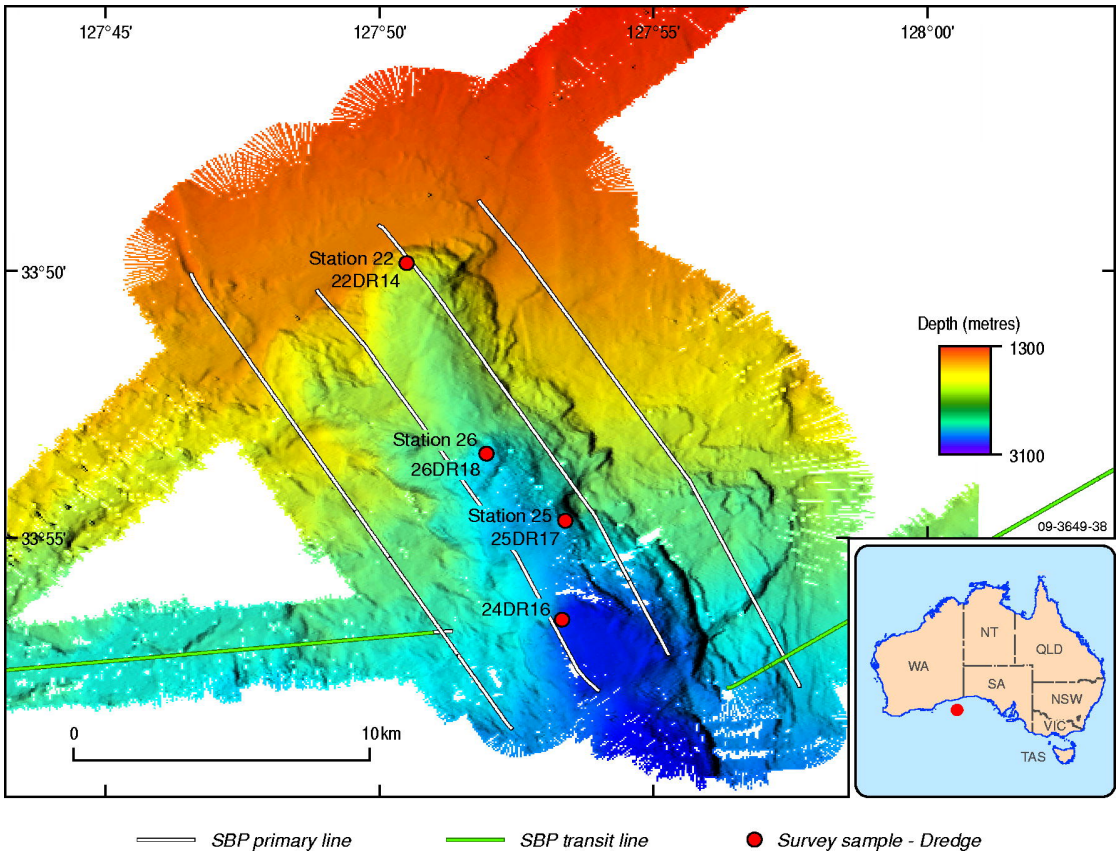

Figure 7.40. *Multibeam swath bathymetry over Area 5b with sample locations.*

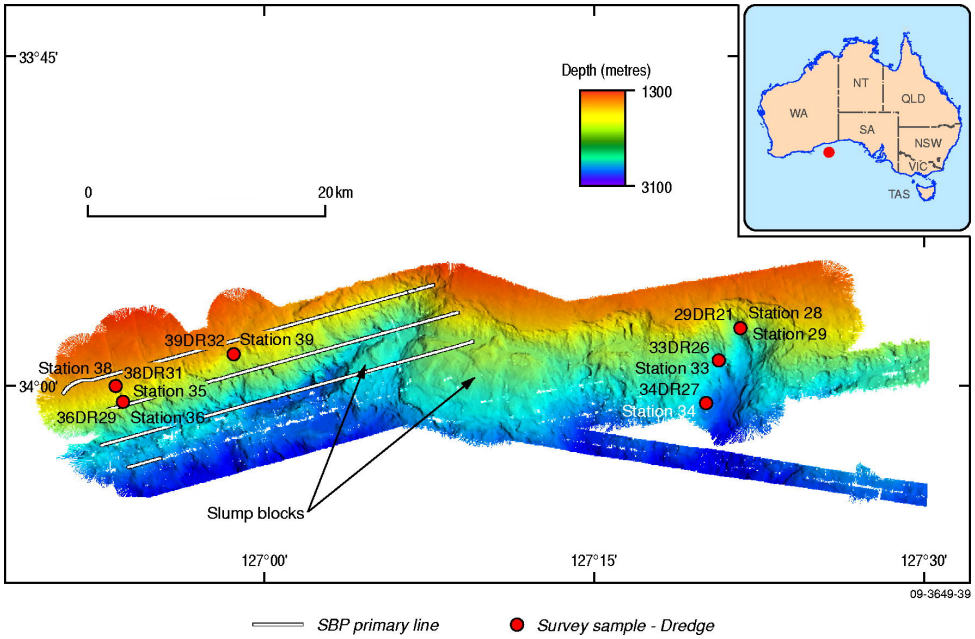

Figure 7.41. *Multibeam swath bathymetry over Area 5c with sample locations.*

Area 5c

Multibeam swath data collected over Area 5c image an east-west trending, generally south-dipping slope, two canyon heads and a significant regional escarpment (Fig. 7.41). The east-west slope feature extends from 1500 m to 3300 m water depth and the regional escarpment occurs at around 1650 m depth. The two canyons initiate from the escarpment and drop to 3300 m. The western canyon contains a large slump block, whereas the eastern canyon has a relatively smooth floor. Between the two canyons a large (~10 km) slump block is present. At least 3 subtle rill features in the west of the area cut into, and terminate below, the 1650 m escarpment.

Samples of the seabed in Area 5c were taken from 12 dredges from Stations 28 to 39 (Fig. 7.41). Sediments collected from the eastern part of Area 5c (Stations 28 to 34) include: dark green, partially lithified mudstone and claystone; black to dark brown and dark olive-grey claystone; micaceous, ferruginous and glauconitic sandstone; fine-grained, lithified, muddy sandstone; partially lithified, dark grey, sandy mudstone; white, partly lithified chalk; and phosphate nodules. Sediments recovered from the western part of Area 5c (Stations 35 to 39) include partially lithified, green mudstone, partially lithified dark greenish-brown to lithified dark grey claystone, pebbly sandstone and pebble- to boulder-sized conglomerate.

Stratigraphy

The sub-bottom profiler data collected over Area 5 have very limited penetration. The majority of the area has a hard surface at the seafloor that limits the penetration of the sub-bottom profiler data. The only area with some seismic penetration is on the transit between Area 5a and Area 5b. This data reveal two units. The oldest unit is highly reflective and is most likely to be the hard, older units exposed to the near seafloor by faulting, as seen on regional seismic data (e.g. Fig. 7.37). The younger unit is difficult to correlate to previously interpreted sub-bottom profiler data and may be related to Pliocene sediment slumping along the slope. The limited sub-bottom profiler penetration within this area may also be due to the extreme water depths and the high speed of the boat during data acquisition.

There is no evidence of hydrocarbon seepage in the sub-bottom profiler data within Area 5.

Area 6

Introduction

Area 6 is located on the lower continental slope above the transition between the northern Ceduna and Recherche sub-basins (Fig. 1.1). The aim of dredging in this area was to sample the interpreted Turonian-Santonian section and mounded seabed features overlying interpreted Albian-Cenomanian mud diapirs and toe-thrusts, and to test for possible hydrocarbon (or other fluid) seepage related to these features (Fig. 7.42).

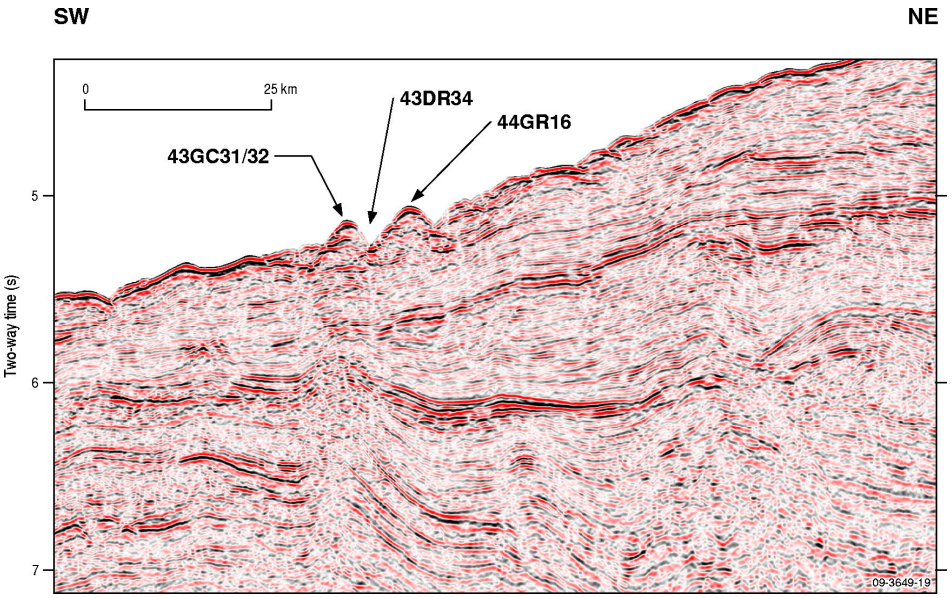

Figure 7.42. *Seismic line from Area 6 showing sampling locations on two mounded features that may be a mud volcano located above a possible mud diapir and toe thrusts (black lines).*

Seabed Morphology and Sedimentology

The multibeam swath data in Area 6 are sparse, with generally single track lines of swath acquisition. This data indicate a slope to the southwest from 3000 m water depth down to 3600 m in the north, 3800 m in the centre and 4000 m in the south of Area 6 (Fig. 7.43). In depths greater than 3300 m the swath indicates an irregular seabed with relatively shallow, indistinct canyon systems reaching 3900 m depth.

Samples of the seabed in Area 6 were collected from dredges and gravity cores from Stations 40 to 43, and one grab from Station 44. The sediments recovered from Station 40 include moderately lithified, brown mudstone and glauconitic mudstone. Station 41 sediment samples include moderately lithified, dark brown mudstone. Weakly lithified, dark brownish-grey mudstone was collected at Station 42, and weakly lithified, dark olive-green mudstone and calcareous foraminiferal ooze from Stations 43 and 44.

Table 7.7: *Area 6 samples.*

Sample Type	Station number	Sample number	Brief description
Grab	Station 40	40GR12	Foraminiferal ooze
Grab	Station 41	41GR13	Pale brown, calcareous, foraminiferal ooze. Somewhat gritty due to common forams, spicules etc.
Grab	Station 42	42GR14	Light greenish-grey, calcareous, foraminiferal ooze. Distinct gritty texture due to abundance of forams, minor spicules etc.
Grab	Station 43	43GR15	Cream coloured (10YR 7/3) foram-rich, fine- to very fine-grained, pelagic calcareous ooze.
Grab	Station 44	44GR16	Calcareous, foraminiferal ooze with dark grey streaks
Gravity Core	Station 40	40GC25	1.3 m. Top section of the core composed of cream coloured (10YR 7/4) calcareous mud overlain by a brown (2.5Y 4/2) sandy layer containing abundant forams. Beneath these is a layer of gravely siltstone that grades to dark mudstone (dark green, highly fossiliferous, heavily bioturbated stiff pyritic mud. Contains numerous fossils and fragments of corals, shells, bryozoa, foraminifera).
Gravity Core	Station 40	40GC26	2.8 m. Light greenish-grey, moderately calcareous, soft runny ooze. Base of core contains some lumps of black stiff mud.
Gravity Core	Station 41	41GC27	1.5 m. Pale grey, largely siliciclastic mud/ooze. Black, micaceous silty mudstone in KK.
Gravity Core	Station 41	41GC28	0.9 m. Mixture of dark, silty mud/mudstone containing glauconite, and siliceous-calcareous pelagic mud.
Gravity Core	Station 42	42GC29	0.5 m. Dark brownish-grey, weakly lithified claystone.
Gravity Core	Station 42	42GC30	0.5 m. Dark brownish-grey, weakly lithified claystone.
Gravity Core	Station 43	43GC31	0.5 m. Dark green, stiff, gritty mudstone capped by pale beige, siliciclastic, slightly calcareous mud.
Gravity Core	Station 43	43GC32	0.8 m. Dark green, highly fossiliferous, heavily bioturbated, stiff pyritic mud. Contains numerous fossils and fragments of corals, shells, bryozoa, foraminifera. Capped by 20 cm pale beige, calcareous mud.

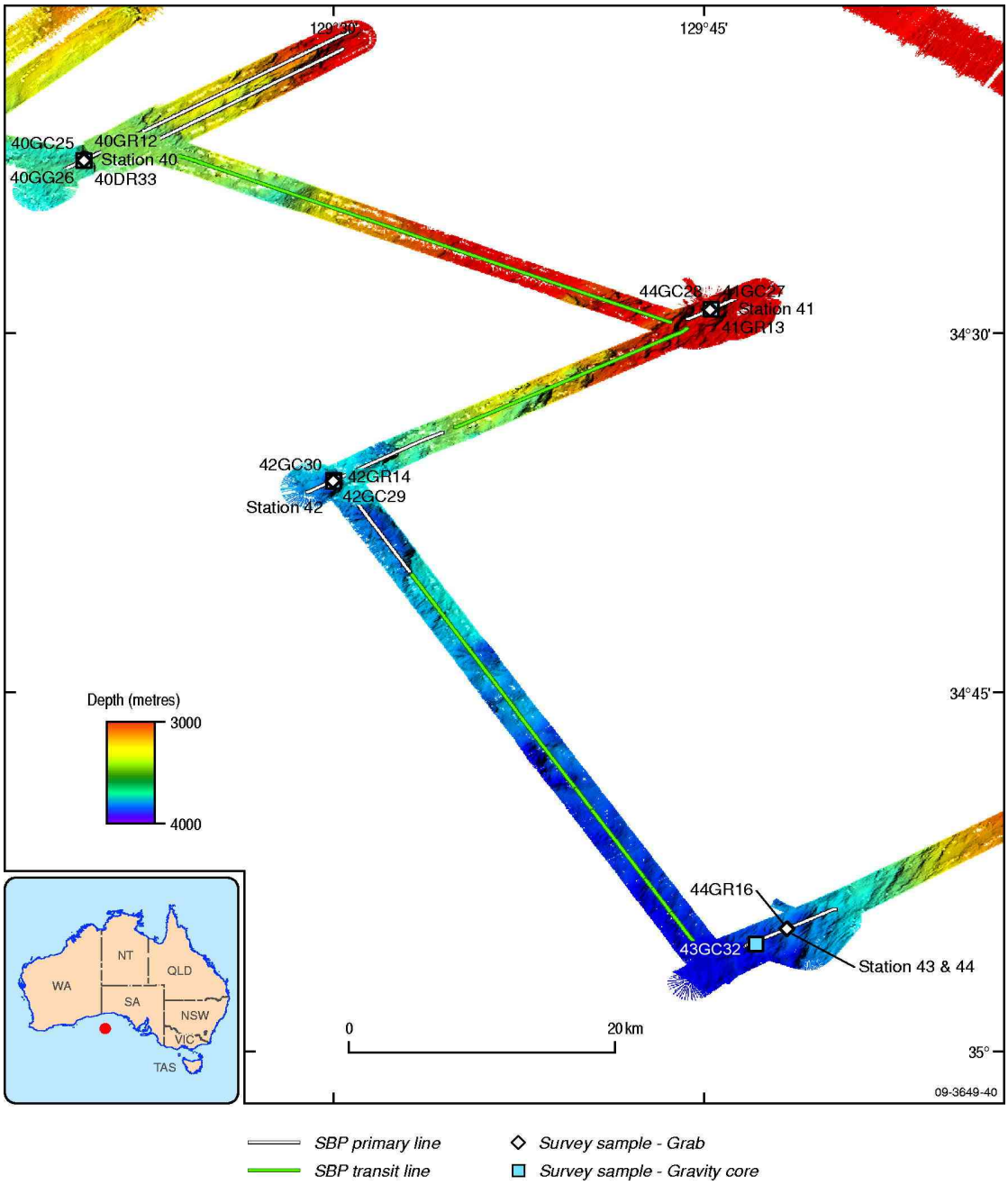

Figure 7.43. *Multibeam swath bathymetry over Area 6 with sample locations.*

Stratigraphy

The sub-bottom profiler data collected over Area 6 have very limited penetration. The area appears to have a hard surface at or near the seafloor and there is no penetration in the sub-bottom profiler data below this surface. The lack of penetration may also be related to the extreme water depths in this area. Therefore, there is no evidence of hydrocarbons seepage within the sub-bottom profiler data.

Station 43 attempted to sample elongate mounds imaged on the regional seismic and bathymetry data that are interpreted to be a mud volcano overlying deeper toe-thrusts and a possible mud diapir

(Fig. 7.42). Gravity core samples collected from this site contained dark green, highly fossiliferous, heavily bioturbated, stiff pyritic mud that was overlain by a thin (20 cm) layer of ooze. The relatively thin layer of ooze compared with other sites in Area 6 (Table 7.7), may indicate relatively recent mud volcano activity, however the sample coverage in the area is too sparse to allow a definitive interpretation.

Geochemistry

As for Areas 2c and 3, screening for thermogenic hydrocarbons through headspace gas and biomarker analyses provided no indication of hydrocarbon seepage in Area 6.

Surface sediments and cores showed a mixed terrestrial and marine signal (Fig. 7.44 and 7.45). Marine inputs increase slightly down core as illustrated by the rise in Marine/Terrestrial ratio in Fig. 7.30.

In Area 6 at Station 43, an interpreted mud volcano was sampled. Palynological analysis of core material collected at 60-80 cm depth indicates that the sediments are Maastrichtian and were deposited in an open marine environment (Appendix 3.1). The age determination and regional seismic data indicate that the sample comes from the Hammerhead Supersequence and was deposited outboard of a large delta system (Totterdell et al., 2000). The biomarker distribution of this sample is largely dominated by linear alkanols and alkanes in the range C_{25}-C_{32} showing carbon number predominance, indicative of a strong terrestrial input (Fig. 7.46). Other major components include polycyclic saturated and aromatic hydrocarbons. In order to study these in more detail, separation of the total organic extract through silica gel liquid chromatography into saturated and aromatic hydrocarbon fractions was carried out and results are summarized below. Algal biomarkers such as sterols or alkenones were either absent or in very low abundances.

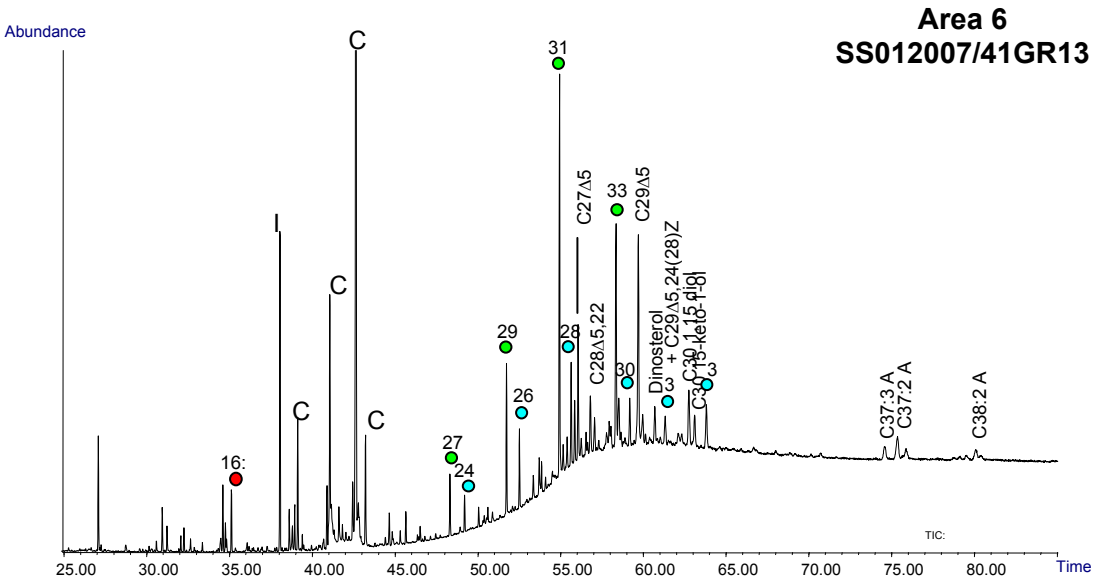

Figure 7.44*. Total ion chromatogram of silylated organic extract from grab sample SS012007/41GR13B. IS: Internal Standard; A: Alkenone; C: Contaminant; $C_{27}\Delta^5$: cholesterol; $C_{28}\Delta^{5,22}$: 24-methylcholesta-5,22E-dien-3β-ol; $C_{29}\Delta^5$: 24-ethylcholest-5-en-3β-ol; $C_{29}\Delta^{5,24(28)Z}$: 24-ethylcholesta-5,24(28)Z-dien-3β-ol.*

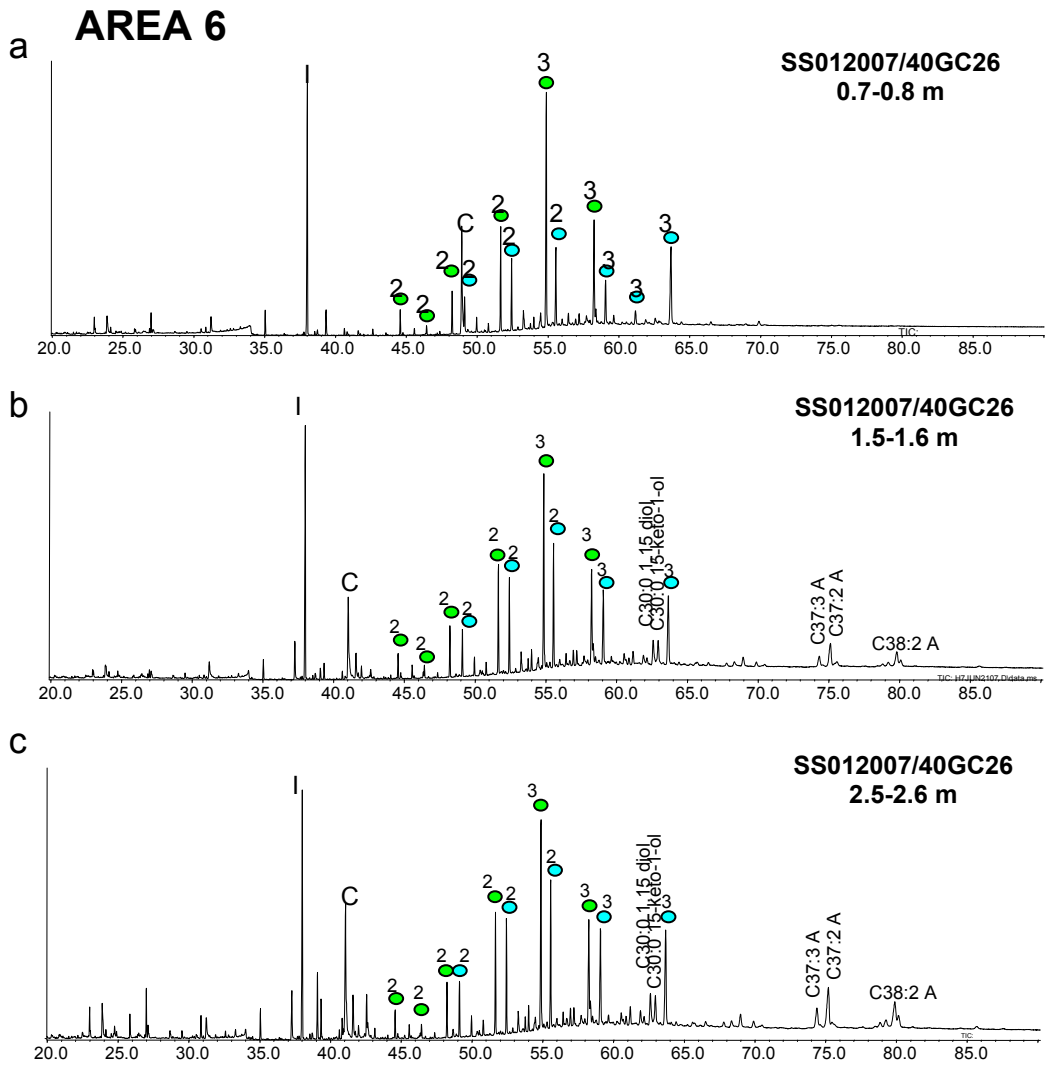

***Figure 7.45**. Total ion chromatograms of silylated organic extracts from Area 6 SS012007/40GC26 core samples: (a) 0.7-0.8 m, (b) 1.5-1.6 m and (c) 2.5-2.6 m. IS: Internal Standard; A: Alkenone; C: Contaminant.*

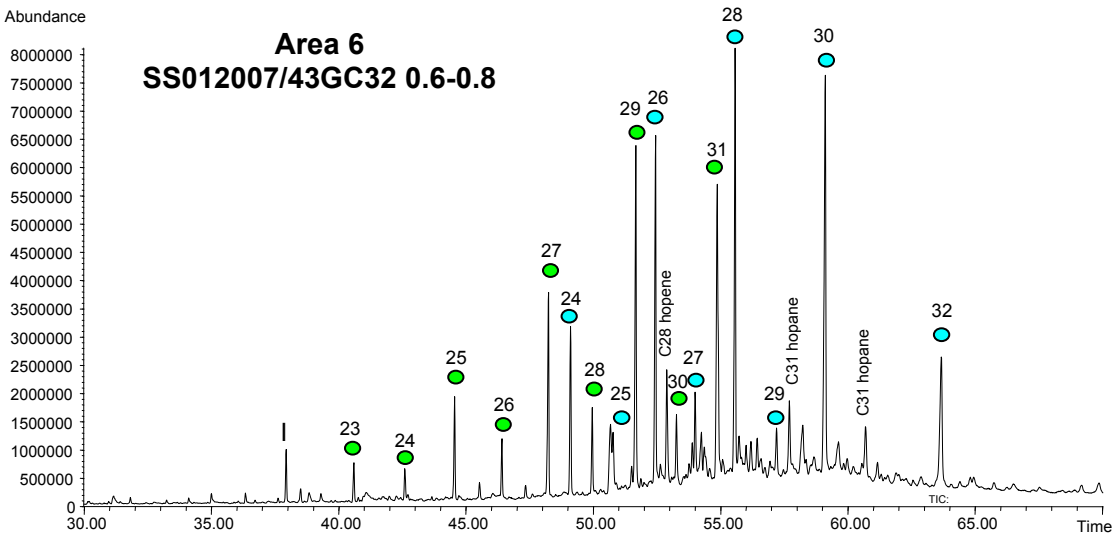

***Figure 7.46**. Total ion chromatogram of silylated organic extract from core sample SS012007/43GC32 0.6-0.8 m. IS: Internal Standard.*

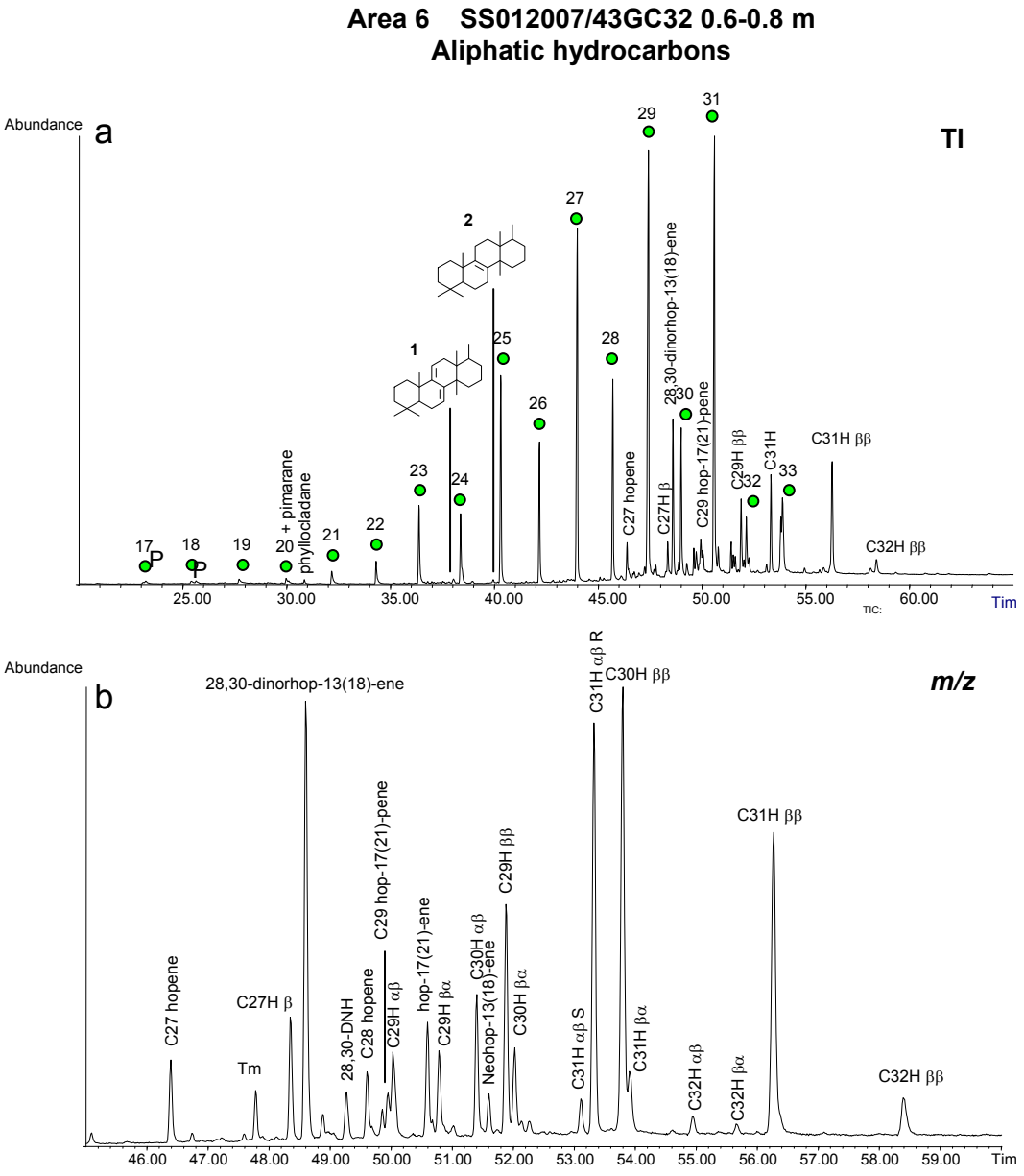

Figure 7.47*. Total ion chromatogram and (b) mass fragmentogram m/z 191 of aliphatic hydrocarbon fraction from core sample SS012007/43GC32 0.6-0.8 m. Pr: Pristane; Ph: Phytane; H: hopane.*

Aliphatic hydrocarbons

The distribution of normal alkanes ranges from C_{17} to C_{33} and is dominated by long-chain C_{25}-C_{31} homologues showing a strong odd over even carbon number predominance characteristic of terrigenous higher plant waxes (Eglinton & Hamilton, 1967) (Fig. 7.47a). Normal alkanes ranging from C_{17} to C_{22} and acyclic isoprenoids pristane and phytane are minor components of the sample. Major cyclic hydrocarbons consist mainly of hopanes and hopenes whose distribution is shown in Fig. 7.47b. The distribution of regular hopanes extends from C_{27} to C_{33} and is dominated by 17β(H),21β(H) isomers, which suggests the sample is immature. The isomers 17α(H),21β(H) and 17β(H),21α(H) are also present to a limited extent. The immaturity of the sediment is further confirmed by the predominance of 17α(H),21β(H)-22R isomers over 17α(H),21β(H)-22S, as well as by the presence of unsaturated hopanoid derivatives, such as rearranged des-E-hopanoid hydrocarbons 1 and 2 (Hauke et al., 1993), hop-17(21)-enes and neohop-13(18)-enes (Fig. 7.47a and 7.47b). Small amounts of 28,30-dinorhopane are present and occur along large concentrations of 28,30-dinorhopene, tentatively identified as 28,30-dinorhop-13(18)-ene, which was proposed as a precursor for 28,30-dinorhopane (Nytoft et al., 2000) (Fig. 7.47b). High abundances of 28,30-dinorhopane are usually encountered in petroleum source rocks deposited under anoxic conditions (Curiale et al., 1985; Mello et al., 1988). Although the origin of this compound is unknown, it is thought to be a product of early diagenetic bacterial reworking (Curiale et al., 1985) and possibly synthesized by sulphur-oxidizing bacteria (Williams, 1984). On the other hand, an alternative origin from ferns was proposed (Seifert et al., 1978). The large amounts of hopanoid derivatives in the aliphatic fraction attest to a significant bacterial contribution to the sediment. However, trace abundances of tentatively identified pimarane and phyllocladane also suggest small inputs from gymnosperms (mainly conifers) (Noble et al., 1985; Noble et al., 1986; Otto & Wilde, 2001). Steroid derivatives including steranes and sterenes were present only in trace amounts.

Aromatic hydrocarbons

The aromatic hydrocarbon fraction is dominated by higher plant-derived compounds. A series of A-ring monoaromatic triterpenoids was identified as 24,25-dinoroleana-1,3,5(10),12-tetraene, 24,25-dinorursa-1,3,5(10),12-tetraene and 24,25-dinorlupa-1,3,5(10)-triene based on mass spectral data (Wolff et al., 1989; Stout, 1992). Triaromatic hydrocarbons 1,2,4a,9-tetramethyl-1,2,3,4,4a,5,6,14bβ-octahydropicene and 1,2,4aβ,9-tetramethyl-1,2,3,4,4a,5,6,14bβ-octahydropicene and tetraaromatic hydrocarbons 1,2,9-trimethyl-1,2,3,4-tetrahydropicene and 2,2,9-trimethyl-1,2,3,4-tetrahydropicene were detected and identified based on published mass spectra (Chaffee & Johns, 1983; Hazai et al., 1989). These aromatic compounds are thought to be derived from the progressive aromatization of higher plant precursors such as β-amyrin and therefore, their abundance in the aromatic fraction indicates a strong terrigenous contribution to the sediment. Interestingly, no derivatives of terrigenous triterpenoids such oleanenes could be found in the aliphatic hydrocarbon fraction. Murray et al. (1997) observed a correlation between increasing abundances of saturated oleanoid derivatives with increasing marine influence in fluvio-deltaic sediments.

Area 7

Introduction

Area 7 is located on the seaward edge of the central Ceduna Terrace (Fig. 1.1). This area was targeted for potential seepage sites associated with recently reactivated Late Cretaceous growth faults extending to the seafloor (Fig. 7.48).

Seabed Morphology and Sedimentology

The multibeam swath data in Area 7 imaged the largest canyon head system observed during this survey – the Nullarbor canyon (Hill et al., 2001; Rollet et al., 2001; Fig. 7.49). The Nullarbor Canyon trends NNE-SSW and the head of the canyon lies in 1925 m water depth. The head of the canyon is sharp, comprising a semi-circular escarpment with a near-sheer relief of up to 250 m. The canyon is at least 10 km wide. Below the first major escarpment, the seafloor is relatively flat, before rising about 30 m to the possible remnants of a slump feature. The canyon contains a series of depressions, irregularities and escarpments, which become more acute with depth (Hill et al., 2001).

Samples of the seabed in Area 7 include dredge and gravity cores taken from Stations 52 to 59 (Table 7.8). Sediments recovered from Stations 52 to 55 include grey, calcareous, foraminiferal ooze, dark grey, argillaceous limestone, ferruginous and dark green mudstone, and lithified grey to black claystone.

Stratigraphy

Sub-bottom profiler penetration in Area 7 was limited to water depths of less than 2000 m. Lack of penetration in deeper water was probably related to both water depth and the steep gradient of the seabed. Where the sub-bottom profiler data did penetrate below the seafloor, the maximum data record was 0.25 s TWT (~185 m) in the centre of the area. Correlation with the regional seismic data suggests that the basal enhanced reflection observed in the sub-bottom profiler data in the centre of the area may correlate to the base of the Dugong Supersequence. An Oligocene horizon identified in the regional seismic data can also be correlated to the sub-bottom profiler data (Fig. 7.50). The Dugong Supersequence has a mid-Eocene to Recent age and contains basal coarse sandstone overlain by a carbonate succession (Totterdell et al., 2000). In the western and eastern parts of Area 7, a well stratified unit that can be seen on the sub-bottom profiler data possibly correlates to the early Pleistocene unit interpreted in Area 2c. The underlying unit is not clearly imaged in these areas but likely correlates to the Pliocene and older sediments of the Dugong Supersequence.

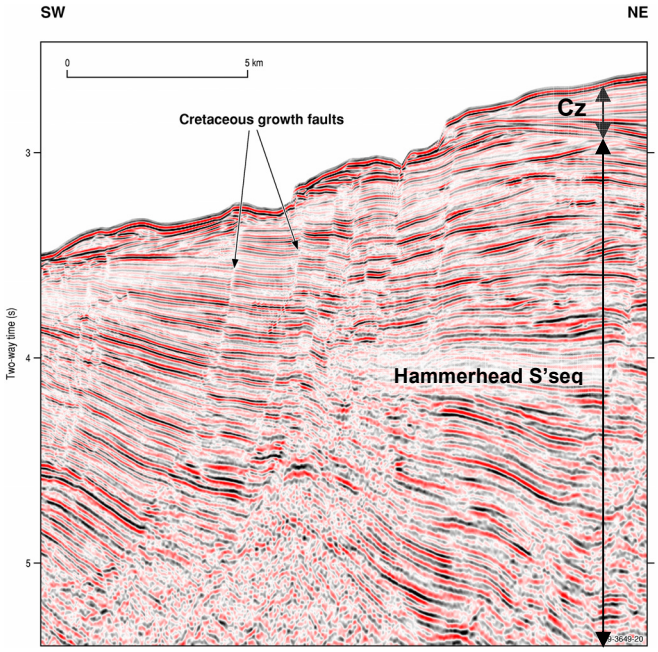

Figure 7.48. *Regional seismic line in Area 7 displaying reactivated growth faults within the late Cretaceous Hammerhead Supersequence that extend to the seafloor. Cz=Cenozoic.*

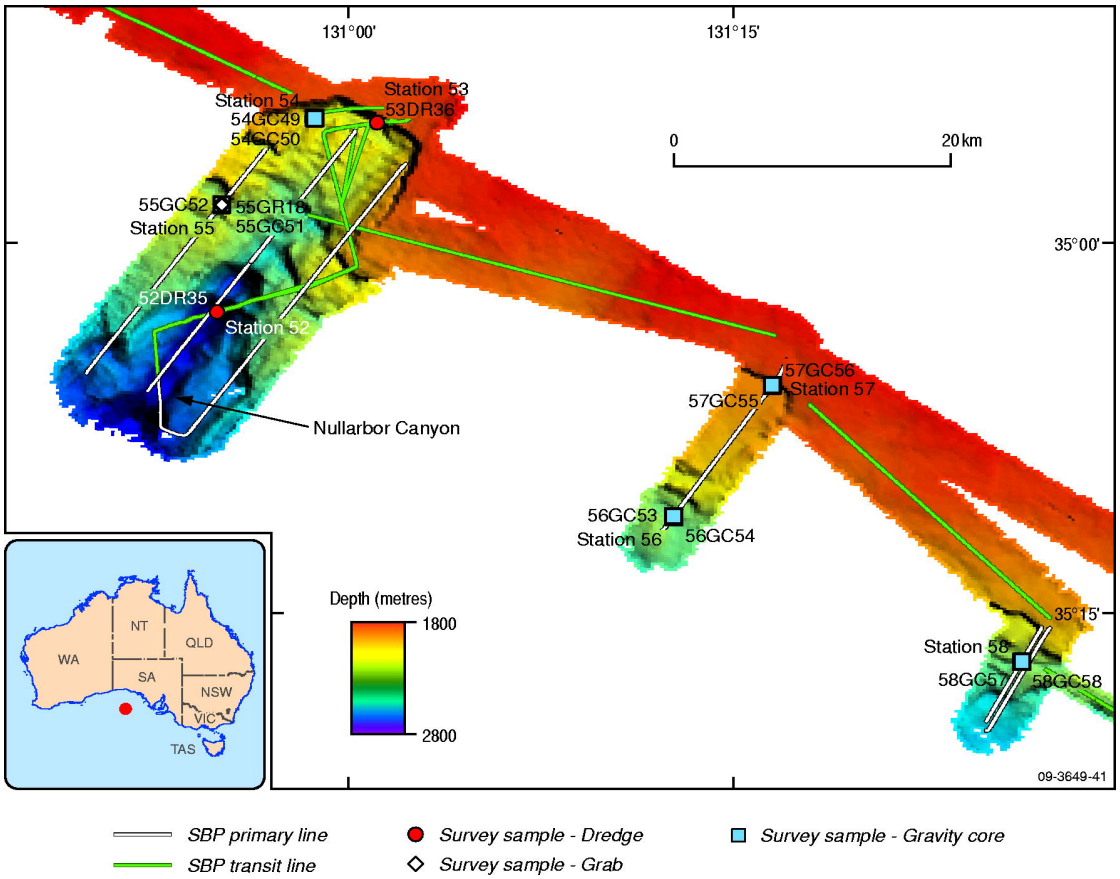

Figure 7.49. *Multibeam swath data collected over Area 7 with sample location.*

Table 7.8: *Area 7 samples*

Sample Type	Station number	Sample number	Brief description
Grab	Station 55	55GR18	Cream coloured, fine- to very fine-grained, foraminiferal, calcareous/siliceous ooze/mud.
Gravity Core	Station 54	54GC49	3.5 m. Dark yellowish-brown ooze at top; black, calcareous ooze with carbonaceous flecks, H_2S and pteropods; light greenish-grey, bryozoan sand/gravel with gastropods; and dark grey, bryozoan sand with chalk pebbles, minor gastropods and brown to black ooze at the base core.
Gravity Core	Station 54	54GC50	3.3 m. Dark yellowish-brown ooze at top; green-brown, mottled, slightly silty, calcareous ooze; very dark greenish-grey, calcareous ooze with strong H_2S odour; black calcareous ooze with carbonaceous flecks, H_2S and pteropods; and light greenish-grey, bryozoan sand/gravel with gastropods and chalk pebbles at base.
Gravity Core	Station 55	55GC51	1.6 m. Grey mottled, gritty, slightly calcareous foraminiferal mud.
Gravity Core	Station 55	55GC52	2.9 m. Dark green, stiff, siliceous mud with smooth plastic texture overlain by beige, gritty, foraminifera-rich, calcareous ooze.
Gravity Core	Station 56	56GC53	2.2 m. Stiff, sticky, beige mud with forams at top; mottled, calcareous, bioturbated mud with some forams; and grey, gritty, calcareous foraminiferal mud at base.
Gravity Core	Station 56	56GC54	1.8 m. Slightly mottled and bioturbated, pale greenish-grey, calcareous, foraminifera-rich mud.
Gravity Core	Station 57	57GC55	2.2 m. Yellowish-brown to light greenish-grey, calcareous, foraminiferal ooze.
Gravity Core	Station 57	57GC56	1.9 m. Light grey to white, calcareous, foraminiferal ooze.
Gravity Core	Station 58	58GR57	1.6 m. Grey, calcareous, foraminiferal ooze.
Gravity Core	Station 58	58GR58	1.3 m. Very pale brown to light greenish-grey to white, calcareous, foraminiferal ooze
Gravity Core	Station 59	59GR59	1.7 m. Pale green, bioturbated, mottled, slightly calcareous, sticky mud with some foraminifera. Small amount of dark green, stiff mud at base.
Gravity Core	Station 59	59GC60	2.6 m. Pale green/grey mottled, bioturbated, slightly calcareous, sticky mud with forams. Dark green, stiff mud at base.

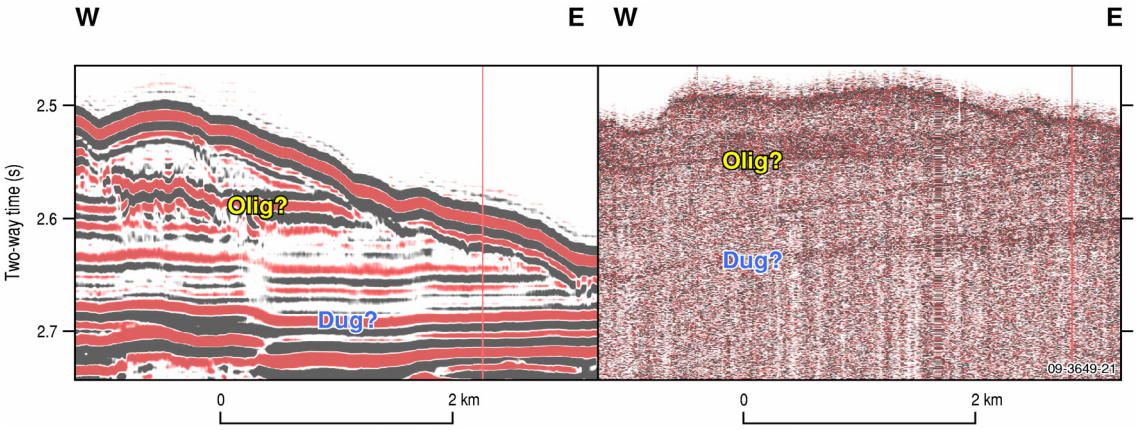

Figure 7.50. *Correlation of the interpreted stratigraphy from the sub-bottom profiler data with regional seismic data interpretation. Olig = Oligocene / late Miocene; Dug = Base Dugong Supersequence.*

Area 8

Introduction

Area 8 is located on the lower continental slope above the transition between the central Ceduna and Recherche sub-basins (Fig. 1.1). This area was targeted for potential seepage sites above interpreted Late Cretaceous shale ridges (Fig. 7.51).

Seabed Morphology and Sedimentology

The multibeam swath data collected over Area 8 show some evidence of mass movement on the slope below 3000 m water depth, however these features have not coalesced into discrete canyons (Fig. 7.52). Samples of the seabed in Area 8 include one gravity core from Station 61 and one dredge from Station 60. Sediments collected by the dredge include lithified mudstone and very weakly lithified claystone. Sediments recovered from the core include partially lithified dark greyish brown claystone.

Stratigraphy

The sub-bottom profiler data collected over Area 8 show very limited, if any, penetration. The lack of penetration in this area is likely to be related to the extreme water depths and steep slope of the seabed. Therefore, there is no evidence of hydrocarbon seepage within the sub-bottom profiler data within Area 8.

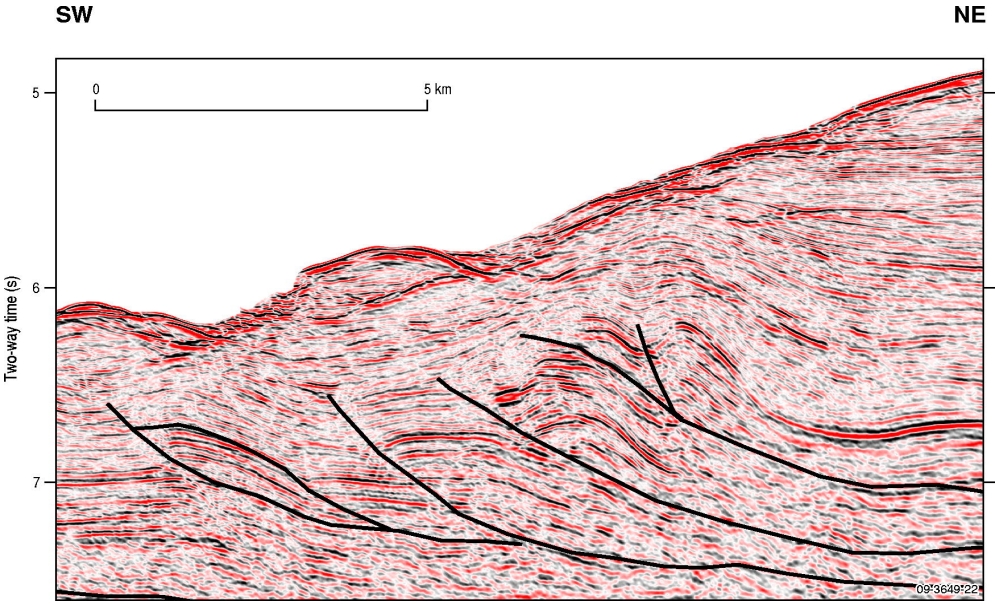

Figure 7.51. *Regional seismic data in Area 8 showing interpreted Late Cretaceous shale ridges associated with toe-thrusts (black lines).*

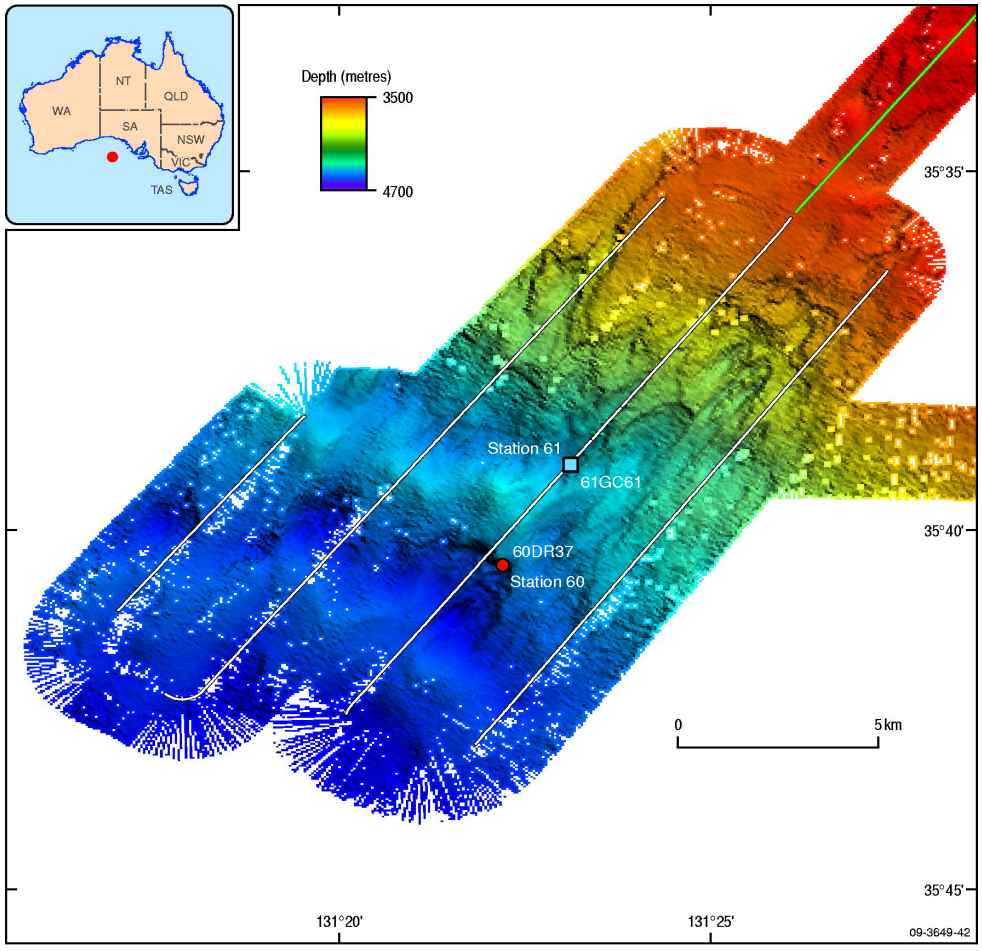

Figure 7.52. *Multibeam swath data collected over Area 8 with sample locations.*

Area 9

Introduction

Area 9 is located on the continental slope above the southeastern Ceduna Sub-basin (Fig. 1.1). This area was targeted for potential seepage sites above Late Cretaceous faults exposed by canyon erosion (Fig. 7.53).

Seabed Morphology and Sedimentology

The multibeam swath data collected over Area 9 partially cover four deeply incised, submarine canyons – from west to east, the Ceduna and Fowlers canyons, shallow canyons that are probably the head of the Nuyts Canyon, and the Pearson Canyon (Fig. 7.54; National Mapping and Information Group, 2008). Where surveyed, these canyons are narrow (3 to 4 km wide) and steep sided, and contain a series of closely spaced and abrupt escarpments. Only the eastern half of the Ceduna Canyon was surveyed; this canyon wall is an extremely steep slope that drops over 500 m into the channel axis. The second system (Fowlers Canyon) contains two nested escarpments, with evidence of a depression to the north. The Nuyts Canyon is narrow (1.8 km), smooth sided and around 100 m deep. Elongate, flow-parallel bedforms occur within this feature at a depth of ~1850 m. Similarly, the easternmost shallow canyon (Pearson Canyon) contains possible bedforms and is bordered to the east by a steep escarpment. A scalloped depression also occurs in the northern part of the canyon axis. The intervening seabed features highly irregular, low profile escarpments.

Samples of the seabed in Area 9 are from gravity cores taken at Stations 62 to 64 (Table 7.9). The sediment recovered from the surface of these cores included greenish to grey calcareous foraminiferal ooze. Station 64 recovered sticky foraminiferal mud and Station 62 also recovered some coal.

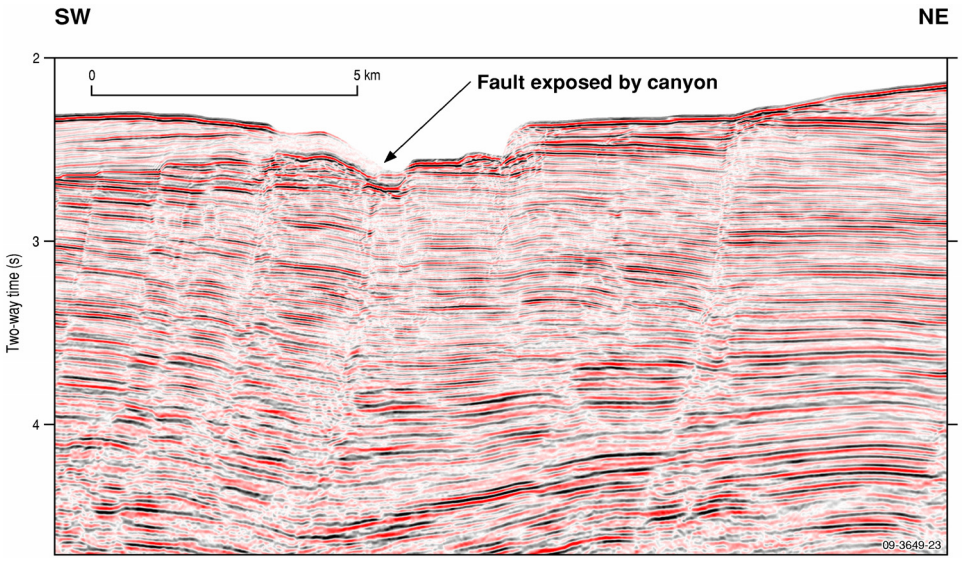

Figure 7.53. *Regional seismic line from Area 9 showing faults exposed at the seafloor due to canyon erosion.*

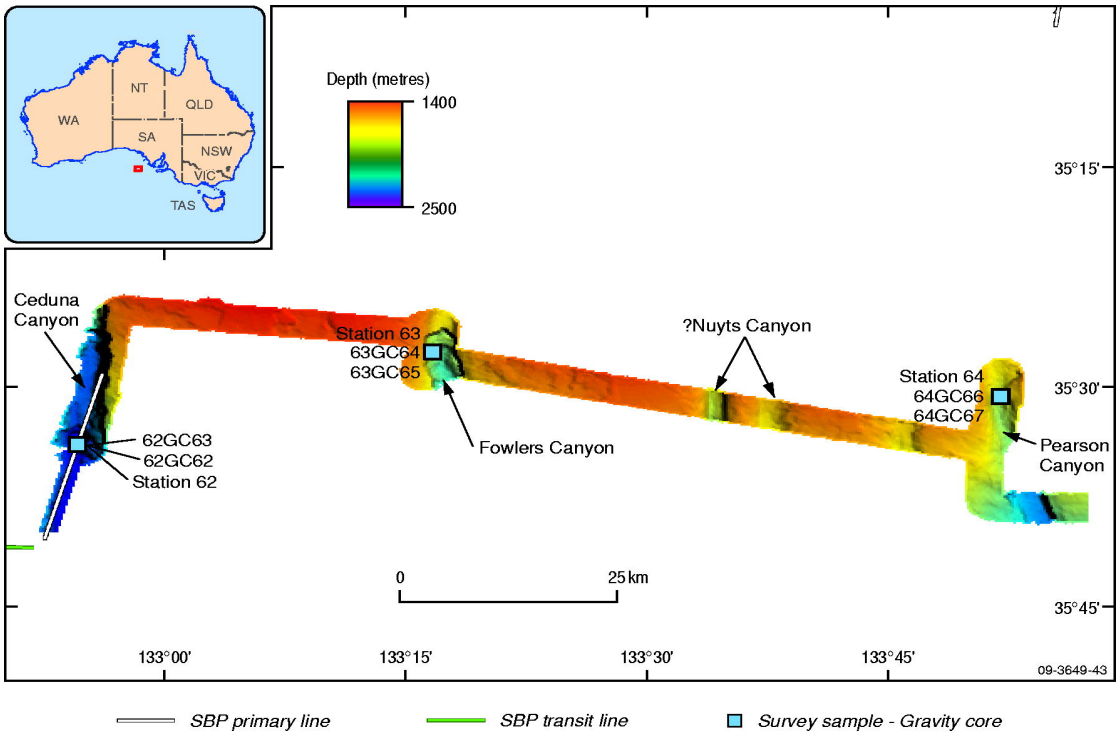

Figure 7.54. *Multibeam swath data collected over Area 9 with sample location*

Stratigraphy

The sub-bottom profiler data collected over Area 9 has very limited if any penetration. The lack of penetration within the sub-bottom profiler data in this area is likely related to the water depth and a hard surface at the seafloor preventing penetration. Therefore, there is no evidence of hydrocarbons seepage within the sub-bottom profiler data within Area 9.

Table 7.9: *Area 9 samples.*

Sample Type	Station number	Sample number	Brief description
Gravity Core	Station 62	62GC62	1.8 m. Greenish-grey, mottled, unconsolidated slightly calcareous mud.
Gravity Core	Station 62	62GC63	3.4 m. Pale green, sticky, slightly gritty and calcareous mud with some foraminifera.
Gravity Core	Station 63	63GC64	0.8 m. Pale green, soft, slightly calcareous mud and minor forams.
Gravity Core	Station 63	63GC65	Very dark brown, slightly micaceous claystone; semi-lithified, very friable(cc & kk recovered only).
Gravity Core	Station 64	64GC66	Grey, calcareous, foraminiferal and spicular ooze with some white, weakly lithified chalk.(cc & kk recovered only).
Gravity Core	Station 64	64GC67	2.0 m. White, weakly lithified chalk rubble with calcareous ooze matrix.

DISCUSSION AND SUMMARY

Geochemistry

Diverse geochemical methods were used to screen samples obtained during Geoscience Australia survey SS012007 for gas and liquid hydrocarbons to search for evidence of natural hydrocarbon seepage. Geochemical analysis of gravity cores from the Bight Basin survey failed to yield any evidence of thermogenic hydrocarbons. However, the analyses provided a range of information on the origin of organic matter in the near-surface and surface sediments.

Headspace gas

The primary objective of the geochemical sampling was to look for indication of natural hydrocarbon seepage. To address this, cores were sub-sampled for headspace gas analysis to establish the nature of pore space gases. Concentrations of methane (C_1), wet gases ethane, propane, butane and pentane (C_2-C_5), and carbon dioxide were determined for each sample.

The total headspace gas (Σ C_1 to C_5) range from less than 0.8 to 11.3 ppm. All of the Bight cores contain total headspace gas less than 50 ppm and are considered background based on the Surface Geochemistry Calibration database (Energy and Geoscience Institute, University of Utah) and other calibration studies (Logan et al., in press). The Bight total hydrocarbon sediment gases are some of the lowest background concentrations of any Australian or international studies (Logan et al., in press). All samples have elevated wet gas fraction values (Σ C_2-C_5/Σ C_1-C_5 greater than 0.05), which are due to differential volatile loss, i.e. greater loss of methane relative the wet gases (Abrams, 2005) and are not indicative of migrated thermogenic derived gases.

The headspace carbon dioxide range from less than 55.8 to 2,536 ppm. All of the Bight cores contain headspace carbon dioxide less than 10,000 ppm, which is the threshold value generally considered as anomalous based on worldwide surveys (Abrams, 2005).

These extremely low C_1 to C_5 gas concentrations suggest that there is no migration of biogenic or thermogenic gases at the sample sites or in situ methane generation.

High-molecular weight hydrocarbons (C_{12} plus)

Core sediments were analysed for their biomarker contents to primarily investigate the presence of seepage-related hydrocarbons. High-molecular weight petrogenic hydrocarbons (e.g., C_{12}^{+} linear alkanes with no carbon number preference) were not detected in any of the core samples. Specific biomarkers associated with methane-related microbial processes, such as anaerobic oxidation of methane (Niemann and Elvert, 2008), were also not detected. Therefore, analysis of high-molecular weight hydrocarbons showed no evidence for hydrocarbon seepage at any site. However, these biomarker data provide information for the environment of deposition and sources of organic matter in near-surface sediments.

Near-surface and surface sediments

Core samples taken during this survey show a strong terrestrial influence. Terrestrial biomarkers can be introduced into the marine environment either by fluvial or aeolian transport. Core sites are too distant from the continent to be affected by fluvial inputs. On the other hand, atmospheric transport via continental wind blown dust has long been recognized as a substantial mechanism for the supply of terrigenous lipids to marine sediments (Pancost & Boot, 2004). The prevalence of linear alkanes over linear alkanols has been suggested as an indication for aeolian inputs rather than fluvial,

because UV photo-oxidation of Aeolian-derived organic matter degrades *n*-alkanols preferentially compared to *n*-alkanes (Ten Haven et al., 1987). However, water depth and sedimentation rates are also thought to control the relative abundance of *n*-alkanols vs. *n*-alkanes (Westerhausen et al., 1993).

In contrast to the core samples, surface grab samples showed a more pronounced marine influence mixed with inputs from land plant material. Marine contribution is evidenced by the occurrence of various algal sterols including brassicasterol ($C_{28}\Delta^{5,22}$) and dinosterol (Fig. 7.28a). Brassicasterol is commonly used as a proxy for diatom abundances (Calvo et al., 2004; Schubert et al., 1998), but can also arise from other microalgae, such as haptophytes or cryptophytes (Volkman et al., 1998). Dinosterol is thought to derive primarily from dinoflagellates (Volkman, 2003). Such sterols were below detection limit in core samples from this survey. Absolute concentrations of terrestrial lipids (linear C_{27}-C_{33} alkanes and C_{26}-C_{32} alkanols) in surface grabs were similar to those of core samples, indicating that terrigenous inputs remained constant over time, while marine contributions decreased (with core depth) in Area 2c.

The geochemistry of surface and core sediments in Area 2c is consistent with the fact that there has been very little recent carbonate deposition in this region. The terrigenous geochemical signature appears to dominate the interpreted well-stratified Early Pleistocene unit and the marine signal likely relates to the Late Pleistocene to Recent marine carbonate deposition. Therefore, the Early Pleistocene unit in Area 2c probably has an abundant aeolian component along with reworked and transported shelf sediments deposited in the area. Reworking of sediments (resuspension and resedimentation) is known to lead to enrichment of more refractory terrestrial biomarkers versus more labile marine lipids accounting for the observed down core biomarker distributions (Colombo et al., 1997; Hoefs et al., 2002). This may also be the reason why the signature in Area 2c is dominantly terrestrial compared to that of Area 3, which is slightly more proximal to its sediment supply.

Seepage indications

Although the geochemistry analysis of the gravity cores sampled yielded no hydrocarbon indications, there were some minor indications of possible shallow gas and seepage within other datasets acquired from the survey. Flares that were identified in the echo-sounder data from Area 1 were possibly related to seepage, particularly as they were located in the vicinity of two third rank SAR slicks. The underlying seismic data indicate zones of vertical disruption, however, the sub-bottom profiler data did not have adequate penetration to identify any shallow gas indicators.

Some potential shallow gas indicators were identified in the sub-bottom profiler data acquired during the transit from Area 1 to Area 2. Because the raw data are not available for this area, seismic attribute analysis was conducted on the processed sub-bottom profiler data. This means that the results of the seismic attribute analysis should be interpreted with some caution. However, the features observed in the data are very different to anything else observed during the survey. The attribute analysis indicated that the features had an enhanced reflectivity, reduced frequency and reversed polarity which all indicate the presence of a low velocity layer that may be shallow gas/fluid.

Area 3 contained an area of pockmarked seafloor that is probably related to fluid escape. The sub-bottom profiler data had minor indications for possible shallow gas below the pockmarks, however, the quality of the data was too poor to conduct attribute analysis. Given the size of these pockmarks (about 150 m diameter and 5 m deep) a large amount of fluid escape would be required to create them. Although dewatering is the most probable cause of these features, gas escape cannot be precluded given the relatively poor quality of the sub-bottom profiler data.

Shallow stratigraphy

The top of the basal unit observed in the sub-bottom profiler data is interpreted as either an Oligocene unconformity or the Middle Miocene unconformity that correlates to MH1 interpreted from ODP sites on the Eyre Terrace. The overlying Pliocene unit was intersected by the ODP sites near the outer edge of the Eyre Terrace and ranged from about 40 to 20 m thick. This is consistent with the interpreted Pliocene unit interpreted from sub-bottom profiler data in Areas 2 and 3 which has an approximate maximum thickness of 30 m.

The early Pleistocene unit interpreted from sub-bottom profiler data is thickest in Area 3 with an estimated 45 m of stratified sediment. Area 2c is located near the Ceduna Terrace margin close to the continental rise in the central GAB. The sub-bottom profiler data indicates that this area has had very little recent deposition with the Early Pleistocene unit shallowly buried or exposed at the seafloor.

Area 6, located off the continental rise, sampled an interpreted mud volcano. The base of the gravity core sampled middle to late Campanian dark mud mounded on the seafloor. This mud was overlain by approximately 20 cm of calcareous ooze, suggesting either that the mud volcano had been active relatively recently, or there has been little to no recent deposition.

The presence of the phosphate nodules in Area 5 is likely to be related to high nutrient upwelling currents and a low recent sedimentation rate. Hughes et al. (2009) reported that in summer months, episodic reversal of the normally eastward-flowing South Australian Current can lead to upwelling via the submarine canyons that incise the continental slope in the GAB.

8. Summary of Survey SS01/2007 Results

J. Totterdell

INTRODUCTION

The Bight Basin Sampling and Seepage Survey (SS01/2007), was designed to address two key petroleum systems issues in the Bight Basin. In order to assist in our understanding of the distribution of source rocks in the basin, the survey aimed to sample the distal facies of potential source intervals of Albian-Santonian age at locations on the seaward edges of the Ceduna and Eyre Terraces. Secondly, the survey aimed to investigate the presence of active petroleum systems by obtaining seabed samples and geophysical data at potential natural hydrocarbon seepage sites across the Ceduna Sub-basin.

Nine areas of interest were identified for surveying in the eastern Bight Basin, including areas where the targeted Albian-Santonian section outcrops on the seafloor, and areas where there was seismic and other geophysical and remotely sensed evidence of possible hydrocarbon seepage. The survey, which was conducted using the Marine National Facility vessel RV *Southern Surveyor*, took place from 24 February–17 March 2007 and successfully sampled all nine targeted areas.

The survey collected 37 dredge hauls, 69 gravity cores and 15 grab samples, as well as 8825 km^2 of swath bathymetry data, and 2400 km of sub-bottom profiler data.

DREDGE SAMPLING SURVEY

The survey was very successful in addressing the most critical of its objectives, recovering samples from the exposed up-dip northwestern edge of the Ceduna Sub-basin that provide the first evidence for a world-class marine Cretaceous source rock in the Bight Basin.

Geochemical and biostratigraphic analysis of dredge samples from Area 5 identified a suite of rocks with the following characteristics:

- Good-very good organic richness: TOC 2–6.9% (17 samples)
- Good to excellent liquids potential: HI 274–479 mgHC/gTOC (11 samples)
- Samples with highest liquids potential have highest TOC (Dredge 17)
- Organic matter has a marine signature and was deposited under reducing (anoxic) conditions
- A close geochemical relationship between these samples and asphaltites recovered as coastal bitumen strandings
- Geochemical comparisons between the potential source rocks and the asphaltites suggests the presence of richer source rocks elsewhere in the basin
- Biostratigraphy: Latest Cenomanian–earliest Turonian
- Age and geochemistry of these organic-rich rocks suggest that they are a local expression of the global Oceanic Anoxic Event 2

These rocks are the best evidence to date of the presence of liquids-prone source rocks in the Bight Basin, and significantly upgrade its petroleum prospectivity by reducing uncertainty regarding this fundamental element of the petroleum system.

Overall, the survey recovered clastic rocks ranging in age from Cenomanian to Maastrichtian, with depositional environments ranging from delta plain to open marine. In addition, several Cenozoic

carbonate rocks were recovered. In the key sampling area, Area 5, the biostratigraphic results indicate that stratigraphic units sampled were the targeted White Pointer and Tiger Supersequences. The best potential source rocks, which straddle the Cenomanian-Turonian boundary, are interpreted to represent the basal Tiger Supersequence.

SEEPAGE SURVEY

The results of the seepage survey were more equivocal. No direct evidence of hydrocarbon seepage was found, despite targeting of a range of promising localities across the basin. Organic geochemical analyses of gravity core samples failed to detect any thermogenic hydrocarbons.

Indirect evidence of possible high-level gas was provided by the sub-bottom profiler data collected in transit between Areas 1 and 2, and in Area 3. Data collected in these areas included some features that can be interpreted as indicating the presence of shallow gas. In addition, echo-sounder data in Area 1 captured flares of unknown origin immediately overlying a possible seepage site identified on seismic data.

There are several possible reasons for failure to directly detect any hydrocarbons during the seepage survey, including hydrocarbons not being preserved in the very shallow section (<10 m) that was sampled by the gravity corer, poor targeting of potential seepage sites, or the lack of any hydrocarbon seepage. This question will probably not be resolved until further sampling work is carried out in the basin, using equipment capable of taking deep cores.

9. Acknowledgements

The authors wish to thank the scientific, technical & ship's crew of the RV *Southern Surveyor,* particularly ship's master Ian Taylor, and CSIRO Ships Manager Ron Plaschke. Special thanks to Geoscience Australia's Palaeontology and Sedimentology Laboratory, Organic and Isotope Geochemistry Laboratory and Field and Engineering Support group. We also thank Heike Struckmeyer and Andrew Jones for their helpful reviews, and David Arnold and Chris Evenden for drafting the figures.

10. References

Abrams, M.A., 2005. Significance of hydrocarbon seepage relative to petroleum generation and entrapment. Marine and Petroleum Geology, 22, 457-477.

Arthur, M.A., Schlanger, S.O. and Jenkyns, H.C., 1987. The Cenomanian–Turonian Oceanic Anoxic Event, II: Palaeoceanographic controls on organic-matter production and preservation. In: Brooks, J. and Fleet, A.J. (Eds), Marine petroleum source rocks. Geological Society Special Publication 26, 401–420.

Bein, J. and Taylor, M.L., 1981. The Eyre Sub-basin: recent exploration results. The APEA Journal, 21, 91–98.

Bernard, B.B., 1978. Light hydrocarbons in marine sediments. Ph.D. dissertation, Texas A&M University, College Station, Texas, 144 p.

Blevin, J.E., Totterdell, J.M., Logan, G.A., Kennard, J.M., Struckmeyer, H.I.M. and Colwell, J.B., 2000. Hydrocarbon prospectivity of the Bight Basin—petroleum systems analysis in a frontier basin. In: 2nd Sprigg Symposium – Frontier Basins, Frontier Ideas, Adelaide, 29–30 June, 2000. Geological Society of Australia, Abstracts 60, 24–29.

Boreham, C. J., 1992. Reversed-phase high-performance liquid chromatography of metalloporphyrins. In: Moldowan, J.M., Albrecht, P. and Philp, R.P. (Eds), Biomarkers in sediments and petroleum- a tribute to W. Seifert, Prentice Hall, 301–312.

Boreham, C.J. and Ambrose, G., 2007. Cambrian petroleum systems in the southern Georgina Basin, Northern Territory, Australia. In: Munson, T.J. and Ambrose, G.J. (Eds). Proceedings of the Central Australian Basins Symposium, Alice Springs, 16–18th August, 2005. Northern Territory Geological Survey, Special Publication 2, 254–281. http://conferences.minerals.nt.gov.au/cabsproceedings/georgina.htm

Boreham, C., Davenport. R. and Hong, Z., 2005. Petroleum geochemistry – source rock characterisation. In: Blevin, J. E. (compiler), Geological framework of the Bremer and Denmark sub-basins, southwest Australia. R/V *Southern Surveyor* Survey SS03/2004, Geoscience Australia Survey 265: Post-survey report and GIS. Geoscience Australia Record 2005/05, Appendix J.

Boreham, C.J. and Fookes, C.J.R., 1989. Separation of nickel(II) alkylporphyrins by reversed-phase high-performance liquid chromatography. Methodology and application. Journal of Chromatography, 467, 195–208.

Boreham, C.J., Krassay, A.A. and Totterdell, J.M., 2001. Geochemical comparisons between asphaltites on the southern Australian margin and Cretaceous source rock analogues. In: Hill, K.C. and Bernecker, T. (Eds), Eastern Australasian Basins Symposium: a refocused energy perspective for the future. Petroleum Exploration Society of Australia, Special Publication, 531–541.

Boreham, C.J. and Powell., T.G., 1987. Sources and preservation of organic matter in the Cretaceous Toolebuc Formation, eastern Australia. Organic Geochemistry, 11, 433–449.

Bradshaw, B.E., Rollet, N., Totterdell, J.M. and Borissova, I., 2003. A revised structural framework for frontier basins on the southern and southwestern Australian continental margin. Geoscience Australia Record 2003/03.

Brassell, S.C., Eglinton, G., Marlowe, I.T., Pflaumann, U. and Sarnthein, M., 1986. Molecular stratigraphy: a new tool for climatic assessment. Nature 320, 129–133.

Brocks, J.J., Love, G.D., Summons, R.E., Knoll, A.H., Logan, G.A. and Bowden, S.A., 2005. Biomarker evidence for green and purple sulphur bacteria in a stratified Palaeoproterozoic sea. Nature 437, 866–870.

Bruins, J., Longley, I.M., Fitzpatrick, J.P., King, S.J. and Somerville, R.M., 2001. The Ceduna Sub-basin—an exploration update. In: Hill, K.C. and Bernecker, T. (Eds), Eastern Australasian

Basins Symposium: a refocused energy perspective for the future. Petroleum Exploration Society of Australia, Special Publication, 655–658.

Calvo, E., Pelejero, C., Logan, G. and De Deckker, P., 2004. Dust-induced changes in phytoplankton composition in the Tasman Sea during the last four glacial cycles. Paleoceanography 19, PA2020, doi:10.1029/2003PA000992.

Chaffee, A.L. and Johns, R.B., 1983. Polycyclic aromatic hydrocarbons in Australian coals. I. Angularly fused pentacyclic tri- and tetraaromatic components of Victorian brown coal. Geochimica et Cosmochimica Acta, 47, 2141–2155.

Clegg, H., Horsfield, B., Stasiuk, L., Fowler, M. and Vliex, M., 1997. Geochemical characterisation of organic matter in Keg River Formation (Elk point group, Middle Devonian), La Crete Basin, Western Canada. Organic Geochemistry, 26(11-12), 627–643.

Colombo, J.C., Silverberg, N. and Gearing, J.N., 1997. Lipid biogeochemistry in the Laurentian Trough--II. Changes in composition of fatty acids, sterols and aliphatic hydrocarbons during early diagenesis. Organic Geochemistry 26, 257–274.

Copard, Y., Disnar, J.R. and Becq-Giraudon, J.F., 2002. Erroneous maturity assessment given by Tmax and HI Rock-Eval parameters on highly mature weathered coals. International Journal of Coal Geology, 49, 57–65.

Curiale, J.A., Cameron, D. and Davis, D.V., 1985. Biological marker distribution and significance in oils and rocks of the Monterey Formation, California. Geochimica et Cosmochimica Acta 49, 271–288.

Davies, H. L., Clarke, J. D. A., Stagg, H. M. J., Shafik, S., McGowran, B. and Alley, N. F., 1989. Maastrichtian and younger sediments from the Great Australian Bight: Bureau of Mineral Resources, Geology and Geophysics, Report 288, 1–40.

di Primio, R., Horsfield, B., 2006. From petroleum type organofacies to hydrocarbon phase prediction. AAPG Bulletin, 90(7), 1031–1058.

Edwards, D., McKirdy, D.M. and Summons, R.E., 1998. Enigmatic asphaltites from the southern margin: molecular and carbon isotopic composition. PESA Journal, 26, 106–123.

Edwards, D.S., Preston, J.C., Kennard, J.M., Boreham, C.J., Van Aarssen, B.G.K., Summons, R.E. and Zumberge, J.E., 2004. Geochemical characteristics of hydrocarbons from the Vulcan Sub-basin, western Bonaparte Basin, Australia. Timor Sea Symposium, Darwin. 169–201.

Eglinton, G. and Hamilton, R.J., 1967. Leaf epicutilar waxes. Science, 156, 1322–1324.

Erbacher, J., Friedrich, O., Wilson, P.A., Birch, H. and Mutterlose, J., 2005. Stable organic carbon isotope stratigraphy across Oceanic Anoxic Event 2 of Demerara Rise, western tropical Atlantic. Geochemistry Geophysics Systems, 6, Q061010, doi:10.1029/2004GC000850.

Espitalié, J. and Bordenave, M.L., 1993. Rock-Eval pyrolysis. In: Bordenave, M.L. (Ed), Applied Petroleum Geochemistry, Éditions Technip, Paris, 237–261.

Farrimond. P., Eglinton, G. and Brassell, S.C., 1990. The Cenomanian/Turonian anoxic event in Europe: an organic geochemical study. Marine and Petroleum Geology, 7, 75–89.

Feary, D.A., et al., 1993. Geological sampling in the Great Australian Bight: scientific post-cruise report – R/V *Rig Seismic* cruise 102. Australian Geological Survey Organisation, Record 1993/18.

Feary, D.A., Hine, A.C., James, N.P. and Malone, M.J., 2004. Leg 182 synthesis: exposed secrets of the Great Australian Bight. In: Hine, A.C., Feary, D.A. and Malone, M.J. (Eds) Proceedings of the Ocean Drilling Program: Scientific Results, 182, Chapter 1, 1–30.

Feary, D. A. and James, N. P., 1998. Seismic stratigraphy and geological evolution of the Cenozoic, cool-water Eucla Platform, Great Australian Bight. American Association of Petroleum Geologists Bulletin 82, 792–816.

Fraser, A.R. and Tilbury, L.A., 1979. Structure and stratigraphy of the Ceduna Terrace region, Great Australian Bight. The APEA Journal, 19(1), 53–65.

Gradstein, F.M., Ogg, J.G. and Smith, A.G., 2004. A geologic time scale 2004. Cambridge University Press, 589p.

Hallam, A., 1981. A revised sea-level curve for the Early Jurassic. Journal of the Geological Society, 138, 735–743.

Hallam, A., 1992. Phanerozoic sea-level changes. Columbia University Press, New York, 266p.

Haq, B.U., Hardenbol, J. and Vail, P.R., 1988. Mesozoic and Cenozoic chronostratigraphy and eustatic cycles. In: Wilgus, C.K., Hastings, B.S., Kendall, C.G.St.C., Posamentier, H.W., Ross, C.A. and Van Wagoner, J.C. (Eds), Sea-level changes: an integrated approach. Society of Economic Paleontologists and Mineralogists, Special Publication 42, 71–108.

Hartgers, W.A., Sinninge Damste, J.S., Requejo, A.G., Allan, J., Hayes, J.M. and de Leeuw, J.W., 1994. Evidence for only minor contributions from bacteria to sedimentary organic carbon. Nature, 369, 224–227.

Hauke, V., Graff, R., Wehrung, P., Hussler, G., Trendel, J.M., Albrecht, P., Riva, A. and Connan, J., 1993. Rearranged des-E-hopanoid hydrocarbons in sediments and petroleum. Organic Geochemistry, 20, 415–423.

Hautevelle, Y., Michels, R., Malartre, F. and Trouiller, A., 2007. The initiation and the resumption of the Callovo-Oxfordian crisis of carbonate productivity: relations with anoxic events and palaeoclimate. IMOG 2007 P106-MO.

Hayes, J.M., Strauss, H. and Kaufman, A.J., 1999. The abundance of ^{13}C in marine organic matter and isotopic fractionation in the global biogeochemical cycle of carbon during the past 800 Ma. Chemical Geology 161, 103–125.

Hazai, I., Alexander, G. and Szekely, T., 1989. Study of aromatic biomarkers in brown coal extracts. Fuel 68, 49–54.

Hesselbo, S. P. and Jenkyns, H. C., 1998. British Lower Jurassic sequence stratigraphy. In: de Graciansky, P.-C., Hardenbol, J., Jacquin, T. and Vail, P. (Eds), Mesozoic and Cenozoic sequence stratigraphy of European basins. Society of Economic Paleontologists and Mineralogists Special Publication 60, 561–581.

Hill, A.J., 1991. Revisions to the Cretaceous stratigraphic nomenclature of the Bight and Duntroon Basins, South Australia. Geological Survey of South Australia, Quarterly Notes, 120, 2–20.

Hill, A.J., 1995. Bight Basin. In: Drexel, J.F. and Preiss, W.V. (Eds), The geology of South Australia. Vol. 2, The Phanerozoic. South Australia, Geological Survey, Bulletin, 54, 133–149.

Hill, P., Rollet, N and Symonds, P., 2001. Seafloor mapping of the South-east Marine Region and adjacent waters – AUSTREA final report: Lord Howe Island, south-east Australian margin (includes Tasmania and South Tasman Rise) and central Great Australian Bight. Australian Geological Survey Organisation Record 2001/08.

Hine, A.C., Brooks, G.R., Mallinson, D., Brunner, C.A., James, N.P. and Feary, D.A., 2004. Data Report: Late Pleistocene-Holocene sedimentation along the upper slope of the Great Australia Bight. In: Hine, A.C., Feary, D.A. and Malone, M.J. (Eds) Proceedings of the Ocean Drilling Program: Scientific Results, 182, Chapter 8, 1–24.

Hoefs, M.J.L., Rijpstra, W.I.C. and Sinninghe Damste, J.S., 2002. The influence of oxic degradation on the sedimentary biomarker record I: evidence from Madeira Abyssal Plain turbidites. Geochimica et Cosmochimica Acta, 66, 2719–2735.

Hoefs M.J.L., van Heemst J.D.H., Gelin, F., Koopmans M.P., van Kaam-Peters H.M.E., Schouten S., de Leeuw J.W. and Sinninghe-Damste J.S., 1995. Alternative biological sources for 1,2,3,4-tetramethylbenzene in flash pyrolysates of kerogen. Organic Geochemistry 23, 975–979.

Holbourn, A.E., Drexler, T.M., Howd P., Marlowe, I.T., Brassell, S.C., Eglinton, G. and Green, J.C., 1984. Long chain unsaturated ketones and esters in living algae and marine sediments. Organic Geochemistry 6, 135–141.

Holbourn, A. and Kuhnt, W., 2002. Cenomanian–Turonian palaeoceanographic change on the Kerguelen Plateau: a comparison with Northern Hemisphere records. Cretaceous Research, 23, 333–349.

Holdway, D., Radlinski, A.P., Exon, N., Auzende, J-M. and Van de Beuque, S., 2000. Continuous multi-spectral fluorescence and absorption spectroscopy for hydrocarbon detection in ocean waters: Fairway Basin, Lord Howe Rise. AGSO Record 2000/35, 57 pp.

Horsfield, B., 1989. Practical criteria for classifying kerogens: Some observations from pyrolysis-gas chromatography. Geochimica et Cosmochimica Acta, 53, 891–901.

Horsfield, B., 1997. The bulk composition of first-formed petroleum in source rocks. In: Welte, D. H., Baker, D. R. and Horsfield, B., Petroleum and Basin Evolution. Springer, Berlin, 337–402.

Hughes, M.G., Nichol, S., Przeslawski, R., Totterdell, J., Heap, A., Fellows, M. and Daniell, J., 2009. Ceduna Sub-basin: environmental summary. Geoscience Australia record 2009/09.

James, N.P., Bone, Y. Collins, L.B. and Kyser K., 2001. Surficial sediments of the Great Australian Bight facies dynamics and oceanography on a vast cool-water carbonate shelf. Journal of Sedimentary Research, 71, 549–567.

James, N.P and von der Borch, C.C., 1991. Carbonate shelf edge off southern Australia: A prograding open-platform margin. Geology, 19, 1005–1008.

Jenkyns, H.C., 1980. Cretaceous anoxic events: from continents to oceans. Journal of the Geological Society, London, 137, 171–188.

Jenkyns, H. C. and Clayton, C. J., 1986. Black shales and carbon isotopes in pelagic sediments from the Tethyan Lower Jurassic. Sedimentology, 33, 87–106.

Jones, A.T., Kennard, J.M., Ryan, G.J., Bernardel, G., Earl, K., Rollet, N., Grosjean, E. and. Logan, G.A., 2007. Geoscience Australia marine survey SS06/2006: post-survey report: natural hydrocarbon seepage survey on the central North West Shelf. Geoscience Australia Record 2007/21.

Judd, A.G. and Hovland, M., 2007. Seabed Fluid Flow: The impact on Geology, Biology and the Marine Environment. Cambridge University Press, New York, 475 pp.

Kerr, A.C., 1998. Oceanic plateau formation: a cause of mass extinction and black shale deposition around the Cenomanian–Turonian boundary. Journal of Geological Society, London, 155, 619–626.

King, S.J. and Mee, B.C., 2004. The seismic stratigraphy and petroleum potential of the Late Cretaceous Ceduna Delta, Ceduna Sub-basin, Great Australian Bight. In: Boult, P.J., Johns, D.R. and Lang, S.C. (Eds), Eastern Australasian Basins Symposium II. Petroleum Exploration Society of Australia, Special Publication, 63–73.

Kolonic, S., Wagner, T., Sinninghe Damsté, J.S., Walsworth-Bell, B., Erba, E., Turgeon, S., Brumsack H-J., Chellai, E. H., Tsikos, H., Kuhnt, W. and Kuypers, M.M., 2005. Palaeoceanography, 70, PA1006, doi:10.1029/2003PA000950.

Koopmans, M.P., Köster, J., van Kaam-Peters, H.M.E., Kenig, F., Schouten, S., Hartgers, W.A., de Leeuw, J.W. and Sinninghe Damsté, J.S., 1996. Diagenetic and catagenetic products of isorenieratene: molecular indicators for photic zone anoxia. Geochimica et Cosmochimica Acta, 60, 4467–4496.

Krassay, A.A. and Totterdell, J.M., 2003. Seismic stratigraphy of a large, Cretaceous shelf-margin delta complex, offshore southern Australia. AAPG Bulletin, 87(6), 935–963.

Kuypers, M.M.M., Pancost, R.D., Nijenhuis, I.A. and Sinninghe Damsté, J.S., 2002. Enhanced productivity led to increased organic carbon burial in the euxinic North Atlantic basin during the Cenomanian oceanic anoxic event. Palaeoceanography, 17, 1051, doi:10.1209/2000PA000569.

Lewan, 1984. Factors controlling the proportionality of vanadium to nickel in crude oils. Geochimica et Cosmochimica Acta, 48, 2231–2238.

Li, Q.,. Simo, J.A.. McGowran, B. and Holbourn, A., 2004. The eustatic and tectonic origin of Neogene unconformities from the Great Australian Bight. Marine Geology, 203, 57–81.

Logan, G.A., Jones, A.T., Kennard, J.M., Ryan, G.J. and Rollet, N., in press. Australian offshore natural hydrocarbon seepage studies, an evaluation and re-assessment. Marine and Petroleum Geology.

Lüning, S., Kolonic, S., Belhadj, Z., Cota, L., Barić, G. and Wagner, T., 2004. Integrated depositional model for the Cenomanian–Turonian organic-rich strata in North Africa. Earth-Science reviews, 64, 51–117.

Marlowe, I.T., Brassell, S.C., Eglinton, G. and Green, J.C., 1984. Long chain unsaturated ketones and esters in living algae and marine sediments. Organic Geochemistry, 6, 135–141.

Mello, M.R., Telnaes, N., Gaglianone, P.C., Chicarelli, M.I., Brassell, S.C. and Maxwell, J.R., 1988. Organic geochemical characterisation of depositional palaeoenvironments of source rocks and oils in Brazilian marginal basins. Organic Geochemistry, 13, 31–45.

Messent, B.E.J., 1998. Great Australian Bight: well audit. Australian Geological Survey Organisation Record 1998/37.

Meyers, P.A., Yum, J.-G. and Wise, S.W., 2007. Confirmation of Cenomanian-Turonian black shales at high-latitude ODP Site 1138 on the Kerguelen Plateau. In: Farrimond, P. et al. (Eds), 23rd International Meeting of Organic Geochemistry, Torquay, England, 9–14 September 2007, Book of Abstracts, P99-MO.

Mohr, B.A.R., Wähnert, V. and Lazarus, D., 2002. Mid-Cretaceous paleobotany and palynology of the central Kerguelen Plateau, southern Indian Ocean (ODP Leg 183, Site 1138). In: Frey, F.A., Coffin, M.F., Wallace, P.J., and Quilty, P.G. (Eds), Proceedings of the Ocean Drilling Program, Scientific Results, 183, 1–39. http://wwwodp.tamu.edu/publications/183_SR/VOLUME/CHAPTERS/008.PDF.

Monteil, E., Macphail, M. and Partridge, A.D., 2008. Results of palynostratigraphic and palaeoenvironmental analyses of 281 dredge samples from the Great Australian Bight (GAB), southern margin, Australia. TimeMatters Biostratigraphic Services report for Geoscience Australia (unpublished).

Morgan, R.P., 1999. Palynology review of the pre-Tertiary of the Bight–Duntroon basins. Report for Primary Industries and Resources South Australia (unpublished).

Murray, A.P., Sosrowidjojo, I.B., Alexander, R., Kagi, R.I., Norgate, C.M. and Summons, R.E., 1997. Oleananes in oils and sediments: Evidence of marine influence during early diagenesis? Geochimica et Cosmochimica Acta, 61, 1261–1276.

Muscio, G.P.A., Horsfield, B. and Welte, D.H., 1994. Occurrence of thermogenic gas in the immature zone – implications from the Bakken insource reservoir system. Organic Geochemistry, 22, 461–476.

National Mapping and Information Group, 2008. Gazetteer of Australia 2008. Geoscience Australia, Canberra. Geocat 65589.

Niemann, H. and Elvert, M., 2008. Diagnostic lipid biomarker and stable carbon isotope signatures of microbial communities mediating the anaerobic oxidation of methane with sulphate. Organic Geochemistry, 39, 1668–1677.

Noble, R.A., Alexander, R., Kagi, R.I. and Knox, J., 1985. Tetracyclic diterpenoid hydrocarbons in some Australian coals, sediments and crude oils. Geochimica et Cosmochimica Acta, 49, 2141–2147.

Noble, R.A., Alexander, R., Kagi, R.I. and Knox, J., 1986. Identification of some diterpenoid hydrocarbons in petroleum. Organic Geochemistry, 10, 825–829.

Norvick, M.S. and Smith, M.A., 2001. Mapping the plate tectonic reconstruction of southern and southeastern Australia and implications for petroleum systems. The APPEA Journal, 41(1), 15–35.

Nytoft, H.P., Bojesen-Koefoed, J.A. and Christiansen, F.G., 2000. C26 and C28-C34 28-norhopanes in sediments and petroleum. Organic Geochemistry, 31, 25–39.

O'Brien, G.W. and Woods, E.P., 1995. Hydrocarbon-related diagenetic zones (HRDZs) in the Vulcan Sub-basin, Timor Sea: recognition and exploration implications. The APEA Journal, 35(1), 220–252.

Otto, A. and Wilde, V., 2001. Sesqui-, di- and triterpenoids as chemosystematic markers of extant conifers - a review. The Botanical Review, 67, 141–238.

Pancost, R.D. and Boot, C.S., 2004. The palaeoclimatic utility of terrestrial biomarkers in marine sediments. Marine Chemistry, 92, 239–261.

Peters, K.E., 1986. Guidelines for evaluating petroleum source rock using programmed pyrolysis. AAPG Bulletin, 70, 318–329.

Peters, K.E., Walters, C.C. and Moldowan, J.M., 2005. The Biomarker Guide Volume 2: biomarkers and isotopes in petroleum exploration and Earth history. Cambridge University Press, 1155pp.

Petsch, S.T., Berner, R.A. and Eglinton, T.I., 2000. A field study of the chemical weathering of ancient sedimentary organic matter. Organic Geochemistry, 31, 475–487.

Raza, A., Hill, K.C. and Korsch, R.J., 1995. Mid-Cretaceous regional uplift and denudation of the Bowen–Surat basins, Queensland and its relation to Tasman Sea rifting. In: Follington, I.L., Beeston, J.W. and Hamilton, L.H. (Eds), Bowen Basin Symposium 1995—150 years on. Geological Society of Australia, supplement.

Richardson, L., Mathews, E. and Heap, A., 2005. Geomorphology and sedimentology of the Southwestern Planning Area of Australia. Geoscience Australia Record 2005/17.

Robl, T.J. and Davis, B.H., 1993. Comparison of the HF–HCl and HF–BF3 maceration techniques and the chemistry of resultant organic concentrates. Organic Geochemistry, 20, 249–255.

Rollet, N. Fellow, M.E., Struckmeyer, H.I.M. and Bradshaw, B.E., 2001. Seabed character mapping in the Great Australian Bight. Geoscience Australia Record 2001/42, 1–23.

Ruble, T.E., Logan, G.A., Blevin, J.E., Struckmeyer, H.I.M., Liu, K., Ahmed, M., Eadington, P.J. and Quezada, R.A., 2001. Geochemistry and charge history of a palaeo-oil column: Jerboa-1, Eyre Sub-basin, Great Australian Bight. In: Hill, K.C. and Bernecker, T. (Eds), Eastern Australasian Basins Symposium: a refocused energy perspective for the future. Petroleum Exploration Society of Australia, Special Publication, 521–530.

Sayers, J., Symonds, P., Direen, N.G. and Bernardel, G., 2001. Nature of the continent–ocean transition on the non-volcanic rifted margin of the central Great Australian Bight. In: Wilson, R.C.L., Whitmarsh, R.B., Taylor, B. and Froitzheim, N. (Eds), Non-volcanic rifting of continental margins: a comparison of evidence from land and sea. Geological Society of London, Special Publications, 187, 51–77.

Schlanger, S.O., Arthur, M.A., Jenkyns, H.C. and Scholle, P.A., 1987. The Cenomanian–Turonian Oceanic Anoxic Event, I: Stratigraphy and distribution of organic carbon-rich beds and the marine $\delta^{13}C$ excursion. In: Brooks, J. and Fleet, A.J. (Eds), Marine petroleum source rocks. Geological Society Special Publication 26, 371–399.

Schlanger, S.O. and Jenkyns, H.C., 1976. Cretaceous oceanic anoxic events; causes and consequences. Geologie en Mijnbouw, 55, 179–184.

Schofield, A. and Totterdell, J.M., 2008. Distribution, timing and origin of magmatism in the Bight and Eucla basins. Geoscience Australia Record 2008/24

Schubert, C.J., Villanueva, J., Calvert, S.E., Cowie, G.L., von Rad, U., Schulz, H., Berner, U. and Erlenkeuser, H., 1998. Stable phytoplankton community structure in the Arabian Sea over the past 200,000 years. Nature, 394, 563–566.

Seifert, W.K., Moldowan, J.M., Smith, G.W. and Whitehead, E.V., 1978. First proof of structure of a C28-pentacyclic triterpane in petroleum. Nature, 271, 436–437.

Smith, M.A. and Donaldson, I.F., 1995. The hydrocarbon potential of the Duntroon Basin. The APEA Journal, 35(1), 203–219.

Somerville, R., 2001. The Ceduna Sub-basin – a snapshot of prospectivity. The APPEA Journal, 41(1), 321–346.

Stagg, H.M.V., Cockshell, C.D., Willcox, J.B., Hill, A.J., Needham, D.V.L., Thomas, B., O'Brien, G.W. and Hough, L.P., 1990. Basins of the Great Australian Bight region, geology and petroleum potential. Bureau of Mineral Resources, Australia, Continental Margins Program Folio, 5.

Stout, S.A., 1992. Aliphatic and aromatic triterpenoid hydrocarbons in a Tertiary angiospermous lignite. Organic Geochemistry, 18, 51–66.

Struckmeyer, H.I.M., O'Brien, G.W., Hatch, L., Heighway, K. & Nigel Press Associates LTD/TREICO LTD, 2000. Great Australian Bight: Remote sensing of hydrocarbon seepage. Australian Geological Survey Organisation, AGSOCAT 31222 (ArcView GIS CDROM & reports).

Struckmeyer, H.I.M., Totterdell, J.M., Blevin, J.E., Logan, G.A., Boreham, C.J., Deighton, I., Krassay, A.A. and Bradshaw, M.T., 2001. Character, maturity and distribution of potential Cretaceous oil source rocks in the Ceduna Sub-basin, Bight Basin, Great Australian Bight. In: Hill, K.C. and Bernecker, T. (Eds), Eastern Australian Basin Symposium: a refocused energy perspective for the future. Petroleum Exploration Society of Australia, Special Publication, 543–552.

Struckmeyer, H.I.M., Williams, A.K., Cowley, R., Totterdell, J.M., Lawrence, G. and O'Brien, G.W., 2002. Evaluation of hydrocarbon seepage in the Great Australian Bight. The APPEA Journal, 42, 371–385.

Summons, R.E., Powell, T.G., 1987. Identification of aryl isoprenoids in source rocks and crude oils: Biological markers for the green sulphur bacteria. Geochimica et Cosmochimica Acta, 51, 557–566.

Tapley, D., Mee, B.C., King, S.J., Davis, R.C. and Leischner, K.R., 2005. Petroleum potential of the Ceduna Sub-basin: impact of Gnarlyknots-1A. The APPEA Journal, 45(1), 365–380.

Teasdale, J.P., Pryer, L.L., Stuart-Smith, P.G., Romine, K.K., Etheridge, M.A., Loutit, T.S. and Kyan, D.M., 2003. Structural framework and basin evolution of Australia's southern margin. The APPEA Journal, 43, 13–37.

Ten Haven, H.L., Baas, M., De Leeuw, J.W., Schenck, P.A. and Brinkhuis, H., 1987. Late Quaternary Mediterranean sapropels II. Organic geochemistry and palynology of S1 sapropels and associated sediments. Chemical Geology, 64, 149–167.

Thurow, J., Brumsack, H.-J. and Rullkötter, J., 1992. The Cenomanian/Turonian boundary event in the Indian Ocean – a key to understanding the global picture. In: Duncan, A. et al. (Eds) Synthesis of results from scientific drilling in the Indian Ocean. American Geophysical Union, Geophysical Monograph 70, 253–273.

Tikku, A.A. and Cande, S.C., 1999. The oldest magnetic anomalies in the Australian–Antarctic Basin: are they isochrons? Journal of Geophysical Research, B1, 104, 661–677.

Tissot, B.P. and Welte, D.H., 1984. Petroleum Formation and Occurrence. Springer-Verlag, Berlin. 699p.

Totterdell, J.M., Blevin, J.E., Struckmeyer, H.I.M., Bradshaw, B.E., Colwell, J.B. and Kennard, J.M., 2000. A new sequence framework for the Great Australian Bight: starting with a new slate. The APPEA Journal, 40, 95–117.

Totterdell, J.M. and Bradshaw, B.E., 2004. The structural framework and tectonic evolution of the Bight Basin. In: Boult, P.J., Johns, D.R. & Lang, S.C. (Eds), Eastern Australasian Basins Symposium II. Petroleum Exploration Society of Australia, Special Publication, 41–61.

Totterdell, J.M. and Krassay, A.A., 2003a. The role of shale deformation and growth faulting in the Late Cretaceous evolution of the Bight Basin, offshore southern Australia. In: Van Rensbergen, P., Hillis, R.R.., Maltman, A.J. and Morley, C.K. (Eds), Subsurface sediment mobilisation. Geological Society of London, Special Publications, 216, 429–442.

Totterdell, J.M. and Krassay, A.A., 2003b. Sequence stratigraphic correlation of onshore and offshore Bight Basin successions. Geoscience Australia Record 2003/02.

Totterdell, J.M., Struckmeyer, H.I.M., Boreham, C.J., Mitchell, C.H., Monteil, E. and Bradshaw, B.E., 2008. Mid–Late Cretaceous organic-rich rocks from the eastern Bight Basin: implications for prospectivity. In: Blevin, J.E., Bradshaw, B.E. and Uruski, C. (Eds) Eastern Australasian Basins Symposium III. Petroleum Exploration Society of Australia, Special Publication, 137–158.

Tsikos, H., Jenkyns, H.C., Walsworth-Bell, B., Petrizzo, M.R., Forster, A., Erba, E., Premoli Silva, I., Baas, M., Wagner, T. and Sinninghe Damsté, J.S., 2004. Carbon-isotope stratigraphy recorded by the Cenomanian-Turonian Oceanic Anoxic Event: correlation and implications based on three key localities. Journal of Geological Society, 161(4), 711–719.

Turgeon, S.C. and Creaser, R.A., 2008. Cretaceous oceanic anoxic event 2 triggered by a massive magmatic episode. Nature, 454, 323–326.

van Bentum, E., Forster, A., Reichart, G-J. and Sinninghe Damsté, J.S., 2007. Rapid changes in oceanic stratification during the Cenomanian/Turonian oceanic anoxic event at Demerara Rise. International Meeting on Organic Geochemistry, Torquay, England, September 2008. Book of Abstracts P97-MO.

van de Meent, D., Brown, S.C., Philp, R.P. and Simoneit, B.R.T., 1980. Pyrolysis-high resolution gas chromatography and pyrolysis gas chromatography-mass spectrometry of kerogens and kerogen precursors. Geochimica et Cosmochimica Acta, 44(7), 999–1013.

Veevers, J.J., Powell, C.Mca. and Roots, S.R., 1991. Review of seafloor spreading around Australia. I. Synthesis of the patterns of spreading. Australian Journal of Earth Sciences, 38(4), 373–89.

Volkman, J. K. 2003. Sterols in microorganisms. Applied Microbiology and Biotechnology, 60, 495–506.

Volkman, J.K., Barrett, S.M., Blackburn, S.I., Mansour, M.P., Sikes, E.L. and Gelin, F., 1998. Microalgal biomarkers: A review of recent research developments. Organic Geochemistry, 29, 1163–1179.

Walker, T.R., 2007. Deepwater and frontier exploration in Australia─historical perspectives, present environment and likely future trends. The APPEA Journal, 47 (1), 15–38.

Wanglu, J., Ping´an, P., Chiling, Y. and Zhongyao, X., 2007. Source of 1,2,3,4-tetramethylbenzene in asphaltenes from the Tarim Basin. Journal of Asian Earth Sciences, 30, 591–598.

Waschbusch, P., Beaumont, C. and Korsch, R.J., 1999. Geodynamic modelling of aspects of the New England Orogen and adjacent Bowen, Gunnedah and Surat Basins. In: Flood, P.G. (Ed.), New England Orogen: regional geology, tectonics and metallogenesis. Earth Sciences, University of New England, Armidale, 203–210.

Westerhausen, L., Poynter, J., Eglinton, G., Erlenkeuser, H. and Sarnthein, M., 1993. Marine and terrigenous origin of organic matter in modern sediments of the equatorial East Atlantic: the $\delta^{13}C$ and molecular record. Deep Sea Research Part I: Oceanographic Research Papers, 40, 1087–1121.

Willcox, J.B. and Stagg, H.M.J., 1990. Australia's southern margin: a product of oblique extension. Tectonophysics, 173, 269–281.

Williams, L.A., 1984. Subtidal stromatolites in Monterey Formation and other organic-rich rocks as suggested source contributors to petroleum formation. AAPG Bulletin, 68, 1879–1893.

Wolff, G.A., Trendel, J.M. and Albrecht, P., 1989. Novel monoaromatic triterpenoid hydrocarbons occurring in sediments. Tetrahedron, 45, 6721–6728.